The role of the LAMMER kinase Kns1 and the calcium/calmodulin-dependent kinase Cmk2 in the adaptation of *Saccharomyces cerevisiae* to alkaline pH stress

Dissertation

zur Erlangung des akademischen Grades

doctor rerum naturalium

(Dr. rer. nat)

Im Fach Biologie (Molekularbiologie)

eingereicht an der

Mathematisch-Naturwissenschaftlichen Fakultät I

der Humboldt-Universität zu Berlin

von

Frau Dipl.-Biochem. M. Nieves Martínez Marshall

Präsident der Humboldt-Universität zu Berlin:
Prof. Dr. Jan-Hendrik Olbertz

Dekan der Mathematisch-Naturwissenschaftlichen Fakultät I:
Prof. Dr. Andreas Herrmann

Gutachter:
1. Prof. Dr. Harald Saumweber
2. Prof. Dr. Thomas Sommer
3. Prof. Dr. Udo Heinemann

eingereicht am: 27.10.2011
Tag der mündlichen Prüfung: 18.07.2012

Abstract

The LAMMER protein kinases, termed after a unique signature motif found in their catalytic domains, are an evolutionary conserved family of dual-specificity kinases that are present in most eukaryotes including humans, yeast and protozoa. Members of this family have been implicated in key cellular functions such as splicing, transcription, translation, differentiation and stimuli-induced signal transduction.

Here I report the first functional characterization of one of the most unexplored members of the LAMMER family, the budding yeast Kns1. Phenotypic analysis uncovered a crucial role for Kns1 in the control of the yeast tolerance to high pH stress. Deletion of the *KNS1* gene conferred high sensitivity to alkaline pH, whereas its overexpression increased tolerance to this stress. Further analysis established that Kns1 promotes growth under alkaline pH stress using not only its catalytic activity but also non-catalytic mechanisms. Large-scale purification of full-length Kns1 from *E. coli* allowed for the identification of nine *in vitro* autophosphorylation sites on Kns1 by mass spectrometry. Mutation of the threonine residue at position 562 (Thr^{562}), an autophosphorylation site located within the LAMMER motif, to a non-phosphorylatable residue yielded a kinase that preserves intrinsic catalytic activity *in vitro* but mostly behaves like the catalytically inactive mutant *in vivo*. This finding showed the physiological importance of autophosphorylation site Thr^{562} in the regulation of Kns1 function.

The protein Cmk2, a calcium/calmodulin-dependent protein kinase II with autocatalytic properties, has been previously proposed as a possible *in vitro* substrate for Kns1. Here I demonstrate that Kns1 phosphorylates Cmk2 *in vitro* using a catalytically inactive Cmk2 mutant as substrate and show that Cmk2, as opposed to Kns1, acts to restrict alkaline tolerance. Genetic evidence suggested that both proteins act in concert on a common pathway, in which Kns1 may downregulate Cmk2 to confer alkaline tolerance. Identification of *in vitro* phosphorylation sites in Cmk2 followed by mutational analysis indicated that autophosphorylation of Cmk2 at Thr^{69} may prevent its downregulation by Kns1 under alkaline pH stress.

In conclusion, this thesis describes a novel and crucial role for Kns1 and its *in vitro* substrate Cmk2 in the adaptation of yeast to alkaline stress and provide valuable insights into their regulation as well as into their functional interplay.

Key words: LAMMER kinase, Kns1, calcium/calmodulin-dependent protein kinase II, Cmk2, alkaline pH stress, Saccharomyces cerevisiae.

Zusammenfassung

Die LAMMER-Kinasen sind Dual-Spezifität-Proteinkinasen, die durch das namensgebende einzigartige LAMMER-Motiv in der katalytischen Subdomäne X gekennzeichnet sind. Sie sind evolutionär hoch konserviert und in den meisten Eukaryonten wie Menschen, Hefen und Protozoen vorhanden. Mitglieder dieser Familie sind mit wichtigen zellulären Prozessen wie Spleißen, Signaltransduktions-wegen, Transkription, Translation und Differenzierung assoziiert.

Die vorliegende Arbeit stellt die erste funktionelle Charakterisierung eines bisher kaum erforschten Vertreters der LAMMER-Proteinkinase Familie Kns1 aus der Bäckerhefe dar. Phänotypische Analysen belegten eine entscheidende Rolle für Kns1 in der Regulation der Toleranz gegenüber basischem pH-Stress. Das Entfernen des *KNS1* Gens führte zu einer gesteigerten Empfindlichkeit der Zellen gegenüber basischen Wachstumsbedingungen, während seine Überexpression in einer erhöhten Stresstoleranz resultierte. Weitere Analysen zeigten, dass Kns1 neben der katalytischen Aktivität auch nicht-katalytischen Mechanismen zur Förderung des Zellwachstums unter alkalischem pH-Stress nutzt. Die Reinigung des Kns1 Proteins in voller Länge aus *E. coli* ermöglichte die Identifizierung von neun *in vitro*-Autophosphorylierungsstellen mittels Massenspektrometrie. Die Mutation von Thr^{562}, eine Autophosphorylierungsstelle innerhalb des LAMMER-Motivs, zu Alanin ergab *in vitro* eine Kinase mit intrinsischer katalytischer Aktivität, die sich jedoch *in vivo* hauptsächlich wie die katalytisch inaktive Kns1-Mutante verhielt. Dieser Befund belegt die physiologische Bedeutung von Thr^{562} in der Regulation der Kns1 Funktion.

Die Calcium/Calmodulin-abhängige Proteinkinase II Cmk2, die konstitutiv autokatalytische Eigenschaften besitzt, wurde früher als mögliches *in vitro* Substrat von Kns1 vorgeschlagen. In dieser Arbeit beweise ich durch Verwendung einer katalytisch inaktiven Cmk2-Mutante als Substrat, dass Kns1 Cmk2 *in vitro* phosphoryliert. Darüber hinaus zeige ich, dass Cmk2 die basische pH-Toleranz der Zellen beschränkt. Gestützt durch genetische Hinweise agieren beide Proteine gemeinsam bei der Regulation der alkalischen Stresstoleranz, wobei Kns1 möglicherweise Cmk2 herabreguliert. Die Identifizierung der *in vitro* Phosphorylierungsstellen von Cmk2, gefolgt von gerichteten Mutagenesestudien dieser Stellen wiesen darauf hin, dass Autophosphorylierung des Restes Thr^{69} von Cmk2 bei alkalischem Stress die Herabregulation durch Kns1 *in vivo* verhindert.

Zusammenfassend beschreibt diese Arbeit eine neue und entscheidende Rolle von Kns1 und Cmk2 bei der Anpassung der Hefe an alkalisches Milieu und gibt wertvolle Einblicke in Regulation und funktionellem Zusammenspiel beider Faktoren.

Schlagwörter: LAMMER-Kinase, Kns1, Calcium/Calmodulin-abhängige Proteinkinase II, Cmk2, alkalische pH-stress, *Saccharomyces cerevisiae*.

Table of contents

1. Introduction

1.1 Protein kinases

Reversible protein phosphorylation is one of the most important control mechanisms of protein function. It is the most widespread type of post-translational modification in intracellular signal transduction and also plays a critical role in the regulation of many other cellular processes. Thus, protein phosphorylation virtually affects every aspect of cell life including metabolism, transcription, cell cycle progression, cytoskeletal organization, organelle trafficking, stress responses, apoptosis and differentiation[1].

Protein phosphorylation is catalysed by protein kinases, which transfer the γ-phosphate from a nucleoside triphosphate (usually ATP) onto an acceptor amino acid in the substrate protein[2]. The addition of a phosphate molecule has profound consequences on the target protein. The attribute of a double negative charge and the capacity of the phosphoryl oxygens to form hydrogen-bond interactions can promote conformational changes in the protein that affect self-association, recognition by other proteins, activation or inhibition of its enzymatic activity[3,4].

1.1.1 Protein kinase classification

The large family of protein kinases is classified based on the target amino acid specificity. There are three major subfamilies responsible for phosphorylation on hydroxy-amino acids in eukaryotic cells: (a) protein tyrosine (Tyr) kinases that phosphorylate the phenolic hydroxyl group of tyrosine, (b) protein serine/threonine (Ser/Thr) kinases that phosphorylate the hydroxyl group on the β-carbon of serine and threonine and (c) dual-specificity protein kinases that are capable of phosphorylating serine, threonine and tyrosine residues[5,6].

1.1.1.2 Serine/Threonine and Tyrosine protein kinases

Ser/Thr and Tyr protein kinases differ principally in the depth of their catalytic cleft, as underscored by the comparison between the tridimensional structure of the prototypical Ser/Thr cAMP-dependent protein kinase (PKA) and Tyr protein kinase Insulin receptor kinase (IRK)[7,8]. A number of differences in the primary structure of Ser/Thr and Tyr protein kinases contribute to the creation of a different residue environment and conformation of the active site[8,9]. Among these differences, there are

three distinctive signature motifs that are traditionally used to predict amino acid specificity[10,11]. These are found in regions close to the site of phosphotransfer *i.e.*, in the catalytic loop (subdomain VIb) and in the P+1 loop (subdomain VIII), which is the docking site for the residue adjacent to the target phosphorylation site. One signature motif is the DLKPEN sequence in the catalytic loop of Ser/Thr kinases that is replaced by DLAARN in Tyr kinases[9]. The second distinctive signature is in the P+1 loop; where in Ser/Thr kinases there is a threonine (Thr^{201} in PKA) or serine, in Tyr kinases there is a conserved proline, which forms hydrophobic interactions with the aromatic ring of the substrate tyrosine[9,12]. Lastly, a characteristic common to all Tyr kinases is the presence of a conserved tryptophan (Trp^{1175} in IRK) in their P+1 loop. This tryptophan contributes to the positioning of the tyrosine ring and also interacts directly with the arginine in the DLAARN motif to link the catalytic with the P+1 loops[8,9]. In Ser/Thr kinases, this link is established through the interaction between Thr^{201} with the lysine residue in the DLKPEN motif, thereby resulting in a closer conformation of the catalytic cleft[8].

1.1.1.3 Dual-specificity protein kinases

Dual-specificity protein kinases bear in their catalytic domains the signature motifs of Ser/Thr protein kinases[6,13]. Therefore, since their discovery, the assumption that the amino acid specificity of a protein kinase can be predicted from its primary sequence had to be reevaluated. Given the significant differences in size and hydrophobicity between the aliphatic Ser/Thr and the aromatic Tyr residues, it is currently believed that the distinct conformation of the catalytic cleft is what basically conditions the discrimination between Ser/Thr and Tyr residues[14]. Therefore, dual-specificity kinases must possess specific sequence determinants conferring permissive substrate usage *i.e.*, flexibility in the active site region to accommodate either type of hydroxyl residues. However, the attempt to identify such determinants through sequence alignment analysis did not yield any obvious consensus motif[6].

The best characterized dual-specificity kinases are the mitogen-activated protein (MAP) kinase kinases *e.g.,* mammalian MEK1/MKK1 and yeast Ste7[15,16]. They typically participate in sequentially activated kinase signalling modules that consist of a minimum of three kinases: an upstream Ser/Thr kinase, a middle dual-specificity kinase and a downstream Ser/Thr kinase. Such signalling modules mediate cellular responses to a myriad of extracellular stimuli and conditions of cellular stress[17,18]. Owing to their physiological importance, MAP kinase pathways have been conserved throughout eukaryotic evolution[19]. Two other major subfamilies of dual-specificity protein kinases are also well-conserved from yeast to mammals: (i) the family of the dual-specificity tyrosine-phosphorylation-regulated kinases (DYRKs), whose members include

mammalian DYRK1 and *S. cerevisiae* Yak1, and (ii) the family of the Cdc2-like kinases (CLKs), herein termed LAMMER kinases, which have as a founding member murine Clk/Sty kinase (mCLK1)[20–24].

1.2 The LAMMER family of protein kinases

The LAMMER family of protein kinases are found in most eukaryotes and belong to the group of eukaryotic signature proteins (ESPs) that were essential for the evolution of eukaryotic cells[25]. Members of this family include Kns1 from *S. cerevisiae*, Lkh1/Kic1 from *S. pombe*, PfLammer from *P. falciparum*, AFC1-3 from *A. thaliana*, PK12 from *N. tabacum*, DOA from *D. melanogaster*, mCLK1-4 from murine and hCLK1-4 from human[13,24,26–32].

All LAMMER kinases tested so far exhibit autophosphorylation activity on Ser, Thr and Tyr residues *in vitro*[33–35]. Autophosphorylation on Tyr residues has only been demonstrated *in vivo* on mCLK1 when overexpressed in mouse[36,37]. Although some doubt has been raised about the extent and relevance of Tyr autophosphorylation under physiological conditions, biochemical data support the hypothesis that dual-specificity might be of importance for LAMMER kinase function[38,39]. For instance, the fact that changes in the pattern of CLK1 autophosphorylation *i.e.*, the extent of Ser/Thr *versus* Tyr phosphorylation, influences CLK1 autophosphorylation activity and activity towards specific substrates *in vitro*[39,40]. So far, dual-specificity does not seem to extend to exogenous substrates, which are phosphorylated by LAMMER kinases preferentially on Ser and, to a lesser extent, on Thr residues[34,41,42]. Alternatively, Tyr phosphorylation may be restricted to specific physiological substrates that are yet to be discovered.

1.2.1 Structural features

LAMMER kinases are characterized by and termed after a unique and highly conserved amino acid signature motif located within the subdomain X of their kinase domains; the EHLAMMERILG (or LAMMER) motif[29]. Based on structure analogies with other kinases, the LAMMER motif was initially predicted to lie below the substrate-binding cleft, suggesting a role in substrate recognition[29,43,44]. However, more recently, determination of the crystal structures of mammalian CLK1 and CLK3 showed that the LAMMER motif is situated at the bottom of the large C-terminal kinase lobe in the small αG-helix, which is buried and packed against an adjacent helix (αH) making it solvent-inaccessible and; therefore, less likely to be involved in substrate recognition[42]. Consistent with this, studies of the LAMMER homologue of tobacco plants, PK12, revealed that mutations disrupting the LAMMER motif abrogated catalytic activity *in*

vitro and caused aberrant subnuclear localization of the kinase but did not interfere with substrate binding[45,46]. However, in the fission yeast, disruption of the LAMMER motif of Lkh1 not only resulted in the abolition of catalytic activity *in vitro* but also in reduced substrate binding capacity[47]. Currently, it is unclear whether these outcomes relate to the actual role of the LAMMER motif *in vivo* and to what extent this role is conserved among evolutionary diverged species.

The catalytic domain of LAMMER kinases is located at the carboxyl (C)-terminus of the protein and is extremely conserved throughout evolution, in particular, in those subdomains responsible for phosphotransfer and substrate recognition[29]. The non-catalytic amino (N)-terminal domain is the most divergent part of the protein, varying greatly in length among species[29]. Animal LAMMER kinases contain a region enriched in short arginine/serine repeats (RS motifs) located at their amino-terminal domains, which contributes to establish optimal interactions with SR proteins[34,48,49]. Although the molecular mechanism of LAMMER kinase regulation is currently unclear, it has been proposed that the N-terminal domain may comprise a regulatory domain and a dimerization domain, as suggested by studies of mammalian CLK1 and fission yeast Lkh1[36,40,50].

1.2.2 Functions

The best characterized and most conserved function of LAMMER kinases in metazoans is the modulation of alternative splicing through the phosphorylation of serine/arginine (SR)-rich proteins[37,39,48,51,52]. Phosphorylation of the SR protein ASF/SF2 within the SR-rich domain by mCLK1 promotes the release of ASF2/SF2 from nuclear speckles and its recruitment to the sites of active transcription[48,51,53]. Furthermore, mCLK1 directly modulates the splicing activity of ASF2/SF2 *in vitro* and affects its ability to interact with other splicing factors and RNA molecules[52,54]. In *Drosophila*, mutations of the *Doa* locus result in hypophosphorylation of the SR-splicing factors TRA and TRA2, which in turn, cause aberrant splicing of the *doublesex* (*dsx)* transcript, thus altering sexual differentiation[49]. Dysregulation of alternative splicing is linked to a number of human cancers and hereditary diseases[55–57]. Given the importance of CLK1 on the control of alternative splicing, the pharmacological inhibition of mammalian CLK kinases has emerged as a potential tool for the therapeutic manipulation of abnormal splicing in pathological states[42,58]. The role of LAMMER kinases in splicing could be also conserved in plants, as PK12 from tobacco plants has been shown to bind and phosphorylate SR proteins *in vitro* and modulate the alternative splicing pattern of endogenous genes in living cells[34,45,46].

Aside from participating in splicing control in diverse species, LAMMER kinases play a role in the oxidative stress responses of fission yeast, fruit fly and humans. In the fission yeast, Lkh1 positively regulates the expression of antioxidant enzymes, as loss of the *lkh1+* gene resulted in greater sensitivity to oxidative stress owing to a reduced expression of catalase (*ctt1+*) and Cu,Zn-superoxide dismutase (*sod1+*)[59]. Lkh1 was later shown to phosphorylate the RNA-binding protein Csx1, which is known to stabilize the mRNA of the transcription factor Atf1 responsible for the induction of *ctt1+* and other genes in response to oxidative stress[50,60,61]. In higher eukaryotes, however, LAMMER kinases exert opposite effects on the expression of antioxidant enzymes. Mutations in the *Doa* gene were reported to protect adult flies against oxidative stress possibly due to the increased protein levels and activity of superoxide dismutase (SOD1). Similarly, the knockdown of CLK1 in human cells led to an increase in SOD1 protein levels and activity[62]. Although the LAMMER kinases seem to act in opposite ways in fission yeast and higher eukaryotes to modulate the expression of antioxidant enzymes, it remains possible that these LAMMER kinases share a conserved underlying mechanism. Yet, their exact mechanism of action in this process awaits further investigation.

Several lines of evidence implicate LAMMER kinases in further stimuli-induced signal transducing pathways. Increased expression of mCLK1 in neuronal cells induces cell cycle arrest and triggers differentiation through the activation of the MAP kinases ERK1 and ERK2, thereby mimicking the activation of the neuronal growth factor (NGF)-dependent transduction pathway[63]. Mammalian CLK1 and CLK2 phosphorylate human PTP-1B, a cytosolic Tyr phosphatase involved in insulin signalling, and its yeast homologue Ptp1 *in vivo*[41]. The LAMMER kinase from *A. thaliana*, AFC1, suppresses defects in the mating-pheromone signalling pathway of *S. cerevisiae* through the stimulation of the transcription factor Ste12, thereby complementing the function of the yeast MAP kinases Kss1 and Fus3[28,64]. The activity and transcription of the tobacco LAMMER kinase PK12 are induced in response to the hormone ethylene, which is known to activate the signalling cascade implicated in a variety of stress responses and developmental processes in plants[35,65]. Evidence for a role of the LAMMER kinases in signalling has recently been provided by the finding that mCLK2 activity is regulated through phosphorylation by Akt (or Protein kinase B) in response to insulin signalling. Upon phosphorylation by Akt, mCLK2 undergoes autophosphorylation, becomes stabilized and phosphorylates the transcriptional co-activator PGC1-α, causing the repression of gluconeogenic gene expression[66]. The identification of PGC1-α as a mCLK2 substrate hints at the idea that LAMMER kinases may act at the final stages of the signalling cascades. Among other LAMMER kinase targets influencing

transcriptional regulation are the aforementioned global regulator of gene expression Csx1 and the transcriptional repressors Tup11 and Tup12 from *S. pombe*[47,50,67].

LAMMER kinases have been implicated in further cellular functions including translational elongation[68], cellular growth and differentiation[29,69], cell-cycle progression and autophagy in *Drosophila*[70–73] as well as in cell division, filamentous growth and flocculation in *S. pombe*[27,74]. These kinases are thus emerging as important players in a wide-range of key cellular functions in many organisms.

1.2.3 Subcellular localization

In concordance to their role in the regulation of SR splicing factors, mammalian CLKs (CLK1-4) have been found to be localized within the nucleus[36–38,48,51]. The bulk of LAMMER kinases analysed bears a presumptive nuclear localization signal at their N-terminus, which suggests that their nuclear targeting might be evolutionary conserved[13,29,37]. However, recent studies have reported that CLK1 and CLK3 are cytosolic proteins[40,75]. On the one hand, part of the discrepancy among the localization data of mammalian LAMMER kinases has been attributed to the different fixation agents used to perform immunostaining experiments[40]. On the other hand, it has also been proposed that the unique N-terminal features of each LAMMER family member contain the molecular determinants that dictate the isoform-specific differences in subcellular localization, as it appears to be the case for the *Drosophila* LAMMER homologue, DOA[76]. There are two isoforms of the DOA kinase that differ mostly in the size of their N-terminal non-catalytic domains. Remarkably, these two isoforms are distinctly distributed within the cell; the 55-kDa isoform is primarily localized to the nucleus whereas the 105-kDa isoform localizes exclusively to the cytoplasm[76]. Altogether, the finding that certain members of the LAMMER family reside in the cytosol reinforces the hypothesis that these kinases also act in cellular processes that take place outside the nucleus (described in 1.2.2).

1.2.4 Kns1, the LAMMER kinase family member of *S. cerevisiae.*

Kns1, the *S. cerevisiae* member of the LAMMER kinase family, is among the most diverged members in the family. Kns1 is one of the largest LAMMER kinases due to an extended N-terminal non-catalytic domain, which contains presumptive nuclear localization signals but lacks the signature region enriched with the RS motifs found in animal LAMMER kinases[29]. Spacing between the catalytic subdomains is highly conserved within the family except for Kns1, which possesses several small inserts

within the catalytic domain that are absent in those of higher eukaryotes[29]. In addition, the LAMMER motif of Kns1 differs in three amino acids from that of its mammalian counterparts, deriving in the EHMAMMQRING sequence (Fig. 1.1)[29].

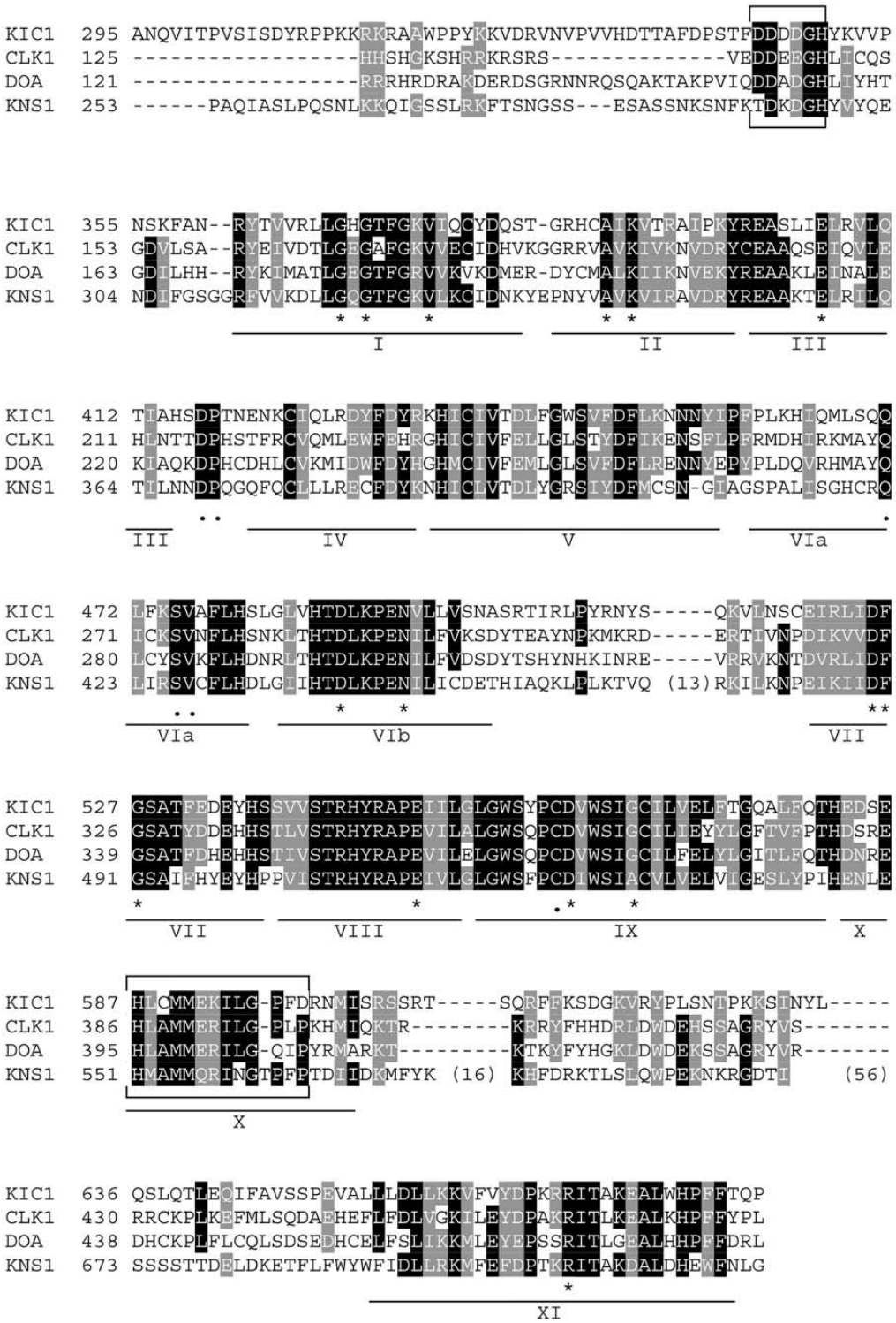

Figure 1.1. Sequence alignment of the catalytic domains of *S. pombe* (Kic1/Lkh1), *H. sapiens* (CLK1), *D. melanogaster* (DOA) and *S. cerevisiae* (Kns1) LAMMER kinases.

Taken from Tang *et al*. (2003)[74].

The function of the yeast LAMMER kinase remains unknown. No subcellular localization, protein interactors or cellular functions have been yet ascribed to Kns1. Large-scale immunolocalization studies reported that epitope-tagged and overexpressed Kns1 shows some cytoplasmic staining and a granular staining of unknown nature; yet, no cellular compartment was conclusively assigned to Kns1[77]. In another large scale study, genomically GFP-tagged Kns1 could not be visualized[78]. A number of yeast proteins have been reported to associate with Kns1 in high-throughput protein-protein interaction studies (see Table 6.1 in Appendix), but it remains to be confirmed whether these proteins are *bona fide* binding partners of Kns1[79–84].

Previous studies have shown that the catalytic domain of Kns1 interacts with and phosphorylates mammalian SR proteins *in vitro*[34], suggesting that Kns1 might be involved, like its counterparts in higher eukaryotes, in alternative splicing. However, although animals and budding yeasts share the basic splicing machinery, they mostly differ in the incidence of alternative splicing, which is rather marginal in the budding yeast[85]. Alternative splicing is mainly regulated by SR proteins in animals[86,87]. While SR proteins exist throughout the entire animal kingdom[88], and even in the fission yeast[89], genuine SR proteins are apparently missing from the budding yeast[90]. For these reasons, the finding that Kns1 is capable of interacting with mammalian SR proteins could be considered, at first, of dubious biological significance. Yet, the budding yeast does possess three SR-like proteins; Npl3, Gbp2 and Hrb1[91,92]. These proteins have been originally implicated in mRNA export[91–94]. More recently, Npl3 has been shown to be required for the efficiency of pre-mRNA splicing[95]. Thus, the possibility of Kns1 playing a role in regular splicing *e.g.*, through the interaction with a SR-like protein, remains conceivable.

The gene encoding the dual-specificity LAMMER kinase in yeast, *KNS1,* is not essential for viability under standard laboratory conditions[26]. This may indicate that the function of its gene product could be compensated for by a different protein or pathway[96,97]. However, previous attempts to identify gene products that are functionally redundant with Kns1 using synthetic lethal screening have so far failed (M. Horn, T. Kinzy and Rabinow, unpublished results)[29]. Alternatively, it is conceivable that the *KNS1* gene is required for growth under specific conditions[98]. This possibility is supported by the finding in a genome-wide phenotypic study that the growth of cells lacking *KNS1* (Δ*kns1*) is inhibited in the presence of exogenous oleate[99]. This growth inhibition by oleate has been ascribed to the toxicity of the unsaturated fatty acid rather than the inability of being used as a carbon source[99]. Oleate toxicity has been

hypothesized to principally rely on the over-incorporation of oleate in the plasma membrane and concomitant increase in fluidity caused by disruption of acyl-chain packing in the lipid bilayer[99]. Other studies have suggested that the deleterious effects of the excess of oleate are due to altered membrane phospholipid composition[100,101]. Therefore, it has been proposed that oleate sensitive mutants could be impaired in functions that are directly or indirectly related to lipid and membrane homeostasis[99]. Whether that is the underlying defect causing the oleate sensitivity of the Δ*kns1* mutant is yet to be investigated.

Recently, a map of the yeast phosphorylome has been created using proteome microarrays coupled with high-throughput *in vitro* kinase assays[102]. This seminal study has provided an overall picture of the substrate preferences of 87 yeast protein kinases, covering ~70% of the yeast kinome and identifying over 4000 phosphorylation events involving 1325 different proteins. Kns1, which was among the kinases assayed, showed the ability to phosphorylate five from about 4400 proteins included in the array[102] (Table 1.1). Based on the phosphorylation signal shown for each substrate, the Ca^{2+}/calmodulin-dependent kinase Cmk2 was the protein phosphorylated by Kns1 to the greatest extent among all substrates.

Table 1.1. Kns1 *in vitro* substrates previously identified in a yeast proteome array screen[102].

ORF Name	Standard Name	Phosphorylation Signal	Description[1]
YOL016C	Cmk2	33508.54	Calmodulin-dependent protein kinase; may play a role in stress response, many Ca^{2+}/Calmodulin dependent phosphorylation substrates demonstrated *in vitro*, amino acid sequence similar to Cmk1 and mammalian CaM Kinase II.
YGL180W	Atg1	11370.53	Protein serine/threonine kinase, required for vesicle formation during autophagy and the cytoplasm-to-vacuole targeting (Cvt) pathway.
YAR019C	Cdc15	6809.37	Protein kinase of the Mitotic Exit Network that is localized to the spindle pole bodies at late anaphase; promotes mitotic exit by directly switching on the kinase activity of Dbf2.
YLR044C	Pdc1	5039.62	Major of three pyruvate decarboxylase isozymes, key enzyme in alcoholic fermentation, decarboxylates pyruvate to acetaldehyde.
YMR102C	Ymr102c	4897.90	Protein of unknown function; transcription is activated by paralogous transcription factors Yrm1 and Yrr1 along with genes involved in multidrug resistance; mutant shows increased resistance to azoles; YMR102C is not an essential gene.

[1]ORF names, standard names and descriptions according to Saccharomyces Genome Database (http://www.yeastgenome.org/)

A growing number of drug discovery strategies is exploiting the budding yeast as model organism (reviewed in [103,104]). The advantages of this simple organism include a high degree of functional conservation of basic pathways between yeast and humans, high genetic tractability and an extensive repertoire of genetic and molecular techniques available for use in genome-wide approaches[105,106]. In this context, a genome-wide screen for the identification of therapeutic targets for Parkinson's disease revealed that the lack of the *KNS1* gene suppresses the toxicity of α-synuclein polypeptide expression, suggesting Kns1 as an enhancer of α-synuclein-associated toxicity[107]. In another large-scale screen, *KNS1* was identified as a gene that alters cellular sensitivity to the anticancer drug tirapazamine (TPZ), which targets topoisomerase II[108]. These findings highlight the importance of elucidating the roles of the Kns1 in the budding yeast and the extent to which these are shared with its human eukaryotes to enhance the scope of the yet limited knowledge about the LAMMER kinase family and enable the future development of novel therapeutic strategies for the treatment of diseases caused by LAMMER kinase dysregulation.

1.3 The calcium/calmodulin-dependent protein kinase II family

1.3.1 Ca^{2+}/CaM-dependent protein kinase II in higher eukaryotes

Calcium/calmodulin (Ca^{2+}/CaM)-dependent protein kinase type II (CaMKII) is a crucial mediator of calcium signalling in the brain, heart and other tissues[109–112]. CaMKII was initially discovered in the central nervous system, where it is highly enriched constituting up to 2% of the total protein in the hippocampus of rodents[113,114]. There, it modulates most aspects of neuronal function and plays a key role in learning and memory[115].

CaMKII has also been implicated in regulating many other aspects of cellular function in response to Ca^{2+} influx, including the regulation of carbohydrate, amino acid and lipid metabolism, ion channels and receptors, neurotransmitter synthesis and release, transcription and translation, cytoskeletal organization and calcium homeostasis[116].

1.3.1.1 Structure and isoform diversity

The CaMKII monomer consists of an NH_2-terminal catalytic domain, a centrally located regulatory domain and a COOH-terminal association domain. The catalytic domain contains the ATP- and substrate-binding sites typical of serine/threonine kinases, as well as sites for interaction with anchoring proteins. The regulatory domain comprises a pseudosubstrate/autoinhibitory sequence that, under basal conditions, binds and constrains the catalytic domain and a calmodulin (CaM) binding domain. The association domain is responsible for the assembly of the CaMKII holoenzyme, the native form of the enzyme (Fig. 1.2A)[117].

The ~600 kDa holoenzyme is composed of 12-14 subunits of several isoforms in varying molecular ratios organized into a two stacked ring-like structure that is formed by the interaction of multiple association domains in a central ring from which an outer ring, consisting of the regulatory and catalytic domains, arises[118,119]. This complex oligomeric structure is essential to warrant accurate decodification by CaMKII of the information conveyed by the amplitude, duration and frequency of intracellular Ca^{2+} transients[120,121].

In mammals, the four known isoforms of CaMKII (α, β, γ, δ) are encoded by separate genes and share approximately 89-93% sequence similarity in their catalytic and regulatory domains[122]. Each isoform ranges in molecular weight from 50 to 70 kDa. The primary difference among the CaMKII isoforms is the variable region, which is a product of alternative splicing, and consists of a series of inserts located between the regulatory and association domain[123]. In some cases, alternative splicing results in the acquisition of particular subcellular targeting sequences[124–126]. Another difference between isoforms is their distribution among tissues. The predominant neuronal isoforms of CaMKII are α and β, whereas the γ and δ isoforms are expressed in diverse tissues including the heart[122].

1.3.1.2 Molecular mechanisms of regulation

CaMKII is subjected to complex regulatory mechanisms that comprise intramolecular interactions modulated by Ca^{2+}/CaM and autophosphorylation, interactions with scaffolding proteins and specific subcellular targeting[127,128]. This intricate regulation ensures signalling fidelity in spite of the broad substrate specificity and high cellular abundance of CaMKII.

The most remarkable feature of CaMKII is its ability to act as molecular switch, being able to retain a ‘‘memory’’ of prior activation by Ca^{2+}/CaM[115]. This ability is

acquired by a two step activation process, consisting of a first activation step upon Ca^{2+}/CaM binding and a subsequent autophosphorylation step (Fig. 1.2B)[117].

Under resting conditions, intracellular Ca^{2+} concentration is low and most CaMKII is held inactive by intramolecular binding of the autoinhibitory sequence to the catalytic domain, which prevents substrate and ATP binding[129,130]. Upon an increase in intracellular Ca^{2+}, CaM binds Ca^{2+} and, subsequently, the regulatory domain of CaMKII, inducing a conformational change that promotes a displacement of the autoinhibitory region from the catalytic domain allowing ATP access to the ATP-binding pocket, thereby disinhibiting the kinase[131]. This allosteric rearrangement of CaMKII exposes a regulatory residue, Thr^{287} (in β, γ and δ isoforms, Thr^{286} in α), that becomes phosphorylated by another kinase domain within the oligomeric holoenzyme kinase[120,132,133].

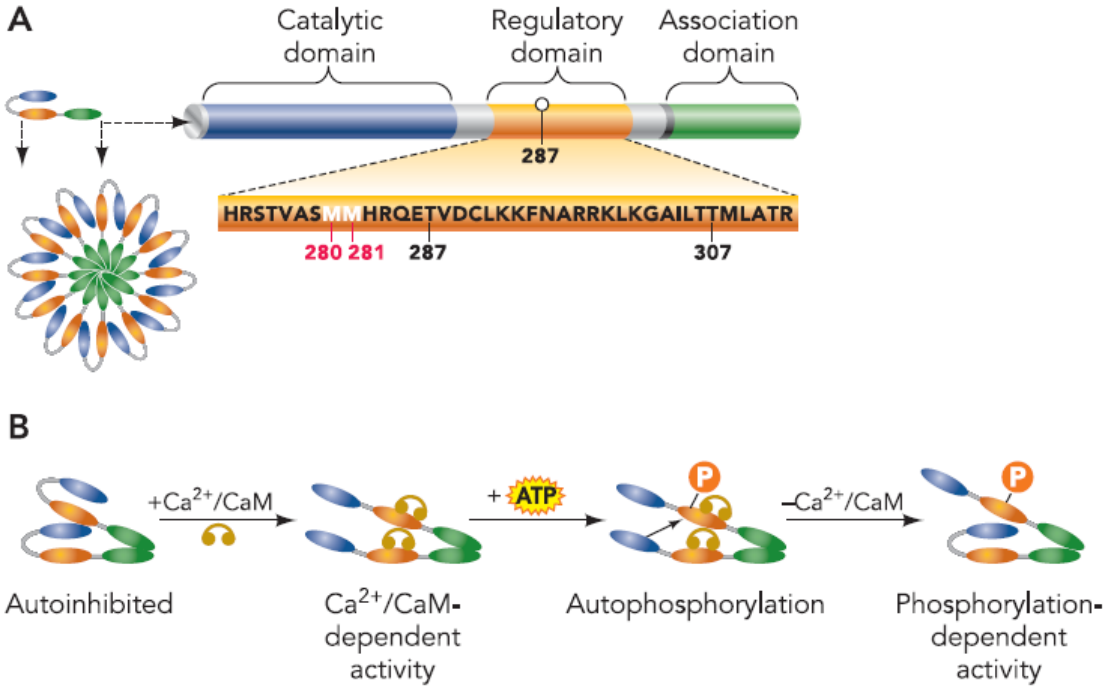

Figure 1.2. Schematic diagram of the CaMKII structure and activation mechanism upon Ca^{2+}/CaM binding.

(A) CaMKII structure. (B) CaMKII activation. See text for details. Taken from Couchonnal and Anderson (2008)[134].

Autophosphorylation at Thr^{287} has two important consequences for CaMKII activity. First, it prevents reassociation of the catalytic and regulatory domains even after dissociation of CaM, thereby rendering the kinase Ca^{2+}/CaM-independent[135,136]. Second, autophosphorylation increases the affinity of CaM-CaMKII binding

substantially (over 1000-fold), a phenomenon termed as “CaM trapping”, which has been suggested to be induced by a local conformational change that allows formation of additional, stabilizing interactions between CaM and Phe[293], Asn[294] and Arg[287] of CaMKII[131,137,138]. Bound Ca^{2+}/CaM eventually dissociates from the kinase when Ca^{2+} concentration reverts to the basal level, thus uncovering additional autophosphorylation sites (Thr[305] and Thr[306]) that were protected by bound CaM[139]. Autophosphorylation at these additional sites prevents subsequent reactivation by Ca^{2+}/CaM, a process termed “CaM capping”[140]. Recently, a novel mechanism for CaMKII activation via oxidation of two methionine residues (Met[281] and Met[282]) located next to the regulatory domain has been further described[141].

1.3.1.3 Subcellular localization

Being a multifunctional kinase, CaMKII is capable of phosphorylating numerous substrates[116]. As CaMKII substrates are distributed in essentially every subcellular compartment, effective targeting is imperative to ensure optimal CaMKII function. Appropriate intracellular targeting is achieved by a combination of activation-dependent and -independent translocation mechanisms that involve interaction with anchoring proteins and organelle localization sequences[142]. Certain CaMKII isoforms possess distinctive segments within the variable region, which result from alternative splicing, that promote specific targeting. That is the case of isoform α_B and δ_B, which bear functional nuclear localization signals, and isoform β, which bears an insert within the association domain that induces cytoskeletal targeting by promoting interaction with F-actin[124–126]. Isoform α-KAP, which lacks the catalytic domain and has a short hydrophobic sequence instead, serves as an integrated anchoring appendage for the CaMKII holoenzyme that tethers coassembled catalytic-competent subunits to the membranes of the endoplasmic reticulum[143]. Furthermore, isoforms with different localization signals can coassemble into the same holoenzyme, whose localization is determined by its isoform composition[125,128].

1.3.2 Ca^{2+}/CaM-dependent protein kinases in *S. cerevisiae*

S. cerevisiae possesses two genes (*CMK1* and *CMK2*) that encode protein kinases with sequence homology and structural organization similar to mammalian CaMKII and whose activity is stimulated by Ca^{2+}/CaM[144,145]. Yeast Ca^{2+}/CaM-dependent kinases Cmk1 and Cmk2 display ~ 41% amino acid sequence identity with mammalian CaMKII and 60% amino acid identity and 90% similarity between each other[145]. The homology

between the catalytic domain of Cmk1 and Cmk2 is particularly high (75.4% amino acid identity), whereas that between their calmodulin binding domains is only 21%[144]. Despite their divergence, both CaM domains contain the basic residues that can be arranged into an amphipathic α-helix to form a canonical CaM-binding site[146]. Consistent with this, Cmk1 and Cmk2 are able to interact with calmodulin[145]. Although both kinases undergo autophosphorylation and show increased *in vitro* kinase activity towards a number of substrates in the presence of Ca^{2+}/CaM, only Cmk2 acquires Ca^{2+}/CaM-independent activity upon autophosphorylation, thus displaying an autoregulatory behaviour most similar to mammalian CaMKII[145,147]. Remarkably, Cmk1 and Cmk2 bear a conserved Thr residue within the putative regulatory region that corresponds to the autophosphorylation site responsible for conferring calmodulin-autonomous activity to mammalian CaM kinase II (Thr^{287}). However, only Cmk2 has the Arg residue situated three positions upstream necessary to configure the core consensus sequence of CaM kinases (RxxT/S)[148].

Unlike their mammalian counterparts, yeast CaM kinases are able to phosphorylate conventional substrates, such as Kemptamide and Myelin Basic Protein (MBP), in the absence of Ca^{2+}/CaM[144]. Another difference between yeast and mammalian CaM kinases is that both yeast kinases lack the carboxy-terminal region that in higher eukaryotes is implicated in subunit assembly[145,149,150]. Accordingly, fractionation studies of yeast CaM kinase preparations indicated that Cmk1 and Cmk2 do not seem to assemble into large oligomers as mammalian CaMKII[151].

The physiological roles of yeast CaM kinases remain largely unknown, as well as the identity of their *in vivo* targets. In early studies, apart from a defect in spore germination observed in cells lacking *CMK2* (Δ*cmk2*), no other defects could be detected in growth, mating efficiency, meiosis or spore formation[144,145]. More recently, Cmk2 has emerged as an important factor for survival in the absence of calcineurin signalling during endoplasmic reticulum (ER) stress[152]. Calcineurin is an evolutionary conserved Ca^{2+}/CaM-activated phosphatase responsible for the regulation of a stress-induced transcriptional program, progression through the cell cycle and Ca^{2+} homeostasis in yeast[153]. Calcineurin-induced gene expression is necessary for cell survival under specific stress conditions such as heat shock, exposure to high concentration of ions (OH^-, Ca^{2+}, Mn^{2+}, and Na^+/Li^+), prolonged incubation with mating pheromone and in situations that compromise cell wall integrity[153]. The activation of calcineurin is also required to promote long-term survival during ER stress[154]. In calcineurin-deficient cells exposed to ER-stress eliciting agents such as miconazole, tunicamycin, or dithiothreitol, Cmk2 seems to delay cell death by preventing the accumulation of reactive oxygen species (ROS)[152]. The underlying mechanism of

Cmk2 action in this process is not completely understood; however, while being independent of calcineurin, it has been suggested that it may operate in concert with calcineurin on a common point[152].

Calcineurin and yeast CaM kinases function in separate but overlapping pathways involved in the maintenance of cell survival during prolonged incubation with mating pheromones[155]. In *S. cerevisiae*, exposure to mating pheromones during sexual conjugation elicits transcriptional and morphological changes that ultimately result in a reversible arrest at the G_1-phase of the cell cycle[156]. To recover from this pheromone-induced arrest, cells must be able to stimulate Ca^{2+} uptake, which is necessary for a rise in cytoplasmic Ca^{2+} that, in turn, activates the calcineurin pathway required for survival[157]. Like calcineurin, CaM kinases also sustain cell survival after pheromone-induced arrest, as simultaneous loss of *CMK1* and *CMK2* (Δ*cmk1*Δ*cmk2*) results in decreased cell viability after exposure to the pheromone[155]. Since the individual effects of Cmk1 and Cmk2 actions were not explicitly tested, it remains unknown which one of them is in fact responsible for sustaining cell survival or whether both kinases act in redundant pathways implicated in the recovery from pheromone-induced arrest.

Interestingly, the expression of *CMK2*, and not of the *CMK1* gene, is induced in a Ca^{2+}/calcineurin-dependent manner[158]. This fact, together with the distinct ability to be converted to a Ca^{2+}/CaM-independent state and their involvement in apparently different processes, suggests that Cmk1 and Cmk2 may be differently regulated by Ca^{2+}/CaM and may function in independent pathways.

1.4 pH homeostasis in yeast

Almost every biological process is pH dependent. Changes in the pH inside the cell affect the charge of metabolites, the solubility of essential elements and enzyme activity. It also influences the electrostatic interactions between charged groups on the surface of biomolecules, thus altering their function and conformational stability (reviewed in [159,160]). Consequently, intracellular pH is an important physiological parameter that must be strictly regulated in all cellular systems.

In the budding yeast, the maintenance of a cytosolic pH around neutrality mainly relies on the activity of the P2-type plasma membrane H^+-ATPase Pma1, which hydrolyzes ATP to pump protons out of the cell[161,162]. This activity is crucial for the generation of the electrochemical proton gradient that drives the uptake of nutrients and cations from the medium and, in consequence, essential for yeast survival[161,163,164]. Another key contributor to cytosolic pH homeostasis is the vacuolar membrane proton pump (V-ATPase), which extrudes protons out of the cytosol to the interior of the

vacuole and further organelles of the secretory pathway[165]. In addition, cation/H^+ exchangers such as the Na^+/H^+ antiporter Nha1 and K^+ transporters Trk1 and Trk2 also play a role in cytosolic pH homeostasis[166,167].

1.4.1 Effects of high pH stress on the yeast physiology

Alkalinization of the external milieu (*i.e.,* to pH>7.5) disrupts the established proton gradient across the plasma membrane required for nutrient acquisition, constituting a stress situation for yeast[161,168]. It interferes with the maintenance of intracellular pH homeostasis and decreases cell proliferation, ultimately leading to viability loss[169,170].

The large set of genes that are induced (~ 400) or required for growth (~ 200) under high pH stress indicates that this stress exerts widespread effects on the yeast physiology[171–175]. For instance, high pH seems to elicit a situation of phosphate starvation, as inferred by the increased expression of genes encoding phosphate transporters *e.g.,* Pho84 and Pho89, and the alkaline hypersensitivity exhibited by mutants lacking genes involved the adaptive transcriptional response *e.g.*, Pho4, Pho81, and Pho85[175,176]. Similarly, the induction upon high pH stress of genes implicated in glucose transport and metabolism implies that yeast cells face glucose deprivation[174,177]. This is further supported by the finding that the AMP-activated protein kinase (AMPK) Snf1, which is necessary for the adaptation of yeast to glucose limitation, is activated by and required for growth under high pH stress[178,179]. The expression of genes implicated in the uptake and metabolism of iron and copper is also induced, which has been suggested to be required to counterbalance the reduced solubility of these essential metals at high pH[175,176]. It has been further proposed that high pH causes oxidative stress, as it leads to the generation of reactive oxygen species (ROS) and the induction of a set of genes involved in the oxidative stress response[175,176]. Consistently, mutants lacking superoxide dismutases Sod1 and Sod2, which play a critical role in oxygen radical detoxification, display alkaline sensitivity[180,181].

The activity of the V-ATPase becomes essential for survival under pH stress conditions[172,182]. Mutants lacking genes encoding for V-ATPase subunits or assembly factors (*vma* mutants) are impaired in organelle acidification[183], which, in turn, is required for endocytosis, intracellular protein sorting, processing and turnover as well as metabolite storage and osmoregulation (reviewed in [184–186]). Consistent with the need of a functional V-ATPase for growth at high pH, a number of mutations with repercussions on V-ATPase assembly, transport and regulation have been observed to result in enhanced sensitivity to high pH stress[172,187,188].

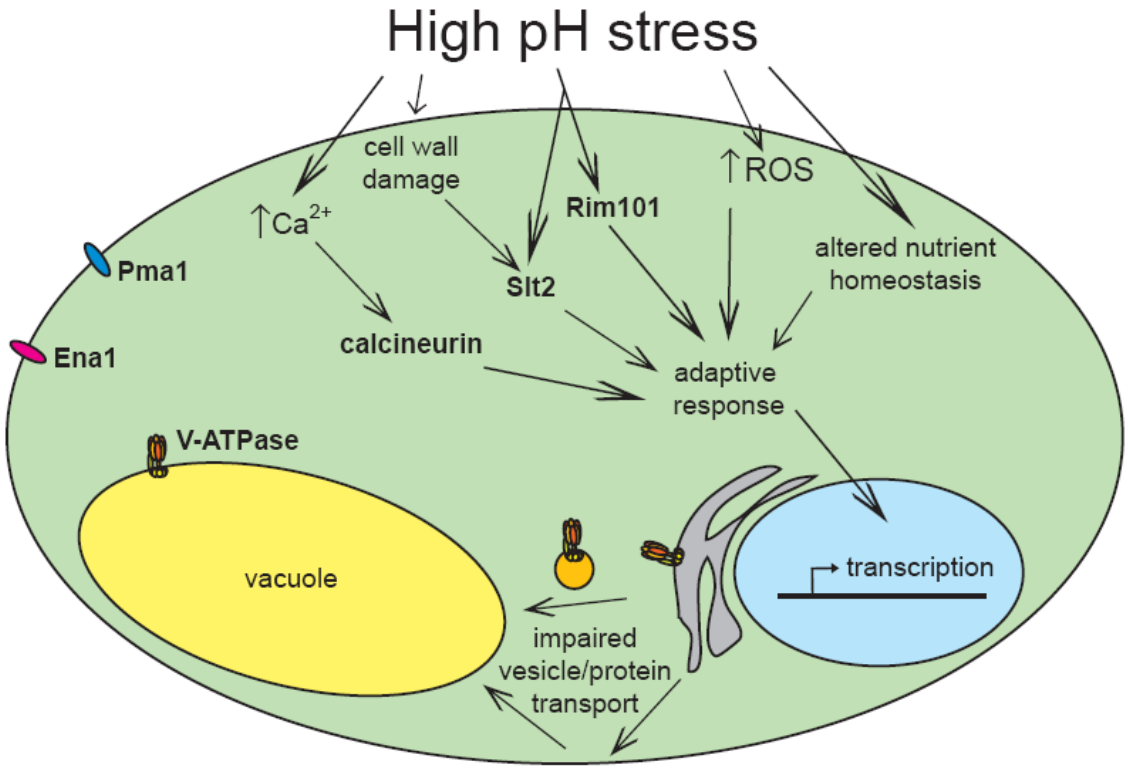

Figure 1.3. Major effects of high pH stress on the physiology of *S. cerevisiae* and known adaptive response signalling pathways.

See text for details.

Yeast cells undergo extensive transcriptional remodelling to withstand alkaline stress. So far, at least three signalling pathways have been identified to be implicated in the adaptive response to high pH stress; the Rim101, the Slt2 MAP kinase and the calcineurin pathway (reviewed in [189]). Activation of the transcriptional repressor Rim101 upon high pH stress leads to an increase in the expression of the plasma membrane Na^+-ATPase Ena1/Pmr2 and Vma4, a subunit of the vacuolar proton pump V-ATPase that is required for multimer assembly[190–192]. The Slt2 MAP kinase pathway is crucial for cell wall biogenesis and for the maintenance of cell wall integrity (CWI) in the face of damaging insults (reviewed in [193]). Recently, exposure to alkaline pH has been shown to specifically activate this pathway[177]. As this activation was mediated by the cell wall stress sensor Wsc1, it has been suggested that alkaline stress causes cell wall damage[177]. In response to high pH, cells become depolarized and, in turn, the Mid1-Cch1 Ca^{2+}-channel rapidly activated, triggering Ca^{2+} entry and concomitant activation of the Ca^{2+}-dependent phosphatase calcineurin[174]. Activated calcineurin dephosphorylates Crz1, a transcription factor that induces a genetic program required for the endurance of high pH stress[174,176].

In summary, a wide variety of processes are involved in the optimal adaptation of yeast to external alkalinization (Fig. 1.3). The integrity of housekeeping processes such as vesicle transport, cell wall and vacuolar organization, phosphate and glucose metabolism as well as metal cation homeostasis is crucial to endure high pH stress[171,180,189]. In addition, the activation of the Slt2 MAP kinase, calcineurin, Snf1 and Rim101 pathways play an important role in the acquisition of high pH tolerance. Yet, despite its obvious importance on the yeast physiology, there is still limited information concerning the extent and general features of the mechanisms governing the acquisition of high pH tolerance.

1.5 Aims

Given their implication on vital cellular processes, the LAMMER kinases are emerging as a potential targets for the treatment of cancer, neurodegenerative and metabolic disorders[42,58,66,107,108,194–196]. Hence, understanding the roles of Kns1 in the budding yeast is key to the use of this genetically tractable organism as a model system for the future development of therapeutic strategies targeting LAMMER kinases.

The function of Kns1 has not been yet investigated in the cellular context. Most of the data available for Kns1 has been obtained within the scope of large-scale surveys. It is known that Kns1 is not essential for viability under standard conditions; however, little is known about the conditions that may render Kns1 indispensable. Analysis of Kns1 localization has yielded thus far inconclusive results[77,78]. Biochemical characterization of Kns1 has been precluded by the difficulty in purifying the full-length kinase from *E. coli.* Hence, all data regarding Kns1 autocatalytic activity derive from analysis of the truncated protein, which was shown to undergo autophosphorylation at Ser, Thr and Tyr residues[33]. Yet, the exact sites of phosphorylation, their physiological significance and evolutionary conservation as well as whether dual-specificity extends to exogenous substrates remain obscure. High-throughput screening for potential kinase target proteins identified five *in vitro* substrates for Kns1 but none of them have been further validated[171]. Furthermore, it is an open question whether Kns1 shares functions with its counterparts.

The present study aimed to unravel cellular roles and regulatory mechanisms of Kns1 in the budding yeast. To this end, the following specific objectives were established:

- To analyse the effects that *KNS1* gene deletion causes on cell fitness under environmental stress conditions.
- To examine the intracellular localization of Kns1 in living cells by fluorescence microscopy.
- To optimize the recombinant expression and purification of full-length and catalytically competent Kns1 for use in biochemical studies.
- To identify the *in vitro* autophosphorylation sites on Kns1 by mass spectrometry and investigate the role of relevant sites on Kns1 function by site-directed mutagenesis.
- To validate *in vitro* candidate substrates for Kns1 and assess their potential physiological relevance. As several Kns1 homologues have been implicated in

signal transducing pathways activated by extracellular stimuli, I speculated that Kns1 may serve similar roles in yeast. Among the *in vitro* candidate substrates reported for Kns1, the Ca^{2+}/CaM-dependent kinase Cmk2 was the candidate with the highest potential significance owing to its suggested roles in stress response pathways[152,155,158]. Therefore, the secondary aim of this thesis was to evaluate the potential relevance of Cmk2 as Kns1 target. For this purpose, I set out to:

- carry out the validation of Cmk2 phosphorylation by Kns1 *in vitro,*
- identify potential Kns1 target site(s) on Cmk2,
- analyse the genetic relationship between *CMK2* and *KNS1* genes,
- assess whether Cmk2 and Kns1 physically interact *in vivo*,
- gain insights into the function, subcellular localization and regulation of Cmk2 and examine whether Kns1 influences any of these aspects.

2. Materials and methods

2.1. Materials

2.1.1 Strains

2.2.1.1 Bacteria strains

Table 2.1: Bacteria strains used in this study.

Name	Genotype	Source
XL1-Blue™	*endA1 gyrA96(nalR) thi-1 recA1 relA1 lac glnV44 F'[::Tn10 proAB+ lacIq Δ(lacZ)M15] hsdR17(rK- mK+)*	Stratagene
DH5α™	F⁻ Φ80*lac*ZΔM15 Δ(*lac*ZYA-*arg*F) U169 *rec*A1 *end*A1 *hsd*R17 (rK–, mK+) *pho*A *sup*E44 λ– *thi*-1 *gyr*A96 *rel*A1	Invitrogen
DB3.1™	F⁻ *gyr*A462 *end*A1 Δ(sr1-*rec*A) *mcr*B *mrr hsd*S20(rB–, mB–) *sup*E44 *ara*-14 *gal*K2 *lac*Y1 *pro*A2 *rps*L20(SmR) *xyl*-5 λ– *leu mtl*1	Invitrogen
Rossetta™ 2	F⁻ *ompT hsdS*$_B$(r_B^- m_B^-) *gal dcm* pRARE2 (Cam^R)	Novagen

2.2.1.2 Yeast strains

The *Saccharomyces cerevisiae* (hereafter termed yeast) S288C-derived strain DF5 (Table 2.2) was used throughout this work, unless indicated otherwise.

Table 2.2: Yeast strains used in this study.

Name	Genotype	Source
BY4741	*s288c; MATa, his3Δ1, leu2Δ0, met15Δ0, ura3Δ0*	C.B. Brachmann[197]
DF5	*a/α, trp1-1(am)/trp1-1(am), his3-Δ200/his3-Δ200, ura3-52/ura3-52, lys2-802/lys2-801, leu2-3,-112/leu2-3,-112*	D. Finley[198]
KL1	*MATa, his3Δ200, leu2-3,-112, ura3-1, trp1Δ1, ade2-1, can1-100, Kan- PGAL1-GST-prp8Δaa1-78, otherwise as BMA38a*	J.D. Beggs[199]
PJ69-4α	*W303; MATa, trp1-901, leu2-3,112, ura3-52, his3-200,gal4Δ, gal80Δ LYS2::GAL1-HIS3, GAL2-ADE3, met2::GAL7-lacZ*	Phillip James[200]
sUB62	*s288c; MATa, ura3–52, his3Δ-200, trp1–1, leu2–3,112 lys2–801*	G.A. Dittmar[198]
Y01507	*BY4741; Mat a; his3D1; leu2D0; met15D0; ura3D0; YLL019c::kanMX4*	Deletion consortium strain
Y16473	*BY4742; Mat α; his3Δ1; leu2Δ0; lys2Δ0; ura3Δ0; YOL016c::kanMX4*	Euroscarf
yAS005	*MATa, kns1Δ::natMX4*	This study

yBM87	*yWO1; MATα vps23::HIS3*	Birgit Meusser
yNM195	*MATa, vma1Δ::kanMX4*	This study
yNM414	*MATa, cmk2::kanMX4*	This study
yNM454	*MATa, cmk2:: KANMX4, kns1Δ::natMX4*	This study
yNM459	*MATa, natNT2::Cup1-1::GFP-KNS1*	This study
yNM555	*MATa, natNT2::Cup1-1::GFP-CMK2*	This study

*All yeast strains created during the course of this study were constructed by me except for yAS5, which was constructed by Andreas Schlundt during his practical placement in the laboratory.

2.1.2 Plasmids

Table 2.3: Bacterial plasmids used in this study.

Name	Description	Selectable marker	Source
pDESTco	*6xHIS attR1 CmR ccdB attR2*	AmpR CmR	Scheich et al. 2007[201]
pDONR221	*attP1 CmR ccdB attP2*	KanR CmR	Invitrogen
pGEX-4T-1	*GST*	AmpR	Amersham Pharmacia
pNM11	(pGEX-4T-1) *GST KNS1*	AmpR	This study
pNM14	(pDONR221) *attL1 KNS1 attL2*	KanR	This study
pNM33	(pDONR221) *attL1 KNS1^{D440A} attL2*	KanR	This study
pNM34	(pDONR221) *attL1 KNS1^{T562A} attL2*	KanR	This study
pNM37	(pGEX-4T-1) *GST KNS1^{D440A}*	AmpR	This study
pNM38	(pDESTco) *6xHIS attB1 CMK2 attB2*	AmpR	This study
pNM39	(pDESTco) *6xHIS attB1 CMK2^{S328E} attB2*	AmpR	This study
pNM43	(pDESTco) *6xHIS attB1 CMK2^{T406A} attB2*	AmpR	This study
pNM44	(pDESTco) *6xHIS attB1 CMK2^{T406D} attB2*	AmpR	This study
pNM45	(pDESTco) *6xHIS attB1 CMK2^{D171A} attB2*	AmpR	This study
pNM47	(pDONR221) *attL1 CMK2 attL2*	KanR	This study
pNM50	(pDONR221) *attL1 CMK2^{D171A} attL2*	KanR	This study
pNM54	(pGEX-4T-1) *GST-KNS1^{T562A}*	AmpR	This study
pNM55	(pDESTco) *6xHIS attB1 CMK2^{Y47F} attB2*	AmpR	This study
pNM56	(pDESTco) *6xHIS attB1 CMK2^{T52A} attB2*	AmpR	This study
pNM58	(pDESTco) *6xHIS attB1 CMK2^{T69A} attB2*	AmpR	This study
pNM59	(pDESTco) *6xHIS attB1 CMK2^{S328A} attB2*	AmpR	This study

pNM60	(pDESTco) *6xHIS attB1 CMK2^{S379A} attB2*	AmpR	This study
pNM75	(pDESTco) *6xHIS attB1 CMK2^{T316A} attB2*	AmpR	This study
pNM76	(pDESTco) *6xHIS attB1 CMK2^{T316E} attB2*	AmpR	This study
pNM77	(pDESTco) *6xHIS attB1 CMK2^{S379E} attB2*	AmpR	This study
pNM78	(pDESTco) *6xHIS attB1 CMK2^{Y47D} attB2*	AmpR	This study
pNM79	(pDESTco) *6xHIS attB1 CMK2^{T52D} attB2*	AmpR	This study
pNM80	(pDESTco) *6xHIS attB1 CMK2^{T69D} attB2*	AmpR	This study
pNM85	(pDONR221) *attL1 CMK2^{Y47F} attL2*	KanR	This study
pNM86	(pDONR221) *attL1 CMK2^{T52A} attL2*	KanR	This study
pNM88	(pDONR221) *attL1 CMK2^{T69A} attL2*	KanR	This study
pNM89	(pDONR221) *attL1 CMK2^{S328A} attL2*	KanR	This study
pNM90	(pDONR221) *attL1 CMK2^{S379A} attL2*	KanR	This study
pNM91	(pDONR221) *attL1 CMK2^{T316A} attL2*	KanR	This study
pNM92	(pDONR221) *attL1 CMK2^{T316E} attL2*	KanR	This study
pNM93	(pDONR221) *attL1 CMK2^{S379E} attL2*	KanR	This study
pNM94	(pDONR221) *attL1 CMK2^{Y47D} attL2*	KanR	This study
pNM95	(pDONR221) *attL1 CMK2^{T52D} attL2*	KanR	This study
pNM96	(pDONR221) *attL1 CMK2^{T69D} attL2*	KanR	This study
pNM98	(pDONR221) *attL1 CMK2^{T406A} attL2*	KanR	This study
pNM99	(pDONR221) *attL1 CMK2^{T406D} attL2*	KanR	This study
pNM100	(pDONR221) *attL1 CMK2^{S328E} attL2*	KanR	This study
pYM-N1	*natNT2 CUP1-1 yeGFP*	AmpR	Janke et al. 2004[202]

Table 2.4: Yeast plasmids used in this study

Name	Description	Selectable marker	Reference/Source
Type	**2µm**		
pGO45	*P_{ADH} GFP-CPS*	AmpR URA3	S.D. Emr[203]
pMD299	(pSV52) *P_{GAL4} EGFP attR1 CmR ccdB attR2*	AmpR CmR TRP1	M. Dahlmann
pNM18	(pSV52) *P_{GAL4} 10xHIS-HA attB1 CMK2^{T129A} attB2*	AmpR TRP1	This study
pNM36	(pNM67) *P_{CUP1-1} EGFP attB1 CMK2^{D171A} attB2*	AmpR TRP1	This study
pNM53	(pNM67) *P_{CUP1-1} EGFP attB1 KNS1^{D440A} attB2*	AmpR TRP1	This study
pNM67	(pMD299) *P_{CUP1-1} EGFP attR1 CmR ccdB attR2*	AmpR CmR TRP1	This study
pNM73	(pNM67) *P_{CUP1-1} EGFP attB1 CMK2 attB2*	AmpR TRP1	This study
pNM74	(pNM67) *P_{CUP1-1} EGFP attB1 KNS1 attB2*	AmpR TRP1	This study
pNM101	(pNM67) *P_{CUP1-1} EGFP attB1 CMK2^{Y47F} attB2*	AmpR TRP1	This study

pNM102	(pNM67) P_{CUP1-1} *EGFP attB1 CMK2*^{T52A} *attB2*	AmpR TRP1	This study
pNM110	(pNM67) P_{CUP1-1} *EGFP attB1 CMK2*^{S328A} *attB2*	AmpR TRP1	This study
pNM111	(pNM67) P_{CUP1-1} *EGFP attB1 CMK2*^{S379A} *attB2*	AmpR TRP1	This study
pNM112	(pNM67) P_{CUP1-1} *EGFP attB1 CMK2*^{T316A} *attB2*	AmpR TRP1	This study
pNM113	(pNM67) P_{CUP1-1} *EGFP attB1 CMK2*^{T406A} *attB2*	AmpR TRP1	This study
pNM116	(pNM67) P_{CUP1-1} *EGFP attB1 CMK2*^{T69A} *attB2*	AmpR TRP1	This study
pNM121	(pNM67) P_{CUP1-1} *EGFP attB1 KNS1*^{T562A} *attB2*	AmpR TRP1	This study
pNM125	(pNM67) P_{CUP1-1} *EGFP attB1 CMK2*^{Y47D} *attB2*	AmpR TRP1	This study
pNM126	(pNM67) P_{CUP1-1} *EGFP attB1 CMK2*^{T52D} *attB2*	AmpR TRP1	This study
pNM127	(pNM67) P_{CUP1-1} *EGFP attB1 CMK2*^{T69D} *attB2*	AmpR TRP1	This study
pNM128	(pNM67) P_{CUP1-1} *EGFP attB1 CMK2*^{T316E} *attB2*	AmpR TRP1	This study
pNM129	(pNM67) P_{CUP1-1} *EGFP attB1 CMK2*^{S328E} *attB2*	AmpR TRP1	This study
pNM130	(pNM67) P_{CUP1-1} *EGFP attB1 CMK2*^{S379E} *attB2*	AmpR TRP1	This study
pNM131	(pNM67) P_{CUP1-1} *EGFP attB1 CMK2*^{T406D} *attB2*	AmpR TRP1	This study
pSV52	P_{GAL4} *10xHIS-HA*	AmpR CmR TRP1	Gheysen et al. 1982[204]
Type	**CEN ARS**		
pMD302	(pOAD1) P_{ADH1} *GAL4(AD) attR1 CmR ccdB attR2*	AmpR CmR LEU2	M. Dahlmann
pMD303	(pOBD2) P_{ADH1} *GAL4(BD) attR1 CmR ccdB attR2*	AmpR CmR TRP1	M. Dahlmann
pNM61	(pRS414) P_{CMK2} *CMK2*	AmpR TRP1	This study
pNM63	(pNM61) P_{CMK2} *EGFP attR1 CmR ccdB attR2*	AmpR CmR TRP1	This study
pNM65	(pNM63) P_{CMK2} *EGFP attB1 CMK2 attB2*	AmpR TRP1	This study
pNM103	(pMD302) P_{ADH1} *GAL4(AD) attB1 KNS1 attB2*	AmpR LEU2	This study
pNM104	(pMD302) P_{ADH1} *GAL4(AD) attB1 CMK2 attB2*	AmpR LEU2	This study
pNM105	(pMD303) P_{ADH1} *GAL4(BD) attB1 KNS1 attB2*	AmpR TRP1	This study
pNM106	(pMD303) P_{ADH1} *GAL4(BD) attB1 CMK2 attB2*	AmpR TRP1	This study
pRS414		AmpR TRP1	Sikorski et al. 1989[205]
pMR29	(pOBD2) P_{ADH1} *GAL4(BD) attB1 SNU66 attB2*	AmpR TRP1	Hyun-Mi Ryu
pGD240	(pOAD1) P_{ADH1} *GAL4(AD) attB1 HUB1 attB2*	AmpR LEU2	G. Dittmar
pGD252	*attB1 KNS1 attB2*	AmpR TRP1	G. Dittmar
pGD253	*attB1 CMK2 attB2*	AmpR TRP1	G. Dittmar

2.1.3 Oligonucleotides

Table 2.5: Oligonucleotides used in this study

Oligo name	Sequence	Purpose
Kan&His	TGGGCCTCCATGTCGCTGG	Control primer for kan & his tagging vectors from Schiebel set, reverse (rev).
oGD70	GTCGTCAAGAGTGGTACCCATGG	Control primer binds to ATG of *NAT* gene (460 bp from p-tef), rev.
oMD135	CCCGGATCCATGTCACAGAATATTCAAATTGGC	BamHI *KNS1* cloning, forward (fwd).
oMD136	CCCGGGCCCCTATCCTTGGGTATTATTATAAGTTGC	XmaI/SmaI *KNS1* cloning, rev.
oMD141	GAAGATTTAGCACAACAAAGACTAATC	*KNS1* k.o. check 80 bp upstream of ATG, fwd.
oMD175	ATGGACCCACATAATCCAATTG	RT-PCR, binds upstream of *ARP2* intron; 200bp/323bp
oMD176	AGATAAGAGCGAACTTCACTTGC	RT-PCR, binds downstream of *ARP2* intron; 200bp/323bp
oMD177	GAAAATTTACTGAATTAACAATGGATTCTG	RT-PCR, binds upstream of *ACT1* intron; 200bp/508bp
oMD178	GGATTGAGCTTCATCACCAAC	RT-PCR, binds downstream of *ACT1* intron; 200bp/508bp
oMD179	ACAATGAGAGAAGTTATTAGTATTAATG	RT-PCR, binds upstream of *TUB1* intron; 200bp/316bp
oMD180	GCCCTTGGAACGAACTTACC	RT-PCR, binds downstream of *TUB1* intron; 200bp/316bp
oNM62	ACGCATACTGCTCTTCTTCATTATTGCTTTATCTTCCGCG TACCTTAGTTATGCGTACGCTGCAGGTCGAC	*KNS1* N-terminal tagging, fwd.
oNM63	TTCATATTTGCTCTTGAACGTTTTCTAGTGCCAATTTGAAT ATTCTGTGACATCGATGAATTCTCTGTCG	*KNS1* N-terminal tagging, rev.
oNM76	CGTCACCTTTTCTTCTATCACATCGCCAATATAAATATAG ACACCAAAAATGCGTACGCTGCAGGTCGAC	*CMK2* N-terminal tagging, fwd.
oNM77	GGACATCTACATGAAATTCAGAATTTATGACCTCTGACTC CTTGGGCATCGATGAATTCTCTGTCG	*CMK2* N-terminal tagging, rev.
oNM78	GTGTGCAAGGTATACAAAGCAGAATG	RT-PCR, binds upstream of *VMA10* intron; 273bp/434bp
oNM79	CTCAGCTAATTCACCTTGCACAC	RT-PCR, binds downstream of *VMA10* intron; 273bp/434bp
oNM80	CAATTATACGGACACGATGAAG	RT-PCR, binds upstream of *SEC27* intron; 345bp/544bp
oNM81	GTTGGATGTACAGCAATGGAACG	RT-PCR, binds downstream of *SEC27* intron; 345bp/544bp
oNM82	GTCAAGGACTGCGGAACTAC	RT-PCR, binds upstream of *SNC1* intron; 258bp/370bp
oNM83	CAATGGGGACGATGATTACAAC	RT-PCR, binds downstream of *SNC1* intron; 258bp/370bp
oNM86	CCAGTCGTTGAGCATCATATG	*CMK2* k.o., binds 279 bp upstream of *ATG*, fwd.
oNM87	CTGAGTGAGGAGAATACATTG	*CMK2* k.o., binds 303 bp downstream of stop codon, rev
oNM94	ACCATCATGCCATGGGATACCCTTATGATGTTCCAGATTA CGCTTCTTTGACAAGTTTGTACAAAAAAGCAGGCTCTATG CCCAAGGAGTCAGAGGT	Gap repair in pSV52 (BamHI, HindIII) *CMK2*, fwd.
oNM95	TGAGCGGATAACAATTTCACACAGGAAACAGCTATGACC ATGATTACGCCACCACTTTGTACAAGAAAGCTGGGTCTTA GTCTTCTGACTTCGACT	Gap repair in pSV52 (BamHI, HindIII) *CMK2*, rev.
oNM96	ACCATCATGCCATGGGATACCCTTATGATGTTCCAGATTA CGCTTCTTTGACAAGTTTGTACAAAAAAGCAGGCTCTATG TCACAGAATATTCAAATTG	Gap repair in pSV52 (BamHI, HindIII) Kns1, fwd.
oNM97	TGAGCGGATAACAATTTCACACAGGAAACAGCTATGACC ATGATTACGCCACCACTTTGTACAAGAAAGCTGGGTCCT ATCCTTGGGTATTATTATAAG	Gap repair in pSV52 (BamHI, HindIII) Kns1, rev.
oNM146	CCT TTT CTT CTA TCA CAT CGC CAA TAT AAA TAT AGA CAC CAA AAC	Cloning pNM63, fwd.

oNM147	TTT TGA GCT CCC ATT ACC GAC ATT TGG GCG	Cloning pNM67, fwd.
oNM148	CCC CAG ATC TCA GTT TGT TTT TCT TAA TAT C	Cloning pNM67, fwd.
oNM153	CTT CAA AGA GAG TTG AAG CTA GCA ATA TTT TAC CAG ACG	SDM fwd, Cmk2 insert mutation T316A, RE site NheI.
oNM154	CGT CTG GTA AAA TAT TGC TAG CTT CAA CTC TCT TTG AAG	SDM rev, Cmk2 insert mutation T316A, RE site NheI.
oNM155	GAG AGT TGA AGA TAG TAA TAT TTT ACC AGA CGT CAA GAA AGG G	SDM fwd, Cmk2 insert mutation T316D, RE site AatII.
oNM156	CCC TTT CTT GAC GTC TGG TAA AAT ATT ACT ATC TTC AAC TCT C	SDM rev, Cmk2 insert mutation T316D, RE site AatII.
oNM157	CGG CGT CAC ACA TGA GCT CGA TGA TTT ACG TC	SDM fwd, Cmk2 insert mutation S379E, RE site SacI.
oNM158	GAC GTA AAT CAT CGA GCT CAT GTG TGA CGC CG	SDM rev, Cmk2 insert mutation S379E, RE site SacI.
oNM159	GTC AAC AGG ACT AAT GAT ATC TTC GGT CGA ACA CTG	SDM fwd, Cmk2 insert mutation Y47D, RE site EcoRV.
oNM160	CAG TGT TCG ACC GAA GAT ATC ATT AGT CCT GTT GAC	SDM rev, Cmk2 insert mutation Y47D, RE site EcoRV.
oNM161	TAT ATT TTC GGT CGA GAC CTT GGT GCC GGT TCC TTC	SDM fwd, Cmk2 insert mutation T52A, RE site StyI.
oNM162	GAA GGA ACC GGC ACC AAG GTC TCG ACC GAA AAT ATA	SDM rev, Cmk2 insert mutation T52A, RE site StyI.
oNM163	GAG ACA AGC CAG AAA GCT TTC CGA TAA TGA AGA TGT TGC	SDM fwd, Cmk2 insert mutation T69D, RE site HindII.
oNM164	GCA ACA TCT TCA TTA TCG GAA AGC TTT CTG GCT TGT CTC	SDM rev, Cmk2 insert mutation T69D, RE site HindII.
oNM166	GAC GTT AAG AAA GGG TTT GAG CTC CGT AAG AAA TTA CGT GAC G	SDM fwd, Cmk2 insert mutation S328E, RE sites SacI/EcoRV.
oNM167	CGT CAC GTA ATT TCT TAC GGA GCT CAA ACC CTT TCT TAA CGT C	SDM rev, Cmk2 insert mutation S328E, RE sites SacI/EcoRV.
oNM168	GAA ATT GAA GTC TGC CTT GGC AAA GGA TGC CTT TGT TC	SDM fwd, Cmk2 insert mutation T406A, RE site StyI
oNM169	GAA CAA AGG CAT CCT TTG CCA AGG CAG ACT TCA ATT TC	SDM rev, Cmk2 insert mutation T406A, RE site StyI
oNM170	GAA ATT GAA GTC TGC CTT GGA TAA GGA TGC CTT TGT TC	SDM fwd, Cmk2 insert mutation T406D, RE site StyI
oNM171	GAA CAA AGG CAT CCT TAT CCA AGG CAG ACT TCA ATT TC	SDM rev, Cmk2 insert mutation T406D, RE site StyI

2.1.4 Antibodies

Table 2.6: Antibodies used in this study

Antibody	Source
Rabbit Peroxidase anti-Peroxidase soluble complex antibody (PAP)	Sigma Aldrich
Affinity-purified mouse monoclonal (IgG2a) anti-GFP antibody (JL-8)	BD Livingcolors
Donkey anti-Rabbit IgG (H+L) peroxidase-conjugated, polyclonal	Jackson Immuno Research

Donkey anti-Goat IgG (H+L) peroxidase-conjugated, polyclonal	Jackson Immuno Research
Mouse anti-Pgk1, monoclonal antibody	Sigma
Mouse anti-Pentahistidine, monoclonal antibody	Qiagen
Goat anti-Glutathione-S-Transferase (GST) antibody, polyclonal antibody	GE life sciences

2.1.5 Proteins

Table 2.7: Proteins used in this study

Protein	Description	Source
Bovine serum albumin (Fraction V)	66 kDa	Sigma-Aldrich
Myelin basic protein	18.14 KDa	Sigma-Aldrich
Calmodulin	16.8 KDa	Sigma-Aldrich

2.1.6 Enzymes

- Taq DNA Polymerase (New England BioLabs, Inc.)
- Expand™ Long Template PCR System (Roche)
- *PfuTurbo*® DNA-polymerase (Stratagene)
- Phusion™ High-Fidelity DNA Polymerase (New England BioLabs, Inc.)
- T4 DNA Ligase (New England BioLabs, Inc.)
- Zymolyase-20T from *Arthrobacter luteus* (MP Biomedicals; Inc.)
- OneStep RT-PCR Enzyme Mix, contains Omniscript Reverse Transcriptase, Sensiscript Reverse Transcriptase, and HotStarTaq DNA Polymerase (QIAGEN)
- Restriction endonucleases (New England BioLabs, Inc.)

2.1.7 Chemicals and other products

Radioactive isotopes

[γ^{32}-P]-ATP Redivue™ (specific activity 3000 Ci/mmol, 10 µCi/µl) was purchased from GE healthcare.

Chemicals

Chemicals were purchased from Bio-Rad, Becton and Dickinson, Invitrogen, Merck, Roche, PAA industrials, Invitrogen, Fermentas, Roth, Serva, Roche, GE Healthcare, Calbiochem, Amersham, Gibco, Fluka or Sigma-Aldrich.

Table 2.8: Chemicals used in this study

Acrylamide/bisacrylamide solution (37.5:1)
Adenine
Agarose
Ammoniumpersulfate (APS)
Ampicillin
Arginine
Bacto Pepton
Bacto Agar
Bromphenol blue
Chloramphenicol
Chloroform
Complete mini™ EDTA-free protease inhibitor cocktail tablets
Cycloheximide
Diethylpyrocarbonate (DEPC)
Dimethyl sulfoxide (DMSO)
Dithiothreitol (DTT)
DNA ladder (O'GeneRuler™)
DNTPs
Ethanol absolute
Ethylenediaminetetraacetic acid (EDTA)
Ethidium bromide
Ficoll
Geniticin (G418)
Glucose
Glycerine
Glycine (MP Biochemicals)
Herring sperm DNA Skimmed dry milk
Histidine
Hoechst 33258
Hydrochloric acid (HCl)
Hydroxyethyl piperazineethanesulfonic acid (HEPES)
IgG Sepharose™ 6 Fast Flow
Isoleucine
Isopropanol
Isopropyl β-D-1-thiogalactopyranoside (IPTG)
Kanamycin
Leucine
Lithium acetate
Lysine
2-Mercaptoethanol
Methanol absolute
Methionine

Nourseothricin (Werner BioAgents)

Orange G

PageRuler^{TM} Prestained protein ladder (10-170 KDa)

PEG (Polyethylene glycol)

Phenol:chloroform:isoamyl alcohol (25:24:1)

Phenylalanine

PMSF (phenylmethanesulphonylfluoride)

Sodium azide (NaN_3)

Quinacrine dihydrochloride

Sodium chloride (NaCl)

Sodium dodecyl sulfate (SDS)

Sodium hydroxide (NaOH)

Sucrose

Tetramethylethylenediamine (TEMED)

Texas Red®-X phalloidin

Threonine

Tris-Base (tris(hydroxymethyl)aminomethane)

Triton®X-100

Tryptophane

Tween®-20

Uracil

Urea

Yeast Extract

Yeast Nitrogen Base (YNB)

2.1.8 Growth media

2.1.8.1 Bacteria growth media

E.coli strains used for plasmid amplification were cultured according to standard procedures at 37°C in Luria Bertani (LB) medium supplemented, if required, with the appropriate antibiotic (Table 2.9)[206].

Table 2.9: Bacteria growth media components

Luria Bertani (LB)		5 g/l Yeast extract 10 g/l Tryptone 10 g/l NaCl
Additives	Antibiotics	100 µg/ml Ampicillin (Amp) 25 µg/ml Chloramphenicol (Cm) 25 µg/ml Kanamycin (Kan)

2.1.8.2 Yeast growth media

Yeast strains were cultured according to standard procedures either in rich (also termed YPD) or synthetic dextrose (SD) medium. SD medium was supplemented with the required aminoacids and nitrogen bases (see table 2.10) to obtain synthetic complete (SC) medium[207]. SC dropout medium was prepared by including all the required aminoacids and nitrogen bases except those used as auxotrophy markers. All media were autoclaved for 20 min at 120 °C. Solid media were prepared by adding bacto-agar at a final concentration of 2 % (w/v).

Solid growth medium containing oleate (STYO) was prepared with 0.67 % yeast nitrogen base (YNB), 0.05 % yeast extract, 1 % Triton®-X100, 0.1 % oleate, the required amino acids and nitrogen bases and 2 % bacto-agar. Oleate was dissolved in warm (~50 °C) 10% Triton®-X100 before being added to the other components. Control plates (STYD) contained 2 % D-glucose instead of oleate.

High pH rich growth medium was prepared by adding HEPES to a final concentration of 100 mM to YPD medium and titrating with 25% HCl to either pH 7.8, 8 or 8.2 before autoclaving. To prepare high pH synthetic complete (SC) dropout medium for studies with overexpression plasmids, the medium was supplemented with copper (100 µM $CuSO_4$) to induce expression and with HEPES added to a final concentration of 10, 15 or 17.5 mM. The pH of these plates after autoclaving was 7.8, 8.0 or 8.2, respectively, as determined using a surface electrode. SC dropout media with higher concentrations of HEPES and pH ≥ 8.0 could not be used owing to the tendency of

yeast nitrogen base to precipitate in these conditions. Copper was added to both control (without HEPES; pH ~ 6.5) and high pH plates.

Table 2.10: Yeast media components

YPD		10 g/l Yeast extract 20 g/l Peptone 20 g/l D-glucose
SD (synthetic dextrose)		1.7 g/l Yeast nitrogen base (YNB) w/o amino acids 5 g/l Ammonium sulfate 20 g/l D-glucose
Additives	Amino acids	20 mg/l L-Arginine 30 mg/l L-Histidine 60 mg/l L-Isoleucine 40 mg/l L-Lysine 20 mg/l L-Methionine 60 mg/l L-Phenylalanine 50 mg/l L-Threonine 40 mg/l L-Tryptophan 60 mg/l L-Leucine
	Nitrogen base	20 mg/l Uracil 20 mg/l Adenine sulphate
	Antibiotics	200 mg/l Geneticin (G418) 100 mg/l Nourseothricin (cloNAT) 0.1-1 µg/ml Cycloheximide
	Others	HEPES 100 µM Copper sulfate

2.1.9 Buffers and solutions

Table 2.11: Solutions used in this study

Solution	Composition*
Ammonium persulfate (APS)	10% (w/v) Ammonium persulfate
ATP solution	1 mM Na_2ATP 1 mM $MgCl_2$
ATP/[γ-^{32}P]ATP solution	100 µM Mg/ATP 1 µCi/µl [γ-^{32}P]ATP (33 nM ATP)
Blocking solution	1x TBS-T 5% (w/v) Skim milk
Blotting buffer pH ~8.3	25 mM Tris-HCl 192 mM Glycine 20% (v/v) Methanol
Coomassie Brilliant Blue (10x)	0.05% (w/v) Coomassie blue 50% (v/v) Methanol 10% (v/v) Acetic acid in ddH2O
DNA loading buffer (5x)	15% (w/v) Ficoll Orange G

Solution	**Composition***
Genomic DNA extraction buffer	10 mM Tris-HCl pH 8 100 mM NaCl 1 mM EDTA 1% (w/v) SDS 2% (v/v) Triton®-X100
Laemmli sample buffer	62,5 mM Tris-Cl pH 6,8 2% (w/v) SDS 10% (w/v) Glycerol 50% (w/v) DTT 0,02% (w/v) Bromophenol blue
Lysis buffer A	50 mM Tris-HCl pH 8 150 mM NaCl 5 mM EDTA 1x Proteinase inhibitor mix (Roche) 0,1 mM PMSF
Phosphate Buffered Saline (PBS) pH 7.4	137 mM NaCl 2.7 mM KCl 4.3 mM Na_2HPO_4 1.47 mM KH_2PO_4
Phenylmethanesulphonylfluoride (PMSF)	PMSF (100 mM in methanol absolute)
PEG	40% (v/v) Polyethylene glycol
SDS electrophoresis buffer pH 8.3	25mM Tris-HCl 19.2mM Glycine 0.1% (w/v) SDS
SDS-polyacrylamide gel pH 8.8 Resolving gel (10%)	30% Acrylamide/0.8% bisacrylamide (v/v) 375 mM Tris-HCl pH 8.8 0.1% (w/v) SDS 0.1% (w/v) Ammonium persulafte TEMED (1:1000 dilution)
SDS-polyacrylamide gel ~6.8 Stacking gel (4%)	30% Acrylamide/0.8% bisacrylamide (v/v) 125 mM Tris-HCl pH 6.8 0.1% (w/v) SDS 0.1% (w/v) Ammonium persulafte TEMED (1:1000 dilution)
Sodium acetate	3 M Sodium acetate Adjust pH to 5.2 with 3 M acetic acid
TAE electrophoresis buffer pH ~8.5	40 mM Tris-acetate 2 mM EDTA
TBS-T	20 mM Tris-HCl pH 7.6 137 mM NaCl 0.1% (v/v) Tween-20
TE pH ~8.0	10 mM Tris-HCl pH 8.0 1 mM EDTA pH 8.0
TEL pH ~8.0	10 mM Tris-HCl pH 8.0 1 mM EDTA pH 8.0 100 mM Lithium acetate
TES	10 mM TrisCl pH 7.5 10 mM EDTA 0.5% (w/v) SDS

Solution	Composition*
Zymolyase solution	0.5 mg/ml Zymolyase-100T in 1 M Sorbitol

*Unless indicated otherwise, chemical substances were dissolved or diluted with deionized water.

2.1.10 Reaction systems, kits

- Western Lightning Chemiluminescence Reagent *PLUS* (Perkin Elmer)
- Expand High Fidelity PCR system (Roche)
- QuikChange® Site-Directed Mutagenesis Kit (Stratagene)
- Gateway® BP and LR Clonase® II enzyme mix (Invitrogen)
- Invisorb® Spin Plasmid Mini Two (Invitek)
- QIAprep MIDI Plasmid Purification Kit (Qiagen)

2.1.11 Consumables

- Centrifuge propylene tubes, 15ml and 50ml (Roth)
- Chromatographie Papier, 3mm (Whatman)
- Eppendorf tubes, 1.5ml (Eppendorf)
- PCR tubes 0.2 ml (Biozym)
- Glass beads 425-600 µm, acid-washed (Sigma)
- X-ray films, Kodak® BioMax® XAR (Sigma-Aldrich)
- Microscope Glass Slides 76 x 26 mm (Menzel-Gläser)
- Coverslips 18 x 18 mm (Roth)
- Nitrocellulose membrane, 0.2 µm (Bio-Rad)
- Petridishes (Roth)

2.1.12 Laboratory hardware equipment

- Mini Gel Electrophoresis System Gel X_L^{Plus} (Labnet International Inc.)
- Heating block Techne DB-2A (Eppendorf)
- Centrifuge 4K15 z.3, 11156/13115 Rotor (Sigma)

- Centrifuge 5415D (Eppendorf)
- Centrifuge RC5C, S3/SS34 Rotor (Sorvall Instr. Du Pont)
- Micromanipulator MSM system (Singer Instruments)
- Microscope Axioplan 2 (Carl Zeiss)
- Mini Protean III System (Bio-Rad)
- Mini Trans Blot Cell (Bio-Rad)
- MJ Mini Personal PCR Thermal Cycler (Bio-Rad)
- Power supply (Bio Rad)
- UV/visible Spectrophotometer Ultra spec 3100 pro (Amersham Biosciences)
- Thermomixer (Eppendorf)
- Vortex (Scientific Ind.)
- *Gene Pulser*® II Electroporation System (BioRad)
- Imaging plate (Fuji Imaging Plate BAS-TR2025, Fuji Photo Film Co., Ltd., Tokyo, Japan)
- Phosphorimager (Fuji Analyzer BAS-1800)

2.2. Methods

2.2.1 *E. Coli* methods

2.2.1.1 Preparation of electrocompetent E.coli and transformation by electroporation

For the preparation of electrocompetent *E. coli* cells, 10 ml of Luria Bertani (LB) starter culture was inoculated with a single colony of *E. coli*, grown overnight at 37 °C in a shaker (250 r.p.m.) to saturation and diluted into 1l of LB media. Cells were grown at 37 °C to an optical density (OD_{600}) of 0.6-0.8 and then chilled by placing the culture flask on ice for 20 min. Cells were harvested at 5000 *xg* for 20 min at 4 °C. Cell pellet was resuspended in 100 ml ice-cold deionized sterile water and centrifuged at 4500 r.p.m. for 20 min at 4 °C twice. Cell pellet was resuspended in 20 ml ice-cold 10% glycerol, centrifuged again and resuspended in the same volume (w/v) of ice-cold 10%

glycerol. Cell suspension was aliquoted in eppendorf tubes (50 µl) and freezed in liquid nitrogen (N_2) and stored at -80 °C.

Transformation was carried out by incubation of 50 µl electrocompetent *E. coli* cells with 0.5 µl plasmid DNA preparations for 5 min on ice followed by electroporation in 2 mm cuvettes using an electroporation apparatus (Bio-Rad). After electroporation, transformed cells were immediately resuspended in pre-warmed LB medium, incubated for 30 min with vigorous shaking by 37 °C and plated onto LB-agar plates supplemented with the appropriate antibiotic. The *E. coli* strain XL1-Blue™ (Stratagene) was used for the maintenance and propagation of all plasmids with the exception of Gateway® constructs, which were propagated using the DH5α™ and DB3.1™ strains (Invitrogen). The Rossetta™ 2 strain (Novagen) was used for the expression of recombinant proteins.

2.2.1.2 Plasmid preparation

The alkaline lysis protocol was used for the small-scale purification of plasmid DNA for restriction endonuclease digestions and cloning. A 3 ml *E. coli* culture was grown overnight to saturation in LB media under selective pressure at 37 °C with shaking (250 r.p.m.). Cells were harvested in eppendorf tubes by centrifugation (16000 x*g* for 2 min, room temperature (RT)) and resuspended in 250 µl resuspension buffer (50 mM Tris-Cl, pH 8.0, 10 mM EDTA, 100 µg/ml RNase A). Upon addition of 250 µl lysis buffer (200 mM NaOH, 1% SDS (w/v)), cell suspensions were mixed by gently inverting the tubes 3 times and incubated for 2 min prior to the addition of 250 µl neutralization solution (3.0 M potassium acetate pH 5.5). The lysate was cleared by centrifugation (16000 x*g* for 10 min, RT). The supernatant was transferred to a fresh tube and plasmid DNA was desalted and concentrated by isopropanol precipitation. The pellet was then washed once with 70% (v/v) ethanol, dried under vacuum, resuspended in 50 µl sterile deionized water and stored at -20 °C.

Highly purified plasmid DNA for sequencing purposes was obtained using the Invisorb® Spin Plasmid Mini Two (Invitek) following manufacturer's instructions. Plasmid DNA for large-scale preparative purposes was purified using the QIAprep MIDI Plasmid Purification Kit (Qiagen) following manufacturer's instructions.

2.2.1.3 Recombinant protein purification

Plasmid pGEX-2TK (GE Healthcare) carrying the *KNS1* coding sequence (pNM11) was transformed into *E. coli* Rossetta™ 2 (Novagen). A single clone of transformed bacteria was grown overnight to saturation in 100 ml of LB media containing 100 µg/ml

ampicillin (Amp) (LB^{Amp}) at 37 °C and then diluted 1:50 in fresh LB^{Amp}. Cells were grown at 37 °C until OD_{600} reached 0.5 and chilled in water bath at 16 °C for at least 1 h. Expression of GST-Kns1 was induced when OD_{600} reached 0.7 by adding Isopropyl β-D-1-thiogalactopyranoside (IPTG; 0.2 mM). After 4h of induction at 16 °C, bacteria were harvested at 5000 *xg* for 15 min and resuspended in 400 ml ice-cold lysis buffer LB1 (10 mM Tris pH 7.6, 10 mM EDTA, 150 mM NaCl and freshly added 1 mM DTT and 0.1 mM PMSF). Cell suspension (100 ml) was lysed by sonication in 6 cycles of 20 sec sonication-30 sec pause (Settings for Branson Sonifier 450 using a horn with 1cm of diameter Tip: 70% Duty Cycle, 4-5 Output control). After sonication, cell lysate was diluted 1:2 with extraction buffer EB (10 mM Tris pH 7.6, 10 mM EDTA, 150 mM NaCl, 1 mM DTT and 2% Triton®-X100) and incubated for 1 h with gentle shaking at 4 °C. Cell debris was pelleted by centrifugation 12000 *xg* for 30 min. The supernatant was transferred to a new tube and incubated with 1ml of 50 % (v/v) slurry of glutathione-Sepharose™ 4B resin (GE Healthcare) pre-equilibrated in buffer LB1. After 2 h incubation at 4 °C with slow tilt rotation, the resin was transferred into an empty column and washed with 500 ml of buffer LB1. Fusion protein GST-Kns1 was eluted from the resin with 1ml elution buffer EB1 (10 mM Tris pH 8, 10 mM EDTA, 150 mM NaCl, 1 mM DTT and 10 mM GSH). Elution was repeated 5 times. Eluates were aliquoted, freezed in liquid N_2 and stored at -80 °C.

Plasmid pDESTco (Invitrogen) carrying the *CMK2* coding sequence (pNM38) was transformed into *E. coli* Rossetta™ 2 (Novagen). A single clone of transformed bacteria was grown overnight to saturation in 25 ml of LB media containing 100 µg/ml ampicillin (Amp) and 25 µg/ml chloramphenicol (Cm) ($LB^{Amp/Cm}$) at 37 °C and then diluted 1:50 in fresh $LB^{Amp/Cm}$. Cells were grown at 37 °C until OD_{600} reached 0.6-0.7 and then expression of 6His-Cmk2 was induced by adding IPTG (0.2 mM). After 2h of induction at 30 °C, bacteria were harvested at 12000 *xg* for 20 min and resuspended in 50 ml ice-cold lysis buffer LB2 (50 mM Tris HCl pH 7.6, 5 mM imidazol and freshly added 0.1 mM PMSF). Cell suspension (50 ml) was lysed by sonication in 6 cycles of 20 sec sonication-30 sec pause as described above. After sonication, cell debris was pelleted by centrifugation 12000 *xg* for 30 min. The supernatant was transferred to a new tube and incubated with 50 µl of NiNTA-Agarose resin (Qiagen). Prior to use, the Ni-NTA bead resin (100 µl of 50 % (v/v) slurry) was washed 3 times with 1 ml buffer LB2 and incubated with high concentration of bovine serum albumin (BSA) *i.e.*, 50 µg BSA in 500 µl resin/buffer LB2 suspension, for 10 min with rotation to block non-specific protein-bead interactions. After 30 min incubation at 4 °C with slow tilt rotation, the resin was transferred into an empty disposable plastic column (Pierce) and washed with 25 ml of buffer WB (50 mM Tris pH 7.6, 300 mM NaCl, 70 mM KCl, 1 mM $MgCl_2$, 5

mM imidazol). Fusion protein 6His-Cmk2 was eluted from the resin by adding 100 µl of elution buffer EB2 (10 mM Tris pH 7.6, 100 mM NaCl and 5 mM EDTA) and incubating with gentle mixing for 10 min. The use of EDTA in the elution buffer was necessary due to the high affinity of the recombinant protein for the resin.

2.2.2 Yeast methods

2.2.2.1 Cultivation of yeast strains

Yeast strains were cultured using standard microbiological methods[207]. Liquid cultures were inoculated from a fresh pre-culture or a single colony and grown overnight (at least 12 h) in rich (YPD) or synthetic complete (SC) drop-out medium in flasks with shaking (225 r.p.m) or in tubes with tilt rotation. To cultivate yeast on solid agar plates, small aliquots of yeast were streaked out from glycerol stocks with sterile inoculation loops on plates containing either YPD or SC media. Strains were grown at 30 °C, unless otherwise noted. Yeast strains were stored for short periods of time on solid agar plates at 4 °C and for long-term periods at -80 °C in 15% glycerol (v/v). The genotype of the strains used in this work is described in table 2.2.

The cell density of yeast cultures was determined by measuring its optical density at 600 nm (OD_{600}) in a spectrophotometer. For reliable measurements, cultures were diluted so that the OD_{600} was <1. An OD_{600} of 1 is equivalent to ~ 3×10^7 cells/ml[208]. The growth stage and rate of cell division of yeast are a function of the cell density of the culture. The exponential phase of growth is referred as log-phase and can be divided into three stages. Early-log phase is the period when cell densities are $<10^7$ cells/ml. Mid-log phase cultures have densities between 1 and 5×10^7 cells/ml. Late-log phase occurs when cell densities are between 5×10^7 and 2×10^8 cells/ml. At a density of 2×10^8 cells/ml yeast cultures are said to be saturated and the cells enter stationary, or G_0 phase[208].

2.2.2.2 Yeast transformation

Transformation of yeast was performed using the modified lithium acetate (LiAc) method by Gietz *et al.* (1992)[209]. Yeast cells were transformed with either plasmids or linear DNA fragments. Briefly, yeast cells were grown overnight in liquid YPD media at 30 °C until OD_{600} reached 0.5-1. Approximately 5 OD_{600} units of cells were gently pelleted by centrifugation (2000 *xg* for 2 min) and washed twice with sterile deionized water and once with sterile TE/LiAc solution (10 mM Tris-HCl pH 8.0, 1 mM EDTA, 100 mM LiAc). Cells were resuspended in a total volume of 40 µl of TE/LiAc solution and

supplemented with 50 µg of single-stranded herring sperm carrier DNA (10 mg/ml, Sigma) and either 40-200 ng plasmid DNA or up to 1 µg linear DNA to be transformed. Then, 350 µl of sterile TE/LiAc-PEG solution (40 % (w/v) PEG 4000 in TE/LiAc) was added, mixed thoroughly with cell suspension and incubated for 30 min at 30 °C. After subsequent heat shock in water bath at 42 °C for 15 min, cells were gently sedimented by centrifugation (1000 *xg* for 1 min, RT), supernatant was removed and cell pellet was resuspended in TE to plate on the appropriate selection medium. For selection of auxotrophic markers (*e.g.* the TRP1 or URA3 selection markers contained in plasmid vectors), synthetic complete (SC) medium lacking the corresponding amino acid was used. When selection of dominant markers (*e.g.* the G418R marker) was necessary, transformed cells were first resuspended in 1 ml YPD medium and incubated for 2 h at 30 °C with rotation to allow the expression of the marker before plating.

2.2.2.3 Creation of yeast mutants

The endogenous *CMK2* gene was disrupted using a PCR-based strategy. The complete coding sequence of *CMK2* was replaced by the heterologous dominant drug resistance cassette *kanMX4*. The module containing *kanMX4* was amplified from the genomic DNA extracted from strain Y16473 (*cmk2*Δ::*kanMX4*) of the Euroscarf deletion set by PCR using primers homologous to a 20 bp genomic sequence located 300 bp up and downstream of the *CMK2* coding sequence (oNM86/oNM87)[210]. PCR was carried out using the Phusion™ High-Fidelity DNA Polymerase (New England BioLabs, Inc.) and following the manufacturer's instructions. The PCR-product was transformed into diploid yeast cells. Diploid cells that correctly integrated the *kanMX4* cassette into the genome (yNM413) by homologous recombination, acquired resistance to geneticin (G418R) conferred by the *kanr* open reading frame (ORF) of *E. coli* transposon *Tn*903[211] and were thus selectable on YPD plates containing 200 µg/ml of G418-sulphate (Calbiochem). Positive clones were verified by PCR using oNM86 and Kan&His primers. The creation of Δ*vma1* (yNM194) diploid cells was achieved by the same approach. Haploid deletion mutant strains were obtained by sporulation and tetrad dissection (described below).

The endogenous *KNS1* gene was genomically tagged at the N-terminus with the enhanced GFP tag (EGFP, hereafter termed GFP) using a PCR-mediated strategy[202] to create strain yNM459. A module containing the drug resistance cassette *natNT2,* the *CUP1-1* promoter and the GFP tag was amplified by PCR using plasmid pYM-N4 as template[202]. The insertion of the *CUP1-1* promoter upstream of the *KNS1* gene allowed the strong induction of *KNS1* expression upon $CuSO_4$ addition. The forward primer oNM62 is composed of the 45 nucleotides upstream of the ATG (including ATG) of the

KNS1 gene followed by 18 nucleotides that anneal to the 5'-end of the cassette. The backward primer oNM63 is composed of the reverse complement of the 45 nucleotides downstream of the ATG of the gene *KNS1* (excluding ATG) followed by 20 nucleotides that anneal to the 3'-end of the cassette. PCR was carried out using the Phusion™ High-Fidelity DNA Polymerase following the manufacturer's instructions. After module amplification, the PCR-product was transformed into wild-type haploid yeast strain sUB62. Cells that acquired resistence to nourseothricin conferred by the *natNT2* gene from *Streptomyces noursei* were selectable on YPD plates containing 100 µg/ml of clonNAT (Nourseothricin, Werner BioAgents). Positive clones were verified by PCR using oGD70 and oMD141 primers. The module containing *natNT2, CUP1-1* and GFP was integrated upstream of the endogenous *CMK2* gene using the same approach and the primer set oNM76/77 for module amplification.

2.2.2.4 Diploid creation, sporulation and tetrad analysis

To create a diploid yeast strain possessing different genetic modifications, two haploid strains of the opposite mating type carrying distinct selectable markers were mated on the surface of YPD agar plates[212]. After 4h of mating at 30 °C, the mating mixture was streaked onto a plate that selected for the diploid genotype. Meiosis and subsequent sporulation of the diploid cell was induced by nitrogen starvation. In principle, a fresh liquid culture from a single colony of the diploid strain was grown overnight until it reached the log-phase. A fraction of this culture (50 µl) was diluted in 2 ml of pre-sporulation media (0.8% yeast extract, 0.3% peptone, 10% dextrose) and let grown for approximately 6-8 hours. Cells were then harvested, exhaustively washed to eliminate traces of pre-spo media and resuspended in 2 ml of sporulation media (0.1% yeast extract, 0.05% dextrose, 1% potassium acetate). After 2-3 days of incubation with rotation at 30 °C, the culture was examined microscopically for spore formation. Tetrads, which are composed of four haploid spores surrounded by a thick-cell wall (ascus), were prepared for dissection by incubating a 10 µl aliquot of the sporulated culture with 1 µg of Zymolyase-100T (MP Biomedicals, Inc.) in Zymolyase solution (0.5 mg/ml Zymolyase-100T in 1 M Sorbitol) for 10 min at RT to disrupt the cell wall. Subsequently, the cell suspension was streaked out onto YPD plates. During tetrad dissection, asci were visualized under a dissection microscope using a 100x magnification and the spores from one ascus were separated using the glass tip of the micromanipulator. Once tetrad analysis is completed, plates were incubated at 30 °C to let spores germinate. After 3 days, the spores formed colonies that could be replica plated for genotyping and further characterization. In this manner, the sporulation of the diploid strains and subsequent tetrade dissection led to the creation of the following

haploid strains; yNM195 (*vma1*Δ::*kanMX4*), yNM414 (*cmk2*Δ::*kanMX4*), yNM454 (*cmk2*Δ::*kanMX4*, *kns1*Δ::*natNT2*) (see table 2.2 for further genotype details).

2.2.2.5 Serial dilution spotting assay

The sensitivity of wild-type and deletion mutant yeast strains to different stress conditions (*e.g.* high pH) was assessed by spotting serial dilutions of yeast cultures on solid agar plates. Cell cultures were grown overnight to mid-log phase in liquid media at 30 °C with rotation, diluted first to an OD_{600nm} of 0.25 in a 96-well microtiter plate and then successively diluted 1 to 5. These dilutions were spotted using a Steers-type inoculum replicator onto agar plates containing the indicated chemicals compounds and/or buffers (described in section 2.1.8.2). Plates were incubated, unless stated otherwise, at 30 °C and photodocumented after the indicated days. Sensitivity to a particular condition was regarded qualitatively as the relative growth of each deletion mutant strain compared with growth of the isogenic wild-type strain on the same plate.

Quantitation of the approximate cell population density of yeast strains grown at high pH was performed by densitometry (ImageJ, NIH). The approximate cell population of each mutant was expressed relative to that of wild-type cells (set to 1.0).

2.2.2.6 Yeast two-hybrid analysis

Yeast two-hybrid assays were performed using the GAL4-based system developed by Fields *et al.*(1989)[213]. Combinations of bait plasmid bearing the *GAL4* binding domain (OBD) fused to the coding sequence of Kns1 (pNM105), prey plasmid bearing the *GAL4* activation domain (OAD) fused to Cmk2 (pNM104) and the respective empty plasmids were transformed as indicated into the host yeast strain PJ69-4A. PJ69-4A allows for stringent growth selection on SC-His and SC-Ade media[200]. Transformants were streaked out on synthetic complete (SC) medium lacking Trp and Leu (SC-Trp-Leu; control) to select for both Gal4-fusion plasmids and then single colonies were selected and streaked onto SC-Trp-Leu medium additionally lacking either His (SC-Trp-Leu-His; reporter 1) or Ade (SC-Trp-Leu-Ade; reporter 2) to assay for reporter activation. Negative controls consisted of cells cotransformed with the following combination of plasmids; pNM105 (*OBD-KNS1*) with pMD302 (*OAD* alone) and *OAD-CMK2* with pMD302 (*OBD* alone). In addition, bait plasmid bearing OBD fused to Cmk2 (pNM106; *OBD-CMK2*), prey plasmid bearing OAD fused to Kns1 (pNM103; *OAD-KNS1*) and the respective empty plasmids were assayed. The reported interaction between Snu66 and Hub1 was tested in parallel as a positive control for the assay using plasmids expressing OBD fused to Snu66 (pMR29; *OBD-SNU66*) and OAD

fused to Hub1 (pGD240; *OAD-HUB1*)[214], which were kindly provided by Dr. Gunnar Dittmar. Plates were incubated for 3 days at 30 °C before photodocumentation.

2.2.2.7 Isolation of genomic DNA from yeast

The preparation of genomic DNA from yeast for use in PCR amplification reactions was performed using the procedure described by Hoffman *et al*. (1987)[215]. A 5 ml yeast cell culture was grown in YPD to saturation (OD_{600}>2), harvested and resuspended in 200 µl DNA extraction buffer (10 mM Tris-HCl pH 8, 100 mM NaCl, 1 mM EDTA, 1% SDS, 2% Triton-100). After addition of 200 µl phenol:chloroform:isoamyl alcohol (25:24:1), cells were disrupted with glass beads (Sigma) by vortexing for 3 min. Cell lysate was spun for 5 min and aqueous phase was transferred to a new tube. To precipitate isolated genomic DNA, 1 ml 100% EtOH and 20 µl 3 M sodium acetate (pH 5.2) were added and mixed by inversion. Finally, after 10 min incubation and 10 min high speed centrifugation (16000 *xg*), pellet was washed once with 70% EtOH, dried in a speed vacuum and dissolved in 50 µl TE buffer (10 mM Tris-HCl pH=8, 1 mM EDTA).

2.2.2.8 Preparation of whole yeast cell extracts

Whole cell extracts were prepared from cultures grown overnight to log-phase in liquid media at 30 °C. Cells were harvested by centrifugation at 2000 x*g* for 5 min, resuspended in 1x cell pellet volume of lysis buffer (50 mM Tris pH 8, 100 mM NaCl, 10mM EDTA) supplemented with an EDTA-free protease inhibitor cocktail tablet (Roche) and phenylmethanesulfonyl fluoride (PMSF; 1 mM). After cell disruption with acid-washed glass beads by vortexing at full speed for 3 min, 3x cell pellet volume of lysis buffer was added. Cell lysate was then cleared of cellular debris with a 5 min 1000 x*g* spin followed by a 10 min 16000 x*g* spin. Supernatant was transferred to a new microcentrifuge tube, Laemmli sample buffer (62.5 mM Tris-Cl pH 6.8, 2% (w/v) SDS, 10% (w/v) Glycerol, 50% (w/v) DTT) was added and the mixture was boiled at 95 °C for 5 min to allow protein denaturation. Aliquots of 0.1 OD_{600} units/µl were resolved by electrophoresis on 8, 10 or 12 % SDS-polyacrylamide gels as indicated.

2.2.2.9 RNA preparation from yeast cells

Total RNA was prepared from intact yeast cells by extraction with hot acidic phenol as described by Collart *et al*. (1993)[216]. Wild-type (sUB62) and Δ*kns1* (yAS5) cells were grown in 10 ml of YPD to mid-log phase (OD_{600}= 0.7). The strain used as positive control for splicing defects, KL1, is impaired in splicing when cultured in glucose medium because the expression of chromosomal *PRP8* is repressed by the galactose

promoter (P_{GAL1})[199]. Thus, KL1 was grown in YPGR (YP + 2% galactose, 2% raffinose) at 30 °C to an OD_{600} of 0.2 and transferred to YPD to repress chromosomal *PRP8* expression and grown until the culture OD_{600} reached 0.7. Cells were harvested and resuspended in 2 ml of TES solution (10 mM Tris-Cl pH 7.5, 10 mM EDTA, 0.5% SDS). After addition of 2 ml of acid phenol followed by 10 s vortexing, samples were incubated for 1 h at 65 °C in water bath. This step ensured cell lysis in a chemical environment that resulted in denaturation of proteins, necessary to rapidly eliminate ribonucleases, and removal of DNA. Then, samples were cooled on ice for 5 min and RNA were fractionated from the other cellular macromolecules by centrifuging 5 min at 1500 x*g* at 4 °C. The aqueous phase was transferred to a new tube and phenol extraction was performed again. Thereafter, addition of 2 ml of chloroform to the aqueous fraction and posterior centrifugation completed the extraction procedure. To achieve concentration and desalting of the purified RNA, 40 µl of 3 M sodium acetate (pH 5.3) and 1 ml of ice-cold 100% ethanol were added to 400 µl aliquots of the samples. Following 1h incubation at -80 °C, RNA was pelleted and washed with 70% ethanol. Finally, RNA was resuspended in 50 µl deionized water. The RNA content and purity was determined by measuring the absorption of the samples at 260 nm (A_{260}) and the ratio of the absorptions at 260 nm and 280 nm (A_{260}/A_{280}), respectively, using quartz cuvettes. Importantly, during all RNA manipulations, rnase-free lab-ware and diethylpyrocarbonate (DEPC)-treated solutions were used to avoid contamination by ribonucleases. 7 OD_{600} cells yielded approximately 250 µg RNA.

2.2.2.10 Partial purification of Pdc1-TAP from yeast

A 3.5 l culture of exponentially growing yeast cells (OD_{600}=0.6) was harvested by centrifugation at 2000 *xg* for 5 min and resuspended in 5 ml of lysis buffer (50 mM Tris pH 8, 150 mM NaCl, 5 mM EDTA and 0.1 % TX-100) supplemented with protease inhibitors (complete mini™ EDTA-free protease inhibitor cocktail and PMSF). After cell disruption with acid-washed glass beads by vortexing at full speed for 3 min, 20 ml of lysis buffer was further added. All subsequent steps were performed at 4 °C. Cell lysate was cleared of cellular debris with a 10 min 1000 x*g* spin followed by a 10 min 10000 x*g* spin. The cleared lysate was incubated with 100 µl of IgG-Sepharose 6 Fast Flow resin (GE Healthcare) for 1 h at 4°C with rotation. The IgG-Sepharose resin (200 µl; 50% (v/v) slurry) was previously equilibrated according to instructions provided by the manufacturer. The resin suspension was loaded onto an empty column and extensively washed with buffer (50 mM Tris pH 8, 150 mM NaCl and 5 mM EDTA). Finally, the washed resin (~100 µl) was transferred to a new microcentrifuge tube and 100 µl of a 10 mM Tris pH 7.5 solution was added.

2.2.3 General molecular techniques

All molecular biology techniques were performed as described in Sambrook and Russell (2001) unless otherwise stated[206].

2.2.3.1 Standard PCR reaction

PCR reactions for the amplification of modules for genomic epitope tagging or drug resistence cassettes for gene deletion were carried out using ~200 ng of DNA template and 300 nM of each set of primers in a 100 µl reaction containing dNTPs (500 µM), 2U of Expand™ Long Template DNA-polymerase (Roche), 10µl of 10x PCR-buffer 2 (with 2.75 mM $MgCl_2$). PCR cycling conditions were as follows: denaturation at 92 °C for 3 min, 35 cycles of 92 °C for 15 s, 52 °C for 30 s and 68 °C for 3 min followed by a final elongation step at 68 °C for 10 min. PCR reactions for the amplification of genes for cloning purposes were carried out using Phusion™ High-Fidelity DNA Polymerase (New England BioLabs, Inc.) and following the manufacturer´s instructions. To test appropriate genomic insertions, standard PCR protocols were performed using Taq-DNA Polymerase (New England BioLabs, Inc.) and isolated genomic yeast DNA as template in 25 µl reaction volume.

2.2.3.2 Site-directed mutagenesis

Single-point mutations were inserted into *KNS1* and *CMK2* coding sequences (CDS) using the QuickChange™ XL Site-Directed mutagenesis Kit (Stratagene) following the manufacturer's instructions. This method is based on the non-strand-displacing action of the *PfuTurbo*® DNA polymerase, which extends the mutagenic primers generating nicked circular strands. PCR reactions were performed using 200ng of the pDONR221 plasmid (Invitrogen) containing either full-length *KNS1* (pNM14) or *CMK2* (pNM47) as template and 125ng of forward and reverse primers carrying the desired mutations. After amplification, the PCR product was digested with 10 U of the *Dpn*I restriction endonuclease for 30 min at 37 °C to remove the non-mutated methylated parental DNA prior to transformation into *E. coli* cells. Mutagenic primers were designed with a silent mutation introducing a restriction site adjacent to the mutation of interest to enable positive mutant screening by restriction endonuclease digestion analysis. All point mutations were further verified through automated DNA sequencing performed by the Invitek sequencing service. Mutagenic primers containing the desired mutations and the accompanying restriction sites are listed in table 2.12.

Table 2.12: Site directed mutagenesis of plasmids.

Name	Template	Gene	Mutation	Primers oNM	Silent RE site
pNM33	pNM14	Kns1	D440A	117/118	StyI
pNM34	pNM14	Kns1	T562A	127/128	SacI
pNM47	pNM47*	Cmk2	A129T	123/124	PvuII
pNM50	pNM47	Cmk2	D171A	111/112	ApaI
pNM85	pNM47	Cmk2	Y47F	129/130	StyI
pNM86	pNM47	Cmk2	T52A	131/132	SacI
pNM88	pNM47	Cmk2	T69A	135/136	HindIII
pNM89	pNM47	Cmk2	S328A	137/138	PvuI
pNM91	pNM47	Cmk2	T316A	153/154	NheI
pNM92	pNM47	Cmk2	T316D	155/156	AatII
pNM93	pNM47	Cmk2	S379E	157/158	SacI
pNM94	pNM47	Cmk2	Y47D	159/160	EcoRV
pNM95	pNM47	Cmk2	T52D	161/162	StyI
pNM96	pNM47	Cmk2	T69D	163/164	HindIII
pNM98	pNM47	Cmk2	T406A	168/169	StyI
pNM99	pNM47	Cmk2	T406D	170/171	StyI
pNM100	pNM47	Cmk2	S328E	166/167	SacI
pNM111	pNM47	Cmk2	S379A	139/140	StyI

2.2.3.3 Restriction Endonuclease digestion and ligation reactions

Restriction endonuclease digestions were carried out following supplier's instructions. A standard reaction mixture of 100µl contained 1-5 µg of plasmid DNA (or PCR product), 1 unit (U) of the appropriate restriction enzyme(s) per µg of DNA (New England BioLabs, Inc.), the recommended buffer and BSA (100 µg/ml) if required. Antarctic Phosphatase (1U/ µg of DNA; New England BioLabs, Inc.) was additionally added to prevent self-ligation of the plasmids. Reaction mixtures were incubated for at least 1 h at 37°C in water bath.

Ligation reactions were performed using 1 U of T4 DNA Ligase enzyme (New England BioLabs, Inc.) per µg of DNA in a 10 µl reaction mixture. Reactions were incubated overnight at 16 °C. The optimal molar ratio of vector to insert was estimated for each ligation reaction.

2.2.3.4 Electrophoretic DNA separation

Horizontal agarose gel electrophoresis was used for the identification of DNA fragments. Because of the negative charge of their phosphate groups, the DNA molecules move through the agarose matrix towards the plus-pole in an electric field. Under constant voltage the migration speed of linear, double-stranded DNA in agarose gels is proportional to the logarithm of its molecular weight. The size of a linear DNA

fragment can be determined by comparison with standard DNA fragments of known size. Depending on the size of the DNA molecules the agarose concentration was chosen between 0.5% and 2.0% (w/v). For the detection of the DNA strands, addition of DNA-intercalating stain ethidium bromide was added to the agarose gels. TAE buffer was used for the preparation of the agarose solution and as electrophoretic buffer. Separated fragments were visualized by UV-light.

2.2.3.5 Plasmid construction

The plasmids used in this work were created combining classic cloning techniques, the Gateway® cloning system (Invitrogen) and gap-repair cloning in yeast. All plasmids created were confirmed by sequencing and are listed in Table 2.3 and 2.4.

The *KNS1* coding sequence was cloned into pGEX-2TK (GE Healthcare) to enable the recombinant expression of N-terminally GST-tagged Kns1 in *E. coli* and purification by glutathione-agarose chromatography. First, the *KNS1* coding sequence was amplified by PCR from wild-type yeast genomic DNA (sUB62) using a forward primer containing the BamHI site (oMD135) and a reverse primer containing the XmaI site (oMD136). Then, PCR-product and pGEX2TK were digested with BamHI/XmaI and ligated according to standard protocols to yield pNM11[206].

The Gateway® cloning technology is based on the bacteriophage lambda (λ)-based site-specific recombination system[217–219]. In particular, the clonase from a LR enzyme mixture transfers the gene of interest (flanked by *att*L1 and *att*L2 sites) from the entry vector into a destination vector which contains a chloramphenicol resistance (CmR) and a *ccd*B gene (flanked by *att*R1 and *att*R2 sites). Upon recombination, the *in vitro* reaction is transformed in *E. coli* strain DH5α. Thus, positive clones can be readily selected on LB plates containing 100 mg/ml ampicillin (LB^{amp}). The toxicity of the *ccd*B gene in the standard laboratory *E. coli* strain DH5α inhibits the growth of transformants containing the original destination vector.

To create *KNS1*- and *CMK2*-bearing plasmids compatible with the Gateway® cloning system (Invitrogen), *KNS1*- and *CMK2* coding sequences were amplified from plasmids (pGD252 and pGD253; kindly provided by Dr. G. Dittmar) using oligonucleotide primer sets containing *attR1* and *attR2* sites flanked by sequences complementary to the ends of BamHI/HindIII-digested pSV52 (oNM94/95, oNM96/97). The PCR-amplified *KNS1*- and *CMK2* coding sequences with *attR1* and *attR2* sites at their respective 5′ and 3′ ends were cloned into pSV52 (kindly provided by S. Sadis and D. Finley) to yield pNM18 and pNM19, respectively. To this end, PCR-products and pSV52 were digested with BamHI/HindIII and each PCR-product was transformed along with linearised pSV52 into yeast cells, which repair the gap in pSV52 by

homologous recombination (gap repair cloning; described by Ma *et al.* 1987[220]). Next, the *CMK2* coding sequence from plasmid pNM18 and *KNS1* from plasmid pNM19 were transferred into pDONR221™ (Invitrogen) by homologous recombination using the BP Clonase enzyme mixture (Invitrogen) and following the manufacturer's instructions to create *CMK2*- (pNM47) and *KNS1*-containing (pNM14) entry vectors. Upon recombination, the *in vitro* reaction was transformed in *E. coli* strain DH5α and positive clones selected on LB plates containing 50 mg/ml kanamycin (LB^{kan}). The inserts of both entry vectors were examined by DNA sequencing. A mutation (T129A) found in *CMK2* from pNM47 was repaired using primers oNM123/124 to yield the wild-type sequence of *CMK2* by site-directed mutagenesis. Then, *CMK2* and *KNS1* were transferred from pNM47 and pNM14 into plasmid pNM67 (2µm, *TRP1*) to yield pNM73 and pNM74, which enable the expression of either N-terminally GFP-tagged Cmk2 or Kns1 driven by the copper-inducible promoter pCUP1-1 in yeast cells. Plasmid pNM67 was created by cloning promoter pCUP1-1 into destination vector pMD299 (kindly provided by M. Dahlmann), which contains a GFP tag (enhanced GFP; EGFP) placed 5' of the Gateway® cloning cassette. Promoter *CUP1-1* was amplified by PCR from pYM-N1 using a forward primer containing the Sac I restriction site (oNM147) and a reverse primer containing the BglII site (oNM148). Both PCR-product and pMD299 were digested with SacI/BglII and ligated according to standard protocols[206]. Similarly, *CMK2* was transferred from pNM47 into destination vector pDESTco[201] (kindly provided by Prof. E. Wanker) using the LR Clonase recombination enzyme mixture (Invitrogen) to yield plasmid pNM38, which enables recombinant expression of 6His-Cmk2 in *E. coli* and purification by nickel chelate chromatography as described above.

For the yeast two hybrid assays, Gateway®-compatible destination vector pMD303 containing the *GAL4* binding domain (based on pOBD2)[83] and pMD302 containing the *GAL4* activation domain (based on pOAD1)[221] were used (kindly provided by M. Dahlmann). Bait plasmids were constructed by transferring either *KNS1* or *CMK2* from pNM47 and pNM14 into pMD303 to create the *OBD-KNS1* (pNM105) or *OBD-CMK2* (pNM106) fusions whereas prey plasmids were constructed by cloning either *KNS1* or *CMK2* from pNM47 and pNM14 into pMD302 to create the *OAD-KNS1* (pNM103) or *OAD-CMK2* (pNM104) fusions.

To express GFP-tagged Cmk2 from a single-copy plasmid and under the control of its endogenous promoter in yeast, I cloned the 5'-UTR (1000 bp) of the *CMK2* locus into pRS414 (*CEN ARS*, *TRP1*)[205] to yield pNM61. The 5'-UTR (1000 bp) region of the *CMK2* locus was amplified by PCR from wild-type yeast genomic DNA (sUB62) using a forward primer containing the EcoRI site (oNM142) and a reverse primer containing the XhoI site (oNM143). Both PCR-product and pRS414 were digested with EcoRI/XhoI

and ligated according to standard protocols[206]. Plasmid pNM61 was converted into a destination vector (pNM63) by inserting the GFP tag (EGFP) and Gateway® cloning cassette via gap repair cloning, which were amplified by PCR from pMD299 using primer set oNM145/146 containing sequences complementary to the ends of XhoI/KpnI-digested pNM61. PCR-product and pNM61 were digested with XhoI/KpnI and transformed into yeast cells to allow homologus recombination. The *E. coli* strain DB3.1™ was used for propagation of the resulting destination vector pNM63. Finally, *CMK2* was transferred from pNM47 into plasmid pNM63 to yield pNM65. The correct functioning of the endogenous promoter of Cmk2 was verified by the induction of expression of N-terminally GFP-tagged Cmk2 upon exposure of yeast cells to high extracellular levels of Ca^{2+}, as previously described[222].

2.2.3.6 Reverse-transcriptase PCR reaction

RNA reverse transcription and subsequent amplification of the resulting cDNA were performed by using One-Step RT-PCR kit (Qiagen) following the manufacturer's instructions. Both enzymatic reactions were carried out in the same tube. The 50 µl reaction mixture contained 1 µg of purified RNA as template, 1 µg of oligo(dT) primers, 0.6 µM of the gene-specific primers, dNTP mix (400 µM of each dNTP), 1x QIAGEN OneStep RT-PCR Buffer and 2 µl of the Qiagen Enzyme mix. During the first incubation step at 50 °C for 30 min, oligo(dT) primers ensured poly(A)-containing mRNA reverse transcription. After cDNA synthesis, a 15 min incubation at 95 °C led to inactivation of the reverse transcriptase, activation of the HotStarTaq DNA-polymerase and denaturation of the cDNA. Then, the PCR reaction started with the following cycling conditions: 25 cycles of denaturing for 20 s at 95 °C, annealing for 30 s at 55 °C, extension for 1 min at 72 °C and one final 10 min extension. Amplified cDNA PCR products were analysed by electrophoresis on 2 % agarose gels.

2.2.4 Protein analysis

2.2.4.1 Determination of protein concentration

The protein concentration was estimated using the Bradford-based Bio-Rad Protein Assay[223]. This assay is based on the shift in the absorbance maximum (from 465 nm to 595 nm) that occurs when the Coomassie Brilliant Blue G-250 dye binds with proteins[224]. A 10 µl aliquot of a protein solution was diluted 1:50 with deionized water and mixed with 500 µl of the Bradford reagent dye (Bio-Rad) in a disposable polystyrene cuvette. After a brief incubation at RT, the absorbance of the sample was measured at 595 nm using a UV/visible spectrophotometer (Ultra spec 3100 pro;

Amersham Biosciences). Serial dilutions of a BSA stock solution of known concentration was prepared and measured in parallel to create a standard curve (from 50 to 2000 µg/ml).

2.2.4.2 SDS-PAGE gel electrophoresis

Analysis of yeast protein extracts was carried out by using discontinuous one dimensional SDS-polyacrylamide gel electrophoresis (SDS-PAGE) under denaturing conditions according to the standard Laemmli protocol[225]. Protein solubilization was achieved by the action of denaturants (SDS), reducing agents (DTT) and heat. Laemmli buffer (6x) was added 1 to 5 to the protein sample, which was then heated for 5 min at 95 °C to allow protein denaturation prior to loading on a SDS-polyacrylamide gel for molecular weight-based separation. For the detection of tagged Kns1 (MW=109 kDa), the percentage of acrylamide used in the separating gel was 8 % and, for tagged Cmk2, was 12 %. SDS electrophoresis buffer (25mM Tris-HCl, 19.2mM Glycine, 0.1% (w/v) SDS) and a 20mA constant current were used as standard running conditions[226]. Vertical electrophoresis was performed using the Mini-PROTEAN 3 system (Bio-Rad). Broad range protein marker (NEB) or pre-stained broad range protein marker (NEB) was used for size-determination.

2.2.4.3 Coomassie staining of polyacrylamide gels

The protein content of polyacrylamide gels was visualized by staining with Coomassie brilliant blue G250. Following electrophoresis, gels were washed 3 times for 5 min with deionized water to remove SDS and buffer salts and then stained for 1 h at RT on a shaker with Coomassie brilliant blue G250 solution according to the manufacturer's instructions. Thereafter, gels were destaining with deionized water.

2.2.4.4 Western blotting

Electroblotting of proteins from polyacrylamide gels onto nitrocellulose membranes was performed essentially as described by Burnette *et al*. (1981)[227] and using the tank transfer system from BIO-RAD (Mini-Trans-Blot) according to the manufacturer´s guidelines. The gel and the nitrocellulose membrane were placed into the semi-dry blot apparatus between two piles of two 3MM filter-papers (Millipore) soaked with transfer buffer (20 mM Tris-base, 192 mM Glycine, 20 % (v/v) Methanol). Electrophoretic transfer was accomplished by applying 70 mA constant current for 1 hour or at 20 mA overnight in transfer buffer. After blotting, the membrane was blocked with proteins from bovine milk to avoid unspecific binding of the antibodies for 1 h at RT in Tris-

buffered saline (20 mM Tris-HCl pH 7.6, 137 mM NaCl) supplemented with 0.1 % (v/v) Tween-20 (TBS-T) and 5% (w/v) skim milk powder. Subsequently, the membrane was incubated with the primary antibody diluted in blocking solution for 1 h at RT or overnight at 4 °C on a shaker. After three washes of 5 min with TBS-T, the membrane was incubated for 1 h at RT with the respective horseradish peroxidase (HRP)-coupled secondary antibody on a shaker. Finally, the membranes were washed at least 3 times for 10 min with TBS-T. Detection by enhanced chemiluminescence (ECL) was performed using the ECL detection system as recommended by the manufacturer (Perkin Elmer). The light emitted by oxidized luminol from the reaction catalysed by the horseradish peroxidase was recorded on X-ray films (Kodak® BioMax® XAR, Sigma-Aldrich).

2.2.4.5 In vitro phosphorylation assays

The autophosphorylation capabilities of wild-type GST-Kns1 (pNM11), GST-Kns1^{D440A} (pNM37) and GST-Kns1^{T562A} (pNM54) were tested *in vitro* in phosphorylation buffer (25 mM Tris pH 7.5, 10 mM $MgCl_2$, 1 mM DTT and 0.2 µg/µl BSA) by incubating 62.5 ng (~ 0.625 pmol) of kinase with 0.5 µl of [γ-^{32}P]ATP (10 µCi/µl; 3000 Ci/mmol) in a total volume of 20.5 µl for 15 min at 30 °C (Fig. 3.8 and 11).

The assessment of Cmk2 *in vitro* phosphorylation by Kns1 was performed by incubating 250 ng (~ 5 pmol) of wild-type 6His-Cmk2 (pNM38) or catalytically inactive 6His-Cmk2^{D171A} (pNM45) with either 50 ng (~ 0.5 pmol) of wild-type GST-Kns1 (pNM11) or catalytically inactive GST-Kns1^{D440A} (pNM37) in 20.5 µl of reaction mix containing phosphorylation buffer (25 mM Tris pH 7.5, 10 mM $MgCl_2$, 1 mM DTT and 0.2 µg/µl BSA) and 0.5 µl of [γ-^{32}P]ATP for 15 min at 30 °C (Fig. 3.14).

Phosphorylation of Pdc1 by Kns1 was tested *in vitro* by incubating Pdc1-TAP, which was affinity-purified on matrix-bound IgG from yeast extracts (described in 2.2.2.10), with either 50 ng wild-type GST-Kns1 (pNM11) or catalytically inactive GST-Kns1^{D440A} (pNM37) in 20.5 µl of reaction mix containing phosphorylation buffer (25 mM Tris pH 7.5, 10 mM $MgCl_2$, 1 mM DTT and 0.2 µg/µl BSA) and 0.5 µl of [γ-^{32}P]ATP for 15 min at 30 °C (Fig. 13). 50 µl of the 200 µl IgG-Sepharose resin suspension containing Pdc1-TAP (50% (v/v) slurry of beads in 10 mM Tris pH 7.5) were used for each kinase reaction. Beads were gently spun down, the supernatant was carefully removed by pipetting and 20 µl of the reaction mix containing the kinase in phosphorylation buffer was added.

The phosphorylation activities of 6His-Cmk2 and phosphorylation site mutants were assayed by measuring their ability to phosphorylate the exogenous model

substrate MBP (Sigma-Aldrich). Reactions were performed by incubating MPB (5 µM) with the indicated 6His-Cmk2 version (0.2 µM) in phosphorylation buffer (25 mM Tris pH 7.5, 10 mM $MgCl_2$, 2.5 mM $CaCl_2$ and 0.2 µg/µl BSA) containing a ATP/[γ-^{32}P]ATP solution (10 µM ATP with 0.1 µCi/µl [γ-^{32}P]ATP) in the absence or presence of calmodulin (CaM; 10 µM) for 5 min at 30 °C (Fig. 3.24, 25 and 26).

All kinase reactions were started with the addition of [γ-^{32}P]ATP and terminated by addition of 10 µl of Laemmli sample (6x) buffer and immediate boiling for 5 min. Preincubations were performed on ice. Samples (5 µl) were resolved by SDS-PAGE. 8 % polyacrylamide (PA) gels were used for autophosphorylation assays, 10 % PA gels for Cmk2 *in vitro* phosphorylation by Kns1 assays and 18 % PA gels for MBP phosphorylation assays. After electrophoresis, gels were fixed in fixing solution (50% methanol, 10% glacial acetic acid) for 30 min and dried under vacuum at 80 °C for 1-2h. Subsequently, digital photostimulated luminescence (PSL) autoradiography was performed by placing dried PA gels into an exposure cassette with an imaging plate (Fuji Imaging Plate BAS-TR2025, Fuji Photo Film Co., Ltd.). After the appropriate exposure time, the imaging plates were scanned using a phosphorimager (Fuji Analyzer BAS-1800) and data were stored as digital files.

BSA was included in the phosphorylation reactions as a unspecific phosphate-acceptor competitor. Aliquots of the reaction mixtures were taken prior to [γ^{32}-P]ATP addition and resolved by SDS-PAGE followed by Western blotting (WB) with the appropriate antibodies to verify equal protein content of each fusion protein species as indicated. MPB protein content was visualized by staining PA gels after electrophoresis with Coomassie Blue. BSA protein content was detected on Western blots by incubating with Ponceau S-staining solution (0.5 % (w/v) Ponceau S, 1 % (v/v) acetic acid) for 5 min at RT with agitation.

2.2.4.6 Identification of phosphorylation sites by mass spectrometry

For the identification of phosphorylation sites on GST-Kns1 by mass spectrometric (MS) analysis, *in vitro* autophosphorylation reactions were performed on a large scale using 2 µg of GST-Kns1 (wild-type or catalytically inactive) in a 40 µl reaction mix containing phosphorylation buffer (25 mM Tris pH 7.5, 10 mM $MgCl_2$, 1 mM DTT) and 50 µM ATP for 30 min at 30 °C. For the identification of phosphorylation sites on 6His-Cmk2 by MS analysis, *in vitro* phosphorylation reactions were performed by incubating 10 µM 6His-Cmk2 (wild-type or catalytically inactive) with 2 µg of wild-type GST-Kns1 in a 40 µl reaction mix containing phosphorylation buffer (25 mM Tris pH 7.5, 10 mM

$MgCl_2$, 1 mM DTT) and 50 µM ATP for 30 min at 30 °C. Additional reaction mixtures devoid of ATP were incubated and analysed in parallel as negative controls. Reaction mixtures were subjected to SDS-PAGE followed by staining with Imperial™ Protein Stain (Pierce). Protein bands containing either 6His-Cmk2 or GST-Ksn1 were excised from the gel. Both proteins were converted to peptides by an in-geld digestion with trypsin and the resulting peptides were extracted as described in Shevchenko *et al*. (2006)[228]. Analysis by mass spectrometry of the resulting peptides was performed by Dr. Gunnar Dittmar in the Mass Spectrometry Core Facility at the Max-Delbrück Centrum (Berlin). The recovered peptides were separated on a 10 cm Pepmap column and directly sprayed into the mass spectrometer using electrospray ionization. Spectra were recorded using a Waters Q-TOF premier or an ABSciex Q-TRAP 4000 mass spectrometer. For the analysis of the recorded spectra the MASCOT software package (Matrix Science) was used.

2.2.5 Data analysis

Phosphate [γ^{32}-P] incorporation into MBP was quantified via densitometric analysis using an image-analysis software (TINA 2.1, Raytest Isotopenmessgeräte GmbH). All raw phosphorylation values of MBP were firstly corrected for background activity and then normalized to the phosphorylation value of MBP incubated with wild-type 6His-Cmk2 either in the absence or presence of CaM/Ca^{2+} as indicated (Fig. 3.24, 25 and 26). Average MBP phosphorylation values and standard deviations were calculated from data derived from three independent experiments. Two-tailed unpaired Student´s *t*-tests were performed to show whether the difference in phosphorylation efficiency between wild-type 6His-Cmk2 and the phosphorylation site mutant cells was significant. Significance levels are indicated in the figures as follows; **p*≤0.05 (n=3), ***p*≤0.01 (n=3). .

2.2.6 Live fluorescence microscopy

All microscopy was performed using the Axioplan II fluorescence microscope (Zeiss). Images were acquired with the Axiocam charge-coupled device camera (Zeiss). The AxioVision 3.0 software was used to control the stage, filter sets and image acquisition. Exposure time, magnification and software settings were kept constant for all acquisitions taken during each experiment. GFP and Hoechst or GFP and Phalloidin images were merged using Adobe Photoshop 4.0 (Adobe Systems, Inc.).

2.2.6.1 GFP fluorescence imaging and Hoechst staining

Cells carrying genome-integrated GFP fusion proteins (yNM459, yNM555 and yNM574) controlled by the copper-inducible promoter (P_{CUP1-1}) were grown overnight in YPD to mid-log phase at 30 °C, induced with 100 µM $CuSO_4$ for 60 min and visualized by fluorescence and differential interference contrast (DIC) microscopy. Cells carrying the genome-integrated GFP-Kns1 fusion protein (yNM459) were stained with the DNA dye Hoechst 33258 (final concentration 1 µg/ml, Molecular Probes) for 5 min at RT.

Cells expressing GFP-Cmk2, GFP-Kns1 fusion proteins or any of the GFP-tagged phosphorylation mutants under the control of the copper-inducible promoter from high-copy plasmids were grown overnight in synthetic complete media lacking tryptophan (SC-Trp) to log phase at 30 °C, induced with 100 µM $CuSO_4$ for 60 min and visualized by fluorescence and DIC microscopy. Images were acquired within an hour after addition of copper. For GFP-Kns1 localization studies under high pH stress, cells grown overnight in SC-Trp were inoculated into YPD buffered to pH 8 with 100 mM HEPES (YPD/pH 8). After overnight culture to log phase, cells were induced with 100 µM $CuSO_4$ for 60 min and subjected to hyperosmotic stress (1M Sorbitol for 10 min) prior to visualization by fluorescence microscopy.

For GFP-Cmk2 localization studies under hyperosmotic stress, cells grown overnight in SC-Trp were inoculated into rich culture media (YPD). After overnight culture to log phase, cells were induced with 100 µM $CuSO_4$ for 60 min and subjected to hyperosmotic stress (1M Sorbitol for 10 min) prior to visualization by fluorescence microscopy. Overnight growth in YPD prior to the hyperosmotic treatment was done to emulate the conditions used for cells carrying genome-integrated GFP fusion proteins. As growth in selective synthetic medium constitutes a mild stress situation to which cells seem to adapt, cells did not perceive and respond to the hyperosmotic treatment when cultured in SC-Trp as when cultured in YPD.

Cells expressing the GFP-Cps1 fusion protein from episomal plasmid pGO45 (generous gift from Prof. S.D. Emr) were grown overnight to log phase in synthetic complete media lacking uracil (SC-Ura) at 30 °C and directly visualized by fluorescence and differential interference contrast (DIC) microscopy.

2.2.6.2 Quinacrine staining

To assess vacuole acidification *in vivo*, yeast cells were stained with quinacrine essentially as described by Weisman *et al.* (1987)[229]. Wild-type (sUB62), Δ*kns1* (yAS5) and Δ*vma1* (yNM195) cells were grown to early-log phase (1ml, OD_{600} 0.2), harvested by centrifugation at 2000 x*g* and resuspended in 500 µl YPD buffered with 100 mM

Hepes (pH 7.6). Upon addition of quinacrine dihydrochloride to a final concentration of 200 µM, cells were incubated for 5 min protected from light at RT. Subsequently, cells were spun and washed twice with a solution containing 2% glucose buffered with 100 mM Hepes (pH 7.6). Cells were examined immediately under the fluorescence microscope using a fluorescein isothiocyanate (FITC) filter set (<0.2 s exposure time). Images were acquired within 10 min after labelling.

2.2.6.3 Labelling of F-actin with rhodamine-tagged phalloidin

The labeling of filamentous actin with rhodamine-phalloidin was performed following the protocol described by Hasek (2006)[230] with minor modifications. Cells expressing GFP-tagged Cmk2 (yNM555) from the genomic locus and under the control of the copper-iducible promoter (P_{CUP1-1}) were grown to log phase (OD_{600} 0.5) in YPD and induced with 100 µM $CuSO_4$. After 60 min of induction, 900 µl of cell culture was fixed by adding formaldehyde to a final concentration of 3.7% (v/v) and incubated for 10 min at 30 °C with gentle rotation. Cells were washed two times in phosphate buffered saline (PBS) and then resuspended in 20 µl PBS containing 25 % (v/v) methanol, to which 2 µl of Texas Red®-X phalloidin (Molecular Probes, Invitrogen) solution was added (0.2 U/µl in methanol). After a 15 min of incubation in the dark with agitation, cells were washed three times in PBS and visualized under the microscope using a fluorescein isothiocyanate (FITC) filter (L5) for GFP-Cmk2 and a rhodamine B-isothiocyanate (RITC) filter (TX2) for Texas Red Phalloidin-stained actin.

3. Results

3.1 Analysis of the Δkns1 phenotype

3.1.1 Δ*kns1* mutants display high sensitivity to environmental alkaline stress.

Several lines of evidence support a role for Kns1 homologues in signal transducing pathways that respond to environmental stress or external stimuli[28,41,50,59,231]. Thus, to gain insight into the physiological function of Kns1, I set out to determine the phenotype of a yeast strain lacking the *KNS1* gene (Δ*kns1*) under a number of environmental stress conditions. Previous phenotypic analysis performed in our laboratory ruled out oxidative, salt and osmotic stress as limiting growth conditions for Δ*kns1* (data not shown; M. Dahlmann, personal communication). I thus subjected Δ*kns1* cells to other commonly tested restrictive conditions such as growth at high (37° C) or low (16° C) temperatures, at high pH (pH 8) and in medium containing a non-fermentable carbon substrate (Glycerol)[171,232]. The sensitivity of Δ*kns1* to these conditions was assessed by spotting serial dilutions of exponentially growing cells on the different test plates (described in Methods 2.2.2.5). This basic phenotypic analysis revealed that Δ*kns1* cells exhibit remarkable high sensitivity to alkaline pH conditions (pH 8) compared to wild-type cells, indicating the *KNS1* gene is required for optimal growth under high pH stress conditions (Fig. 3.1A). The growth of Δ*kns1* and wild-type cells did not differ in the other conditions tested (Fig. 3.1B). Reduced alkaline tolerance was also observed in a Δ*kns1* mutant isogenic to the reference strain BY4741[171,180,197,210,233], confirming that the alkaline sensitivity phenotype exhibited by Δ*kns1* cells is background-independent *i.e*., not caused by strain-specific heterogeneities (Fig. 3.1C).

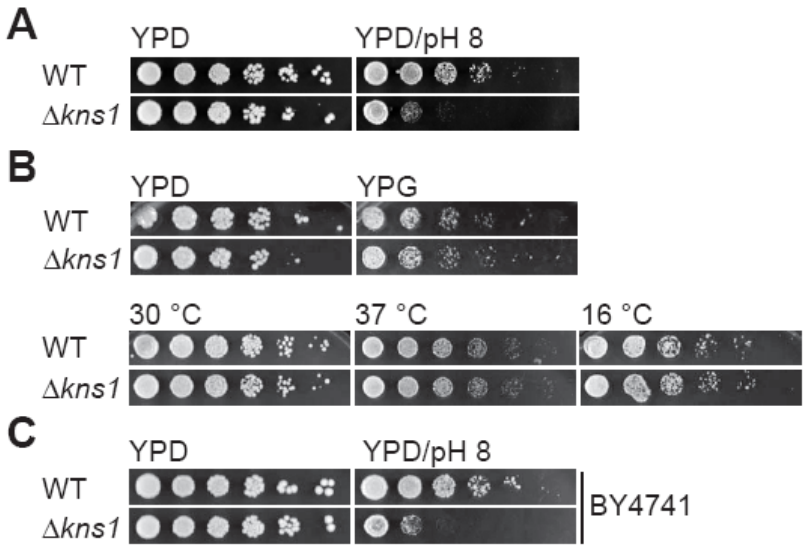

Figure 3.1. The Δ*kns1* deletion mutant strain is highly sensitive to high pH conditions.

(A) Wild-type (WT; sUB62) and Δ*kns1* (yAS5) cells were grown overnight in YPD to mid-log phase at 30 °C, and diluted to an optical density (OD_{600nm}) of 0.25. Five-fold serial dilutions of these diluted cultures were spotted onto rich medium containing glucose (YPD; control, pH ~5.5), YPD containing 100mM Hepes adjusted to pH 8 (YPD/pH 8). (B) WT and Δ*kns1* cells were spotted onto rich medium containing either glucose (YPD; control) or glycerol (YPG) prior wash with medium lacking carbon source (YP). Additionally, cells were spotted in triplicate onto YPD plates, which were incubated either at 30 °C (control), at 37 °C, or 16 °C. (C) WT strain BY4741 and the isogenic Δ*kns1* mutant were grown, diluted and spotted onto YPD (control) and YPD/pH 8 as in (A). Plates were incubated at 30° C for 2 days (controls), for 5 days (YPD/pH) or 3 days (YPG) or at 37 °C or 16 °C for 3 days before photodocumentation. In all cases, the diluted overnight culture (OD_{600nm}=0.25) is shown at the left along with 5-fold serial dilutions going left to right.

To verify that the newly identified alkaline sensitive phenotype of the Δ*kns1* mutant exclusively resulted from the absence of the *KNS1* gene, I tested whether ectopic expression of Kns1 in the Δ*kns1* background restores normal tolerance to high pH conditions. To this end, I first created a plasmid containing the genomic region of *KNS1* (including 1000 bp of the 5'-UTR region followed by the GFP tag and the *KNS1* gene) in an attempt to express Kns1 at endogenous levels; however, I was unable to detect GFP-Kns1 by Western blotting using monoclonal α-GFP antibodies (data not shown). This failure may indicate that either crucial regulatory elements were missing in the cloned 5'-UTR region or that, although less likely, endogenous Kns1 levels were below the detection limit of the Western blot assay. I therefore cloned *KNS1* into a plasmid (2µm) carrying the metallothionein promoter (P_{CUP1-1}) to enable the copper-inducible overexpression of N-terminally GFP-tagged Kns1 (GFP-Kns1) (described in Methods 2.2.3.5)[202,234]. The created vector was then

transformed into the haploid deletion strain Δ*kns1* in order to avoid the effects of endogenous *KNS1* gene product. The copper-induced expression of the GFP-Kns1 fusion protein was verified by Western blotting of yeast cell extracts using α-GFP antibodies (Fig. 3.2A, lane 4). Note that GFP-Kns1 can be observed in the extract prepared from non-induced cells (Fig. 3.2A, lane 3), indicating leaky expression. In addition, increasing the concentration of copper ameliorates, in part, growth at high pH, as it has been suggested to compensate for the reduced solubility this essential metal cation at high pH[172]. For these reasons, alkaline sensitivity was regarded qualitatively as the relative growth of Δ*kns1* cells harbouring the vector alone compared with the growth of Δ*kns1* cells overexpressing GFP-Kns1 on the same plate (supplemented with copper; 100 µM $CuSO_4$).

As shown in fig. 3.2B, overexpression of *GFP-KNS1* restored the growth of Δ*kns1* to wild-type levels in medium buffered to pH 8, thereby demonstrating that the Δ*kns1* phenotype is exclusively caused by the loss of *KNS1*. Furthermore, this result indicates that the fusion protein preserved the biological function of Kns1 *i.e.*, the N-terminal GFP tag did not interfere with the kinase role in conferring alkaline stress tolerance.

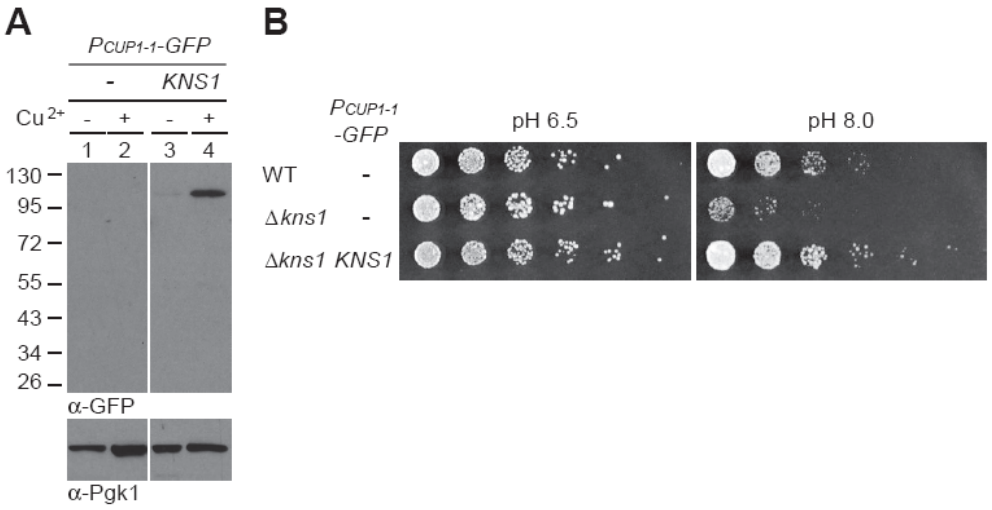

Figure 3.2. Kns1 overexpression suppresses the alkaline sensitivity of Δ*kns1* cells.

(A) Western blot analysis showing copper (Cu^{2+})-induced expression of GFP-Kns1 from a high-copy plasmid in Δ*kns1* cells. Δ*kns1* (yAS5) cells were transformed with either copper-inducible high-copy empty plasmid (P_{CUP1-1}-GFP; pNM67) or plasmid encoding wild-type Kns1 (P_{CUP1-1}-GFP-Kns1; pNM74). Transformants were grown overnight to log-phase in synthetic complete medium (SC-Trp) and then either directly harvested (lanes 1 and 3) or induced with Cu^{2+} (100 µM $CuSO_4$) for 30 min at 30 °C (lanes 2 and 4). Whole-cell extracts were prepared and analysed by SDS-PAGE, followed by Western blotting with α-GFP and α-Pgk1 antibodies as described in Methods 2.2.4. Pgk1 was detected to confirm equal protein loading. Space between lanes corresponds to lanes that have been spliced out.

(B) Wild-type (WT; sUB62) cells harbouring an empty plasmid (pNM67) and Δ*kns1* cells harbouring either empty plasmid (pNM67) or plasmid encoding GFP-Kns1 (pNM74) were grown overnight at 30 °C in SC-Trp to log-phase and diluted to an optical density (OD_{600nm}) of 0.25. Five-fold serial dilutions of this diluted culture were spotted onto either SC-Trp (pH ~6.5) or SC-Trp containing 15 mM Hepes (pH 8.0). All plates were supplemented with 100 µM $CuSO_4$ to induce GFP-Kns1 expression. Cell growth was monitored after incubation at 30 °C for 3 days (pH 6.5) or 6 days (pH 8.0).

3.1.2 Deletion of *KNS1* does not cause global splicing defects in yeast

The best characterized role of LAMMER kinases in higher eukaryotes is the regulation of splicing through the phosphorylation of serine/arginine (SR)-rich splicing factors[37,39,48,51,52]. Kns1 has been reported to phosphorylate and interact with mammalian SR proteins[34]. Although the budding yeast does not seem to possess genuine SR proteins, it does have SR-like proteins implicated in splicing[95,235]. For this reason, I contemplated the possibility of Kns1 being involved in splicing in the budding yeast. Unspliced pre-mRNAs are generally targeted for degradation to prevent their translation into non-functional or truncated proteins[236–238]. Thus, if Kns1 were required for efficient splicing, the increased alkaline sensitivity of Δ*kns1* cells could be explained by the inefficient splicing of pre-mRNAs encoding proteins essential for normal alkaline tolerance as *e.g.*, the subunit of the vacuolar proton pump (V-ATPase) Vma10*,* whose absence hinders growth at pH 7.5[239]. A similar scenario in which failure to splice a particular transcript causes pleiotropic effects on other processes has been previously reported[240]. Loss of factors required for splicing typically leads to the accumulation of unspliced mRNA[241,242]. To test whether Kns1 is necessary for effective pre-mRNA splicing, I determined the relative levels of spliced and unspliced mRNA in Δ*kns1* cells. For this, I performed a reverse-transcriptase PCR (RT-PCR) on total RNA purified from Δ*kns1* and wild-type (WT) using intron-flanking oligonucleotides (described in Methods 2.2.3.6 and 2.2.2.9). The gene transcripts assayed included *VMA10,* along with *SNC1* and *SEC27*, which were arbitrarily chosen, and commonly tested transcripts *ACT1*, *ARP2* and *TUB1*[243–245]. The oligonucleotides used in the RT-PCR were designed to hybridize with the two exons encompassing the intron to differentiate pre-mRNA (unspliced) from the mature mRNA (spliced) (Fig. 3.3A). I included the KL-1 mutant strain (kindly provided by Prof. J.D. Beggs) in the assay as the positive control strain for splicing defects[199]. In this strain, the expression of the essential *PRP8* gene, which encodes a crucial component of the U4/U6-U5 snRNP complex required for

splicing[246], is strongly repressed by the galactose promoter (P_{GAL1}) in glucose medium. KL1 cells display reduced splicing activity when grown in glucose medium and are still viable due to the ectopic expression of a truncated Prp8 form that is inefficiently transported to the nucleus[199]. As shown in fig. 3.3B, the predominant mRNA species in Δ*kns1* and WT cells was spliced mRNA. KL-1 mutant cells showed greater accumulation of unspliced pre-mRNA than WT, being the unspliced form predominant in most cases (Fig. 3.3B), as expected[199]. This result indicates that loss of *KNS1* does not affect the splicing efficiency of the transcripts assessed *i.e.*, it does not cause a global splicing defect.

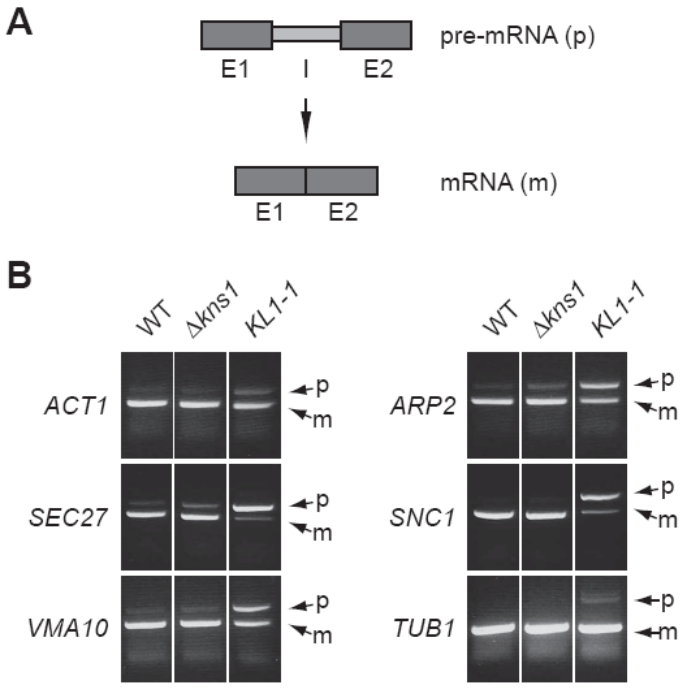

Figure 3.3. Deletion of *KNS1* does not globally affect pre-mRNA splicing in yeast.

(A) Schematic representation of pre-mRNA (unspliced) and mature mRNA (spliced). Oligonucleotides for the RT-PCR reaction were designed to hybridize with the two exons (E1 and E2) encompassing the intron (I) of each of the gene transcripts assessed in (B). (B) Δ*kns1* cells efficiently splice the pre-mRNA of reporter transcripts. The splicing-defective mutant (KL1-1) showed greater accumulation of pre-mRNA than WT, as expected[199]. Total RNA was prepared from wild-type (WT; sUB62), Δ*kns1* (yAS5) and KL1-1 as described in Methods 2.2.2.9. RT-PCR reactions were carried out as described in Methods 2.2.3.6. cDNA from the reverse transcriptase (RT) reaction was used as template in PCR reactions with the appropriate intron-flanking oligonucleotide set for the following genes *ACT1*, *ARP1*, *VMA10*, *SNC1*, *SEC27* and *TUB1*. PCR products were resolved on 2% agarose gels and stained with ethidium bromide. Bands representing the PCR products corresponding to the mature mRNA (m) and pre-mRNA (p) are indicated by arrows.

3.1.3 Δ*kns1* cells do not display vacuolar acidification defects

Disruption of genes encoding V-ATPase subunits or regulators typically leads to hypersensitivity to alkaline stress[180,182,188,239,247]. Importantly, the subunit A of the V-ATPase (Vma1/Tfp1) has been reported to co-purify with Kns1 in a large-scale co-immunoprecipitation study[80,248], suggesting the possible association of both proteins *in vivo*. This prompted me to speculate that Kns1 could be linked to V-ATPase function. Thus, if Kns1 were required for proper V-ATPase function, loss of *KNS1* could conceivably elicit defects in vacuolar acidification, thereby explaining the Δ*kns1* phenotype. To investigate this possibility, I assessed whether Δ*kns1* cells were defective in vacuolar acidification using the quinacrine uptake assay (described in Methods 2.2.6.2). Quinacrine is a fluorescent weak base that diffuses freely through membranes and accumulates upon protonation within the acidic vacuolar compartment[229,249]. Cells lacking the *VMA1* gene (Δ*vma1*) showed a complete absence of quinacrine staining (Fig. 3.4B), which has been shown to correlate with loss of V-ATPase-mediated acidification, and the inability to grow at pH 8 characteristic of the *vma* mutants (Fig. 3.4A) [184,188,250]. Δ*kns1* cells showed a severe growth defect at pH 8 (Fig. 3.4A). However, the vacuoles of Δ*kns1* cells, like those of WT cells, were notably stained with quinacrine, indicating that they were properly acidified. This result shows that Δ*kns1* cells do not display notable vacuolar acidification defects.

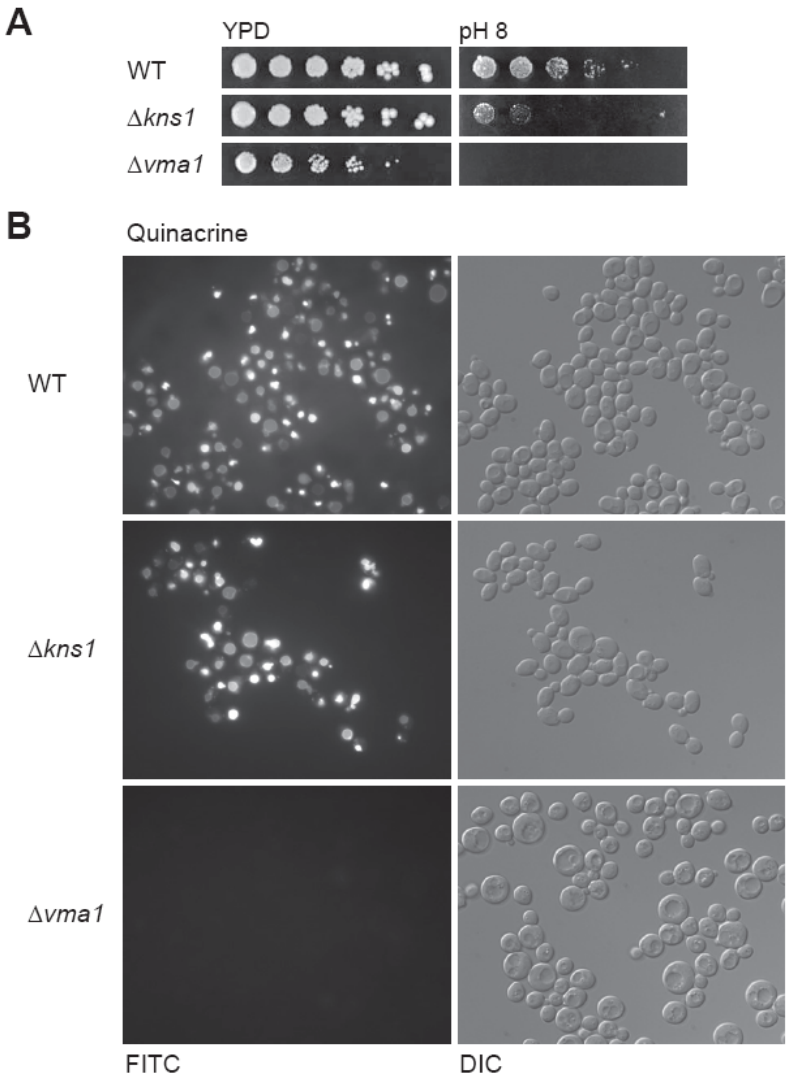

Figure 3.4. The Δ*kns1* mutant displays high pH sensitivity comparable to Δ*vma1* mutant but does not exhibit vacuolar acidification.

(A) Wild-type (WT; sUB62), Δ*kns1* (yAS5) and Δ*vma1* (yNM195) cells were grown overnight in YPD to mid-log phase at 30 °C and diluted to an optical density (OD_{600nm}) of 0.25. Five-fold serial dilutions of this diluted culture were spotted onto rich medium containing glucose (YPD; pH~5.5, control plate), YPD containing 100mM Hepes adjusted to pH 8 (pH 8). Cell growth was monitored after incubation at 30 °C for 2 days (YPD) or 5 days (high pH). (B) The same strains as in (A) were grown to mid-log phase in YPD at 30°C and stained with quinacrine prior to visualization by fluorescence microscopy. WT and Δ*kns1* cells showed notable and equivalent quinacrine staining, whereas no quinacrine staining could be detected in Δ*vma1* cells. Cells were first located under differential-interference contrast (DIC) optics and then visualized under a fluorescein isothiocyanate (FITC) filter with a 100x objective to examine vacuolar staining with quinacrine.

3.1.4 Δ*kns1* cells are not impaired in vacuolar protein transport

I next sought to investigate which underlying defects could cause impaired growth at high pH without affecting vacuolar acidification in the Δ*kns1* mutant. Efficient sorting of vesicles and proteins to the vacuole is sensitive to changes in organelle acidification; therefore, it is particularly compromised under alkaline conditions[251–253]. Conversely, alterations in the vacuolar protein sorting (VPS) system greatly impinge upon alkaline tolerance, as manifested by the finding that many mutants defective in this process *e.g., vps* mutants, display remarkable sensitivity to high pH stress conditions[171,172,188]. To test whether the alkaline sensitivity of Δ*kns1* cells correlates with an underlying failure in vacuolar protein sorting, I examined the delivery of hydrolase carboxypeptidase S (Cps1) via the CPY pathway to the vacuole. The inactive precursor of CPS (pCps1) is a type II integral membrane protein that traverses through the endoplasmic reticulum (ER) and Golgi apparatus to the late endosomal compartment, also termed multivesicular body (MVB), where it is selectively sorted into intralumenal vesicles (reviewed in [254]). Upon fusion of the matured MVB with the vacuole, lumenal vacuolar hydrolases cleave pCps from its transmembrane anchor to form the active and mature CPS form (mCps1) (Fig. 3.5A)[255]. The transport of Cps1 into the vacuolar lumen can be readily monitored by fluorescence microscopy using N-terminally GFP-tagged Cps1, which is a well-established model cargo protein of the VPS/MVB pathway[203,256]. I therefore transformed wild-type and Δ*kns1* cells, as well as Δ*vps23* cells, which served as a positive control for VPS defects, with an high-copy plasmid coding for the GFP-Cps1 fusion protein (a generous gift from Prof. S.D. Emr)[203]. The Δ*vps23* mutant lacks an essential component of the ESCRT-I complex, the endosomal sorting complex required for transport of cargo into the MVBs[256]. This causes the accumulation of cargo proteins destined for the vacuole in an aberrant endosomal compartment termed the class E compartment[256]. Wild-type and Δ*kns1* cells showed GFP fluorescence within the vacuole, indicating that the vesicles containing GFP-Cps1 were adequately transported into the lumenal space (Fig. 3.5B). By contrast, the GFP fluorescence in Δ*vps23* mutants was mainly localized to the vacuolar membrane and in vesicle-like structures adjacent to the vacuole, which were reminiscent of the class E compartment (Fig. 3.5B, indicated by arrows).

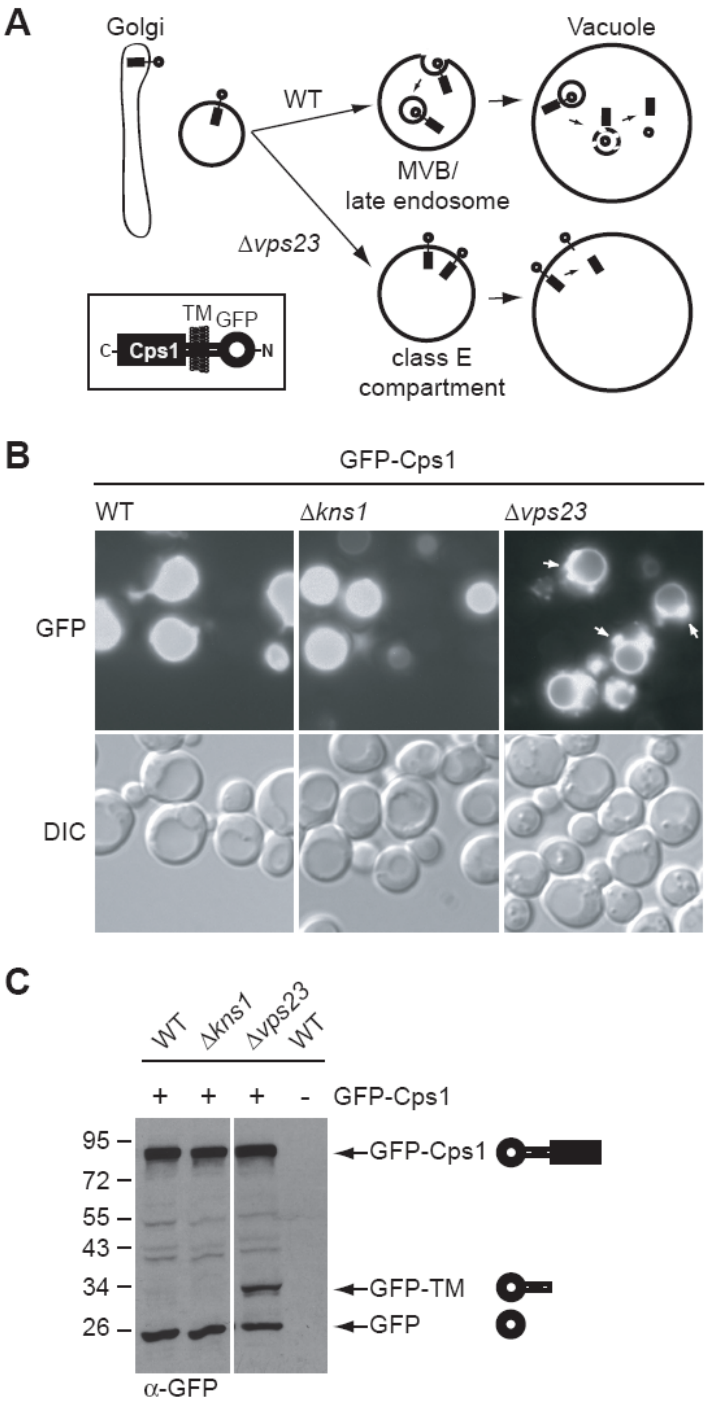

Figure 3.5. The Δkns1 mutant does not exhibit defects in the vacuolar sorting of Cps1.

(A) Schematic depiction of the vacuolar sorting of N-terminally GFP-tagged Cps1 (carboxypeptidase S). GFP-Cps1 traverses the Golgi to the multivesicular body (MVB)/late endosome with the GFP moiety facing the cytosol. In wild-type (WT) cells, GFP-Cps1 is efficiently sorted into MVB intralumenal vesicles and delivered to the vacuolar lumen. In the class E vacuolar protein sorting (*vps*) mutant Δ*vps23,* sorting of cargo into intralumenal vesicles is impaired; hence, upon MVB-vacuolar fusion, GFP-Cps1 remains on the vacuolar membrane with GFP facing the cytosol. TM, transmembrane region of Cps1. Adapted from Katzmann *et al*. 2001[256]. (B) Localization of GFP-Cps1 in WT (sUB62), Δ*kns1* (yAS5) and Δ*vps23* (yBM87) cells. Like WT, Δ*kns1* cells show GFP fluorescence in the vacuolar

lumen, indicating effective GFP-Cps1 vacuolar sorting. Δ*vps23* cells show GFP signal accumulation at the vacuolar membrane and vesicle-like structures adjacent to the vacuole. WT, Δ*kns1* and Δ*vps23* cells expressing GFP-Cps1 from a high-copy plasmid (pGO45) were grown overnight to mid-log phase in liquid SC-Ura at 30 °C and visualized by fluorescence and DIC microscopy. Arrows indicate presumptive class E compartments. (C) Western blot of whole protein extracts from WT, Δ*kns1* and Δ*vps23* cells expressing GFP-Cps1. Whole-cell lysates were prepared and analysed by SDS-PAGE, followed by Western blotting with anti-GFP antibodies. Space between lanes corresponds to lanes that have been spliced out.

Efficient GFP-Cps1 vacuolar delivery in Δ*kns1* cells was further confirmed through the analysis of GFP-Cps1 proteolytic processing. Both full-length GFP-Cps1 (~91 KDa) and free GFP (~27 KDa) were detected in whole-cell protein extracts from wild-type and Δ*kns1* cells expressing GFP-Cps1 (Fig. 3.5C) by Western blotting using α-GFP antibodies. This indicates that GFP-Cps1 reached the vacuolar lumen and was subject to protease-dependent cleavage. In class E *vps* mutants, most of GFP-Cps1 accumulates at the vacuolar membrane with the GFP-tag facing the cytoplasm[203,256]. As a result, vacuolar proteases are unable to process the part of the protein fusion containing the transmembrane domain (TM) and the GFP-tag[203,256]. Therefore, an additional band with the approximate molecular weight of the GFP-TM fusion of GFP-Cps1 (~31 KDa) was detected in Δ*vps23* whole-cell extracts (Fig. 3.5C). Altogether, these data show that Δ*kns1* efficiently transports GFP-Cps1 to the vacuole, ruling out an impairment of the VPS system, in particular, of the CPY/MVB pathway, as the underlying defect responsible for its alkaline sensitive phenotype.

3.2 Analysis of the intracellular localization of Kns1

Determination of protein localization is an important step towards the understanding of the biological function of a protein. In the case of protein kinases, subcellular distribution represents an additional level of regulation, which affects substrate specificity[14,257]. Therefore, to obtain further insight into the function of Kns1, I examined the subcellular localization of GFP-Kns1 by fluorescence microscopy in living cells.

3.2.1 Kns1 localizes predominantly to the nucleus

To visualize Kns1 expressed at endogenous levels, I inserted the GFP-tag at the C-terminus of the *KNS1* genomic locus (*KNS1-GFP*). Yet, endogenously expressed Kns1-GFP did not yield detectable fluorescence signal (data not shown). For this reason, I created cells overexpressing genomic N-terminally GFP-tagged Kns1 (GFP-Kns1) under the control of the copper-inducible metallothionein promoter (P_{CUP1-1}) (described in Methods 2.2.2.3). The P_{CUP1-1} promoter was introduced upstream of the *KNS1* locus to allow culturing cells in rich media, which is a more physiological, less stress-inducing condition than nutrient-limiting synthetic media. As shown in fig. 3. 6, GFP-Kns1 was predominantly localized within the nucleus, as indicated by its colocalization with the DNA-dye Hoechst-33258. GFP-Kns1 was also found uniformly distributed throughout the cytoplasm.

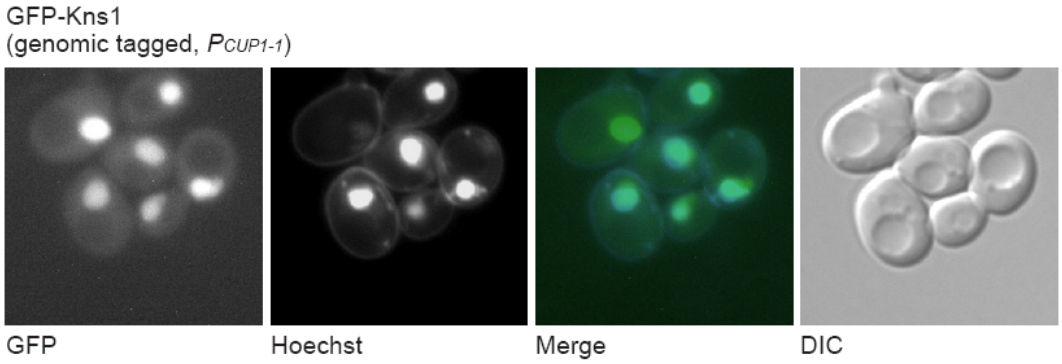

Figure 3.6. Analysis of the localization of genomic tagged GFP-Kns1 shows predominant nuclear localization.

Genomic Kns1 tagged with GFP at its N-terminus (GFP-Kns1) and expressed under the control of the copper-inducible P_{CUP1-1} promoter localizes predominantly to the nucleus, as shown by colocalization with the Hoechst stain. Cells carrying the genome-integrated GFP-Kns1 fusion protein (yNM459) were grown overnight in YPD to mid-log phase at 30 °C and induced with copper (100 µM $CuSO_4$) for 60 min. Cells were then stained with a DNA dye (Hoechst 33258) for 5 min and visualized by fluorescence and differential interference contrast (DIC) microscopy. Fluorescence at the cell periphery in the Hoechst panels is an occasional artefact of the Hoechst staining procedure. Merge indicates the fusion between the GFP (green) and Hoechst (blue) fluorescence images.

3.3 Identification of the in vitro autophosphorylation sites in Kns1

Autophosphorylation constitutes a regulatory mechanism of fundamental importance in protein kinases[258]. Therefore, the identification of the sites of autophosphorylation and elucidation of their role is crucial to define the molecular mechanisms involved in kinase function and regulation. Previous studies using phosphoamino acid analysis have shown that a recombinant truncated form of Kns1 autophosphorylates on Ser, Thr and Tyr residues *in vitro*[33]. The evolutionary conservation of dual-specificity in Kns1 suggests a relevant biological role. However, the identity of the autophosphorylated residue(s) on Kns1 remains unknown. To gain insight into Kns1 autoregulation and obtain direct evidence for dual amino acid specificity, I set out to determine the *in vitro* site(s) of Kns1 autophosphorylation through the analysis of recombinant full-length Kns1 by mass spectrometry.

3.3.1 Expression and purification of recombinant full-length GST-Kns1 in *E.coli*

Attempts in the past to purify recombinant full-length Kns1 have either yielded minimal amounts of intact protein along with several degradation products or failed completely[33,34]. Therefore, most of the biochemical studies on Kns1 have been performed using truncated forms of Kns1 consisting solely of either the non-catalytic or the catalytic domain[33,34]. So far, full-length Kns1 has been only be purified as an N-terminal GST-fusion protein at a small scale for use in proteome microarrays[102,259]. In the present work, I set out to produce full-length GST-Kns1 in a larger scale to perform in-solution *in vitro* kinase assays. To this end, I cloned Kns1 into plasmid pGEX-2TK and undertook the optimization of its expression in *E. coli* (described in Methods 2.2.1.3). When the expression of the enzyme was induced at 37 °C, the vast majority of the protein appeared in the insoluble fraction, probably forming inclusion bodies. Lowering the culture temperature reduces the growth and translation rate of bacteria, which improves recombinant protein folding and, in turn, decreases inclusion body formation[260–262]. Therefore, induction of GST-Kns1 expression was performed at a lower temperature (16 °C), resulting in an increase in solubility. Additionally, bacterial cell lysates were incubated after sonication with the non-ionic detergent Triton® X-100 (1%) for 1 h. This step was included to help

solubilization of the exposed hydrophobic surfaces of the protein and remove major contaminants, such as lipid and membrane-associated proteins as well as *E. coli* cell wall material[263].

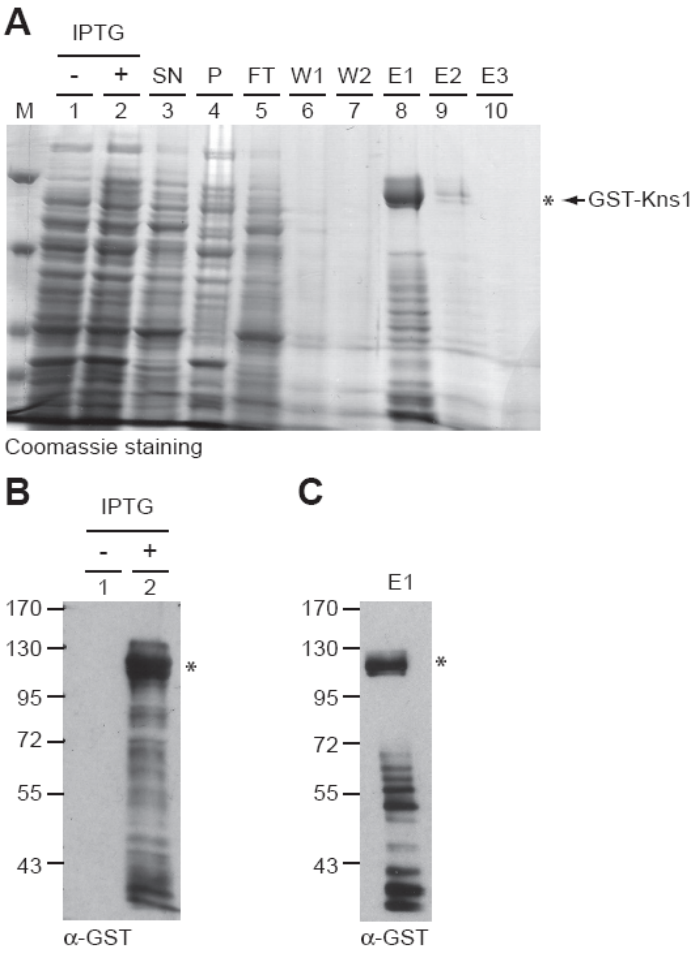

Figure 3.7. Optimized procedure for the purification of full-length GST-Kns1 from *E. coli*.

(A) Purification of GST-Kns1. The recombinant GST-Kns1 protein was purified by glutathione-affinity chromatography as described in Methods 2.2.1.3. Aliquots from indicated steps of the purification protocol were subjected to SDS-PAGE on a 8% polyacrylamide gel followed by Coomassie brilliant blue R250 staining. Lane M; molecular weight marker, lane 1; before IPTG induction, lane 2; after 4h IPTG induction, lane 3; Supernatant, lane 4; Pellet, lane 5; Flow through, lane 6; Wash 1, lane 7; Wash 2, lane 8; Eluate (E) 1, lane 9; Eluate 2, and lane 10; Eluate 3. (B) Western blot analysis with the α-GST antibody of a bacterial cell fraction before (1) and after (2) IPTG induction of GST-Kns1 expression. (C) Western blot analysis with the α-GST antibody of E1 from (A).

An example of the optimized purification of GST-Kns1 is shown in fig. 3.7A. A protein band with the predicted molecular mass of GST-Kns1 (calculated Mr 108 kDa) was detected in the IPTG-induced cell extract (Fig. 3.7B, lane 2) but not in the non-induced cell extract (Fig. 3.7B, lane 1) by Western blotting using α-GST

antibodies, confirming specific IPTG-induction of GST-Kns1. After affinity purification using glutathione Sepharose™ 4B beads, the presence of full-length GST-Kns1 was clearly visible in eluted fractions (E1-3) on Coomassie blue-stained gels (Fig. 3.7A, lanes 8, 9 and 10). Although the full-length protein was the predominant protein species, several low molecular weight proteins were also recovered in the eluate fractions. These proteins appeared to be degradation products of GST-Kns1, as a similar band pattern was detected in the eluate fraction (E1) by Western blotting using α-GST antibodies (Fig. 3.7C). Many of these bands were detected by Western blotting of the IPTG-induced cell fraction removed before the purification procedure, suggesting that most degradation occurred during expression in bacteria (Fig. 3.7B, lane 2).

Previous studies have shown that recombinantly expressed Kns1 exhibits constitutive autophosphorylation activity[33,34]. To test whether the catalytic activity of GST-Kns1 was preserved throughout the purification procedure, I performed an *in vitro* kinase assay to test for autophosphorylation activity (described in Methods 2.2.4.5). Incubation of purified GST-Kns1 in the presence of radiolabed ATP ([γ-^{32}P]-ATP) led to the incorporation of phosphate ([γ-^{32}P]) into GST-Kns1. Phosphorylated GST-Kns1 was detected after resolution of the reaction mixture on SDS-PAGE gels and subsequent autoradiography (Fig. 3.8B, lane 1). This result indicates that the purified enzyme was capable of efficient autophosphorylation, demonstrating intact kinase functionality.

To confirm that GST-Kns1 phosphorylation was solely due to the intrinsic catalytic activity of Kns1, I created a catalytically inactive version of GST-Kns1. For this, I replaced the catalytic base of Kns1 to Ala. The catalytic base is an invariant residue found in the catalytic loop of all protein kinases that is crucial for phosphoryl-transfer and active site conformation[5,264–268]. Mutation of this residue to Ala has been extensively proved to dramatically decrease catalytic activity[102,269–271]. Sequence alignment of the catalytic loops of Kns1 and the prototypical protein kinase A of yeast (Tpk1) and human (PKA) indicated that residue Asp^{440} of Kns1 is the equivalent to the catalytic base of Tpk1 (Asp^{210}) and PKA (Asp^{166}) (Fig. 3.8A)[44,270]. Western blot analysis showed that mutant GST-Kns1^{D440A} migrated slightly faster than wild-type GST-Kns1, probably due to the lack of autophosphorylation (Fig. 3.8B, lane 2, middle panel). The absence of detectable autophosphorylation activity in the reaction mixture containing mutant GST-Kns1^{D440A} demonstrated effective kinase inactivation (Fig. 3.8B, lane 2, upper panel). Furthermore, it confirmed that the incorporation of phosphate [γ-^{32}P] into wild-type GST-Kns1 was the result of

autocatalysis and not due to the catalytic activity of contaminating or copurifying proteins.

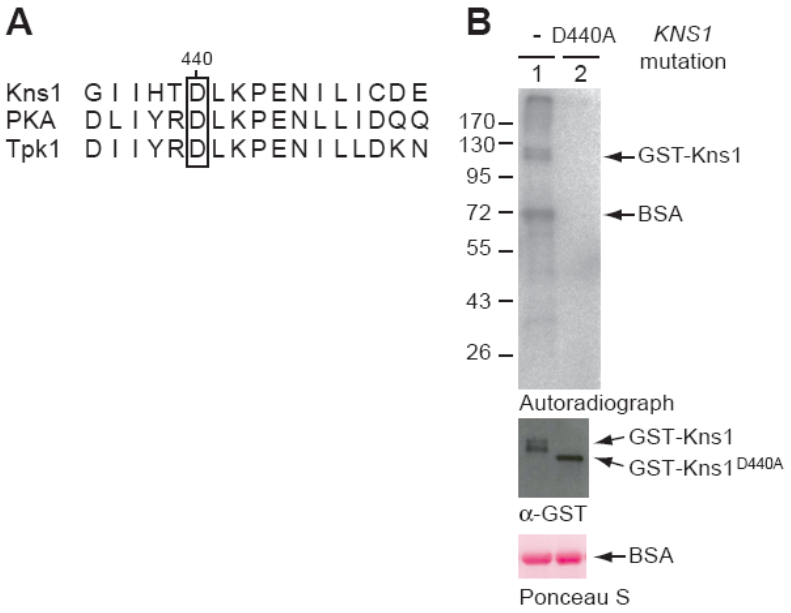

Figure 3.8. Mutation of the catalytic site (D440A) effectively abolishes Kns1 catalytic activity.

(A) Sequence alignment of the catalytic loop of *S.cerevisiae* (Kns1) LAMMER kinase and *H.sapiens* (PKA) and *S.cerevisiae* (Tpk1) Protein kinase A kinases identified Asp^{440} as the presumptive catalytic base of Kns1 (B) *In vitro* autophosphorylating activities of wild-type GST-Kns1 and GST-$Kns1^{D440A}$ mutant. Recombinantly expressed and purified wild-type (WT) GST-Kns1 (1) and GST-$Kns1^{D440A}$ mutant (2) were incubated with [γ-^{32}P]ATP in phosphorylation buffer (25 mM Tris pH 7.5, 10 mM $MgCl_2$, 1 mM DTT) for 15 min at 30 °C and then subjected to SDS-PAGE. BSA was included in the phosphorylation reactions as a unspecific phosphate-acceptor competitor (0.2 µg/µl). Reactions were stopped by addition of Laemmli sample buffer and immediate boiling for 5 min, followed by SDS-PAGE and autoradiography. Upper pannel: ^{32}P autoradiograph, Middle panel: α-GST WB, Bottom panel: Ponceau S staining. The migration positions of molecular mass marker proteins are indicated in kilodaltons (kDa).

3.3.2 Autophosphorylation sites in Kns1

To identify Kns1 autophosphorylation sites, an *in vitro* kinase assay was performed by incubating recombinant wild-type GST-Kns1 with non-radiolabeled ATP (described in Methods 2.2.4.6). Briefly, upon incubation with ATP, the *in vitro* kinase reaction mixture was resolved by SDS-PAGE followed by Coomassie blue staining. The protein band containing full-length GST-Kns1 was excised and digested in-gel with trypsin. Subsequent analysis by mass spectrometry (MS) of the resulting peptides was performed by Dr. Gunnar Dittmar (Head of the Mass Spectrometry Core Facility, Max Delbrück Centrum).

In total, nine Kns1 phosphorylation sites were identified (Table 3.1). Six phosphorylation sites, Thr^{34}, Ser^{57} Thr^{183} Ser^{198} and Thr^{217}, are found distributed along the non-catalytic N-terminal domain (Fig. 3.9A). The three remaining phosphorylation sites are found within the catalytic domain (Fig. 3.9A). Concretely, Thr^{562} is situated within the LAMMER motif, in subdomain X (Fig. 3.9B). Ser^{583} and Ser^{601} are found within the insertions of unknown function between subdomain X and XI, which are characteristic of LAMMER kinases and other members of the CMGC group of protein kinases[5].

Two *in vitro* kinase reactions that served as negative controls were additionally performed and analysed in parallel with the aforementioned reaction: one containing the inactive mutant GST-$Kns1^{D440A}$ and one containing wild-type GST-Kns1 devoid of ATP. No phosphopeptides were detected in these reactions (G. Dittmar, personal communication), which indicates that GST-Kns1 did not undergo autophosphorylation during expression in *E. coli*.

Table 3.1. Phosphopeptides containing the phosphorylation sites identified *in vitro* on Kns1 by mass spectrometry.

Phosphopeptide			
Position	**Sequence[1]**	**Phospho Site**	**Times mapped *in vitro*[2]**
34-43	**T**FLDNFEETR	T34	2
55-64	QN**S**FLTDNLR	S57	2
183-193	**T**ISLPQLPLSK	T183	3
181-193	QRTI**S**LPQLPLSK	S185	3
194-213	LSYQ**S**NYFNVPDQTNAIVPR	S198	1
216-232	V**T**QTENELLHLTGSCAK	T217	2
559-571	ING**T**PFPTDIIDK	T562	2
580-593	LGN**S**PSDLNSTVIK	S583	1
599-607	TL**S**LQWPEK	S601	1

[1]Phosphorylation sites are presented as bold, underlined characters. [2]Indicates the number of independently prepared phosphoprotein-enriched samples that produced spectra matching this phosphopeptide sequence.

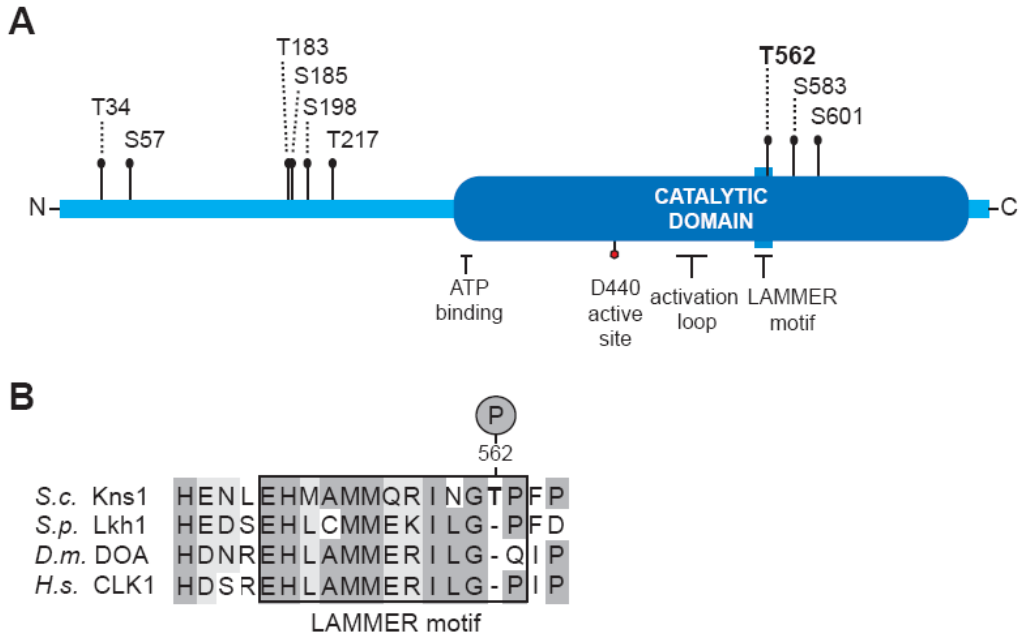

Figure 3.9. Schematic diagram of the *in vitro* autophosphorylation sites identified on Kns1.

(A) The sites of phosphorylation in Kns1 identified by mass spectrometry from the analysis of *in vitro* autophosphorylated GST-Kns1 are indicated by black pins, with residue type and number indicated above. The red pin within the catalytic domain denotes the position of the active site (D440). The phosphorylation site located within the LAMMER motif, T562, is shown in *bold.* The diagram was generated using *MyDomains* from PROSITE (http://us.expasy.org/tools/mydomains) and adapted. (B) Alignment of the sequences containing the LAMMER motif of Kns1 (*S. cerevisiae*), Lkh1/Kic1 (*S. pombe*), DOA (*D. melanogaster*) and CLK1 (*H. sapiens*) (adapted from Tang *et al*. 2002)[74]. The LAMMER motif is marked by a black box. Conserved amino acid residues are highlighted in dark grey and similar residues in light grey.

To graphically visualize the general preferences of Kns1 for specific residues surrounding the identified autophosphorylation sites, I generated a sequence logo from the multiple alignment of the sequences surrounding these sites (Figure 3.10). In this logo, the residues are represented by their one-letter code. Letters are stacked in decreasing order of predominance and their height indicates the relative frequency of a residue at a particular position[272]. On the basis of the type of residues found on top of the stacks at these positions and taking into account that kinases are generally most selective at the P-3 position, followed by the P-2 and P+1 positions[273], it can be inferred that Kns1 prefers basic residues at position P-4 and P-3 (*e.g.* Arg and Lys), an uncharged polar environment at the P-2 position (*e.g.* Asn, Gln and Thr) and hydrophobic residues at the P+1 position (*e.g.* Phe, Leu and Pro).

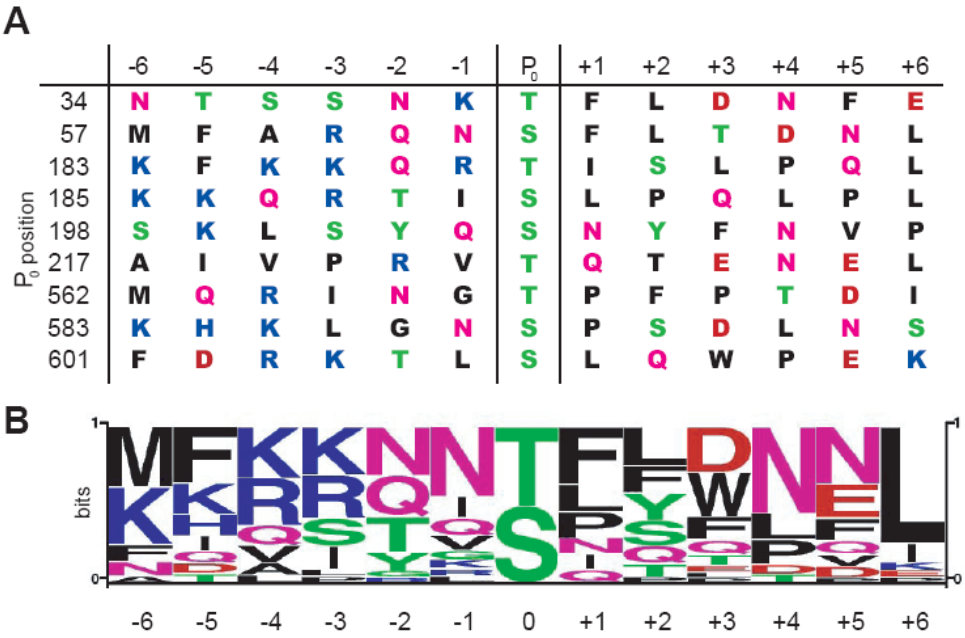

Figure 3.10. Kns1 *in vitro* autophosphorylation site sequence logo.

(A) Multiple alignment of the sequences containing the nine *in vitro* autophosphorylation sites found in Kns1. Sequences were aligned by the autophosphorylated residue (designated as P_0). The residues on the N-terminal side are assigned negative numbers and those on the C-terminal side positive numbers. (B) The Kns1 logo was generated using the multiple sequence alignment shown in A and the *PSP Logo Generator* from http://www.phosphosite.org/homeAction.do. The numbers along the abscissa indicate the position of the residues relative to P_0 within the sequence. The ordinates are in units of bits and are indicative of the information content at each position[272,274]. Residues are represented by their one-letter abbreviations and arranged from top to bottom within stacks, with the highest-frequency residue being on top of the stack and letter height being proportional to the relative frequency of the residue at a particular position[272,274]. Amino acid colour code: basic (blue), acidic (red), polar uncharged non-phosphorylatable (pink), phosphorylatable (polar uncharged or hydrophopic; green) and hydrophobic non-phosphorylatable (black).

3.4 Mutational analysis of Kns1

Among the identified autophosphorylation sites found in this study, residue Thr[562] is one of the most intriguing owing to its proximity in the amino acid sequence to the LAMMER motif of Kns1 (EHMAMMQRING**T**[562]) (Fig. 3.9B). The orientation of Thr[562] in the tridimensional structure of Kns1 is unknown; however, the close proximity of Thr[562] to the LAMMER motif hints at a potential implication of Thr[562] phosphorylation on the role of this signature motif in Kns1 regulation. Mutational analysis of the fission yeast (Lkh1) and tobacco plant (PK12) homologues of Kns1 revealed that their LAMMER motif is required for catalytic activity *in vitro*[45–47]. Although the role of the LAMMER motif in other family members has not yet been explored, the preservation of this unique motif across evolutionarily divergent

species insinuates that its function might be conserved. In order to evaluate the relevance of Thr^{562} phosphorylation in Kns1, I replaced Thr^{562} with the non-phosphorylatable residue Ala (T562A) and analysed the catalytic activity, *in vivo* performance and subcellular localization of the resulting mutant ($Kns1^{T562A}$). Furthermore, I analysed the behaviour of the catalytically inactive Kns1 mutant ($Kns1^{D440A}$) in parallel to assess the contribution of the catalytic activity to the biological function of Kns1.

3.4.1 Effect of the Thr^{562} mutation on the intrinsic catalytic activity of Kns1

To test whether loss of phosphorylation site Thr^{562} affects Kns1 catalytic activity, I examined the ability of recombinantly expressed GST-$Kns1^{T562A}$ to autophosphorylate *in vitro*. The autoradiograph of *in vitro* autophosphorylated wild-type GST-Kns1 and mutant GST-$Kns1^{T562A}$ showed similar levels of phosphate [γ-^{32}P] incorporation in both protein species (Fig. 3.11A). This result shows that the T562A mutation does not noticeably impair Kns1 autophosphorylation, which indicates that residue Thr^{562} is not required for intrinsic catalytic activity *in vitro*.

3.4.2 Effects of catalytic inactivation and Thr^{562} mutation on the role of Kns1 in alkaline tolerance modulation.

To explore whether catalytic inactivating D440A or phosphorylation site T562A mutation affects Kns1 function *in vivo*, I examined to what extent overexpression of GFP-$Kns1^{D440A}$ or GFP- $Kns1^{T562A}$ rescues the growth defect of Δ*kns1* cells in plates buffered to pH 7.8, 8.0 or 8.2 (Fig. 3.11C). The correct expression of GFP-$Kns1^{T562A}$ and GFP-$Kns1^{D440A}$ mutants in yeast was confirmed by Western blot analysis using α-GFP antibodies. As shown in fig. 3.11B, total protein levels of GFP-$Kns1^{T562A}$ and GFP-$Kns1^{D440A}$ were similar to wild-type GFP-Kns1 levels in Δ*kns1* cells under standard conditions. This indicates that neither of the mutations seems to decrease kinase stability.

3.4.2.1 Catalytically inactive Kns1 fails to confer tolerance to mild-alkaline stress but favours growth at higher alkaline stress conditions.

In medium at pH 7.8, Δ*kns1* cells overexpressing active kinase GFP-Kns1 grew considerably better than Δ*kns1* cells overexpressing inactive mutant GFP-Kns1^{D440A}, suggesting that catalytic activity is necessary for Kns1 to increase alkaline tolerance at this external pH (Fig. 3.11C). The fact that Δ*kns1* cells were not compromised at pH 7.8 *i.e.*, grew like wild-type cells (carrying an empty vector), indicates that Kns1 is still dispensable for growth under these conditions (hereafter termed mild-alkaline stress) (Fig. 3.11C). In medium at pH 8, GFP-Kns1^{D440A} had the ability to partially rescue the growth of Δ*kns1* cells *i.e.*, it did not rescue growth to the same extent as the active kinase but to a greater extent than the empty vector (Fig. 3.11C). This result implies that the non-catalytic properties of Kns1 also participate in conferring tolerance to high pH stress. Remarkably, Δ*kns1* cells overexpressing inactive GFP-Kns1^{D440A} displayed greater alkaline tolerance than Δ*kns1* cells overexpressing GFP-Kns1 at pH 8.2 (Fig. 3.11C). This result shows that catalytically inactive Kns1, as opposed to active Kns1, becomes more proficient in promoting growth as external alkalinity increases. In summary, these findings reveal that catalytic and non-catalytic properties of Kns1 positively contribute to the kinase role in sustaining cell growth at high pH conditions.

3.4.2.2 Mutation T562A notably impinges upon Kns1 function in vivo

Although the T562A mutation did not affect the autocatalytic activity of Kns1 *in vitro* (Fig. 3.11A), the possibility of this mutation impairing autocatalytic activity or catalytic activity towards exogenous substrates of Kns1 *in vivo* cannot yet be excluded. I hypothesized that if phosphorylation site Thr^{562} were required for Kns1 catalytic activity *in vivo*, the replacement of Thr^{562} with Ala should yield a Kns1 mutant (GFP-Kns1^{T562A}) that behaves like the inactive kinase (GFP-Kns1^{D440A}) during alkaline stress. In medium at pH 7.8, Δ*kns1* cells overexpressing GFP-Kns1^{T562A} grew like Δ*kns1* cells overexpressing GFP-Kns1^{D440A}, indicating that both Kns1 mutants lack the ability of the active kinase to increase alkaline tolerance at pH 7.8 (Fig. 3.11C). Remarkably, Δ*kns1* cells overexpressing GFP-Kns1^{T562A} exhibited a greater growth defect than Δ*kns1* cells overexpressing GFP-Kns1^{D440A} in medium at pH 8, thus mimicking the growth behaviour of Δ*kns1* cells (carrying an empty vector) (Fig. 3.11C). This finding indicates that the mutation T562A renders Kns1 less capable of supporting cell growth at pH 8 than the inactivating D440A

mutation. At a higher pH (pH 8.2), the effects of GFP-Kns1^{T562A} overexpression reverted, causing an increase in alkaline tolerance similar to that conferred by GFP-Kns1^{D440A} overexpression (Fig. 3.11C). This result shows that the lack of Thr^{562} in Kns1 mostly mimics the consequences of catalytic inactivation *in vivo*. Moreover, it suggests that the phosphorylation state of Thr^{562} regulates the role of Kns1 in modulating cellular tolerance to alkali.

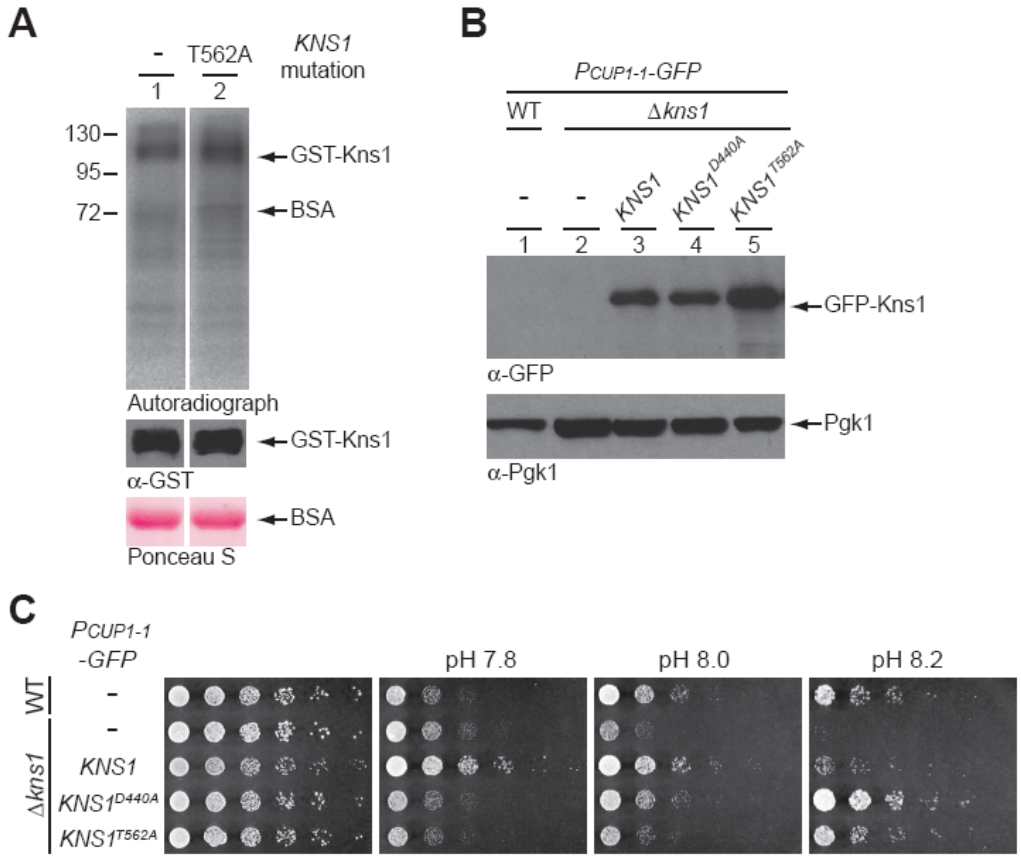

Figure 3.11. Phosphorylation site Thr^{562} (T562), catalytic activity and also non-catalytic properties are required for the role of Kns1 in the modulation of alkaline tolerance.

(A) The GST-Kns1^{T562A} mutant is catalytically active *in vitro*. Recombinantly expressed and purified wild-type (WT) GST-Kns1 (lane 1) and GST-Kns1^{T562A} mutant (lane 2) were incubated with [γ-^{32}P]ATP in phosphorylation buffer as described in fig. 3.8. Reactions were resolved by SDS-PAGE and autoradiography. Upper panel: ^{32}P autoradiograph, Middle panel: α-GST WB, Bottom panel: Ponceau S staining. The migration positions of molecular mass marker proteins are indicated in kDa. (B) GST-Kns1^{D440A} and GST-Kns1^{T562A} mutants are efficiently expressed *in vivo*. Western blot of whole-cell extracts from wild-type (WT; sUB62) and Δ*kns1* (yAS5) cells carrying an empty vector (pNM67) and Δ*kns1* carrying a copper-inducible high-copy plasmid (P_{CUP1-1}) encoding GFP-tagged wild-type Kns1 (pNM74), catalytically inactive Kns1^{D440A} (pNM53) or phosphorylation site mutant Kns1^{T562A} (pNM121). Cells were grown overnight to log-phase in selective synthetic complete medium (SC-Trp) and induced with copper (100 µM $CuSO_4$) for 30 min. Then, whole-cell extracts were prepared and analysed by SDS-PAGE, followed by Western blotting using α-GFP and α-Pgk1 antibodies as described in Methods

2.2.4. Pgk1 was detected to confirm equal protein loading. (C) The same cells as in (B) were grown overnight in SC-Trp at 30 °C to log-phase and diluted to an optical density (OD_{600nm}) of 0.25. Five-fold serial dilutions of this diluted culture were spotted onto SC-Trp (pH 6.5), SC-Trp containing 10 mM Hepes (pH 7.8), 15 mM Hepes (pH 8.0) or 17.5 mM Hepes (pH 8.2) (described in Methods 2.2.2.6). All SC-Trp plates were supplemented with 100 µM $CuSO_4$ to induce GFP-Kns1 expression. Cell growth was monitored after incubation at 30 °C for 3 days (pH 6.5), 5 days (pH 7.8), 6 days (pH 8.0) or 7 days (pH 8.2).

3.4.3 Effect of mutagenesis on Kns1 subcellular localization

The finding that the phosphorylation site mutant GFP-Kns1^{T562A} partially mimicked the inactive mutant GFP-Kns1^{D440A} *in vivo* and that both mutants act in an opposite manner as wild-type GFP-Kns1 implies that autophosphorylation, in particular at the Thr^{562} site, modulates Kns1 function. However, as GST-Kns1^{T562A} showed no apparent impairment in catalytic function *in vitro* nor increased instability *in vivo* (Fig. 3.11A and B), I raised the question of whether autophosphorylation on Thr^{562} affected Kns1 function by inducing changes in its subcellular localization. This postulate was also prompted by the finding that the integrity of the LAMMER motif of PK12, the Kns1 homolgue in tobacco plants, is required for proper subnuclear localization[46]. For this reason, I examined the localization of GFP-Kns1^{T562A} *in vivo*.

3.4.3.1 Neither catalytic activity nor residue Thr^{526} are required for the nuclear localization of Kns1

Expression of wild-type GFP-Kns1 from a high-copy plasmid revealed a predominant nuclear localization and the accumulation of GFP signal in one or two foci that appeared to be close to, or within, the nucleus (Fig. 3.12A). In contrast to the localization of genomically tagged GFP-Kns1 observed in cells cultured in rich medium, the presence of GFP-Kns1 in the cytoplasm was barely detectable when cells were cultured in minimal medium to ensure the maintenance of plasmids with selectable markers. Intriguingly, Δ*kns1* cells overexpressing GFP-Kns1 (wild-type Kns1, Kns1^{D440A} or Kns1^{T562A}) were not permeable to the DNA-dye Hoechst-33258, whereas cells containing an empty vector were. For this reason, co-localization experiments with Hoechst could not be performed. Nevertheless, it could be observed that GFP-Kns1^{D440A} and GFP-Kns1^{T562A} mutants showed similar distribution as wild-type GFP-Kns1, suggesting that neither catalytic activity nor residue Thr^{526} seem to be required for Kns1 localization.

Based on the data presented here implicating Kns1 in the modulation of alkaline stress, the question arose as to whether the localization of Kns1 changes in response to alkaline stress and, if so, whether catalytic activity and residue Thr^{562} are necessary for correct relocalization. To answer this question, Δ*kns1* cells overexpressing GFP-Kns1, GFP-Kns1^{D440A} or GFP-Kns1^{T562A} were subjected to high pH stress (pH 8) for different short (10, 30, 60, 90 and 120 min) and long (overnight; ~15-18 h) time periods and prior to visualization by fluorescence microscopy. Overnight exposure to high pH stress did not noticeably alter the distribution of GFP-Kns1, GFP-Kns1^{D440A} and GFP-Kns1^{T562A} within the cell (Fig. 3.12B) nor at any of the other conditions assessed (data not shown), indicating that Kns1 principally remains in the nucleus upon pH stress independently of its catalytic activity or the phosphorylation state of Thr^{526}.

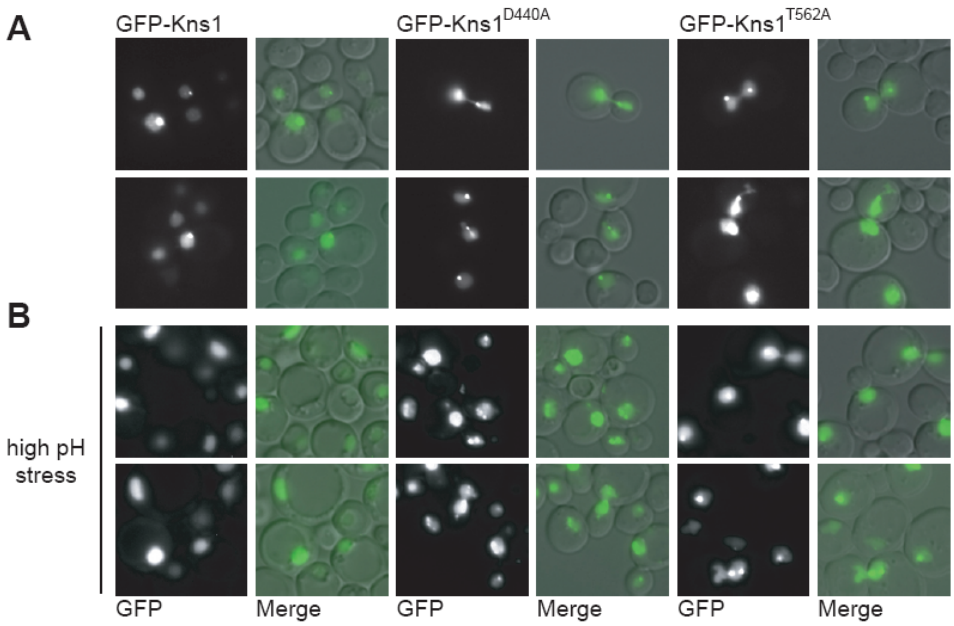

Figure 3.12. Loss of catalytic activity or phosphorylation site Thr^{562} does not affect GFP-Kns1 localization under normal and high pH conditions.

(A) Wild-type (WT) GFP-Kns1, catalytically inactive kinase GFP-Kns1^{D440A} and phosphorylation site mutant GFP-Kns1^{T562A} show similar intracellular distribution. Δ*kns1* cells (yAS5) expressing *GFP-KNS1* (pNM74), *GFP-KNS1^{D440A}* (pNM53) and *GFP-KNS1^{T562A}* (pNM121) from a multicopy plasmid controlled by the copper-inducible promoter P_{CUP1-1} were grown overnight to mid-log phase on selective synthetic complete medium (SC-Trp). Prior to fluorescence microscopy analysis, cells were induced with copper (100 μM $CuSO_4$) for 60 min. (B) GFP-Kns1, GFP-Kns1^{D440A} and GFP-Kns1^{T562A} localization do not remarkably change under high pH stress conditions. The same cells as in (A) were grown overnight in SC-Trp and then diluted to an optical density (OD_{600nm}) of 0.25 in YPD buffered to pH 8 with 100 mM Hepes. After overnight growth under these high pH stress conditions, cells were induced with copper

and visualized as in (A). Merge indicates the fusion between the GFP (green) and differential interference contrast (DIC) images.

3.5 Kns1 phosphorylates Cmk2 in vitro

Environmental alkalinization constitutes a stress situation for yeast cells. In response, they activate signalling pathways that trigger adaptive transcriptional responses required for survival (reviewed in [189]). Consistent with this, mutants lacking key genes involved in these responses have been reported to exhibit increased sensitivity to high pH conditions[171,175,177,275]. The LAMMER kinases of the fission yeast, fruit fly and human have been implicated in a variety of stimuli-induced signalling pathways (see Introduction 1.2.2). Given the possible existence of functional similarities between Kns1 and its counterparts and the hypersensitivity of ∆*kns1* cells to high pH, I speculated that Kns1 may play a role in the adaptive response to high pH. Thus, to gain insight into the mechanism by which Kns1 controls alkaline tolerance, I assessed the functional relevance of the *in vitro* candidate substrates for Kns1 that might function in adaptive response pathways.

The gene encoding the Ca^{2+}/CaM-dependent kinase Cmk2, one of the identified *in vitro* candidate substrates for Kns1[102], has been reported to be greatly induced upon high pH stress[173]. Exposure to high pH stress activates the calcineurin/*CRZ1* pathway, which plays a crucial role in the transcriptional response to high pH[174,176,179]. Importantly, this pathway has been shown to remarkably increase *CMK2* gene expression when activated[158]. These notions altogether prompted me to consider that Cmk2 could be involved in an alkaline response pathway and; thus, be a feasible physiological substrate for Kns1. To evaluate this possibility, I analysed biochemical and functional links between Cmk2 and Kns1.

Recombinantly expressed Cmk2 has been previously shown to exhibit constitutive autophosphorylation activity[144]. Therefore, to confirm the finding of the proteome-wide phosphorylation screen[102], I performed in solution-based *in vitro* kinase assays using catalytically inactive Cmk2. In this manner, *trans*-phosphorylation by Kns1 could be unequivocally detected in the absence of the Cmk2 autophosphorylation background. Wild-type *CMK2* was cloned into bacterial expression vector pDESTco, expressed in *E. coli* as an N-terminal 6xHis-fusion protein (6His-Cmk2) and purified using NiNTA-Agarose (Qiagen) (described in Methods 2.2.1.3). Cells expressing this fusion protein produced two polypeptides of similar size (~ 55-60 KDa) (Fig 3.13A), as seen on Coomassie blue-stained gels.

These bands were confirmed to correspond to 6His-tagged Cmk2 by Western blotting with α-His antibodies, as shown in fig. 3.14. The expression of recombinant Cmk2 as a doublet has been also reported to occur in a previous study and may indicate the eventual production of a truncated protein due to incomplete translation[144].

The catalytically inactive Cmk2 mutant was created by substituting Asp^{171} to Ala to yield 6xHis-$Cmk2^{D171A}$. Residue Asp^{171} was shown to correspond to the catalytic active site of Cmk2 based on sequence homology within the catalytic loop region of Cmk2 with the prototypical protein kinase A of murine (PKA) and yeast (Tpk1) (Fig. 3.13B)[10,44,145]. Akin to wild-type 6xHis-Cmk2, 6xHis-$Cmk2^{D171A}$ migrated also as a double polypeptide. However, in this instance, one of the two 6xHis-$Cmk2^{D171A}$ polypeptides migrated with an apparent lower molecular weight (Fig. 3.13A, marked with an asterisk). This polypeptide was consistently obtained from three different $Cmk2^{D171A}$-bearing vector clones, which may suggest that the D171A mutation inherently leads to translational errors *e.g.,* premature termination, or brings about a specific proteolytic event.

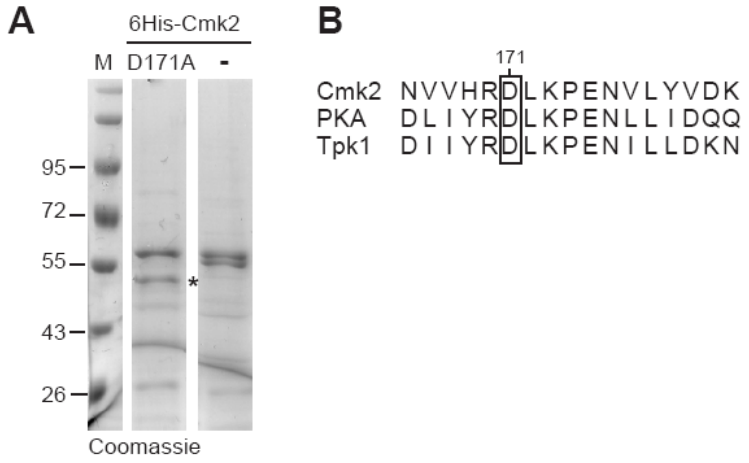

Figure 3.13. Purification of wild-type 6His-Cmk2 and mutant 6His-$Cmk2^{D171A}$ from *E. coli*.

(A) Recombinant 6His-Cmk2 and mutant 6His-$Cmk2^{D171A}$ were purified by Ni-NTA chromatography as described in Methods 2.2.1.3. A sample from each eluate was subjected to SDS-PAGE on a 12 % polyacrylamide gel followed by Coomassie brilliant blue R250 staining. Lane M; molecular weight marker. The migration positions of molecular mass marker proteins are indicated in kDa. (B) Sequence alignment of the catalytic loop of *S. cerevisiae* Cmk2 , *H.sapiens* (PKA) and *S.cerevisiae* (Tpk1) Protein kinase A kinases. By sequence analogy, the residue equivalent to the catalytic base of PKA and Tpk1 in Cmk2 was shown to be Asp^{171}.

In vitro kinase reactions were performed by incubating GST-Kns1 with either 6xHis-Cmk2 or catalytically inactive 6xHis-$Cmk2^{D171A}$ in the presence of [γ-^{32}P]-ATP

(described in Methods 2.2.4.5). As negative controls, further *in vitro* kinase reactions using catalytically inactive mutant GST-Kns1^{D440A} instead of GST-Kns1 were performed to ensure that substrate phosphorylation was solely due to the catalytic activity of GST-Kns1 rather than to the activity of contaminating kinases. In agreement with previous observations made by Ohya *et al.* (1991)[144], incorporation of [γ-^{32}P] into 6xHis-Cmk2 in the kinase reaction containing only 6xHis-Cmk2 (Fig. 3.14, lane 5) demonstrated that the recombinant protein possessed basal autophosphorylation activity, which was independent of the presence of activating kinases or external factors such as *e.g.,* calmodulin (CaM). By contrast, 6xHis-Cmk2^{D171A} displayed no detectable autophosphorylation activity, confirming effective catalytic inactivation (Fig. 3.14, lane 8). Owing to the extent of 6xHis-Cmk2 autophosphorylating activity, the effects of including GST-Kns1 in the *in vitro* kinase reaction did not yield conclusive evidence for *trans*-phosphorylation (Fig. 3.14, lane 3). Yet, *trans*-phosphorylation was clearly evident when inactive mutant 6xHis-Cmk2^{D171A} was incubated with GST-Kns1, as this resulted in the detection of the two radiolabed bands that corresponded to the polypeptides produced by the Cmk2^{D171A}-bearing pDEST vector (Fig. 3.14, lane 6). These radiolabeled bands were not detected after incubation with GST-Kns1^{D440A}, confirming that 6xHis-Cmk2^{D171A} phosphorylation was not due to the action of contaminating kinases but to GST-Kns1 activity (Fig. 3.14, lane 7). In summary, these data unequivocally validate Cmk2 as a genuine *in vitro* substrate of Kns1. Moreover, incorporation of [γ-^{32}P] into the inactive mutant GST-Kns1^{D440A} was observed when 6xHis-Cmk2, but not 6xHis-Cmk2^{D171A}, was present in the reaction, indicating that Kns1 was capable of serving as a substrate for Cmk2 *in vitro* (Fig. 3.14, lanes 4 and 7). It is important to note that, in contrast to Kns1 (see Fig. 3.15 and refs [33,34,102]), Cmk2 has been previously reported to display broad substrate specificity[144]. Hence, it is probable that the observed *in vitro* phosphorylation of GST-Kns1^{D440A} by 6His-Cmk2 might be non-specific.

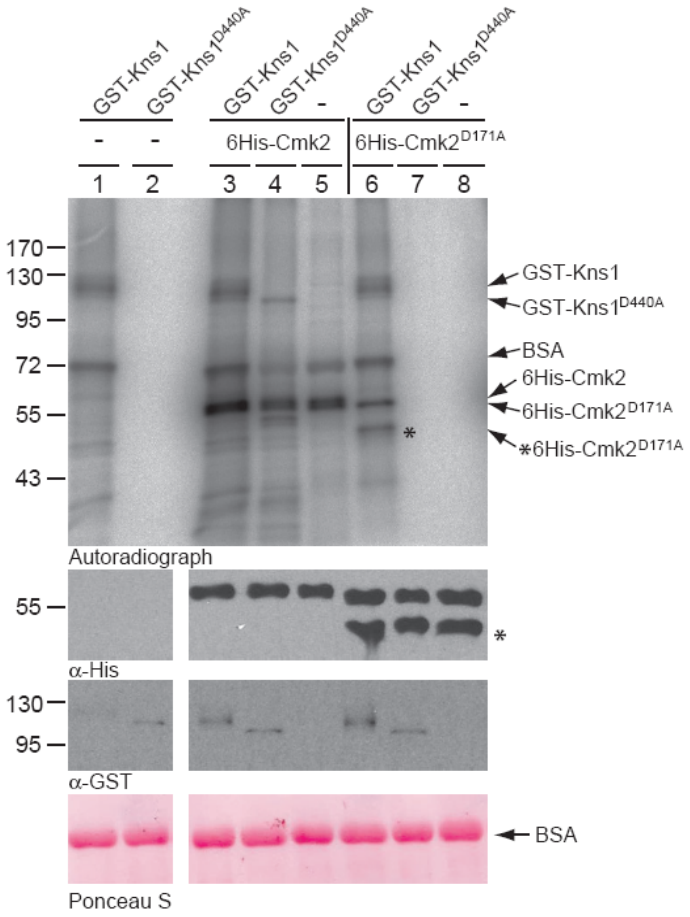

Figure 3.14. Cmk2 is phosphorylated by Kns1 *in vitro*.

Recombinantly expressed and purified wild-type 6His-Cmk2 (pNM38) or catalytically inactive 6His-Cmk2^{D171A} (pNM45) were incubated as indicated with either wild-type GST-Kns1 (pNM11) or catalytically inactive GST-Kns1^{D440A} (pNM37) in phosphorylation buffer (25 mM Tris pH 7.5, 10 mM $MgCl_2$, 1 mM DTT) in the presence of [γ-^{32}P]ATP for 15 min at 30 °C as described in Methods 2.2.4.5. BSA was included at a relatively high concentration (0.2 µg/µl) in the phosphorylation reactions as a non-specific phospho-acceptor competitor. Reactions were stopped by addition of Laemmli sample buffer and immediate boiling for 5 min, followed by SDS-PAGE and autoradiography. Aliquots of the reaction mixtures were taken prior to [γ^{32}P]ATP addition and analysed by SDS-PAGE and Western blotting with α-His and α-GST antibodies. Top: ^{32}P autoradiograph; Middle: α-His and α-GST WB; Bottom: Ponceau S staining. The migration positions of molecular mass marker proteins are indicated in kDa. GST-Kns1 forms are not evident as 100 ng were used to obtain a kinase:substrate molecular ratio of 1:10. The positions of the phosphorylated protein species are indicated by arrows. Marked by an asterisc is a degradation product of one of the two polypeptides expressed by the 6His-Cmk2^{D171A}-bearing plasmid. All samples were analysed on the same gel. The phosphorylation assay shown is representative of at least three independent experiments.

In order to validate further candidate substrates identified by Ptacek *et al.* (2005)[102], I performed an *in vitro* kinase assay using C-terminally TAP-tagged Pdc1 purified from yeast as substrate. Pdc1 was chosen among the Kns1 candidate

substrates (Table 1.1) principally for the convenient availability in the laboratory of the Pdc1-TAP construct. Moreover, comprehensive literature curation together with data obtained in preliminary experimental tests (*i.e.,* phenotypic analysis, data not shown) did not reveal notable links between the other candidate substrates and a potential involvement in alkaline tolerance mechanisms. No phosphorylation of Pdc1-TAP was detected, revealing Pdc1-TAP as a false positive (Fig. 3.15). Importantly, this result underlined the specificity of Kns1 towards Cmk2.

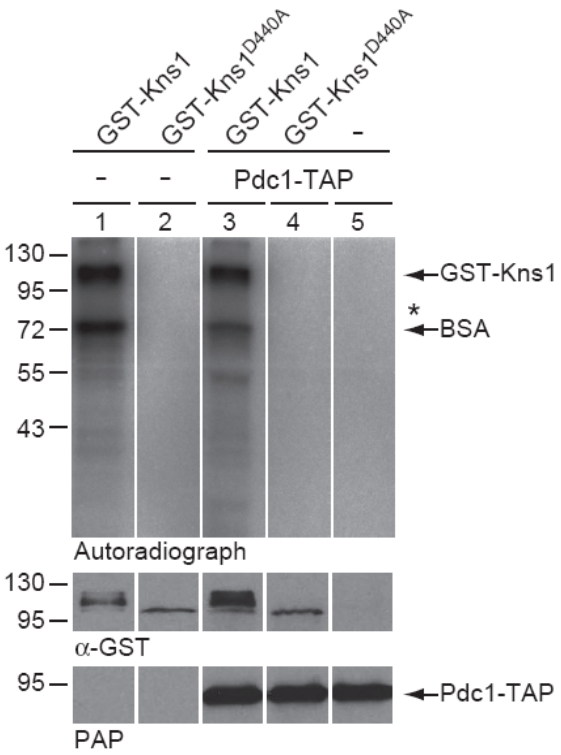

Figure 3.15. Kns1 does not phosphorylate Pdc1 *in vitro*.

Pdc1-TAP was purified from yeast extracts and incubated with either recombinant wild-type GST-Kns1 (pNM11) or catalytically inactive GST-Kns1^{D440A} (pNM37) in phosphorylation buffer in the presence of [γ-^{32}P]ATP for 15 min at 30 °C as described in Methods 2.2.4.5. BSA was included in the reaction as a phosphate-acceptor competitor (0.2 µg/µl). A band corresponding to molecular weight (MW) of the phosphorylated Pdc1-TAP fusion protein was not observed (expected MW=82.7; 61.5 kDa + 21.2 kDa of the TAP-tag, indicated with an asterisk). Although several intervening lanes were spliced out, all samples were analysed on the same gel. Aliquots of the reaction mixtures were taken prior to [γ-^{32}P]ATP addition and analysed by SDS-PAGE and Western blotting with α-GST and Peroxidase anti-Peroxidase soluble complex (PAP) antibodies. Top: ^{32}P autoradiograph; Middle: α-GST and PAP antibody WB. The migration positions of molecular mass marker proteins are indicated in kDa.

3.5.1 Analysis of Kns1-Cmk2 physical interaction

The phosphorylation of Cmk2 by Kns1 inherently implies a direct interaction of Cmk2 with Kns1 *in vitro*. I therefore sought to determine whether such an interaction occurs *in vivo*. Although kinase-substrate interactions are generally of a weak and transient nature, in some cases, these can be more readily detected using the yeast two-hybrid system owing to the high sensitivity of the reporter gene strategy[213,276,277]. I chose this system to test the binding of Kns1 to Cmk2. To this end, I created a plasmid expressing *KNS1* N-terminally fused to the *GAL4* binding domain (*OBD*) and a plasmid expressing *CMK2* fused to the *GAL4* activation domain (*OAD*) both driven by the *GAL1* promoter (P_{GAL1}). Combinations of these constructs with each other, or with empty vectors (used as negative controls), were co-expressed in yeast strain PJ69-4A as indicated in fig. 3.16. The previously reported interaction between splicing factor Snu66 and ubiquitin-like protein Hub1 was tested in parallel as positive control (Fig. 3.16, bottom panels)[214]. Interactions between bait and prey proteins are indicated by the activation of *GAL1* promoter-*HIS3* reporter, which allows growth on medium lacking histidine. The use of Kns1 as bait (*OBD-KNS1*) resulted in auto-activation of the *HIS3* reporter gene (reporter 1) in the absence of prey protein Cmk2 (*OAD-CMK2*) (Fig. 3.16, upper panels). Therefore, I additionally tested *CMK2* as bait (*OBD-CMK2*) and KNS1 as prey (*OAD-KNS1*) (Fig. 3.16, middle panels) as well as a second nutritional reporter gene, *ADE2* (reporter 2). However, this attempt failed to detect a direct physical interaction between Kns1 and Cmk2, as indicated by the absence of growth on medium lacking adenine.

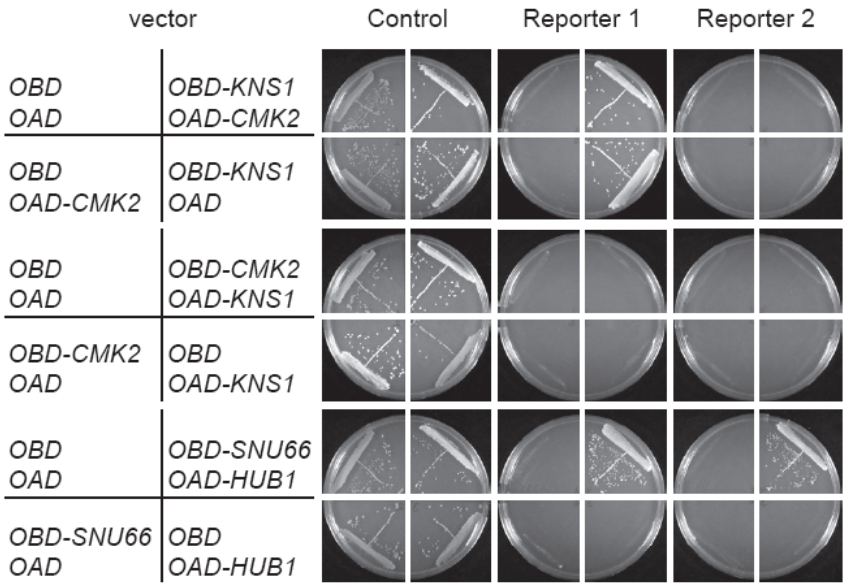

Figure 3.16. Analysis of Kns1-Cmk2 physical interaction using the yeast two-hybrid system.

Host strain PJ69-4A was transformed with combinations of plasmids expressing *GAL4* binding domain (OBD) fused to *KNS1* (*OBD-KNS1*; pNM105) and *GAL4* activation domain fusions (OAD) fused to *CMK2* (*OAD-CMK2;* pNM104) (upper panels) or OBD fused to *CMK2* (*OBD-CMK2;* pNM106) and OAD fused to fused to *KNS1* (*OAD-KNS1;* pNM103) (middle panels). Negative controls consisted of cells co-transformed with combinations of plasmids expressing *OBD-KNS1*, *OAD-CMK2, OAD-KNS1* or *OBD-CMK2* with empty plasmids (*OBD* or *OAD* alone) as indicated. As a positive control for the assay, cells transformed with plasmids expressing OBD fused to *SNU66* (*OBD-SNU66*; pMR29) and OAD fused to *HUB1* (*OAD-HUB1*; pGD240) were used in parallel. Cells were plated on synthetic complete (SC) medium lacking tryptophan and leucine (SC-Trp-Leu) to select for both Gal4-fusion plasmids (control) and on SC medium lacking either histidine (SC-Trp-Leu-His; reporter 1) or adenine (SC-Trp-Leu-Ade; reporter 2) as required to assay for reporter activation. Plates were incubated for 3-4 days at 30 °C before photodocumentation.

3.6 Genetic interactions between KNS1 and CMK2

The confirmation of the *in vitro* phosphorylation of Cmk2 by Kns1 prompted me to investigate whether Kns1 and Cmk2 were *de facto* functionally related *in vivo.* Genetic interactions reflect the extent to which the function of one gene depends on the presence of a second gene, providing a valuable insight into the relationship between their cellular roles[278–285]. In search of physiological evidence for the biochemical interaction observed, I analysed the type of genetic interaction between *KNS1* and *CMK2*. For this purpose, I examined and classified the relation among the phenotypes of cells lacking either *KNS1* ($P_{\Delta kns1}$), *CMK2* ($P_{\Delta cmk2}$) or both

($P_{\Delta kns1\Delta cmk2}$) with respect to the phenotype of wild-type (P_{WT}) cells exposed to alkaline stress (pH 7.8, 8.0 and 8.2) (*P* denotes alkaline pH sensitivity) (Fig. 3.17).

A genetic interaction between two genes *e.g.,* X and Y, is defined by the deviation (ε) of the double deletion mutant phenotype ($P_{\Delta x\Delta y}$) from the expected neutral phenotype ($E_{\Delta x\Delta y}$)[286,287]. *Exy* can be calculated as the product of the individual mutational effects ($E_{\Delta x\Delta y} = P_{\Delta x} {}^{*} P_{\Delta y}$) under the hypothesis that the double mutant carries two non-interacting mutations (Fig. 3.17A)[288,289]. An absolute deviation distinct from zero between $P_{\Delta x\Delta y}$ and $E_{\Delta x\Delta y}$ suggests that the two genes genetically interact whereas a deviation close to zero indicates non-interacting gene pairs[280,290]. To get an estimate of the deviation (ε) between $P_{\Delta kns1\Delta cmk2}$ and $E_{\Delta kns1\Delta cmk2}$, the approximate cell population density of yeast strains grown at high pH was considered as an indicator of cell fitness and quantified by densitometry (ImageJ, NIH). The approximate cell population of each mutant was expressed relative to that of wild-type cells (set to 1.0).

Under all high pH stress conditions tested (pH 7.8-8.2), Δ*cmk2* cells grew better than WT cells (Fig. 3.17B), indicating that loss of *CMK2* increases alkaline tolerance. This implies that Cmk2, as opposed to Kns1, restricts growth under high pH conditions.

At pH 7.8, the lack of Kns1 conferred increased alkaline sensitivity (Fig. 3.17B), which shows that Kns1 is necessary for the acquisition of normal tolerance under these conditions ([1]). The double mutant Δ*kns1*Δ*cmk2* exhibited a phenotype equivalent to the expected phenotype $E_{\Delta kns1\Delta cmk2}$ (ε ~ 0). This result indicates that Kns1 and Cmk2 contribute separately and independently to the pathways responsible for the adaptation of cells to mild alkaline stress (pH 7.8).

At pH 8.0, the loss of *CMK2* partially alleviated the phenotype caused by loss of *KNS1* because the phenotype of Δ*kns1*Δ*cmk2* was less severe than expected ($P_{\Delta kns1\Delta cmk2} > E_{\Delta kns1\Delta cmk2}$), yielding a positive deviation (ε = 0.82) (Fig. 3.17B). This indicates that both genes display an "alleviating" genetic interaction, also termed positive epistasis[389]. This type of interaction commonly occurs when a mutation in

[1] Note that Δ*kns1* cells displayed more alkaline sensitivity than WT cells in rich media buffered to pH 7.8 (Fig. 3.17B) whereas Δ*kns1* grew like WT (carrying empty vectors) in minimal media buffered to pH 7.8 supplemented with copper (Fig. 3.11C). Importantly, nutrient conditions *i.e.,* increased copper concentrations, affect the susceptibility of cells to high pH stress[180]. The growth conditions of the two experiments are not fully comparable and; therefore, their outcomes are not to be considered incongruous.

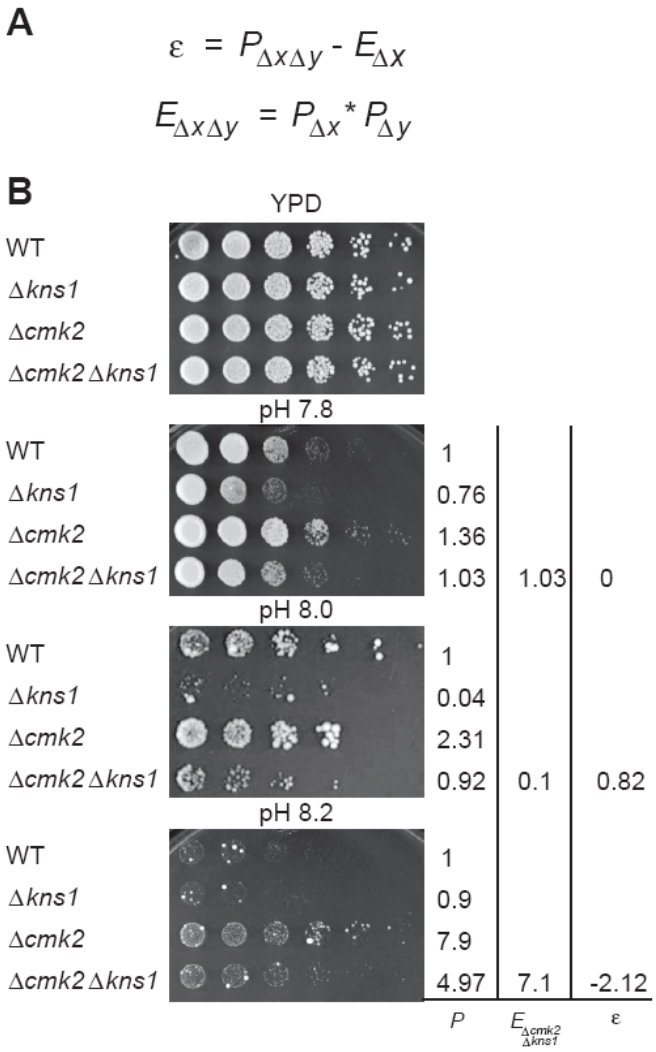

Figure 3.17. Genetic interactions between *KNS1* and *CMK2* under high pH conditions.

(A) A genetic interaction between mutants *x* and *y* can be defined by the deviation (ε) of an observed double-mutant phenotype ($P_{\Delta x\Delta y}$) from the expected neutral phenotype of an organism's fitness ($E_{\Delta x\Delta y}$) under the hypothesis that it carries two non-interacting mutations[290]. (B) Deletion of *CMK2* causes opposite effects as deletion *KNS1* on alkaline pH tolerance. Wild type (WT; sUB62), Δ*kns1* (yAS5), Δ*cmk2* (yNM414) and double deletion mutant Δ*kns1*Δ*cmk2* (yNM454) cells were grown overnight in YPD to mid-log phase at 30 °C and diluted to an optical density (OD_{600nm}) of 0.25. Five-fold serial dilutions of this diluted culture were spotted onto YPD (pH~5.5; control plate) and YPD containing 100mM Hepes adjusted to pH 7.8, 8.0 or 8.2. Cell growth was monitored after incubation at 30 °C for 2 days (YPD), 4 days (pH 7.8), 5 days (pH 8.0) or 7 days (pH 8.2). The approximate cell population density of each strain grown at high pH was quantified by densitometry (ImageJ, NIH) and expressed relative to that of wild-type cells (set to 1.0).

one gene impairs the function of a whole pathway, thereby concealing the consequence of additional mutations in other members of that pathway[280,291,292]. Based on the fact that Kns1 and Cmk2 exert opposite effects on alkaline tolerance,

it can be inferred that, if both proteins act on the same pathway, one protein has to effect a negative regulatory influence on the other.

At pH 8.2, ∆cmk2 grew better than ∆*kns1*∆*cmk2*, indicating that loss of *KNS1* reduces the alkaline tolerance of ∆*cmk2* cells (Fig. 3.17B). Thus, Kns1 positively contributes to alkaline tolerance; yet, only in the absence of Cmk2. Given that WT was barely capable of growing at 8.2, it can be inferred that Kns1 is unable to confer alkaline tolerance in the WT due to the presence of Cmk2. The double mutant phenotype was more severe than expected ($E_{\Delta kns1\Delta cmk2} > P_{\Delta kns1\Delta cmk2}$), resulting in a negative deviation ($\varepsilon = -2.12$). This defines the genetic interaction between *KNS1* and *CMK2* as "aggravating"[389]. This indicates that both proteins also genetically interact under severe alkaline pH stress and are, thus, functionally interconnected.

A systematic genome-wide phenotypic analysis of the haploid yeast deletion collection has previously reported that deletion of *KNS1* elicits an oleate-sensitive phenotype[99]. This phenotype functionally implicates Kns1 in a process required to endure exposure to toxic levels of exogenous oleate. In accordance with that report, the ∆*kns1* mutant grew poorly on media containing oleate as the sole carbon source (Fig. 3.18). I therefore asked whether Cmk2 shared a functional link with Kns1 in this process by examining the effect of deleting *CMK2* on the growth of ∆*kns1* on oleate-containing medium. This revealed that the deletion of *CMK2* partially alleviated the oleate sensitive phenotype caused by deletion of *KNS1* (Fig. 3.18), leading to a double mutant phenotype less severe than expected ($P_{\Delta kns1\Delta cmk2} > E_{\Delta kns1\Delta cmk2}$). This shows that both genes display an alleviating genetic interaction ($\varepsilon = 0.95$), suggesting that both also act in concert to modulate the ability to cope with high levels of oleate.

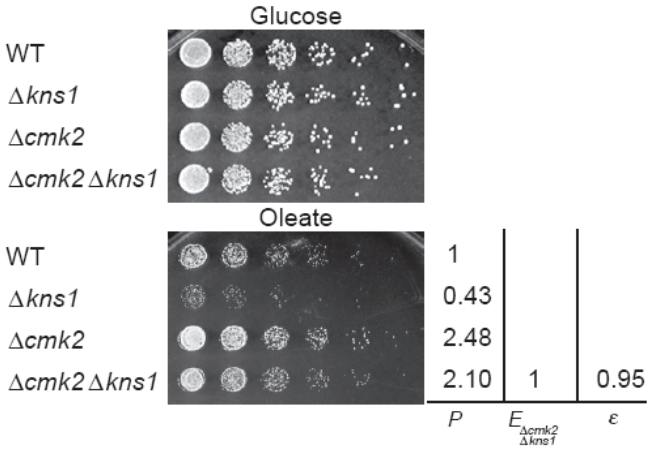

Figure 3.18. Genetic interaction between *KNS1* and *CMK2* displayed upon exposure to high levels of exogenous oleate.

Growth of Δ*cmk2* cells on oleate-containing plates is comparable to that of wild-type cells. The same cells as in (B) were grown overnight in YPD, washed with rich medium lacking carbon source (YP), serially diluted and spotted onto either STY plates containing either 2 % glucose (control) or 0.1% oleate (described in Materials 2.1.8). Cell growth was monitored after incubation at 30 °C for 2 days (STY Glucose) or 7 days (STY Oleate). In all cases, the undiluted culture is shown at the left along with 5-fold serial dilutions going left to right. The approximate cell population density of each strain was quantified as described in fig. 3.17. Genetic interaction is defined by the extent of deviation (ε) of an observed double-mutant phenotype ($P_{\Delta x \Delta y}$) from the expected neutral phenotype of an organism's fitness ($E_{\Delta x \Delta y}$).

Altogether, these genetic data underscore the functional interplay between Kns1 and Cmk2 in the adaptation of yeast to environmental alkalinization and exposure to exogenous oleate. In particular, the alleviating interactions described for *KNS1* and *CMK2* strongly suggest that both proteins act in the same pathway under these particular stress conditions.

3.6.1 Loss of Cmk2 improves cell growth at high pH

To verify that the absence of *CMK2* was solely responsible for the increased resistence of Δ*cmk2* cells to alkaline-induced stress, I performed complementation experiments using a high-copy plasmid overexpressing wild-type N-terminally GFP-tagged Cmk2 under the control of the copper-inducible P_{CUP1-1} promoter. As shown in fig. 3.19A, transformation of Δ*cmk2* cells with the Cmk2-borne plasmid, but not with the empty plasmid, led to the reduction of the alkaline tolerance of Δ*cmk2* cells to wild-type levels. Hence, this result confirms that Cmk2 restricts alkaline tolerance.

In order to perform the complementation experiments under more physiological conditions, the *CMK2* gene was cloned into a single-copy plasmid harboring 1000 bp of the 5'-UTR region of *CMK2* to obtain endogenous levels of Cmk2 expression. Exposure of cells to high concentrations of calcium (Ca^{2+}) induces *CMK2* expression by ~ 5 fold, as reported previously[158]. Therefore, to test whether the 5'-UTR region contained the promoter elements required for correct induction of Cmk2 protein expression, Δ*cmk2* cells carrying the constructed plasmid were incubated for 20, 40, 60 or 100 min with calcium (Ca^{2+}; 200 mM $CaCl_2$). Western Blotting of non-induced and Ca^{2+}-induced cell extracts using α-GFP antibodies showed that addition of Ca^{2+} to the growth media leads to induction of Cmk2 expression, indicating that the plasmid carried a functional Cmk2 promoter (Fig. 3.19D). Comparison of the growth of Δ*cmk2* cells expressing GFP-Cmk2 at endogenous levels with Δ*cmk2* cells overexpressing GFP-Cmk2 from a high-copy plasmid under the control of the P_{CUP1-1} promoter revealed that the mere presence of GFP-Cmk2 restrained growth of cells

exposed to alkaline stress independently of the expressing system used (Fig. 3.19A and B). This shows that the effects caused by the copper-inducible overexpression of *CMK2* are equivalent to those exerted by the kinase expressed under the control of its promoter. Moreover, it indicates that the N-terminal GFP tag does not disrupt kinase function, as evidenced by the restoration of the wild-type phenotype in Δ*cmk2* cells upon expression of the fusion protein GFP-Cmk2.

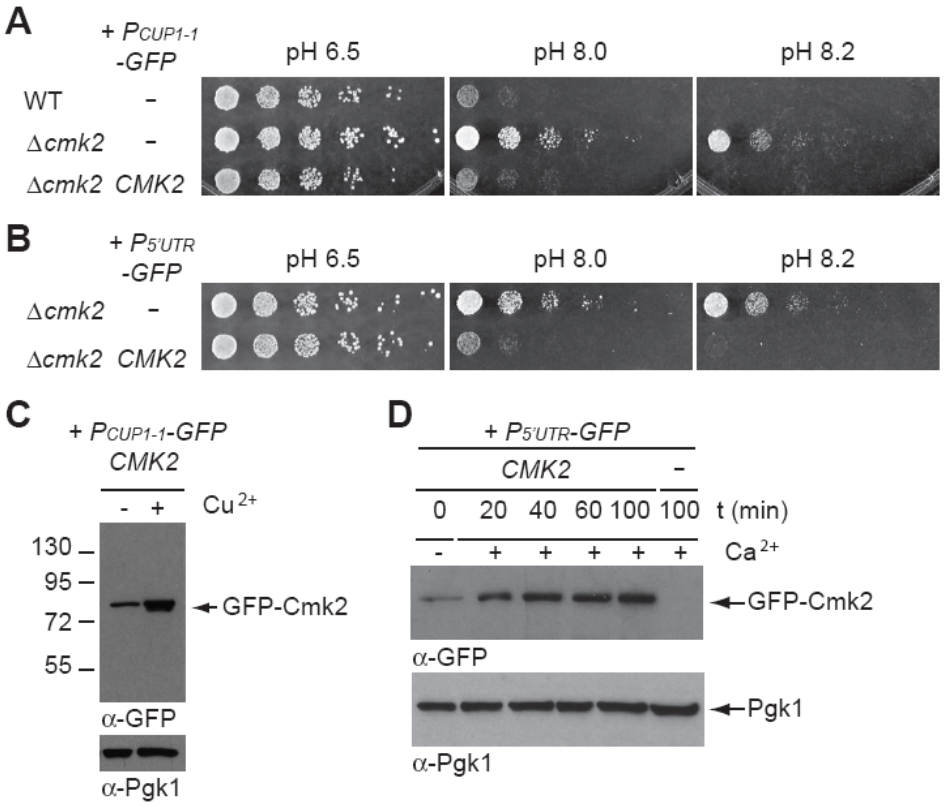

Figure 3.19. GFP-Cmk2 expression decreases the alkaline tolerance of Δ*cmk2* cells to wild-type levels. Effects of *CMK2* expression on alkaline tolerance are independent of the expression system used.

Wild-type (WT; sUB62) cells harbouring an empty plasmid and Δ*cmk2* (yNM414) cells harbouring the plasmid encoding N-terminally GFP-tagged Cmk2 (GFP-Cmk2) under the control of either the copper-inducible promoter (P_{CUP1-1}) (high-copy; pNM73) (A) or the endogenous promoter ($P_{5'UTR}$) (single-copy; pNM65) (B) and Δ*cmk2* cells harbouring the respective empty plasmids (pNM67 or pNM63) were grown overnight at 30 °C in SC-Trp to log-phase and diluted to an optical density (OD_{600nm}) of 0.25. Five-fold serial dilutions of this diluted culture were spotted onto either SC-Trp (pH 6.5) or SC-Trp containing 15 mM Hepes (pH 8.0) or 17.5 mM Hepes (pH 8.2). Cells from (A) and (B) were spotted together onto the same plate. All SC-Trp plates were supplemented with 100 µM $CuSO_4$ to induce GFP-Cmk2 expression from the copper-inducible plasmid. Cell growth was monitored after incubation at 30 °C for 3 days (pH 6.5), 6 days (pH 8.0) or 8 days (pH 8.2). (C) Western blot analysis showing copper (Cu^{2+})-induced expression of GFP-Cmk2 from a high-copy plasmid in Δ*cmk2* cells. Δ*cmk2* cells were transformed with empty plasmid (pNM67) or plasmid encoding GFP-Cmk2 (pNM73) driven by the

copper-inducible promoter (P_{CUP1-1}). Transformants were grown overnight to log-phase in selective synthetic complete medium (SC-Trp) and then either directly harvested (lines 1 and 3) or induced with Cu^{2+} (100 µM $CuSO_4$) for 60 min at 30 °C (lines 2 and 4). The extract prepared from cells carrying the vector encoding GFP-Cmk2 contained detectable amounts of full-length Cmk2 protein before and after Cu^{2+} induction, indicating leaky expression prior to Cu^{2+} addition. (D) The cloning of a functional promoter of the *CMK2* gene was confirmed by the endogenous expression of Cmk2 upon calcium addition. Δ*cmk2* cells harbouring either an empty plasmid (pNM63) or a plasmid encoding GFP-Cmk2 under the control of the endogenous promoter (p5'UTR) containing the endogenous 5'UTR of *CMK2* and the *CMK2* gene fused N-terminally to GFP (pNM65) were grown to log-phase and either mock treated or treated with 200 mM $CaCl_2$ for 20, 40, 60 and 100 min. Cells were harvested and washed with NaN_3. Whole-cell extracts from (C) and (D) were prepared and analysed by SDS-PAGE, followed by Western blotting with α-GFP antibodies and α-Pgk1 as described in Methods 2.2.4. Pgk1 was detected to confirm equal protein loading.

3.6.2 Cmk2 requires catalytic activity to restrict alkaline tolerance.

To learn whether Cmk2 possesses kinase-independent functions, I examined the effect of catalytic inactivation on the role of Cmk2 in the cellular adaptation to alkaline conditions. In pH 8 medium, Δ*cmk2* cells overexpressing catalytically inactive Cmk2 (GFP-$Cmk2^{D171A}$) coped with alkaline stress more efficiently than wild-type (WT) cells (Fig. 3.20). In particular, the effects of overexpressing GFP-$Cmk2^{D171A}$ were akin to those of deleting the *CMK2* gene *i.e.*, both resulted in enhanced cell tolerance to alkaline stress. This result reveals that catalytic inactivation completely abolishes the ability of Cmk2 to restrict alkaline stress tolerance *in vivo*. Hence, it can be concluded that the effects of Cmk2 on alkaline stress tolerance completely rely on its catalytic activity.

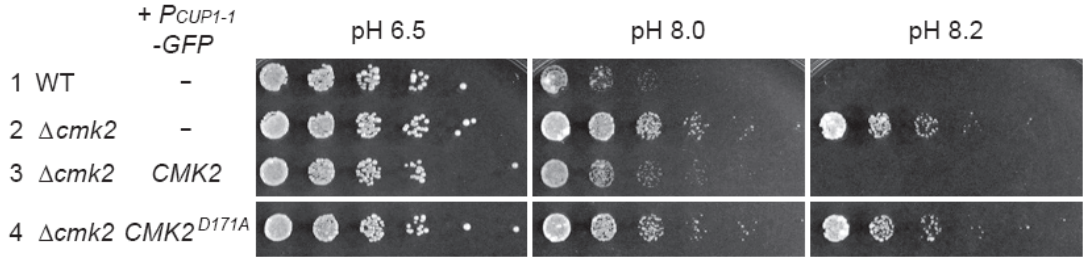

Figure 3.20. Restoration of the wild-type alkaline tolerance conferred by overexpression of *CMK2* requires intact catalytic function.

Wild-type (WT; sUB62) and Δ*cmk2* (yNM414) cells carrying an empty vector (pNM67) and Δ*cmk2* carrying a copper-inducible high-copy plasmid (P_{CUP1-1}-*GFP*) encoding either wild-type Cmk2 (pNM73) or catalytically inactive mutant $Cmk2^{D171A}$ (pNM36) were grown overnight in SC-Trp at 30 °C to log-

phase and diluted to an optical density (OD_{600nm}) of 0.25. Five-fold serial dilutions of this diluted culture were spotted onto either SC-Trp (pH 6.5) or SC-Trp containing 15 mM Hepes (pH 8.0) or 17.5 mM Hepes (pH 8.2). All SC-Trp plates were supplemented with 100 µM $CuSO_4$ to induce GFP-Cmk2 expression. Cell growth was monitored after incubation at 30 °C for 3 days (pH 6.5), 6 days (pH 8.0) or 7 days (pH 8.2). Cells were spotted together onto the same plates.

Genetic analysis indicated that *KNS1* and *CMK2* act antagonistically in a common pathway to govern the tolerance of cells exposed to an external pH of 8.0 (Fig. 3.17). This result together with the finding that both proteins biochemically interact *in vitro* (Fig. 3.14) led to the hypothesis that one may conceivably downregulate the other by phosphorylation. Therefore, the absence of the upstream kinase should lead to the increased activity of the unmodified substrate, which, in turn, should enhance the phenotype of the kinase deletion mutant when overexpressed[293]. This concept is referred to as synthetic dosage enhancement and can be indicative of a kinase-substrate relationship[293,294]. To test this hypothesis, I considered the possibility of Kns1 phosphorylating Cmk2 to downregulate its function *in vivo* and examined the effects that *CMK2* overexpression has on cell growth at pH 8.0 in the presence and absence of *KNS1*. Cmk2 showed greater ability to restrict alkaline tolerance when overexpressed in the absence of *KNS1* than in its presence (Fig. 3.21, row 3 *vs* 5). Overexpression of *CMK2* exacerbated the alkaline sensitive phenotype of ∆*kns1*∆*cmk2* cells (Fig. 3.21, row 4 *vs* 5). However, ∆*cmk2* cells grew better than ∆*kns1*∆*cmk2* cells (both carrying empty vectors) (Fig. 3.21, row 2 *vs* 3), indicating that loss of *KNS1* renders cells more sensitive to high pH stress also in the absence of Cmk2. This shows that Kns1 not only improves alkaline tolerance through the regulation of Cmk2 action but also through the regulation of additional targets with a relevant role in high pH adaptation. For this reason, this result does not conclusively confirm the kinase-substrate relationship on its own. However, it does, together with the finding of an alleviating interaction between the *KNS1* and *CMK2* genes, further support the notion that Kns1 may conceivably inhibit Cmk2 function *in vivo*. Moreover, the possibility that Cmk2 regulates Kns1 by phosphorylation is plausible based on the observation that Cmk2 is capable of phosphorylating Kns1 *in vitro* (Fig. 3.14). However, this hypothesis cannot be evaluated through the examination of the effects of *KNS1* overexpression in the absence or presence of *CMK2* owing to the finding that Kns1 exerts dual functions on alkaline tolerance *i.e.*, a kinase-dependent and independent function (Fig. 3.11).

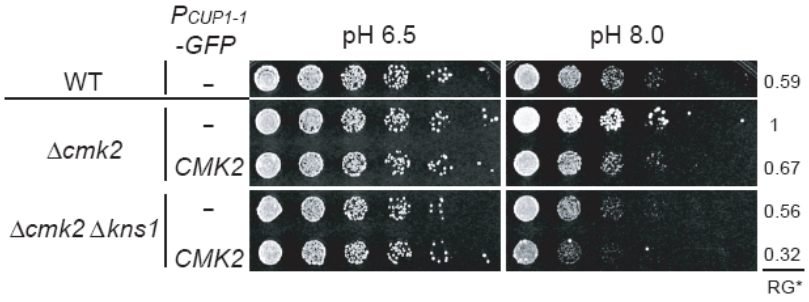

Figure 3.21. Effect of the overexpression of *CMK2* on cell growth at pH 8.0 in the presence and absence of *KNS1*.

Isogenic wild-type (WT; sUB62) and Δ*cmk2* (yNM414) cells carrying an empty vector (pNM67) and either Δ*cmk2* or Δ*kns1*Δ*cmk2* (yNM454) carrying an empty vector or copper-inducible high-copy plasmid (P_{CUP1-1}-*GFP*) encoding wild-type Cmk2 (pNM73) were grown overnight in SC-Trp at 30 °C to log-phase and diluted to an optical density (OD_{600nm}) of 0.25. Five-fold serial dilutions of this diluted culture were spotted onto either SC-Trp (pH 6.5) or 15 mM Hepes (pH 8.0) supplemented with 100 µM $CuSO_4$. Cell growth was monitored after incubation at 30 °C for 3 days (pH 6.5), 6 days (pH 8.0). Cells were spotted together onto the same plates. The approximate cell population density of yeast strains grown at high pH was considered as an indicator of cell fitness, quantified by densitometry (ImageJ, NIH) and indicated as RG (relative growth). The approximate cell population of each strain was expressed relative to that of wild-type cells (set to 1.0).

3.7 Identification of in vitro phosphorylation sites in Cmk2

To further elucidate the significance of Cmk2 phosphorylation by Kns1, I aimed at the identification of the target residues of Kns1 in Cmk2. For this purpose, *in vitro* kinase assays were performed incubating recombinant GST-Kns1 with either 6His-Cmk2 or the inactive 6xHis-Cmk2^{D171A} mutant in the presence of non-radiolabeled ATP. In addition, 6xHis-Cmk2 was incubated alone in the presence and in the absence of ATP (negative control) to identify Cmk2 autophosphorylation sites. *In vitro* kinase reaction mixtures were subjected to mass spectrometric analysis (described in Methods 2.2.4.6).

A summary of all phosphopeptides and phosphorylation sites identified are shown in table 3.2 and 3.3. A total of 13 different Cmk2 phosphopeptides including 19 phosphorylation sites were identified (Table 3.2). A schematic representation of full-length Cmk2 is shown in fig. 3.22 illustrating the fairly dispersed localization of these phosphorylation sites throughout the entire length of Cmk2.

Table 3.2. Phosphopeptides containing the phosphorylation sites identified *in vitro* on Cmk2 by mass spectrometry.

Phosphopeptide		Phospho Site[2,3]	Times mapped *in vitro*[5]	Homologous site in mammalian CaMKII[4]
Position	**Sequence[1]**			
A. Cmk2 phosphopeptides and phosphorylation sites identified only in the GST-Kns1-containing reaction				
325-330	KGF**S**LR	S328	1	
351-384	NMY**S**LGDDGDNDIEENSLNESLLDGVTHSLDDLR	S354	1	
349-384	LRNMYSLGDDGDNDIEENSLNESLLDGVTH**S**LDDLR	**S379**	1	**S318/S319**
B. Cmk2 phosphopeptides and phosphorylation sites identified in the GST-Kns1-containing and autophosphorylation reaction				
30-44	FINKL**S**GQPESYVNR	S35	4	
34-44	LSGQPE**S**YVNR	S40	3	
34-44	LSGQPES**Y**VNR	Y41	2	
34-51	LSGQPESYVNR**T**NYIFGR	T45	3	
45-51	TN**Y**IFGR	Y47	4	**Y13**
52-62	**T**LGAGSFGVVR	T52	6	
52-62	TLGAG**S**FGVVR	S57	5	
66-76	KL**S**TNEDVAIK	**S68**	1	
66-76	KLS**T**NEDVAIK	T69	5	T36
171-182	DLKPENVL**Y**VDK	Y179	2	
292-312	LNPADRP**T**ATELLDDPWITSK	T299	2	T262
292-312	LNPADRPTA**T**ELLDDPWITSK	T301	2	
292-312	LNPADRPTATELLDDPWIT**S**K	S311	1	
313-324	RVE**T**SNILPDVK	T316	7	**T287**
313-324	RVET**S**NILPDVK	S317	5	
403-415	SAL**T**KDAFVQIVK	**T406**	6	**T366**

[1] Phosphosites are presented as bold characters. [2] Residues conserved between yeast CaM kinase Cmk1 and Cmk2 are shown underlined. [3] Phosphosites S68, S379 and T406 have been previously mapped *in vivo* in *S. cerevisiae* Cmk2 and are marked as bold characters[295–298]. [4] Phosphosites that are conserved in mammalian CaMKII and have been found phosphorylated *in vivo* are indicated as bold characters; Y13 of mouse (isoform α), T287 of mouse and human (isoform $\alpha, \beta, \delta, \gamma$), S319 of mouse and human (isoform δ, γ), S318 of mouse (isoform α) and T366 of mouse (isoform β) CaMKII[299–303]. [5] Indicates the number of independently prepared phosphoprotein-enriched samples that produced spectra matching this phosphopeptide sequence.

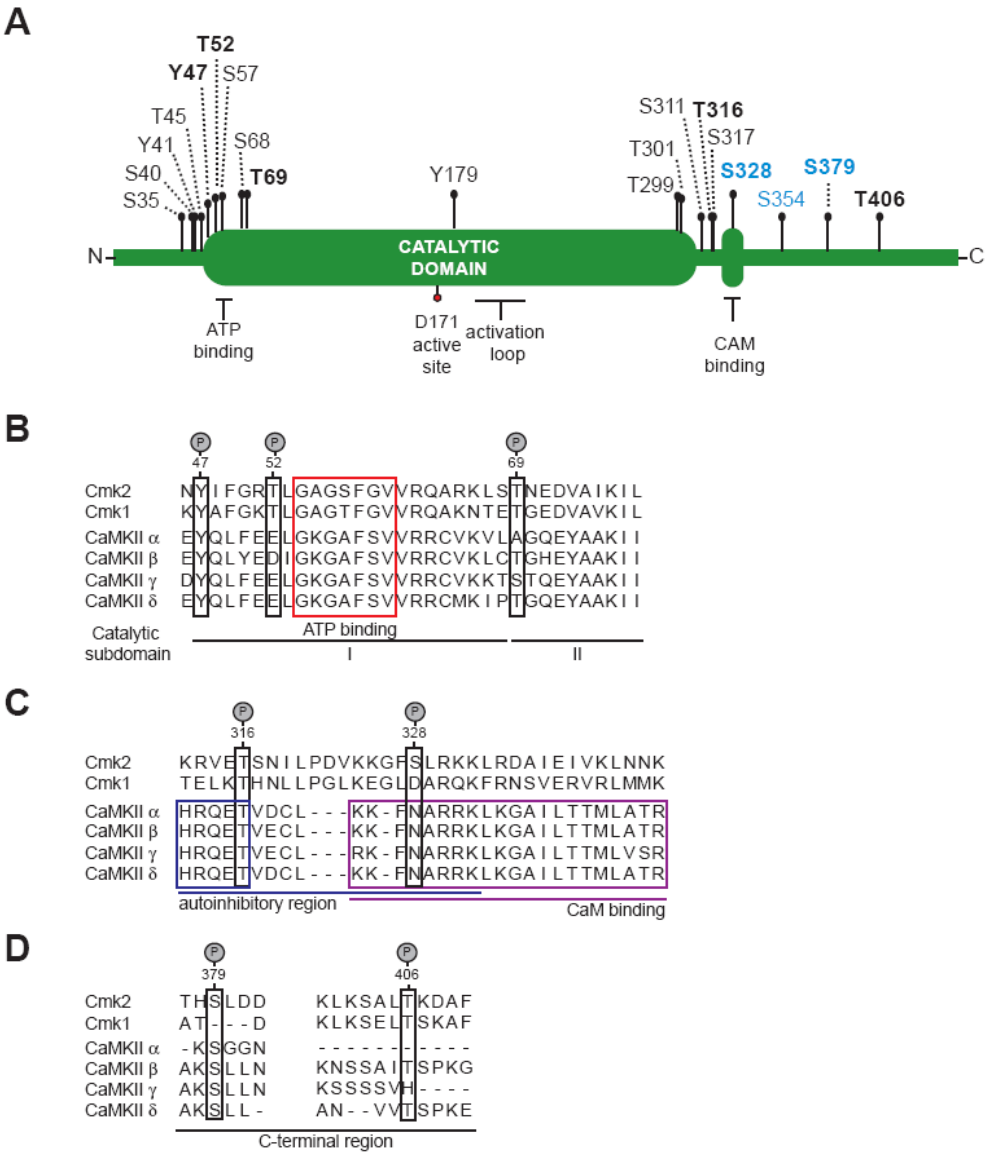

Figure 3.22. Schematic diagram of the *in vitro* phosphorylation sites identified on Cmk2.

(A) The sites of phosphorylation identified by mass spectrometry from the analysis of *in vitro* phosphorylated 6His-Cmk2 are indicated by black pins with residue type and number indicated above. The red pin within the catalytic domain (D171) denotes the position of the active site. Phosphorylation sites chosen for mutagenesis analysis are shown in *bold*. The phosphorylation sites that were only detected when GST-Kns1 was present in the kinase reaction are highlighted in blue. Autophosphorylation sites are indicated in black. The diagram was generated using *MyDomains* from PROSITE (http://us.expasy.org/tools/mydomains). The calmodulin (CAM) binding domain of Cmk2 is represented according to its similarity to mammalian CAM kinases[145]. Sequence alignment of (B) the catalytic domain (subdomain I and part of II), (C) the putative autoregulatory sequence and (D) the C-terminal region of Cmk2 and the equivalent regions of Cmk1 from *S. cerevisiae* and the α, β, γ and δ isoforms of CaMKII from *R. norvegicus*. The identified phosphorylation sites of Cmk2 selected for mutational analysis are indicated by the "P" labelled grey pins and boxed together (black box) with their equivalent residues in the Cmk2 homologues. Relevant regions are indicated with coloured boxes as follows: glycine-rich motif of protein kinases (red box) and key region for autoinhibition (dark blue) and minimal CaM binding domain (violet) of mammalian CaMKII kinases. Numbering is according to the

CMK2 sequence. Dashes indicate single-residue gaps inserted to maximize the alignment of the yeast and mammalian proteins. Adapted from Pausch *et al*. (1991)[145].

Failure to detect any phosphorylation on 6xHis-Cmk2^{D171A} prevented the unequivocal identification of Cmk2 *in vitro* target sites for Kns1. However, of all the residues found phosphorylated on wild-type 6His-Cmk2, three were only detected when GST-Kns1 was present in the kinase reaction; Ser^{328}, Ser^{354} and Ser^{379} (Table 3.2A). Therefore, these residues were contemplated as possible Kns1 candidate target sites. Residue Ser^{328} is located within the region corresponding to the autoregulatory domain of CaMKII kinases, whereas Ser^{354} and Ser^{379} are found within the evolutionary divergent C-terminal region of Cmk2 (Fig. 3.22D). Residue Ser^{379} is conserved among Cmk2 and all isoforms of mammalian CaMKII but not between Cmk2 and Cmk1 (Fig. 3.22D)[145].

Sixteen phosphorylation sites were identified on both the wild-type kinase 6His-Cmk2 incubated under autophosphorylation conditions and on the one incubated with GST-Kns1 (Table 3.2B). None of these phosphorylation sites was detected in the catalytically inactive 6xHis-Cmk2^{D171A} mutant, indicating that these sites result from autocatalytic activity. Of these phosphorylation sites, Ser^{57}, Thr^{301} and Ser^{317} were identified in the kinase reaction devoid of ATP, which implies that 6xHis-Cmk2 underwent autophosphorylation at these residues during expression in *E. coli.*

Five autophosphorylation sites (Tyr^{47}, Thr^{69}, Thr^{299}, Thr^{316} and Thr^{406}) are remarkably conserved throughout evolution, as equivalent residues are found in both yeast Ca^{2+}/CaM-dependent kinases, Cmk1 and Cmk2, as well as in several mammalian CaMKII isoforms, whereas three autophosphorylation sites (Ser^{40}, Thr^{52} and Tyr^{179}) are conserved only within both yeast kinases[145]. Cmk2 has been classified into the group of Ser/Thr protein kinases based on its primary sequence[304]. For this reason, the finding of three tyrosine residues (Tyr^{41}, Tyr^{47} and Tyr^{179}) among the identified autophosphorylation sites was unexpected.

Mass spectrometric analysis of the GST-Kns1 from the kinase reaction containing 6xHis-Cmk2 detected two phosphorylation sites (Table 3.3) in addition to the *in vitro* autophosphorylation sites identified on Kns1 (Table 3.1); Thr^{323} and Ser^{585}. Residue Thr^{323} is situated within the glycine-rich loop of the ATP-binding region and is conserved among Kns1, *S. pombe* Kic1/Lkh1, *D. melanogaster* DOA*, H. sapiens* CLK2 and CLK3[74]. Residue Thr^{585} is located C-terminally to the LAMMER motif of Kns1 (Fig. 3.23). This finding was consistent with the phosphorylation of GST-Kns1^{D440A} by 6His-Cmk2 observed *in vitro* (Figure 3.14, lane 4).

Table 3.3. *In vitro* phosphopeptides and phosphorylation sites identified by mass spectrometry on Kns1 only in the kinase reaction containing 6xHis-Cmk2.

Phosphopeptide		Phospho Site	Times mapped *in vitro*[2]
Position	**Sequence**[1]		
317-326	DLLGQG**T**FGK	T323	1
580-593	LGNSP**S**DLNSTVIK	S585	1

[1] Phosphosites are presented as bold, underlined characters. [2] Indicates the number of independently prepared phosphoprotein-enriched samples that produced spectra matching this phosphopeptide sequence.

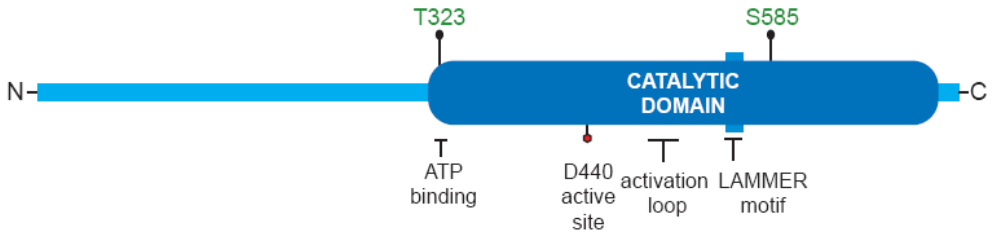

Figure 3.23. Schematic diagram of the *in vitro* phosphorylation sites identified on Kns1 solely in the presence of 6His-Cmk2.

The sites of phosphorylation identified from the analysis by mass spectrometry of *in vitro* phosphorylated GST-Kns1, which were found only when 6His-Cmk2 present in the kinase reaction, are indicated by black pins with residue type and number indicated above in green. The red pin within the catalytic domain (D171) denotes the position of the active site. The diagram was generated using *MyDomains* from PROSITE (http://us.expasy.org/tools/mydomains).

3.8 Mutational analysis of Cmk2

The candidate Kns1 target residues Ser^{328} and Ser^{379} and autophosphorylation sites Tyr^{47}, Thr^{52}, Thr^{69}, Thr^{316} and Thr^{406} were of particular interest due to their evolutionary conservation and location within functionally relevant regions of Cmk2 (Fig. 3.22). To assess the importance of these sites in Cmk2 function, I investigated their role in the *in vitro* substrate phosphorylation activity and *in vivo* function of Cmk2 by individually mutating each residue to either alanine (Ala), to prevent phosphorylation, or to aspartate (Asp) or glutamate (Glu), to partially mimic phosphorylation, in bacterial and yeast Cmk2-borne expressing vectors.

3.8.1 Effect of phosphorylation site mutagenesis on the exogenous kinase activity of Cmk2

The physiological substrates of Cmk2 remain so far unknown. Previous analysis of the *in vitro* kinase specificities of yeast Ca^{2+}/CaM kinases showed that Cmk2 is capable of phosphorylating several substrates such as Kemptamide, Syntide 2, Myelin Basic Protein (MBP), Casein, Histone and Myosin Light Chain[144]. To assess whether the mutation of the selected phosphorylation sites influenced the catalytic capability of Cmk2, I performed *in vitro* kinase assays with wild-type 6His-Cmk2 (WT) or single-point mutant versions of 6His-Cmk2 using MBP as substrate in the presence and absence of calmodulin and Ca^{2+} (Ca^{2+}/CaM) (described in Methods 2.2.4.5). The exogenous kinase activity of 6His-Cmk2 was expressed as relative incorporation of radiolabeled phosphate [γ-^{32}P] from [γ-^{32}P]ATP into MBP.

3.8.1.1 Mutations in the C-terminal region of Cmk2

The C-terminal domain is the most divergent region among members of the CaMKII family. In higher vertebrates, it contains several variable inserts that are isoform specific and confer different properties such as distinct CaM-binding affinities, nuclear targeting inhibitor sequences and SH3-binding potential[149,305–307]. Despite the predominant divergence within the C-terminal region, Cmk2 shares few short stretches of highly conserved residues with CaMKII[145]. The corresponding stretches in CaMKII are embedded within functionally variable inserts[145,308]. Therefore, the finding of two phosphorylated residues, Ser^{379} and Thr^{406}, within these conserved stretches hinted at the possible functional significance for these phosphorylation events *in vivo*.

The candidate Kns1 target site Ser^{379} is remarkably conserved among Cmk2 and all isoforms of mammalian CaMKII (Fig. 3.22D)[145]. In the absence of Ca^{2+}/CaM, mutation Ser^{379} to Ala (S379A) increased Ca^{2+}/CaM-independent catalytic activity whereas mutation Ser^{379} to Glu (S379E) maintained this activity closer to the WT levels. Concretely, the amount of phosphorylated MBP was increased by 1.73-fold by the S379A mutation and by 1.20-fold by the S379E mutation with respect to the amount of MBP phosphorylated by WT (Fig. 3.24B and D). This result hints at an inhibitory role for Ser^{379} phosphorylation in the regulation of the Ca^{2+}/CaM-independent activity of Cmk2 toward exogenous substrate MBP *in vitro*. WT more closely resembled 6His-Cmk2^{S379E} than 6His-Cmk2^{S379A} in terms of Ca^{2+}/CaM-independent activity (Fig. 3.24), suggesting that the recombinant WT enzyme is probably phosphorylated at Ser^{379} in the absence of Ca^{2+}/CaM.

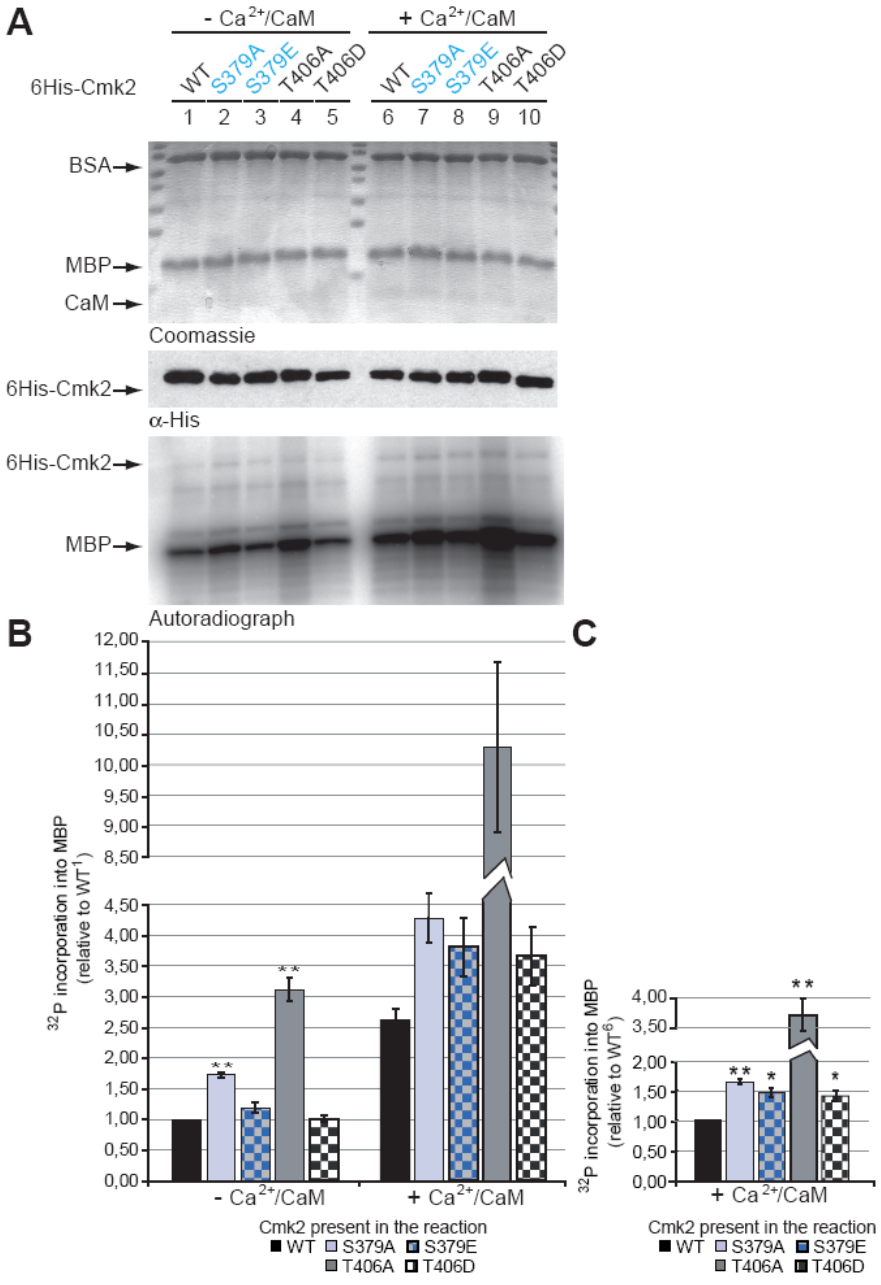

D

		32P incorporation into MBP		
		Relative to WT[1]		Relative to WT[6]
		- Ca2+/CaM	+ Ca2+/CaM	+ Ca2+/CaM
Cmk2	WT	1.00	2.62 ± 0.19	1.00
	S379A	1.73 ± 0.05	4.29 ± 0.40	1.64 ± 0.04
	S379E	1.20 ± 0.08	3.81 ± 0.48	1.45 ± 0.08
	T406A	3.12 ± 0.19	9.73 ± 1.38	3.70 ± 0.27
	T406D	1.01 ± 0.05	3.67 ± 0.48	1.40 ± 0.09

Figure 3.24. Effects of phosphorylation site mutations in the C-terminal domain on the *in vitro* phosphorylation activity of Cmk2 toward the exogenous substrate MBP.

(A) *In vitro* phosphorylation reactions were performed by incubating exogenous substrate MBP (Myelin basic protein; 5 µM) with [γ-^{32}P]ATP and either wild-type (WT) 6His-Cmk2 (pNM38) or one of the

indicated phosphorylation site mutants (0.2 µM) in phosphorylation buffer (25 mM Tris pH 7.5, 10 mM $MgCl_2$, 2.5 mM $CaCl_2$ and 0.2 µg/µl BSA) in the presence or absence of calmodulin (CaM; 10 µM) for 5 minutes by 30 °C as described in Methods 2.2.4.5. The phosphorylation reactions were performed in the absence or presence CaM as indicated. Reactions were stopped by addition of Laemmli sample buffer and immediate boiling for 5 min, followed by SDS-PAGE and autoradiography. The phosphorylation site mutations encoded by the assayed *CMK2* mutants are indicated above each lane and are as follows: S379A (pNM60), S379E (pNM77), T406A (pNM43) and T406D (pNM44). Aliquots of the reaction mixtures were taken prior to [γ^{32}P]ATP addition and resolved by SDS-PAGE followed by either Coomassie staining or Western blotting (WB) with α-His antibodies. Top: Coomassie staining; Middle: α-His WB; Bottom: ^{32}P autoradiograph. All reactions contained BSA as an unspecific phosphate-acceptor competitor (2 mg/ml). The phosphorylation assay shown is representative of three independent experiments. The migration positions of molecular mass marker proteins are indicated in kDa and protein species are indicated by arrows. All samples were analysed on the same gel. (B) Quantification of MBP phosphorylation by the 6His-Cmk2 phosphorylation site mutants. Phosphate [γ-^{32}P] incorporation into MBP was quantified by phosphoimaging and corrected for background activity. The phosphorylation levels measured for MBP incubated with wild-type 6His-Cmk2 in the absence of Ca^{2+}/CaM (lane 1; termed WT^1) were normalized to 1 and those measured for MBP incubated with the indicated 6His-Cmk2 mutants (lines 2 to 10) are presented relative to that value. (C) Quantification of MBP phosphorylation was done as in (B) but the phosphorylation levels measured for MBP incubated with wild type 6His-Cmk2 in the presence of Ca^{2+}/CaM (lane 6; termed WT^6) were normalized to 1 and those measured for MBP incubated with the indicated 6His-Cmk2 mutants (lines 7 to 10) in the presence of Ca^{2+}/CaM are presented relative to that value. Quantification data shown in (B) and (C) represent average MBP phosphorylation values from three independent experiments with standard deviation as indicated. A Student´s *t*-test was performed to show whether the difference in phosphorylation efficiency between wild-type 6His-Cmk2 and phosphorylation site mutants cells was significant. *p* values are indicated with respect to the wild-type value as follows; *p≤0.05 (n=3), **p≤0.01 (n=3). Columns; means, bars; standard deviation. (D) Table showing the quantification data used in (B) and (C).

In the presence of Ca^{2+}/CaM, both Ser^{379}-mutants deviated from the wild-type behaviour, as S379A and S379E mutations increased substrate phosphorylation by 1.64- and 1.45-fold, respectively, with respect to Ca^{2+}/CaM-activated WT (Fig. 3.24C and D).

Thr^{406} is conserved among Cmk2 and isoforms β and δ of CamKII (Fig. 3.22D)[145]. In the absence of Ca^{2+}/CaM, mutant 6His-$Cmk2^{T406A}$ caused a significant (*p<0.01*) 3.12-fold increase in the amount of phosphorylated MBP compared with WT, which reached the activity levels of Ca^{2+}/CaM-activated WT. By contrast, 6His-$Cmk2^{T406D}$ phosphorylated MBP with a similar efficiency as WT (Fig. 3.24B and D). The Thr^{406}-site mutations had similar effects on the exogenous Ca^{2+}/CaM-dependent catalytic activity of Cmk2 (Fig. 3.24). The presence of Ca^{2+}/CaM acted in a cumulative manner with the stimulating effects of the T406A mutation on Cmk2 catalytic activity, resulting in a 3.70-fold increase in the amount of MBP

phosphorylated by 6His-Cmk2^{T406A} relative to that phosphorylated by Ca^{2+}/CaM-activated WT (Fig. 3.24C and D) and a 9.73-fold increase relative to that phosphorylated by WT (in the absence of Ca^{2+}/CaM) (Fig. 3.24B and D). In conclusion, the phosphorylation-mimicking mutation T406D prevented Cmk2 from achieving the enhanced catalytic activity exhibited by the 6His-Cmk2^{T406A} mutant. This result strongly suggests that autophosphorylation at Thr^{406} is likely to play an important role in the inhibition of Cmk2 exogenous kinase activity *in vitro*. Furthermore, the finding that the catalytic behaviour of 6His-Cmk2^{T406D} most closely resembled that of WT in the presence and absence of Ca^{2+}/CaM implies that autophosphorylation of Thr^{406} may occur constitutively and independently of Ca^{2+}/CaM activation.

3.8.1.2 Mutations in the putative autoregulatory region of Cmk2

In the present study, two residues located within the putative autoregulatory domain of Cmk2 were detected phosphorylated *in vitro*; candidate Kns1 target Ser^{328} and autophosphorylation site Thr^{316} (Fig. 3.22C).

The candidate Kns1 target site Ser^{328} is a non-conserved residue located within a region that corresponds, based on sequence similarity, to the CaM binding domain of mammalian CaMKII[145]. In particular, Ser^{328} is embedded within a segment (residues 324-334) that shows a remarkably high degree of evolutionary conservation; yet, Ser^{328} itself is substituted by a non-phosphorylatable polar residue in CaMKII (Asn^{294}; in isoform α) (Fig. 3.22C). Importantly, the segment containing Asn^{294} in mammalian CaMKII (291-297) plays a key role in the stabilization of the autoinhibitory state of CaMKII prior to Ca^{2+}/CaM-activation[131,138]. Hence, if the sequence containing Ser^{328} had a similar function in Cmk2, introduction of a negative charge at position 328 (S328E) would be expected to disrupt a possible inhibitory association of this sequence with the catalytic domain. This would, in turn, enhance Ca^{2+}/CaM-independent activity, as it occurs when a similar mutation at the equivalent position is introduced in CaMKII (N294D)[131]. That was not the case, as 6His-Cmk2^{S328E} did not exhibit greater Ca^{2+}/CaM-independent activity than WT 6His-Cmk2. In fact, 6His-Cmk2^{S328E} exhibited less activity than WT, phosphorylating 0.32-fold less MBP than WT in the absence of Ca^{2+}/CaM (Fig. 3.25B and D). This result shows that a negative charge at position Ser^{328} significantly decreases the Ca^{2+}/CaM-independent exogenous catalytic activity of Cmk2 ($p<0.01$), implying that

the role of Ser^{328} phosphorylation might be inhibitory. There were no significant differences among the substrate phosphorylation efficiencies of WT, 6His-$Cmk2^{S328A}$ and 6His-$Cmk2^{S328E}$ in the presence of Ca^{2+}/CaM, indicating that the phosphorylation state of Ser^{328} is probably irrelevant for Ca^{2+}/CaM-dependent exogenous activity. The observation that 6His-$Cmk2^{S328A}$ most closely mimics the catalytic behaviour of WT leads to infer that the WT enzyme is probably not phosphorylated under assay conditions, favouring the possibility of being Ser^{328} a target site of Kns1.

Thr^{316} is a highly conserved residue embedded within sequence RVE**T**^{316}, which conforms to the minimal consensus motif for CaMKII kinases (RXXS/T)[148]. Autophosphorylation, upon Ca^{2+}/CaM binding, at the homologous residue Thr^{286} in mammalian CaMKII leads to kinase disinhibition due to the disruption of the docked state of Thr^{286} and concomitant displacement of the pseudosubstrate region from the catalytic domain[131]. Unlike mammalian CaMKII, Cmk2 exhibits remarkable basal kinase activity in the absence of Ca^{2+}/CaM. Yet, Cmk2 shows a 2.5- to 4-fold increase in kinase activity in the presence of Ca^{2+}/CaM (Fig. 3.24-26 and refs. [144,147]), suggesting that some kind of regulatory mechanism exists that restrains full active Cmk2 until Ca^{2+}/CaM-mediated stimulation occurs. For these reasons, it was conceivable to speculate that phosphorylation of Thr^{316} could play a role in Cmk2 regulation similar to the role of Thr^{286} in mammalian CaMKII. Thus, if Cmk2 were catalytically constrained by a regulatory segment in a similar way as mammalian CaMKII is prior to Ca^{2+}/CaM activation, introduction of a negative charge at position 316 would be expected to disrupt the autoinhibitory state and increase Ca^{2+}/CaM-independent exogenous kinase activity. However, mutation of Thr^{316} to Asp (T316D) did not increased, but decreased by 0.13-fold, Ca^{2+}/CaM-independent exogenous kinase activity (Fig. 3.25), arguing against the presumption that autophosphorylation at Thr^{316} plays an activating role in Cmk2. In the presence of Ca^{2+}/CaM, 6His-$Cmk2^{T316D}$ exhibited 0.13-fold less substrate phosphorylation efficiency than WT. Altogether, these data indicate that Thr^{316} autophosphorylation does not seem to significantly contribute to the regulation of the catalytic activity of Cmk2 toward exogenous substrates *in vitro*.

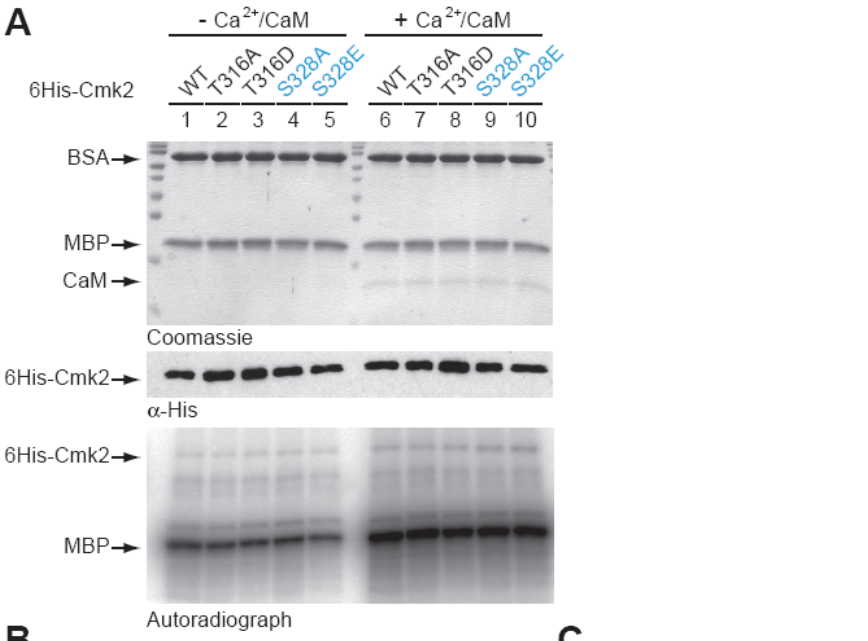

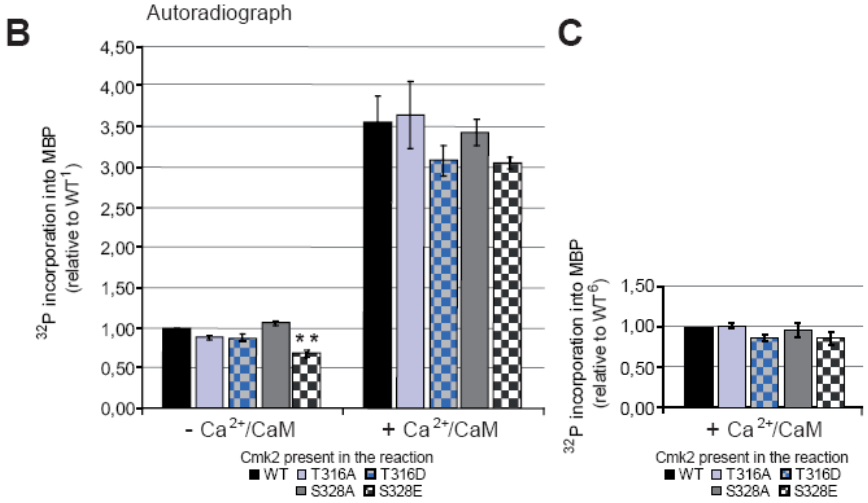

D

		32P incorporation into MBP		
		Relative to WT[1]		Relative to WT[6]
		- Ca2+/CaM	+ Ca2+/CaM	+ Ca2+/CaM
Cmk2	WT	1.00	3.56 ± 0.32	1.00
	T316A	0.88 ± 0.03	3.65 ± 0.41	1.02 ± 0.03
	T316D	0.87 ± 0.04	3.09 ± 0.19	0.87 ± 0.03
	S328A	1.06 ± 0.02	3.43 ± 0.17	0.97 ± 0.09
	S328E	0.68 ± 0.04	3.06 ± 0.07	0.87 ± 0.07

Figure 3.25. Effects of phosphorylation site mutations in the presumptive regulatory domain on the *in vitro* phosphorylation activity of Cmk2 toward the exogenous substrate MBP.

(A) *In vitro* phosphorylation reactions were performed by incubating exogenous substrate MBP (Myelin basic protein) with [γ-^{32}P]ATP and either wild-type (WT) 6His-Cmk2 (pNM38) or one of the indicated phosphorylation site 6His-Cmk2 mutants as described in legend to fig. 3.24. The phosphorylation site mutations encoded by the assayed *CMK2* mutants are indicated above each lane and are as follows: T316A (pNM75), T316D (pNM76), S328A (pNM59) and S328E (pNM39). Aliquots of the reaction mixtures were taken prior to [γ-^{32}P]ATP addition and resolved by SDS-PAGE followed by either

Coomassie staining or Western blotting (WB) with α-His antibodies. Top: Coomassie staining; Middle: α-His WB; Bottom: ^{32}P autoradiograph. The phosphorylation assays shown are representative of three independent experiments. The migration positions of molecular mass marker proteins are indicated in kDa and protein species are indicated by arrows. All samples were analysed on the same gel. (B) and (C) Quantification of MBP phosphorylation by 6His-Cmk2 phosphorylation sites mutants was performed as described in fig. 3.24. *p* values are indicated with respect to the wild-type value as follows; *p≤0.05 (n=3), **p≤0.01 (n=3). Columns; means, bars; standard deviation.

3.8.1.3 Mutations in the ATP binding domain of Cmk2

Residues Tyr^{47} and Thr^{52} are located within subdomain I of the kinase domain of Cmk2 (Fig. 3.26). This subdomain comprises the ATP-binding pocket, where key residues anchor and orientate the ATP molecule for the phosphotransfer reaction[5]. I speculated that phosphorylation at these sites may conceivably affect ATP-binding, as introduction of negative charges through phosphorylation, or mutation to an acidic residue, may possibly disrupt the hydrophobic environment of the ATP-binding pocket that is necessary to enclose the adenine ring of the nucleotide.

Residue Tyr^{47} limits subdomain I at its NH_2-terminus and is highly conserved among Cmk1, Cmk2 and murine CaMKII protein kinases[145]. Mutation of Tyr^{47} to Phe (Y47F) decreased MBP phosphorylation by 0.26-fold in the absence Ca^{2+}/CaM and by 0.17-fold in the presence of Ca^{2+}/CaM compared to the extent of MBP phosphorylation by WT (Fig. 3.26). Mutation of Tyr^{47} to Asp (Y47D) yielded an enzyme that was highly insoluble, yielding a very low concentration of 6His-$Cmk2^{Y47D}$ enzyme preparation. As 6His-$Cmk2^{Y47D}$ could not be adjusted to the same concentration range as the other mutants, it was excluded from the assay.

Thr^{52} is conserved within Cmk1 and Cmk2 and replaced by an acidic residue in isoforms β, δ and γ of murine CaMKII[145]. It is situated next to the highly conserved glycine-rich motif (**T**^{52}LGXGXXG) (Fig. 3.22B), which clamps the non-transferable phosphates of the ATP molecule[309]. In the absence of Ca^{2+}/CaM, 6His-$Cmk2^{T52A}$ phosphorylated 0.29-fold less MBP than WT, whereas, by contrast, the 6His-$Cmk2^{T52D}$ mutant phosphorylated a 1.16-fold more MBP than WT. Both 6His-$Cmk2^{T52A}$ and 6His-$Cmk2^{T52D}$ mutants were able to phosphorylate MBP to a similar extent as WT does in the presence of Ca^{2+}/CaM (Fig. 3.26). This result indicates that autophosphorylation at Thr^{52} might be required to reach the Ca^{2+}/CaM-independent substrate phosphorylation efficiency levels of wild-type Cmk2 *in vitro*.

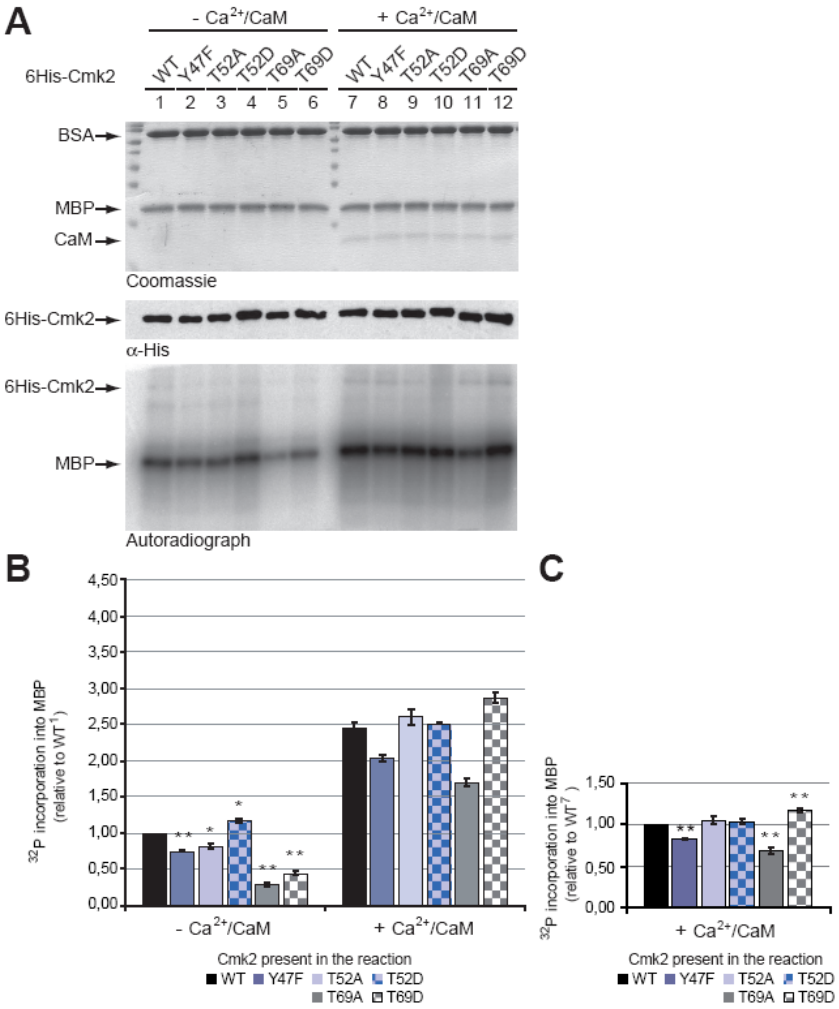

D

Cmk2	32P incorporation into MBP		
	Relative to WT[1]		Relative to WT[7]
	- Ca2+/CaM	+ Ca2+/CaM	+ Ca2+/CaM
WT	1.00	2.45 ± 0,08	1.00
Y47F	0.74 ± 0.02	2.02 ± 0,04	0.83 ± 0,01
T52A	0.81 ± 0.04	2.60 ± 0,11	1.06 ± 0,05
T52D	1.16 ± 0.02	2.51 ± 0,01	1.04 ± 0,03
T69A	0.29 ± 0.02	1.69 ± 0,06	0.70 ± 0,03
T69D	0.43 ± 0.03	2.86 ± 0,07	1.17 ± 0,02

Figure 3.26. Effects of phosphorylation site mutations in the ATP-binding domain on the *in vitro* phosphorylation activity of Cmk2 toward the exogenous substrate MBP.

(A) *In vitro* phosphorylation reactions were performed by incubating exogenous substrate MBP (Myelin basic protein; 5 µM) with [γ-^{32}P]ATP and either wild-type (WT) 6His-Cmk2 (pNM38) or one of the indicated phosphorylation site mutants as described in legend to fig. 3.24. The phosphorylation site mutations encoded by the assayed *CMK2* mutants are indicated above each lane and are as follows: Y47F (pNM55), T52A (pNM56), T52D (pNM79), T69A (pNM58) and T69D (pNM80). Aliquots of the reaction mixtures were taken prior to [γ-^{32}P]ATP addition and resolved by SDS-PAGE followed by either Coomassie staining or Western blotting (WB) with α-His antibodies. Top: Coomassie staining;

Middle: α-His WB; Bottom: ^{32}P autoradiograph. The phosphorylation assay shown is representative of three independent experiments. The migration positions of molecular mass marker proteins are indicated in kDa and protein species are indicated by arrows. All samples were analysed on the same gel. (B) and (C) Quantification of MBP phosphorylation by 6His-Cmk2 phosphorylation sites mutants was performed as described in fig. 3.24. *p* values are indicated with respect to the wild-type value as follows; *p≤0.05 (n=3), **p≤0.01 (n=3). Columns; means, bars; standard deviation.

Thr^{69} limits subdomain II at its NH_2-terminus and is conserved among Cmk1, Cmk2 and murine CaMK II (isoforms β and δ) (Fig. 3.22B)[5,145]. In the absence of Ca^{2+}/CaM, both Thr^{69} mutations significantly (*p<0.01*) decreased the exogenous catalytic activity of Cmk2 toward MBP. Concretely, 6His-$Cmk2^{T69D}$ phosphorylated 0.57-fold less MBP than WT. 6His-$Cmk2^{T69A}$ was even less efficient, phosphorylating 0.73-fold less MBP than WT (Fig. 3.26). This result shows that loss of residue Thr^{69} impairs Ca^{2+}/CaM-independent exogenous kinase activity *in vitro*. Remarkably, both mutants were however able to phosphorylate MBP with efficiencies closer to WT levels in the presence of Ca^{2+}/CaM. In particular, 6His-$Cmk2^{T69A}$ phosphorylated 0.30-fold less MBP than WT. 6His-$Cmk2^{T69D}$ phosphorylated 0.17-fold more MBP than WT (Fig. 3.26). This indicates that both Thr^{69}-mutants undergo a ~6-fold stimulation in the presence of Ca^{2+}/CaM. Yet, only the phosphorylating-mimicking 6His-$Cmk2^{T69D}$ mutant was capable of reaching, and even surpassing, the substrate phosphorylation efficiency of WT (Fig. 3.26). This finding highlights the importance of a negative charge at position 69 for Ca^{2+}/CaM-dependent exogenous kinase activity *in vitro*, implying that the autophosphorylation of Cmk2 at Thr^{69} may be necessary for proper exogenous kinase activity upon Ca^{2+}/CaM activation.

3.8.2 Effect of Cmk2 mutagenesis on cell survival under high pH stress

The inherent complexity of protein kinase regulation demands the analysis of the effects of a particular mutation in a physiological context to reveal the relative contribution of the particular residue in the final biological output. Taking into account that only a fraction of the total amount of protein is normally found phosphorylated at any specific time[310], overexpression of a mutant protein lacking a crucial phosphorylation site or carrying a phosphate-mimic should result in an enhancement of phenotype, which would shed light on the functionality of that residue. Therefore, to evaluate the relevance of the herein identified phosphorylation

sites in the *in vivo* regulation of Cmk2, I analysed the phenotype associated with the overexpression of different GFP-Cmk2 mutants containing non-phosphorylatable or phosphorylation-mimicking residues of cells exposed to alkaline stress (pH 8 and 8.2).

Based on the finding that the effects of Cmk2 on cell tolerance to alkali depend solely on its catalytic activity (Fig. 3.20), I reasoned that the extent of cell growth at high pH that is associated to the overexpression of a particular Cmk2 mutant should indicate whether the corresponding mutation exerts activating or inactivating effects on catalytic activity. Thus, I assessed the growth of Δ*cmk2* cells overexpressing wild-type GFP-Cmk2 or a phosphorylation site mutant Cmk2 on high pH medium (pH 8 and 8.2) and classified the mutations as "activating" if these elicited wild-type alkaline sensitivity (Fig. 3.27A, row 3), or "inactivating" if these resulted in the similar increased alkaline tolerance as that conferred by *CMK2* gene deletion (Fig. 3.27A, row 2).

Single point mutations of either candidate target Ser^{328} or autophosphorylation site Thr^{69} to Ala (S328A, T69A) were classified as "inactivating" because cells overexpressing either GFP-$Cmk2^{S328A}$ or GFP-$Cmk2^{T69A}$ displayed increased alkaline tolerance (Fig. 3.27A, rows 12 and 8), most closely resembling the growth behaviour of Δ*cmk2* cells. By contrast, mutations of either Ser^{328} to Glu (S328E) or Thr^{69} to Asp (T69D) elicited wild-type alkaline sensitivity and were therefore classified as "activating" (Fig. 3.27A, rows 13 and 9). This result indicates that Cmk2 requires a phosphate-mimic at residue Ser^{328} and Thr^{69} to behave like the wild-type protein in conditions of high pH stress.

Mutation of autophosphorylation site Thr^{406} to Ala (T406A) was "activating", as this mutation gave rise to the wild-type alkaline sensitive phenotype (Fig. 3.27A, row 16). Conversely, the phosphorylation-mimicking mutation T406D was classified as "inactivating" owing to its ability to enhance alkaline tolerance (Fig. 3.27A, row 17). These data argue in favour of an inhibitory role for the autophosphorylation at Thr^{406} in the function of Cmk2 *in vivo*.

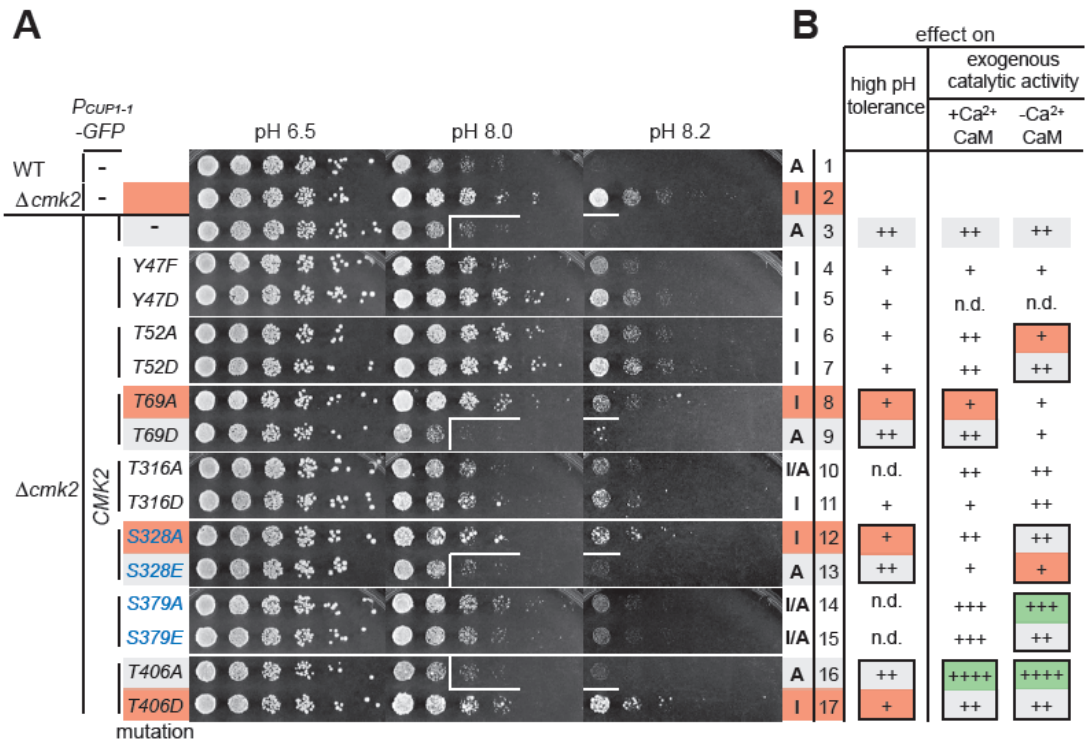

Figure 3.27. Mutational analysis reveals phosphorylation sites relevant for Cmk2 to confer tolerance to alkali.

(A) Overexpression of Cmk2 carrying Y47D, T69A or T406D mutations causes the same increase on alkaline tolerance as *CMK2* deletion. Wild-type (WT; sUB62) and Δ*cmk2* (yNM414) cells harbouring a copper-inducible high-copy empty plasmid (P_{CUP1-1}-GFP; pNM67) and Δ*cmk2* cells harbouring plasmid (P_{CUP1-1}-GFP) encoding either wild-type *CMK2* (pNM73) or *CMK2* carrying one of the following phosphorylation site mutations: Y47F (pNM101), Y47D (pNM125), T52A (pNM102), T52D (pNM126), T69A (pNM116), T69D (pNM127), T316A (pNM112), T316D (pNM128), S328A (pNM110), S328E (pNM129), S379A (pNM111), S379E (pNM130), T406A (pNM113) and T406D (pNM131) were grown overnight on SC-Trp at 30 °C to log-phase. Discernible antagonistic growth effects caused by pairs of mutants for a particular phosphorylation site are highlighted with a white lines. Letter "A" denotes the growth behaviour of Δ*cmk2* cells overexpressing either WT or Cmk2 mutants that mimic WT (*i.e.*, carrying "activating" mutations). Letter "I" denotes the increased alkaline tolerance conferred by either *CMK2* gene deletion or overexpression of Cmk2 carrying "inactivating" mutations. Cells were then diluted, spotted onto SC-Trp (pH 6.5), SC-Trp containing 15 mM Hepes (pH 8.0) or 17.5 mM Hepes (pH 8.2) supplemented with copper and monitored after incubation at 30 °C for 3 days as described in figure 3.19. (B) Summary of the effects phosphorylation site mutations on Cmk2 *in vivo* and *in vitro* function. Two asterisks reflect the effects on catalytic activity or ability to restrict growth at high pH caused by the WT protein or a mutant mimicking WT. If these effects are decreased by a mutation, these are denoted with one asterisk, whereas, if these effects are increased by a mutation, these are denoted with three or four asterisks depending on the extent of the increase. Discernible antagonistic growth effects at high pH or significant changes in catalytic activity caused by pairs of mutants for a particular phosphorylation site are boxed, where effects resembling those caused by WT are highlighted in grey, those reflecting a decrease in WT function (*in vitro* or *in vivo*) in red and those eliciting increased WT activity in green.

Comparison between the *in vivo* and *in vitro* mutational data revealed clear correlation between the effects caused by the Thr^{406}-mutations on the *in vitro* catalytic activity and on the ability to restrict alkaline tolerance *in vivo* of Cmk2 (Fig. 3.27B). Similarly, the effects caused by the Thr^{69}-mutations on the ability of Cmk2 to restrict alkaline tolerance *in vivo* correlated with those on Ca^{2+}/CaM-dependent catalytic activity but not with those on Ca^{2+}/CaM-independent catalytic activity. By contrast, the effects caused by the Ser^{328}-mutations on the *in vitro* Ca^{2+}/CaM-dependent catalytic activity of Cmk2 were opposed to their effects on the ability to restrict alkaline tolerance *in vivo* of Cmk2.

Mutations of either candidate target Ser^{379} or autophoshorylation site Thr^{316} to either Ala or to a phosphorylating-mimicking residue did not elicit discernible antagonistic effects in cell growth at high pH (Fig. 3.27A, rows 10, 11, 14 and 15). Hence, these results indicate that the phosphorylation status of these residues does not notably affect Cmk2 function under such conditions. Any mutation of residue Tyr^{47} or residue Thr^{52} resulted in the alkaline tolerance phenotype of Δ*cmk2* cells, which indicates that loss of either Tyr^{47} or Thr^{52} impairs Cmk2 function *in vivo* (Fig. 3.27A, rows 4-7).

The correct expression of GFP-Cmk2 carrying mutations in residues Tyr^{47}, Thr^{69}, Thr^{406} and Ser^{328} was confirmed under standard conditions by Western blot analysis using the α-GFP antibody (Fig. 3.28). As there were no substantial differences between the protein levels of wild-type Cmk2 and the mutants, it can be inferred that the increased cellular tolerance to alkali elicited by overexpression of Cmk2 carrying the "inactivating" mutations is more likely to correspond with an impairment in Cmk2 function rather than with a failed expression of the mutants.

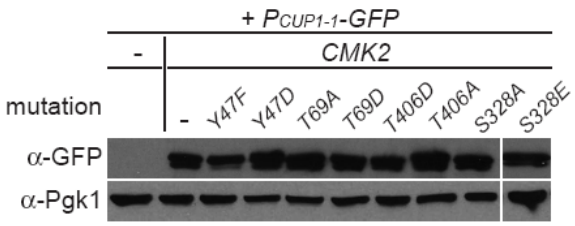

Figure 3.28. Protein levels of wild-type Cmk2 and Cmk2 carrying mutations on residues Tyr^{47}, Thr^{69} and Thr^{406} are similar *in vivo*.

Western blot of whole-cell extracts from Δ*cmk2* (yNM414) cells harbouring empty copper-inducible high-copy plasmid (pNM67) encoding either wild-type *CMK2* (pNM73) or *CMK2* carrying one of the following phosphorylation site mutations: Y47F (pNM101), Y47D (pNM125), T69A (pNM116), T69D (pNM127), S328A (pNM110), S328E (pNM129), T406A (pNM113) and T406D (pNM131). Cells were grown overnight to log-phase in SC-Trp and induced with 100 μM $CuSO_4$ for 30 min. Then, whole-cell

extracts were prepared and analysed by SDS-PAGE, followed by Western blotting with α-GFP and α-Pgk1 antibodies as described in Methods 2.2.4. Although intervening lanes were spliced out, all samples were analysed on the same gel. Pgk1 was detected to confirm equal protein loading.

The alleviating genetic interaction between the *KNS1* and *CMK2* genes indicated that their encoded proteins may conceivably act on the same pathway under high pH stress (pH 8.0) (Fig. 3.17). Furthermore, the increased ability of Cmk2 to restrict alkaline tolerance when overexpressed in the absence of *KNS1* relative to that exhibited in the presence of Kns1 suggested that Kns1 could inhibit Cmk2 activity *in vivo* (Fig. 3.21). Hence, I questioned whether loss of Kns1 distinctively affected the ability of the Cmk2 phosphorylation site mutants to modulate alkaline tolerance. To test this, I examined the alkaline sensitivity phenotype elicited by the overexpression of wild-type GFP-Cmk2 or Cmk2 mutated at the phosphorylation sites that seemed more likely to have relevant roles in the regulation of Cmk2 under high pH stress *i.e.*, Thr^{69}, Ser^{328} and Thr^{406}, in either the Δ*kns1*Δ*cmk2* or the Δ*cmk2* background. No remarkable differences were observed among the growth patterns of cells overexpressing the Ser^{328}- and Thr^{406}-mutants upon *KNS1* loss (data not shown). However, loss of *KNS1* reversed the "inactivating" effect caused by the T69A mutation (Fig. 3.29, row 3 *vs* 5), rendering GFP-$Cmk2^{T69A}$ able to restrict alkaline tolerance like the wild-type kinase. Thus, it can be inferred that Kns1 negatively regulates Cmk2 *in vivo* function if Cmk2 is not phosphorylated on Thr^{69}. Δ*cmk2*Δ*kns1* cells overexpressing GFP-Cmk2 were more sensitive to alkali than those overexpressing GFP-$Cmk2^{T69A}$ (Fig. 3.29, row 2 *vs* 5), indicating that the wild-type kinase is functionally more active than the T69A mutant. This suggests that the T69A mutant might be downregulated in the absence of Kns1 by additional factors.

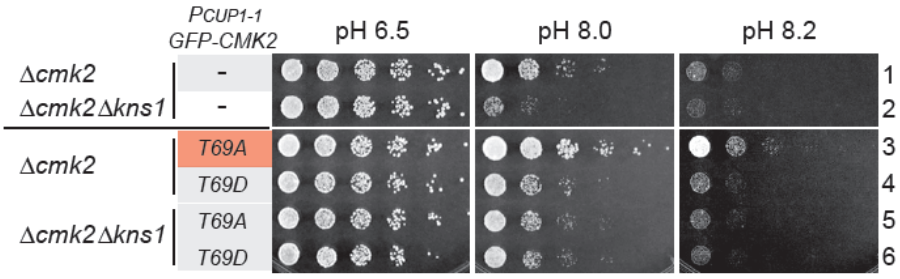

Figure 3.29. The effects of T69A mutation on Cmk2 depends on the presence of Kns1.

Δ*cmk2* (yNM414) and Δ*cmk2*Δ*kns1* (yNM454) cells harbouring a copper-inducible high-copy plasmid empty (P_{CUP1-1}-GFP; pNM67) or plasmid (P_{CUP1-1}-GFP) encoding either wild-type *CMK2* (pNM73) or *CMK2* carrying one of the following phosphorylation site mutations: T69A (pNM116), T69D (pNM127)

were grown overnight on SC-Trp at 30 °C to log phase. Cells were then diluted and spotted onto SC-Trp (pH 6.5), SC-Trp containing 15 mM Hepes (pH 8.0) or 17.5 mM Hepes (pH 8.2) as in figure 3.19. All SC-Trp plates were supplemented with 100 µM $CuSO_4$ to induce GFP-Cmk2 expression. Cell growth was monitored after incubation at 30 °C for 3 days (pH 6.5), 6 days (pH 8.0) or 7 days (pH 8.2).

3.9 Analysis of the intracellular localization of Cmk2

The localization of Cmk2 within the cell has not been yet determined. To test whether Cmk2 coincides with Kns1 in the same intracellular compartment, I examined the intracellular localization of GFP-Cmk2 by fluorescence microscopy. I hypothesized that Kns1 could conceivably regulate Cmk2 function by altering its localization. Therefore, I further examined the localization of GFP-Cmk2 in cells lacking Kns1.

3.9.1 Cmk2 localizes to the cytoplasm

In an attempt to avoid the caveats that protein overexpression has on localization studies, I first aimed at assessing the localization of GFP-Cmk2 expressed under the control of its own promoter. However, GFP-Cmk2 expressed at endogenous levels was not detectable by fluorescence microscopy (data not shown). In order to enable cell culture in rich media and facilitate visualization of GFP-Cmk2, I created cells expressing N-terminally GFP-tagged Cmk2 from the genomic locus under the control of the $P_{CUP1\text{-}1}$ promoter (described in Methods 2.2.2.4). Under standard conditions, GFP-Cmk2 was found diffusely distributed throughout the cytoplasm and excluded from the nucleus, as shown by the lack of overlap with the Hoechst staining (Fig. 3.30A). GFP-Cmk2 overexpressed from the high-copy vector showed cytoplasmic localization in cells cultured in minimal media, indicating that changes in growth media do not affect Cmk2 localization (Fig. 3.30A). Importantly, the localization of GFP-Cmk2 was not affected by the absence of *KNS1* (Fig. 3.30B), indicating that, under non-stressed conditions, Cmk2 localization is independent of Kns1.

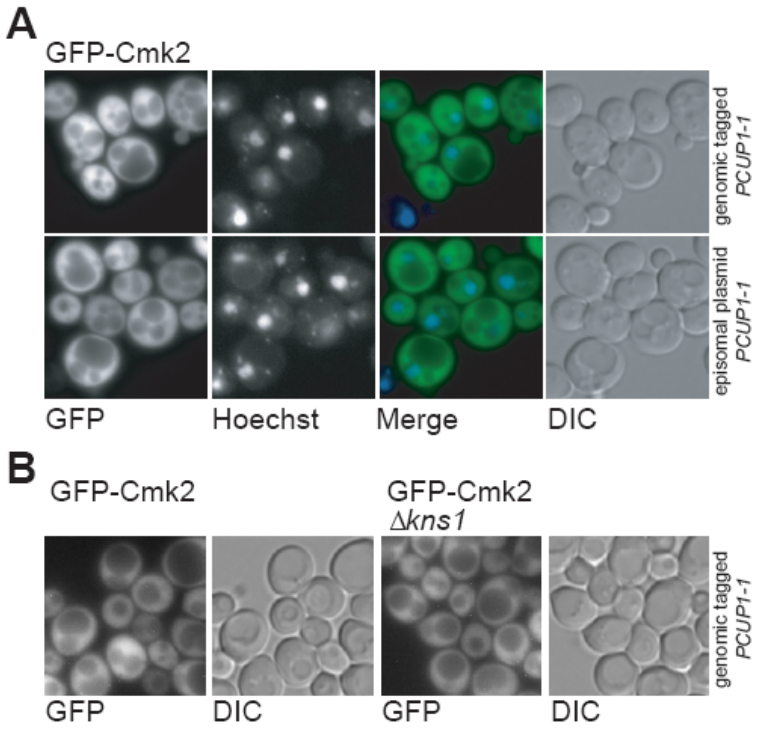

Figure 3.30. GFP-Cmk2 localizes to the cytosol.

(A) Wild-type Cmk2 genomically tagged at its N-terminus with GFP (GFP-Cmk2) and expressed under the control of the copper-inducible promoter (P_{CUP1-1}) localizes to the cytosol and is excluded from the nuclear compartment, as shown by the lack of colocalization with the Hoechst stain. Cells carrying the genome-integrated GFP-Cmk2 fusion protein (yNM555) were grown overnight in YPD to mid-log phase at 30 °C, whereas Δ*cmk2* cells (yNM414) carrying a high-copy plasmid driven by the P_{CUP1-1} promoter (pNM73) where grown in selective synthetic medium (SC-Trp). Cells were induced with 100 µM $CuSO_4$ for 60 min, stained with DNA dye (Hoechst 33258) for 5 min and visualized by fluorescence microscopy. Merge indicates the fusion between the GFP (green) and Hoechst (blue) fluorescence images. Right panels: Nomarski differential-interference contrast (DIC) images. Fluorescence at the cell periphery in the Hoechst panels is an occasional artifact of the Hoechst staining. (B) Cells carrying the copper-inducible GFP-Cmk2 genomic fusion protein in the presence (yNM555; left panels) or absence of Kns1, (Δ*kns1*, yNM574; right panels) show cytosolic GFP-Cmk2 localization. Cells were grown in YPD and induced as described for yNM555 in (A). Fluorescence (GFP) and differential interference contrast (DIC) images are shown.

3.9.1.1 Exposure to osmotic stress induces accumulation of Cmk2 in sub-cytoplasmic patchlike structures

Many kinases, including mammalian CaMKII kinases, are often targeted to distinct subcellular compartments in order to guarantee the appropriate phosphorylation of their substrates[142,311–313]. In particular, cytoplasmic signalling

proteins involved in stress response pathways are occasionally targeted to determined subcellular compartments to ensure signalling fidelity[314]. The ability of Cmk2 to influence cellular tolerance to high pH stress raised the possibility of intracellular Cmk2 repositioning in response to these stress conditions. However, examination of cells overexpressing genomically GFP-tagged Cmk2 subjected to alkaline stress (as described in 3.4.3) did not reveal noticeable changes in GFP-Cmk2 distribution (Fig 3.31B).

It is well-established that the intracellular localization of CaMKII kinases in higher eukaryotes may vary upon a variety of external stimulus[128]. I hypothesized that stress conditions that stimulate Cmk2 protein expression may also alter the localization of Cmk2, which may be influenced by Kns1. Thus, I set out to assess Cmk2 localization under different stress environments. The greatest fold increase in endogenous *CMK2* expression has been reported to occur after 5 to 30 min of exposure to high levels of extracellular Ca^{2+} (~5 fold increase) and after hypo- and hyperosmotic shock (~2.65 fold increase)[158,315]. Therefore, I chose these conditions to challenge cells overexpressing genomically GFP-tagged Cmk2 and assessed GFP-Cmk2 localization. Induction of hyperosmotic stress by addition of sorbitol to the growth media (1M final concentration) resulted in the accumulation of GFP-Cmk2 in discrete cytosolic punctate structures that were mainly concentrated near the plasma membrane, at bud tips and bud neck regions (Fig. 3.31C and G). A similar punctate pattern of distribution was observed under hypoosmotic conditions (Fig. 3.31E). By contrast, addition of calcium (100 mM of $CaCl_2$) to the media followed by 30 min of incubation did not elicit noticeable changes in the diffuse cytosolic distribution of Cmk2 (Fig. 3.31D).

Cells carrying a vector expressing only GFP did not show a punctate pattern upon osmotic stress, indicating that the onset of fluorescence signal at peripheral foci exclusively depends on Cmk2 (Fig. 3.31F). Furthermore, deletion of *KNS1* did not affect the ability of GFP-Cmk2 to concentrate in peripheral foci, which shows that Kns1 is not required for the redistribution of GFP-Cmk2 upon hyperosmotic stress (Fig. 3.31G).

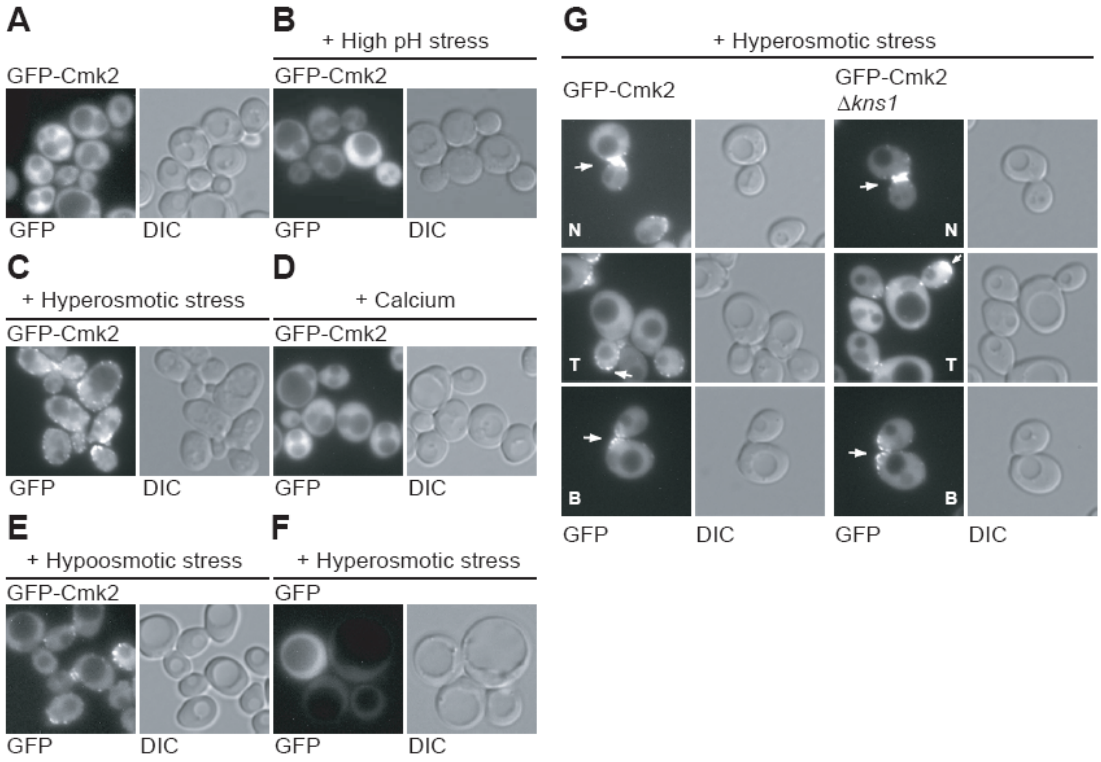

Figure 3.31. GFP-Cmk2 remains cytosolic under high pH stress but it accumulates in discrete punctate structures near the plasma membrane upon osmotic stress independently of Kns1.

Cells carrying the copper-inducible GFP-Cmk2 genomic fusion fusion protein (yNM555) show localization of GFP-Cmk2 in the cytosol when cultured under unstressed conditions (A) and under high pH stress (B). Upon induction of hyperosmotic stress (1 M sorbitol) for 10 minutes, GFP-Cmk2 was observed to accumulate in punctate structures near the plasma membrane (C) in the same cells as in (A). Hypoosmotic stress (wash with distilled water followed by 10 min incubation) (E), but not the addition of calcium to the medium (100 mM of $CaCl_2$) followed by 30 min incubation (D), induced accumulation of Cmk2 in discrete puncta in the same cells as in (A). (F) Cells carrying an empty vector expressing the GFP alone were subjected to hyperosmotic stress as in (A) and did not show a punctate localization pattern for GFP. (G) Accumulation of GFP-Cmk2 in punctate structures is independent of Kns1. Cells carrying the copper-inducible GFP-Cmk2 genomic fusion protein in the presence (yNM555; left panels) or absence of Kns1, (Δ*kns1*, yNM574; right panels) show a similar punctate pattern of GFP-Cmk2 localization. Representative examples of GFP accumulation at bud emergence sites (B), tips (T) and mother-bud neck (N) are indicated by arrows. Cells were grown overnight to mid-log phase at 30 °C in YPD and subjected, or not (in A), to the indicated stress as described above prior to visualization by fluorescence microscopy. In all cases, cells were induced with 100 μM $CuSO_4$ for 60 min prior to visualization. Fluorescence (GFP) and differential interference contrast (DIC) images are shown.

The stress-induced localization of GFP-Cmk2 in punctate foci that accumulated in areas of polarized growth (bud emergence, tips and mother-bud necks) was reminiscent of the characteristic localization of cortical actin patches. Cortical actin patches are discrete cytoskeletal bodies wrapped around plasma membrane invaginations, which are known to be involved in endocytosis and membrane traffic,

and also suggested to constitute possible sites of osmosensing[316–318]. To test whether the punctate distribution of GFP-Cmk2 corresponded with that of cortical actin patches, staining of F-actin with Texas Red Phalloidin was performed in cells overexpressing genomically GFP-tagged Cmk2. As shown in fig. 3.32, GFP-Cmk2 showed partial colocalization with actin patches. In particular, most overlap of GFP signal with the actin staining was observed near bud emergence sites and at the mother-bud neck. However, GFP-Cmk2 was also found in several punctate structures devoid of actin staining and, *vice versa*, various actin cortical patches lacked GFP-Cmk2 signal (Fig. 3.32).

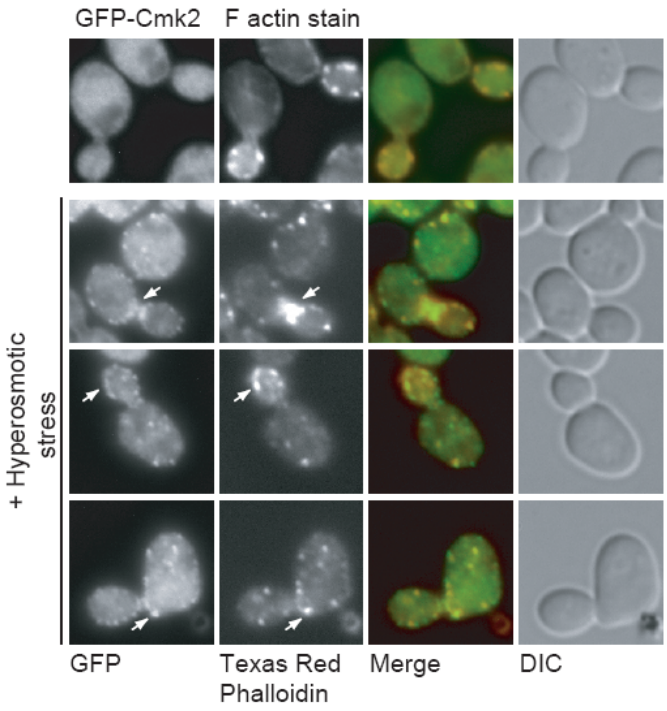

Figure 3.32. GFP-Cmk2 partially colocalizes with cortical actin patches.

Cells carrying the copper-inducible and genome-integrated GFP-Cmk2 fusion protein (yNM555) were grown overnight to log-phase, fixed and stained with Texas Red Phalloidin to visualize F-actin as described in Methods 2.2.6.3. Cells were either immediately harvested (A) or subjected to hyperosmotic stress (1 M Sorbitol for 10 min) (B) before preparation for F-actin staining. Merge indicates the fusion between the GFP (green) and Texas Red Phalloidin (Red) fluorescence images where areas of overlapping localization appear in yellow. Note that cells exposed to hyperosmotic stress show a reduction of polarized actin cables, as previously described[319]. Arrows indicate examples of colocalization of cortical actin patches with GFP-Cmk2 fluorescence.

In summary, these findings show that the cytosolic localization of overexpression GFP-Cmk2 remains unaltered upon alkaline stress but changes in

response to osmotic stress, which elicits the translocation of GFP-Cmk2 to punctate foci that partially colocalize with cortical actin patches and other patchlike structures.

3.9.2 Effect of Cmk2 mutagenesis on localization

Lastly, I investigated whether catalytic inactivation or mutation of the identified phosphorylation sites affects Cmk2 intracellular localization.

3.9.2.1 Catalytic inactivation does not affect Cmk2 localization

Under unstressed conditions, the inactive kinase mutant GFP-Cmk2^{D171A} showed uniform cytoplasmic localization that was identical to that exhibited by the wild-type protein (Fig. 3.33A, upper panels). Next, I asked whether the catalytic activity of Cmk2 was required for patchlike distribution of Cmk2 upon osmotic stress. After exposure of cells to hyperosmotic stress, GFP-Cmk2^{D171A} was translocated to patchlike structures as efficiently as the wild-type protein (Fig. 3.33B, upper panels). This result shows that the stress-stimulated accumulation of Cmk2 in punctate structures does not depend on its intrinsic kinase activity.

3.9.2.2 Cmk2 localization is not affected by the mutation of any of the identified phosphorylation sites

In order to determine whether there is a correlation between the phosphorylation state of Cmk2 and changes in its subcytoplasmic localization, the localization of Cmk2 mutants was examined (Fig. 3.33). None of the mutations caused noticeable changes in the punctate localization pattern of GFP-Cmk2 upon hyperosmotic stress, indicating that repositioning of GFP-Cmk2 does not depend on the phosphorylation state of any of the sites investigated. As the catalytic inactive Cmk2 mutant was still capable of accumulating in cortical punctate structures (Fig. 3.33), it can be concluded that neither autophosphorylation nor phosphorylation of any downstream substrate of Cmk2 plays a role in the regulation of cortical targeting.

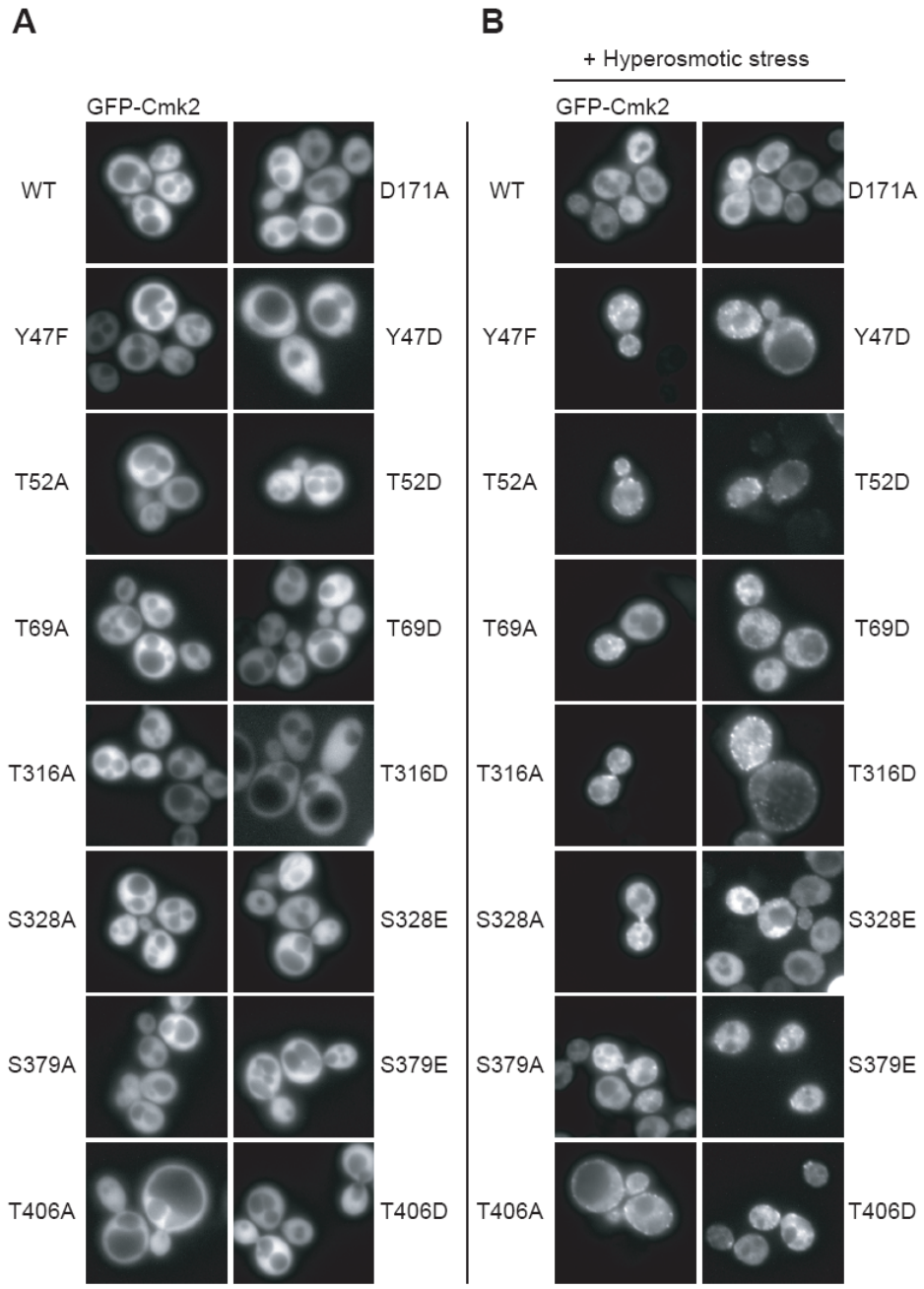

Figure 3.33. Subcellular localization of the GFP-Cmk2 phosphorylation site mutants.

(A) GFP-Cmk2 phosphorylation site mutants localize to the cytosol in the absence of hyperosmotic stress. Δ*cmk2* cells (yNM414) were transformed with a copper-inducible high-copy plasmid ($P_{CUP1\text{-}1}$-GFP) encoding wild-type *CMK2* (pNM73), catalytically inactive $CMK2^{D171A}$ (pNM36) or one of the phosphorylation site *CMK2* mutants carrying the following single point mutations: Y47F (pNM101), Y47D (pNM125), T52A (pNM102), T52D (pNM126), T69A (pNM116), T69D (pNM127), T316A (pNM112), T316D (pNM128), S328A (pNM110), S328E (pNM129), S379A (pNM111), S379E (pNM130), T406A (pNM113) and T406D (pNM131). Cells were grown overnight on selective synthetic medium (SC-Trp) at 30 °C to log-phase, induced with 100 µM $CuSO_4$ for 60 min and visualized by fluorescence microscopy. (B) The phosphorylation site mutations do not affect accumulation of GFP-Cmk2 in peripheral punctate structures upon hyperosmotic stress. The same cells as in (A) were grown overnight to log phase in SC-Trp and then used to inoculate rich culture media (YPD). After overnight

culture in YPD to log phase, cells were induced with 100 µM $CuSO_4$ for 60 min and subjected to hyperosmotic stress (1M Sorbitol for 10 min) prior to visualization by fluorescence microscopy.

4. Discussion

4.1. Kns1 controls alkaline pH stress tolerance in yeast.

In this study, I show that deletion of the yeast LAMMER kinase confers hypersensitivity to alkaline pH stress. For yeast cells to withstand external alkalinization, a myriad of processes must function properly[171–175], making it difficult to discern the physiological defects that underlie the alkaline sensitivity phenotype of Δ*kns1*. Yet, two scenarios can be imagined. In the first one, Δ*kns1* could be defective in a housekeeping process that is particularly necessary for survival under alkaline stress. Here I show that the decreased ability of Δ*kns1* cannot be accounted for, at least, by global defects in splicing (discussed below). In addition, neither vacuolar acidification, a process well-known to be crucial for growth at high pH, nor vacuolar protein transport (via CPY/MVB pathways) is impaired in Δ*kns1* cells (Fig. 3.4 and 3.5). In a second scenario, Δ*kns1* cells could be unable to invoke the appropriate adaptive response (discussed in 4.4.1). A role for Kns1 in alkaline pH stress adaptation would be consistent with previous reports indicating that *KNS1* gene expression is rapidly induced by 4-fold in response to alkaline stress[173].

Consistent with the finding presented herein that Kns1 function is required for optimal growth under high pH stress, recent genome-wide mapping of the quantitative trait loci (QTLs) conferring alkaline tolerance has identified *KNS1* among the genes that contribute to the ability of yeast cells to thrive under high pH stress[320]. However, the alkaline pH sensitivity of Δ*kns1* cells has gone unnoticed in previous genome-wide screens for deletion mutant strains sensitive to high pH[171,172,233]. The missed detection of *bona fide* genes relevant for alkaline tolerance in high-throughput phenotypic approaches is not rare. One notorious example is provided by the fact that the Δ*vma1* mutant and several mutants lacking other components of the vacuolar H^+-ATPase were not reported as high pH sensitive by Giaever *et al.* (2002)[171] nor by Hillenmeyer *et al.* (2008)[233], despite their demonstrated hypersensitivity to alkaline pH conditions[182,188]. Remarkably, both Δ*kns1* and Δ*vma1* mutants showed in those two studies a similar sensitivity score, which lay notably below the cut-off for significance. By contrast, in the present study, these mutants displayed evident poor growth at high pH conditions (Fig. 3.4). The differences between the experimental conditions used in those approaches

and in the present study may account for the discrepancy. For instance, the use of buffers with different buffering capacities (*e.g*, HEPES *vs* Tris-HCl), the use of liquid *vs* solid growth media or the different medium pH used[171,172,233].

4.1.1. Kns1 is mainly located in the nucleus

The finding that Kns1 remains predominantly localized in the nucleus under unstressed and alkaline pH stress conditions (Fig. 3.6 and 3.12) raises a main question: which nuclear process is consistent with the role of Kns1 in the cellular adaptation to alkaline stress?

There are several nuclear processes that are well-known to have a major impact in the adaptive response of yeast to external alkalinization. For instance, the transcription of stress-responsive genes[173,175,176,191]. Recent reports have implicated the fission yeast Lkh1 and mammalian CLK2 LAMMER kinases in the regulation of transcription factors[47,60,66]. It is thus conceivable that a similar role for Kns1 might be conserved in yeast. Alternatively, Kns1 could be implicated in rRNA-related processes, as suggessted by the recent finding that the bulk of proteins associated with Kns1 (13 out of 18) reside within the nucleus and function in processes principally related to rRNA processing and ribosome biogenesis[298]. It is noteworthy that the transcription of rRNA genes has been shown to be highly regulated in response to environmental challenges[321], which would harmonize with the role of Kns1 in alkaline stress tolerance.

In addition, the splicing and nuclear export of alkaline pH stress-related transcripts are further processes taking place within the nucleus that could conceivably affect high pH tolerance. The majority of LAMMER kinases analysed to date have been reported to reside within the nucleus, where they principally modulate splicing processes[36–39,46–48,51,76]. The ability of Kns1 to interact *in vitro*, like its eukaryotic counterparts, with mammalian SR splicing factors together with the existence of a SR-like protein in yeast that is required for the efficiency of pre-mRNA splicing prompted me to speculate the possible involvement of Kns1 in splicing[34,95]. Data presented here show that Δ*kns1* cells do not globally accumulate non-spliced transcripts (Fig. 3.3), advocating against a general role of Kns1 in splicing. The possibility of Kns1 affecting the splicing of other transcripts cannot be completely ruled out given that a limited number of transcripts were assayed in the present study. The development of specialized genome-wide splice-sensitive microarrays *e.g.,* the one created by Clark *et al.* (2002)[241], will be needed in the future to analyse in greater detail splicing efficiency in Δ*kns1* cells.

A role for Kns1 in the nuclear export of mRNA might be also feasible. Recently, a high-throughput mass spectrometric analysis of protein complexes has reported the

association of Kns1 with Gbp2 and Hrb1[298], which are two SR-like proteins implicated in the cytoplasmic delivery of mRNA[93,94]. Hrb1 and Gbp2 share the basic domain structure of canonical SR proteins[94,322]; hence, the ability of Kns1 to interact with these proteins is in line with its ability to interact *in vitro* with mammalian SR splicing factors[34]. Future studies aimed at verifying these associations and investigating their physiological significance may provide key insights into Kns1 nuclear function.

Examination of the localization of GFP-Kns1 overexpressed from a high-copy plasmid further revealed the accumulation of GFP-Kns1 in discrete foci that appeared to be located within, or close to, the nucleus (Fig. 3.12). A potential explanation for the variance observed in GFP-Kns1 intranuclear distribution may relay on the different expression systems used. Since my attempts to visualize endogenously expressed GFP-Kns1 were unsuccessful, I cannot conclude whether Kns1 is actually homogeneously distributed throughout the nucleoplasm or rather specifically concentrated in foci when expressed at physiological levels. Likewise, it remains to be answered whether the cytoplasmic localization of GFP-Kns1 observed when overexpressed from the genomic locus (Fig. 3.6) and in previous localization studies[77,323] is *de facto* biologically relevant or artificially caused by protein overexpression *e.g.,* as a result of the saturation of the nuclear import machinery. Resolving this question will require the analysis of Kns1 localization via biochemical means *e.g.*, using a subcellular fractionation approach.

In conclusion, despite the need for examination under endogenous expression conditions, the presented localization data for Kns1 clearly provide a valuable clue worth to be further explored experimentally: the implication of Kns1 on a nuclear process that is implicated on the adaptation of yeast to high pH stress.

4.2 Identification of the in vitro autophosphorylation sites of Kns1 by mass spectrometry

This work presents the first purification procedure that yields an active and full-length recombinant Kns1 enzyme preparation optimal for in-solution kinase assays and phosphorylation analysis by mass spectrometry (MS). The use of this preparation successfully allowed the identification of eleven phosphorylation sites on Kns1: nine resulting from autophosphorylation (Table 3.2) and two occurring only in the presence of Cmk2 (Table 3.3). Mutational analysis of Thr[562], one of the newly identified

autophosphorylation sites, revealed the importance of this site for Kns1 function *in vivo* (discussed in 4.3.2).

The consensus sequence of Kns1 is yet to be experimentally determined. The characterization of Kns1 phosphorylation specificity using degenerate peptide libraries has been precluded in previous studies owing to the low activity of a recombinant truncated form of Kns1 on exogenous peptides mixtures or proteins[34]. Examination of the sequences surrounding the identified autophosphorylation sites revealed that the residue preferences for Kns1 conform to three of the five criteria reported to describe the optimal consensus sequence of the LAMMER kinase counterparts of Kns1[34,42]. That is, Kns1, like *Drosophila* DOA, human CLK2 and tobacco PK12 LAMMER kinases, seems to generally favour basic residues at position P-4 and P-3, an uncharged polar environment at the P-2 position and hydrophobic residues at the P+1 position (Fig. 3.10). Residues flanking Kns1 *in vitro* autophosphorylation sites Thr^{183}, Ser^{185}, Thr^{562} Ser^{583} and Ser^{601} most closely match these preferences. Remarkably, Thr^{183}, Ser^{185}, Thr^{562} and Ser^{583} have been detected *in vivo* in recent mass spectrometric studies[295,298]. It is thus very likely that these sites constitute physiologically relevant autophosphorylation sites of Kns1.

Previous phosphoamino acid analysis of a truncated form of Kns1 consisting of the catalytic domain (65 KDa) revealed that phosphoserine constituted 51.5%, phosphothreonine 30.2% and phosphotyrosine 18.3% of the total autophosphorylation activity[33]. In the present work, five phosphoserines and four phosphothreonines have been identified by MS on the full-length kinase (Table 3.1). This outcome may indicate that phosphoserine and phosphothreonine residues constitute the most abundant phosphorylated residues of Kns1, as no phosphopeptide enrichment techniques were used prior to MS analysis. This possibility would be consistent with the data obtained from the phosphoamino acid analysis[33]. Remarkably, no phosphotyrosine was detected. Failure to detect phosphotyrosine might be due to several methodological constraints, for instance, the low abundance of phosphotyrosine in Kns1, which might fall below the detection limit of the MS analysis method. Another constraint to consider is the incomplete sequence coverage of the MS analysis, which in the presented study ranged between 40 - 70 % (Dr. G. Dittmar, personal communication). This limited coverage is commonly caused by unfavourable peptide sizes, ion suppression effects and/or insufficient ionization efficiencies for individual peptides[324–326]. In addition, differences between kinase purification methods, *in vitro* kinase assay conditions and/or the phosphorylation analysis approach used in this work and by Lee *et. al.* (1996)[33] may account for the variance of the outcomes. However, it is important to stress that the phosphorylation pattern obtained with the truncated form of Kns1 might

not be an accurate reflection of that obtained herein using the full-length kinase. For instance, tyrosine phosphorylation could be restrained in the full-length kinase. Conversely, a truncated Kns1 might also exhibit artefactual tyrosine phosphorylation as a result from an abnormal conformation or residue exposure.

4.3 Insights into the mode of Kns1 action

In this study, I provide first insights into the mode of Kns1 action *in vivo*. Experimental evidence indicates the following; (i) Kns1 confers alkaline tolerance through catalytic and non-catalytic mechanisms, (ii) the contribution of either of these mechanisms depends on the magnitude of the stress and (iii) the newly identified autophosphorylation site Thr^{562} is crucial for the role of Kns1 in alkaline tolerance.

4.3.1 Kns1 regulates alkaline stress tolerance through catalytic and non-catalytic mechanisms.

The catalytic activity of Kns1 plays a crucial role in the ability of the kinase to modulate the alkaline pH stress tolerance of yeast. This was evidenced by the finding that, unlike overexpression of *GFP-KNS1* (hereafter termed *KNS1*), overexpression of catalytically inactive $KNS1^{D440A}$ was not capable of increasing the tolerance of Δ*kns1* cells to mild alkaline stress (pH 7.8). Remarkably, contrary to the effects of *KNS1* overexpression, the effects of $KNS1^{D440A}$ overexpression gradually become more favourable for survival as pH increases, leading to partial restoration of wild-type alkaline tolerance at pH 8.0. In medium at pH 8.2, the effects on alkaline tolerance elicited by *KNS1* and $KNS1^{D440A}$ overexpression reverted, being $KNS1^{D440A}$ the kinase form that boosts tolerance to the greatest extent (Fig. 3.11). These data demonstrate that Kns1 not only uses its intrinsic kinase activity but also non-catalytic mechanisms to increase alkaline tolerance. This finding would be in line with the regulatory role proposed for the non-catalytic domain of LAMMER kinases in higher eukaryotes[36,40,50]. It is also consistent with the finding that the non-catalytic domain of the LAMMER kinase DOA fulfills separate and essential roles in *Drosophila*[327]. Like DOA, Kns1 possesses an extended N-terminal domain. Therefore, it would be interesting to investigate in the future whether the non-catalytic properties of Kns1 are encompassed within the non-catalytic domain. Non-catalytic properties may comprise protein-binding properties such as target sequestration, scaffolding, anchoring or the ability to oligomerize.

The degree of external alkalinity seems to determine which of both mechanisms is responsible for conferring tolerance and to what extent. This strongly suggests that Kns1 is specifically regulated by a signal elicited by the alkaline stress and that it may function in an adaptive response signalling pathway. Further studies will be needed to establish how Kns1 exert its effects on alkaline tolerance and which alkali-induced factors regulate Kns1 function *in vivo*. Although the molecular bases of these effects are yet to be characterized, I speculate that Kns1 acts on downstream factors that perform condition-specific activities using either its catalytic activity or its non-catalytic qualities *e.g.,* scaffolding properties. Hence, there might be additional Kns1 effectors that are regulated via mechanisms distinct from phosphorylation.

An alternative explanation is conceivable for the phenotypical effects elicited by *KNS1*^{D440A} overexpression. This involves an inherent limitation of the overexpression approach; the indirect effects induced by the sequestration of interacting proteins. Inactivation of the kinase was achieved through the mutation of the invariant aspartyl residue Asp^{440}, which corresponds to the putative catalytic base. This type of mutation has been reported to cause a stabilization of the enzyme-substrate complex in other studies. For instance, in the yeast protein kinase A (Tpk2), mutation of Asp^{210} (Asp^{166} in mammalian PKA) causes a large, 370-fold decrease in k_{cat}; however, it also causes a small increase in K_m for the peptide substrate and ATP[270]. Taking this into account, it cannot be completely ruled out that the effects of *KNS1*^{D440A} overprexpression may result from a functional depletion of Kns1 substrates or interactors due to a “trapping” mechanism. This possibility could be tested in future studies using truncated forms of Kns1 consisting of either the catalytic or the non-catalytic domain alone.

4.3.2 Autophosphorylation site Thr^{562} is crucial for the *in vivo* function of Kns1

Data presented herein support a key role for residue Thr^{562} in modulating Kns1 function *in vivo*. The evidence comes from the finding that the effects of replacing Thr^{562} with Ala (T562A) mostly resemble the effects of a catalytically inactivating mutation (D440A) in the ability of Kns1 to modulate alkaline tolerance (Fig. 3.11). Akin to Kns1^{D440A}*,* Kns1^{T562A} cannot increase alkaline tolerance like the active kinase when overexpressed in cells exposed to an external pH of 7.8. Kns1^{T562A} was even less capable than Kns1^{D440A} of rescuing the growth of Δ*kns1* cells at pH 8.0. In conclusion, these results clearly show that the inability to autophosphorylate on Thr^{562} notably alter the biological function of the kinase, even to a greater extent than loss of catalytic

activity. Hence, it can be inferred that Thr^{562} phosphorylation may be required by Kns1 to behave like the catalytically active kinase *in vivo*.

Residue Thr^{562} is located within the amino acid sequence of the LAMMER motif (EHMAMMQRING**T**^{562}); therefore, I speculated that Thr^{562} phosphorylation might be linked to the role of this signature motif. For the LAMMER kinases of tobacco plants (PK12) and fission yeast (Lkh1), this motif is necessary for catalytic activity and subcellular localization[45,47]. In the present work, mutation T562A did not seem to affect the intrinsic catalytic activity *in vitro* nor localization of Kns1 (Fig. 3.11-12). This could mean that the role of the LAMMER motif is either not functionally connected to Thr^{562}, not conserved in the budding yeast, or both. The fact that the LAMMER motif is less conserved in the budding yeast advocates against complete functional conservation throughout evolution (Fig. 1.1)[29]. Moreover, Thr^{562} lies between two conserved residues within the LAMMER motif but is absent in other members of the family, evidencing that regulation through autophosphorylation at Thr^{562} is exclusive of the budding yeast LAMMER homologue. The main question remains as to how the T562A mutation alters the activity of Kns1 within the cell. It is conceivable that the absence of phosphorylation at position 562 elicits the down-regulation of Kns1 in the cellular context *e.g.*, by altering binding affinities toward external regulators or autoinhibitory regions. Elucidation of the exact molecular mechanism underlying Kns1 regulation through Thr^{562} autophosphorylation will require structural and biochemical characterization of the enzyme.

4.4 Functional links between Kns1 and Cmk2

Previous high-throughput screening for kinase substrates proposed Cmk2 as a candidate *in vitro* substrate for Kns1[102]. In this work, I unequivocally confirmed Cmk2 *in vitro* phosphorylation by Kns1 using catalytically inactive Cmk2 and provide genetic data supporting that both proteins may act in concert on a common pathway, in which Kns1 could conceivably downregulate Cmk2 to confer alkaline tolerance. Mutational analysis of Cmk2 further revealed that autophosphorylation site Thr^{69} might be required to prevent possible inhibition by Kns1 *in vivo* under specific high pH stress conditions. Based on these results, I propose Kns1 as a plausible down-regulator of Cmk2 during alkaline stress and discuss about the feasibility of being Cmk2 a *bona fide* substrate for Kns1.

4.4.1 Genetic interplay between *KNS1* and *CMK2* genes.

A genetic interaction reveals the extent to which the function of one gene is influenced by the presence of a second gene. The analysis of the genetic interaction between the *KNS1* and *CMK2* genes with respect to the cellular response to high pH stress and high levels of exogenous oleate presented in this study provides evidence for the functional interplay of both proteins *in vivo* (described below and depicted in Fig. 4.1).

At an external pH of 7.8, *KNS1* and *CMK2* did not interact genetically, indicating that both proteins modulate the tolerance to mild alkaline stress separately and independently (Fig. 3.17B). At pH 8.0, both genes displayed an alleviating genetic interaction, which commonly arises from pairs of gene products that are in the same complex and/or function in the same pathway[284,285,328–330]. This result indicates that Kns1 and Cmk2 possibly converge in a single pathway to define alkaline tolerance at pH 8.0. Remarkably, alleviating interactions have been recently shown to be particularly enriched among kinases-substrate pairs[331]. Hence, the finding of an alleviating interaction between *KNS1* and *CMK2* together with the demonstration that Kns1 is capable of phosphorylating Cmk2 *in vitro*, and *vice versa*, strengthens the possibility that the kinase-substrate interaction occurs *in vivo*.

The functional relation between Kns1 and Cmk2 in medium at pH 8.0 could be explained by the following hypothetical model: if it is assumed that downregulation of Cmk2 by Kns1 is important for growth at pH 8.0, then loss of the inhibition through *KNS1* deletion (Δ*kns1*) should result in less alkaline pH tolerance due to the increased activity of Cmk2. Conversely, the removal of Cmk2 should disable the detrimental effect conferred by the lack of Kns1, explaining the less severe growth defect exhibited by Δ*kns1*Δ*cmk2* cells. This model would be consistent with the negative regulatory model of Avery and Wasserman[278], which states that when two mutations lead to opposite phenotypic effects *i.e.*, $P_{\Delta x} \neq P_{\Delta y}$, and one suppresses the effect of the other *i.e.,* one is epistatic to the other, it is the downstream mutation that is epistatic to the upstream mutation[278]. As Cmk2 is epistatic to Kns1, Cmk2 should act downstream of Kns1. Epistasis analysis has been used to accurately infer the order of action of pathway components[291,332]. However, it is not a completely reliable method for determining the order of gene action in cases where partial suppression occurs because it could indicate either molecular bypass or counteraction[333]. Here it was observed that loss of *CMK2* did not completely, but partially, suppressed the alkaline sensitive phenotype of Δ*kns1*. One explanation for this partial suppression is that the pathway for adaptation to alkaline pH regulated by Kns1 converges not only with a

Cmk2-dependent pathway, but also with other pathways, as suggested by the finding that loss of *KNS1* renders cells more sensitive to high pH stress in the absence of Cmk2 (Fig. 3.21). A second explanation is that Kns1 may exert, not only upstream, but also further roles downstream of Cmk2. Because the possibility of being Cmk2 upstream of Kns1 cannot be completely ruled out, further work will be required to confirm the model in which Kns1 is positioned upstream of Cmk2 in the regulatory hierarchy. Nonetheless, the weight of the alleviating genetic interaction and the rather specific phosphorylation of Cmk2 by Kns1 (discussed in 4.4.2) lead me to advocate in favour of the possibility that Cmk2 is regulated at pH 8.0 by Kns1 *in vivo*.

At pH 8.2, the *KNS1* and *CMK2* genes displayed an aggravating genetic interaction. Interactions of this kind have been reported to often identify pairs of genes whose products buffer one another and impinge on the same cellular process[105,279,285,328–330]. Owing to the antagonistic nature of Kns1 and Cmk2 effects, this aggravating interaction cannot be interpreted as both proteins acting redundantly on the same process. Based on the observation that Kns1 was unable to confer alkaline tolerance in the wild-type strain, but was able to do that in the Δ*cmk2* background, it can be reasoned that either Cmk2 counteracts the positive effects of Kns1 by directly inhibiting Kns1 or by acting as a major repressor of a downstream target of Kns1 under severe alkaline pH stress conditions (pH 8.2). It has been recently reported that pairs of kinases that act on the same substrate genes commonly display aggravating interactions between themselves[331]. Therefore, a scenario could be envisioned in which both proteins act separately on a common downstream effector that controls adaptation to severe alkaline pH stress. Note that *CMK2* deletion has positive effects on growth even in the absence of *KNS1*, which may implicate that Cmk2 negatively regulates other favorable processes, or stimulate processes that are detrimental for survival at pH 8.2.

The finding that in medium containing oleate the *KNS1* and *CMK2* genes display an alleviating genetic interaction implies that Kns1 and Cmk2 may also function in a common linear pathway to regulate the ability of yeast to cope with high levels of oleate. Oleate sensitivity has been recently hypothesized to underlie the inability to adapt to fluctuations in membrane composition[334]. Consistent with this, oleate sensitive mutants unable to cope with a surplus of unsaturated fatty acids have been shown to direct oleate to phospholipid synthesis, thereby increasing membrane proliferation[100]. Interestingly, situations that lead to plasma membrane stretch or proliferation trigger activation of the cell-wall integrity (CWI) signalling pathway[193], which, in turn, has been related to the alkaline stress response pathway[177,189,335]. In particular, exposure to high pH stress has been proposed to challenge cell-wall integrity, resulting in the specific

activation of the CWI pathway[177]. Hence, the finding that Kns1 and Cmk2 genetically interact under these interconnected stress conditions reinforces the notion that both proteins functionally converge in a common adaptive stress response pathway, which might conceivably overlap with the CWI pathway (further discussed in 4.7).

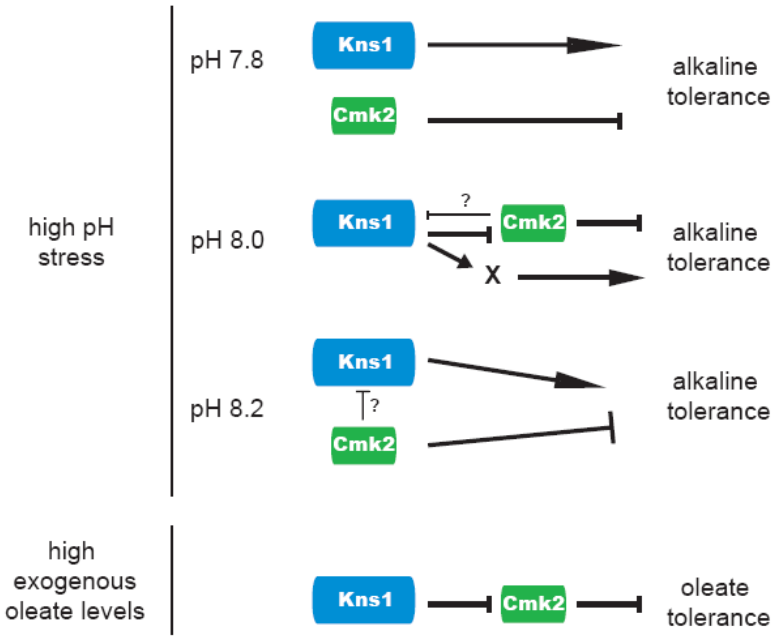

Figure 4.1. Proposed model for the functional interplay between Kns1 and Cmk2 in the regulation of alkaline pH stress tolerance and tolerance to exposure to high levels of exogenous oleate based on genetic analysis.

See text (4.4.1) for detailed description.

Altogether, genetic data presented herein underscore the functional interplay between Kns1 and Cmk2 in the adaptation of yeast to two interconnected stress conditions; environmental alkalinization and exposure to exogenous oleate.

4.4.2 Kns1 phosphorylates Cmk2 *in vitro*

The lack of physiological regulatory constraints in an *in vitro* kinase assay could eventually lead to increased promiscuity of the purified recombinant kinases. The inability of GST-Kns1 to phosphorylate Pdc1-TAP (Fig. 3.15) and the low activity on exogenous peptide mixtures and proteins exhibited by recombinant Kns1 in previous studies strongly suggest that Kns1, unlike Cmk2, does not indiscriminately phosphorylate proteins *in vitro*[33,34,102,144]. Thus, it is conceivable to assume that the *in*

vitro phosphorylation of Cmk2 by Kns1 is rather specific. This notion together with the possibility that Kns1 and Cmk2 may functionally converge in a situation of high pH stress (pH 8.0) favour the hypothesis stated above that Kns1 conceivably regulates Cmk2 by phosphorylation *in vivo* under pH stress (pH 8.0).

Mass spectrometric analysis of wild-type and catalytically inactive 6His-Cmk2^{D171A} incubated under phosphorylating conditions in the presence and absence of GST-Kns1 was performed to identify the targets sites of Kns1 on Cmk2. Ser^{328}, Ser^{354} and Ser^{379} were the only residues found to be phosphorylated in wild-type 6His-Cmk2 exclusively in the presence of GST-Kns1 (Table 3.2A). This led to the suggestion that these residues may constitute possible Kns1 target sites. Yet, the identification of the residues phosphorylated by GST-Kns1 in the catalytically inactive 6His-Cmk2^{D171A} was necessary to unequivocally validate Ser^{328}, Ser^{354} and Ser^{379} as Kns1 target sites. Despite considerable efforts, all attempts to identify the phosphorylation sites in the 6His-Cmk2^{D171A} incubated with GST-Kns1 using mass spectrometry failed. This may have been due to *e.g.,* the low stoichiometric phosphorylation of 6His-Cmk2^{D171A}, loss of phosphoric acid during sample preparation or incomplete sequence coverage[336].

Autophosphorylation events that require prior phosphorylation or “priming” of specific residues by a heterologous kinase are common in the regulation of protein kinases[337–339]. For instance, Akt (Protein kinase B) undergoes autophosphorylation at Ser^{473} exclusively upon previous phosphorylation by PDK-1 (3-Phosphoinositide-dependent protein kinase)[339]. Hence, the possibility that Ser^{328}, Ser^{354} and Ser^{379} phosphorylation resulted, not from direct *trans*-phosphorylation by Kns1, but from autophosphorylation *e.g.*, induced upon phosphorylation of Cmk2 by Kns1 at other residues, cannot be excluded. Nevertheless, biochemical and functional data from the mutational analysis of Ser^{328} and Ser^{379} performed in this work together with the observed preferences of Kns1 for specific residues (discussed in 4.1.2) provided hints on the relevance of these residues in Cmk2 function and their feasibility as targets for Kns1 (discussed in 4.5.1).

4.4.3 Kns1 specifically affects *in vivo* function of the Cmk2 mutant lacking Thr^{69} autophosphorylation site

The mutational analysis presented herein reveals the importance of Thr^{69} phosphorylation in the autoregulation of *in vitro* catalytic activity and *in vivo* function of Cmk2. The significant decrease in substrate phosphorylation elicited by both Thr^{69}-substitutions (T69A or T69D) in the absence of Ca^{2+}/CaM may indicate that either the Asp residue does not appropriately mimic the phosphate in the non-activated (by

Ca^{2+}/CaM) conformation of the kinase or that this threonine residue is structurally required for optimal Ca^{2+}/CaM-independent catalytic activity (Figure 3.26). In any case, both Thr^{69}-mutants underwent remarkable activation in the presence of Ca^{2+}/CaM, which hints at a possible conformational stabilization induced upon CaM binding. Remarkably, only the phosphorylation-mimicking mutant 6His-$Cmk2^{T69D}$ reached the *in vitro* substrate phosphorylation efficiency of wild-type (Fig. 3.26), implying that autophosphorylation at Thr^{69} is likely necessary for Ca^{2+}/CaM-dependent catalytic activity. This stimulatory effect observed *in vitro* correlated with the "activating" effect of the T69D mutation on the function of Cmk2 *in vivo.* Consistently, the T69A mutation was inhibitory *in vitro* and classified as "inactivating" *in vivo*. Given that the $Cmk2^{T69D}$ mutant behaved like its wild-type counterpart both *in vitro* in the presence of Ca^{2+}/CaM and *in vivo* under high pH stress (Fig. 3.26 and 27), it can be speculated that wild-type Cmk2 may be autophosphorylated at Thr^{69} in these situations. Previous work has shown that exposure to alkali provokes a rise in intracellular calcium[174]. Thus, it can be envisaged that Cmk2 is autophosphorylated at Thr^{69} under high pH stress probably due to the Ca^{2+}/CaM-activating conditions brought about by this stress condition[174].

Analysis of the phenotypic effects of mutating Thr^{69} in cells lacking *KNS1* uncovered the protective role of Thr^{69} autophosphorylation against Kns1 downregulation. Overexpression of the GFP-$Cmk2^{T69A}$ mutant did not decrease, like overexpression of the wild-type kinase, the tolerance of Δ*cmk2* cells to high pH stress (Fig. 3.27 and 29). Yet, further deletion of *KNS1* (Δ*cmk2*Δ*kns1*) reversed this behaviour, resulting in a protein GFP-$Cmk2^{T69A}$ that mimicked the wild-type kinase (Fig. 3.29). This strongly suggests that the presence of Kns1 specifically represses the activity of unphosphorylated Cmk2 at position 69 *in vivo*. Moreover, the finding that GFP-$Cmk2^{T69D}$ is functionally independent of Kns1 implies that autophosphorylation at Thr^{69} could prevent downregulation by Kns1.

Altogether, biochemical and physiological evidence underscore the necessity of a negative charge at position 69 for Cmk2 to achieve optimal Ca^{2+}/CaM-dependent kinase activity *in vitro*, emulate the behaviour of the wild-type protein *in vivo* and prevent downregulation by Kns1. Therefore, it can be inferred that, under high pH stress conditions, autophosphorylation of Thr^{69} is required to maintain Cmk2 functionally active. Whether downregulation of $Cmk2^{T69A}$ function by Kns1 occurs via phosphorylation or other non-catalytic mechanisms remains to be elucidated.

4.5 Cmk2 in vitro phosphorylation sites and their potential physiological relevance

This study reports the first mapping of 19 *in vitro* phosphorylation sites on the yeast Ca^{2+}/CaM-dependent kinase Cmk2 by mass spectrometry (Table 3.2). Mutational analysis of two potential Kns1 target sites and five autophosphorylation sites provided key insights into the potential roles of these sites on the regulation of Cmk2 activity (discussed in detail below). The proposed roles for the most relevant sites are summarized as follows:

- Phosphorylation of Thr^{328} inhibits Ca^{2+}/CaM-independent activity *in vitro* . It has opposed effects *in vivo,* possibly due to cellular effectors. It may conceivably be mediated by Kns1.
- Phosphorylation of Ser^{379} inhibits Ca^{2+}/CaM-independent activity *in vitro.* It does not seem to alter the role of Cmk2 in alkaline stress. This phosphorylation event is evolutionary conserved and physiologically relevant, as it has been detected *in vivo* both in yeast and mammals in previous studies. It may result from autocatalysis induced by the presence of Kns1.
- Autophosphorylation at Thr^{406} constitutively inhibits Cmk2 catalytic activity *in vitro* independently of Ca^{2+}/CaM activation. It functionally inactivates Cmk2 *in vivo i.e.*, it renders Cmk2 unable to restrict alkaline pH tolerance. It does not seem to occur under high pH stress. This phosphorylation event has been detected *in vivo* both in yeast and mammals in previous studies.
- Autophosphorylation at Thr^{316} does not notably affect substrate phosphorylation efficiency *in vitro* nor seems to play a role in the ability of Cmk2 to restrain alkaline tolerance.
- Autophosphorylation at Thr^{69} is stimulatory and required for Ca^{2+}/CaM-dependent activity and to display wild-type behaviour *in vivo* under high pH stress. It may prevent downregulation by Kns1.
- Autophosphorylation at Thr^{52} is stimulatory and required for Ca^{2+}/CaM-independent but not for Ca^{2+}/CaM-dependent catalytic activity. Residue Thr^{52} is necessary for Cmk2 to display wild-type behaviour *in vivo* under high pH stress.

4.5.1 Mutational analysis of Kns1 candidate target sites Ser^{379} and Ser^{328}

Ser^{379} is situated within the divergent C-terminal region of Cmk2 and it is highly conserved in mammalian CaMKII kinases (isoforms α, β, γ and δ)[145]. In the absence of Ca^{2+}/CaM, the S379A mutation increased the catalytic activity of Cmk2 whereas the S379E mutation maintained this activity closer to the WT levels (Fig. 3.24). This result strongly suggests a role for Ser^{379} phosphorylation in the inhibition of the Ca^{2+}/CaM-independent activity of Cmk2 toward exogenous substrate MBP *in vitro*. In the presence of Ca^{2+}/CaM, none of the Ser^{379}-mutants resembled the behaviour of wild-type (WT) in terms of *in vitro* substrate phosphorylation efficiency (Fig. 3.24). This has two possible explanations. First, given the enhanced activity of the $Cmk2^{S379A}$ mutant, it is remains feasible that actual Ser^{379} phosphorylation *de facto* inhibits Ca^{2+}/CaM-dependent activity but that the Glu residue does not effectively serve as a reliable phospho-mimic for the Ca^{2+}/CaM-activated kinase. Second, it is possible that non-phoshosphorylated Ser^{379} might be structurally required for normal catalytic function under Ca^{2+}/CaM-activating conditions. Remarkably, no distinguishable antagonistic effects on the ability of Cmk2 to restrain the growth at high pH were elicited by the Ser^{379}-mutations (Fig. 3.27). It is possible that the phosphorylation state of Ser^{379} in particular, or perhaps, Ca^{2+}/CaM-independent activity in general, may not be relevant to the role of Cmk2 in alkaline stress tolerance. Alternatively, Ser^{379} phosphorylation could affect the ability of Cmk2 to govern alkaline tolerance only in combination with other phosphorylation events. Therefore, simultaneous mutagenesis of multiple phosphorylation sites will be needed in the future to unveil possible synergistic effects of Ser^{379} phosphorylation and other phosphorylation events on Cmk2 regulation. Lastly, Ser^{379} phosphorylation may distinctively affect the affinity of Cmk2 towards particular substrates *i.e.*, MBP vs physiological targets.

Although mutation of Ser^{379} did not cause detectable differences in the growth phenotype of cells exposed to alkaline stress, evidence exists in support of the biological relevance of Ser^{379} phosphorylation. This has been provided by the detection of Ser^{379} phosphorylation *in vivo* by large-scale mass spectrometric analysis of the yeast proteome[295,297,298]. In addition, phosphorylation of Ser^{319}, the homologous residue of Ser^{379} in β-CaMKII (isoform 3), has also been detected in human cells[300], which strongly advocates in favor of a conserved role of this phosphorylation event among divergent species.

Ser^{328} is a non-conserved residue situated within an amino acid sequence (residues 324-334) that is remarkably conserved between yeast Cmk2 and mammalian

CaMKII kinases[145]. Arguing against the presumption that this sequence could be involved, like the homologous sequence in CaMKII[131,138], in the stabilization of an autoinhibited form of the kinase, mutation S328E did not increase, but decreased, Ca^{2+}/CaM-independent activity of Cmk2 *in vitro* (Fig. 3.25). This inhibitory effect caused by the S328E mutation *in vitro* did not correlate with the "activating" effect elicited by this mutation *in vivo*. Likewise, the S328A mutation caused a moderate "inactivating" effect *in vivo* but did not alter the catalytic activity of Cmk2 *in vitro*. These discordances might be explained by the possibility that external factors could specifically alter the catalytic properties of the Cmk2 Ser^{328}-mutants in the cellular context.

The question remains whether Ser^{328} and Ser^{379} could be considered feasible targets of Kns1. The only residue known to date to be phosphorylated *in vitro* by Kns1 on an exogenous substrate is the Ser at position 164 on bovine MBP[33]. Comparison of the sequence containing Ser^{164} of MBP with the sequence containing Ser^{328} and Ser^{379} of Cmk2 reveals that the properties of the residues surrounding Ser^{328} conform to a greater degree than Ser^{379} with those of Ser^{164} on MPB. In particular, basic residues are found surrounding Ser^{164} and Ser^{328} (at position P-3, P-4 and P+4) whereas Ser^{379} is surrounded by acidic and hydrophobic residues (Fig. 4.2).

	P_0 position	-4	-3	-2	-1	P_0	+1	+2	+3	+4
MBP	164	S	R	S	G	S	P	M	A	R
Cmk2	328	K	K	Q	F	S	L	R	K	K
	379	G	V	T	H	S	L	D	D	L

Figure 4.2. Alignment of the sequence containing Ser^{164} of bovine MBP and the sequences of Cmk2 containing Kns1 candidate target sites Ser^{328} and Ser^{379}.

Using the designation for the phosphorylated residue as P_0, the residues on the N-terminal side are assigned negative numbers and those on the C-terminal side positive numbers. Amino acid color code: basic (blue), acidic (red), polar uncharged non-phosphorylatable (pink), phosphorylatable (polar uncharged or hydrophopic; green) and hydrophobic non-phosphorylatable (black).

As wild-type 6His-Cmk2 more closely resembled the phosphorylation mimicking mutant 6His-$Cmk2^{S379E}$ than 6His-$Cmk2^{S379A}$ in terms of Ca^{2+}/CaM-independent activity (Fig. 3.24), it might be further inferred that the wild-type recombinant enzyme undergoes constitutive autophosphorylation at Ser^{379} *in vitro*. Conversely, wild-type 6His-Cmk2 behaved more like 6His-$Cmk2^{S328A}$ than like 6His-$Cmk2^{S328E}$ in the absence of Ca^{2+}/CaM. This may indicate that recombinant Cmk2 is not phosphorylated under such conditions and that reduced catalytic activity is only elicited by external factors *i.e.*, the phospho-mimic mutation (S328E) or *trans*-phosphorylation by Kns1. Based on

these notions, Ser^{328} seems a more feasible target of Kns1 than Ser^{379}. However, assuming the hypothesis that Kns1 inhibits Cmk2 activity under high pH stress through the phosphorylation of Ser^{328}, the S328E mutation should have elicited an "inactivating" effect *in vivo*. Since that was not the case, I conclude that Ser^{328} is not the Kns1 target responsible for the downregulation of Cmk2 by Kns1 *in vivo,* or at least, not the only Kns1 target. Importantly, I cannot rule out the possibility that multisite phosphorylation by Kns1 of Ser^{328} and additional target sites, which may be yet to be identified, might be necessary to repress Cmk2 activity *in vivo*.

4.5.2 Autophosphorylation site within the C-terminal domain: Thr^{406}

The present work uncovers a crucial role of Thr^{406} phosphorylation in the regulation of Cmk2 kinase activity. In particular, it shows that the substitution of Thr^{406} with a non-phosphorylatable reside *i.e.,* T406A, causes a 3-4 fold increase in the exogenous catalytic activity of Cmk2 while, conversely, a mimic of Thr^{406} phosphorylation *i.e.,* T406D mutation, prevents Cmk2 from exhibiting that maximal activity (Fig. 3.24). The fact that wild-type 6His-Cmk2 displays similar substrate phosphorylation efficiency as 6His-$Cmk2^{T406D}$ suggests that the wild-type protein might be autophosphorylated on Thr^{406} *in vitro* and, possibly, catalytically repressed. This type of autoregulation appears to occur constitutively, as it is independent of external factors (*e.g.,* Ca^{2+}/CaM).

Physiological evidence supporting the inhibitory role of Thr^{406} phosphorylation in the regulation of Cmk2 activity is provided by the finding that the T406D mutation elicits the effects of the catalytic inactivating mutation D171A, or *CMK2* deletion, on the ability of the kinase to modulate alkaline stress tolerance (Fig. 3.27). Owing to the fact that overexpression of GFP-Cmk2 or GFP-$Cmk2^{T406A}$ causes the same phenotypic consequences on alkaline tolerance, I deduce that Cmk2 is probably not autophosphorylated at Thr^{406} in such conditions. Therefore, it is likely that Cmk2 displays its maximal catalytic activity under high pH stress, as inferred by the enhanced kinase activity exhibited by 6His-$Cmk2^{T406A}$ *in vitro* (Fig. 3.24). It can be envisaged that a specific phosphatase would be required to dephosphorylate Thr^{406} and, supposedly, activate the kinase in that cellular context. Further work will be necessary to identify the extrinsic factors or stimuli that control Thr^{406} dephosphorylation *in vivo.*

Residue Thr^{406} is conserved among budding yeast Cmk1 and Cmk2, and mammalian isoforms β and δ of CaMKII, which suggests that constitutive autoinhibition through phosphorylation might not be a regulatory mechanism exclusive of yeast Cmk2 but shared by several members of the CaMKII family. This conjecture is strengthened

by the fact that both Thr^{406} in Cmk2 and the equivalent residue in murine β-CaMKII, Thr^{366}, have been found to be phosphorylated *in vivo*[302,303,340]. The Thr^{406} residue is embedded within the sequence SAL**T**^{406} located C-terminal to the putative autoregulatory domain of Cmk2. This sequence is analogous to the sequence SAI**T**^{366}, which is located within the variable domain IV/V of β-CaMKII[145]. In higher eukaryotes, the combination through alternative splicing of ten variable domain exons is responsible for the remarkable diversity within the CaMKII kinase family[308]. These variable domains condition isozyme properties such as subcellular targeting to the nucleus, plasma membrane or actin cytoskeleton, the binding affinity for CaM, substrate specificity and the initial rate of autophosphorylation[125,305–307,341–345]. Here I show that the Thr^{406}-mutations do not seem to affect Ca^{2+}/CaM-dependent activation (Fig. 3.24) and do not cause noticeable changes in the subcellular distribution of Cmk2 (Fig. 3.33). Moreover, the catalytic inhibition caused by the T406D mutation was independent of external factors or stimuli. Hence, I propose that Cmk2^{T406D} is probably maintained in a low activity state through an intermolecular or intramolecular association with, possibly, an autoinhibitory domain. Alternatively, the negative charge at Thr^{406} might favor a conformational state that affects ATP or substrate affinity or prevents optimal phosphotransfer. A more detailed kinetic analysis *i.e.,* determination of V_{max} or K_{cat}, will be required to elucidate the exact mechanism of inhibition by Thr^{406} phosphorylation. Future experiments should be aimed at revealing the structural changes that occur in Cmk2 after autophosphorylation and understanding how these contribute to catalytic inhibition.

4.5.3 Autophosphorylation site within the putative autoregulatory domain: Thr^{316}

An important finding of this study is the first identification of Thr^{316} phosphorylation on Cmk2. Residue Thr^{316} is equivalent to Thr^{286} of mammalian CaMKII, whose phosphorylation is crucial for the acquisition of Ca^{2+}/CaM-independent activity by CaMKII[135,136,145]. Previous studies have indicated that Cmk2, like mammalian CaMKII, displays the ability to become Ca^{2+}/CaM-autonomous upon autophosphorylation and pinpointed Thr^{316} as the candidate phosphorylation site accountable for such property[144,147]. The present study shows using mutational analysis that *in vitro* autophosphorylation at Thr^{316} does indeed occur but that it does not seem to affect Ca^{2+}/CaM-independent activity *in vitro* nor the role of Cmk2 in modulating tolerance to high pH conditions.

Prior to Ca^{2+}/CaM activation, CaMKII is kept by the regulatory segment in an inactive state, in which Thr^{286} is buried between the surface of the channel formed by two α-helices of the catalytic domain and the regulatory segment with its side chain located at the negative pole of the αF helix[346]. Therefore, as evidenced in previous mutational studies of murine CaMKII, introduction of an acidic residue at position 286 (T286D mutation) inevitably causes its repulsion from the hydrophopic channel, thereby disrupting the autoinhibitory interaction between the regulatory and catalytic domains, which, in turn, translates into a 7-10% increase in Ca^{2+}/CaM-independent activity toward exogenous substrates[131,347–349]. However, unlike the $CaMKII^{T286D}$ mutant, the 6His-$Cmk2^{T316D}$ mutant did not exhibit greater Ca^{2+}/CaM-independent activity than the 6His-$Cmk2^{T316A}$ mutant (Fig. 3.25). Thus, it is unlikely that Thr^{316} phosphorylation fulfills the same role as the equivalent phosphorylation event in mammalian CaMKII. Alternatively, the catalytic domain of Cmk2 may not interact with the regulatory segment in the same way as occurs in CaMKII and; therefore, it is possible that the T316D mutation (or autophosphorylation at Thr^{316}) is not sufficient on its own to relieve potential inhibitory steric constraints and confer Ca^{2+}/CaM-independent activity in the yeast kinase.

It is important to note that, although both CaMKII and Cmk2 become activated by Ca^{2+}/CaM, one major difference between both proteins is the degree of activation achieved *i.e.,* the fold increase in total catalytic activity. While the basal kinase activity of CaMKII is 100-1000 fold lower than the maximal Ca^{2+}/CaM-stimulated value, that of Cmk2 is only 2.5 to 8 fold lower than the Ca^{2+}/CaM-stimulated activity (Figure 3.24-26)[144,147]. Another difference between Cmk2 and CaMKII is the presence of an association domain at the C-terminus of CaMKII responsible for the dodecameric arrangement of the holoenzyme, which in Cmk2 is lacking[144,149,150]. These differences may account for the divergence in the mechanisms of autoinhibition used by both kinases.

4.5.4 Autophosphorylation site in the ATP-binding domain: Tyr^{47}.

Perhaps the most intriguing finding of this study concerns the identification of three tyrosine autophosphorylation sites on Cmk2 (Tyr^{47}, Tyr^{41} and Tyr^{179}) (Table 3.2B). This implies that Cmk2 exhibits dual-specificity instead of the expected specificity restricted to Ser/Thr. Yet, several protein kinases that were initially considered to exclusively possess Ser/Thr kinase activity have been also shown to display Tyr kinase activity. For instance, casein kinase I and II, glycogen synthase kinase-3β/Mck1, Rim11 and

Spk1 among others[259,350–355]. Moreover, dual-specificity has been previously detected in another Ca^{2+}/CaM-dependent kinase family member. In particular, a chimeric CaMKII protein, consisting of the CaMKII catalytic fragment fused N-terminally to the subdomain I of CaMKI, has been shown to autophosphorylate *in vitro* on Tyr as result of an intramolecular reaction[356]. CaMKII has been also reported to display Tyr phosphorylating activity toward the synthetic substrate poly(Glu/Tyr)[353]. In conclusion, these studies in conjunction with the present work support the notion that the ability to phosphorylate Tyr *in vitro* is a conserved property of Ca^{2+}/CaM-dependent protein kinases. It thus remains to be determined whether acceptor promiscuity only occurs under the non-physiological conditions of the *in vitro* assays or is *de facto* biologically relevant. Remarkably, the residue equivalent to Tyr^{47} in α-CaMKII, Tyr^{13}, has been found to be phosphorylated in the murine brain[299]. As data presented here show that Cmk2 autophosphorylates at a Tyr in the same position *in vitro*, it can be speculated that both phosphorylation events might play a conserved autoregulatory role in both CaMKII family members. To confirm this hypothesis in future studies, it will be necessary to identify Tyr^{47} phosphorylation in Cmk2 *in vivo* and establish whether Tyr^{13} results from the autocatalytic activity of α-CaMKII.

Residue Tyr^{47} is located seven positions upstream of the glycine consensus motif of Cmk2, limiting the ATP-binding domain at its N-terminus (Fig. 3.22B). The close proximity of Tyr^{47} to the ATP-binding domain of Cmk2 hints at the possibility that autophosphorylation at Tyr^{47} might inhibit kinase activity by introducing a steric or electrostatic hindrance that prevents effective ATP or peptide binding. Inhibition by phosphorylation within the ATP-binding domain was initially described for the cyclin-dependent kinase Cdc2 in *S. pombe*, which is down-regulated by phosphorylation of a conserved tyrosine (Tyr^{15}) located within its glycine motif[357–360]. Whether mutation Y47D reduces catalytic activity remains unknown due to the instability of 6His-$Cmk2^{Y47D}$, which prevented its efficient purification from *E. coli*. The instability caused by mutation Y47D *in vitro* raises the suspicion that the functional impairment of GFP-$Cmk2^{Y47D}$ might be accounted for by the instability of the mutant *in vivo*. However, this seems unlikely, as GFP-$Cmk2^{Y47D}$ was correctly expressed in yeast cells, at least, under unstressed conditions (Fig. 3.28). Bulky hydrophobic residues are commonly found in the position occupied by Tyr^{47} in protein kinases[5]. Therefore, the finding that, not only the phosphorylation-mimicking mutation Y47D, but also the Y47F mutation, elicited an increase in alkaline tolerance similar to that caused by the catalytic inactivation or deletion of the kinase (Fig. 3.20 and 27), suggests a key role for the Tyr^{47} residue in the maintenance of the structural integrity of the ATP-binding domain.

The finding that a similar phosphorylation event has been found to occur *in vivo* in α-CaMKII[299] suggests that Tyr[47] autophosphorylation could in fact have a significant role in Cmk2. However, it remains possible that the use of Glu as a phosphomimic may have prevented the identification of such role. Although acidic residues lacking the aromatic ring (Asp and Glu) have been successfully used to mimic phosphotyrosine in several studies[355,361–363], one major caveat of this approach is the obvious structural differences between these residues and Tyr. Future work aimed at elucidating the role of Tyr[47] autophosphorylation should include the use of a better analogue of phosphotyrosine *e.g.,* the chemical compound pCMF (p-Carboxymethyl-l-phenylalanine)[364].

4.6 Cmk2 localization

Here I show that GFP-Cmk2 is uniformly localized in the cytosol under standard conditions of growth, under high pH stress and exposure to high levels of extracellular Ca^{2+}. In addition, I show that, in response to osmotic stress, GFP-Cmk2 rapidly translocates to discrete punctate structures that are dispersed throughout the cytosol and enriched in areas of polarized growth (Fig. 3.31).

Localization data indicate that Kns1 and Cmk2 reside in different subcellular compartments under standard conditions (Fig 3.6 and 30). Given the genetic and biochemical evidence supporting the potential interaction of both proteins *in vivo* and their regulation of the adaptation of yeast to alkaline stress, it was conceivably to expect their co-localization under high pH stress. However, I could not observe co-localization of GFP-Kns1 and GFP-Cmk2. Since Kns1 is capable of directly phosphorylating Cmk2 *in vitro,* it is possible that distinct subcellular compartmentalization serves to regulate this phosphorylation event *in vivo*. Future studies should be aimed at investigating the conditions in which Kns1 and Cmk2 may eventually coincide in the same compartment.

Cortical actin patches consist of plasma membrane invaginations to which actin and other cytoskeletal bodies associate[318]. They are complex and dynamic in composition (reviewed in [365,366]) and their distribution changes dramatically throughout the cell cycle and in response to external stimuli[318,319,367]. Cortical actin patches are considered sites of endocytosis[368]. Among the proteins typically found in, or near, cortical patches are cytoskeletal proteins and their regulators, endocytic adaptors and scaffolds[365,369]. At the sites of polarized growth such as bud sites, bud tips and mother-bud necks, cortical actin patches coincide with other cortical structures that contain proteins involved in the establishment of polarity, growth of the cell surface and actin

assembly[370–372]. The finding that GFP-Cmk2-containing punctate structures partly co-localize with cortical actin patches (Fig. 3.32) suggests a possible interaction of Cmk2 with cortical actin patches components. In support of this possibility, recent genome global interaction studies have identified Cmk2 in protein complexes containing a number of cortical actin patch components and endocytic factors including Ede1, Cof1, Syp1, Myo2, Myo3, Myo4 and Myo5[79,80,298]. Hence, these proteins may constitute possible cortical actin anchors of Cmk2. Like Cmk2, endocytic proteins Ede1 and Syp1 partly colocalize with cortical actin patches[373,374] However, what makes Cmk2 different is that its localization is principally induced by osmotic stress. Thus, it would be interesting to assess in future experiments whether Cmk2 directly binds any of these proteins and, if that were the case, whether these associations occur under normal, or only, under stress conditions. Owing to the fact that the mammalian homologue of Cmk2, β-CaMKII, is capable of associating with F-actin[345], it is also possible that Cmk2 conserves the same property and is thus recruited to cortical patches via an interaction with actin.

Exposure to hyperosmotic conditions elicits the rapid disassembly of the actin cytoskeleton[319]. Efficient recovery from an hyperosmotic shock requires proper activation of the high-osmolarity glycerol (HOG) MAP kinase pathway and the reorganization of the actin cytoskeleton[317,319,375,376]. The finding that, in response to hyperosmotic shock, Cmk2 is brought to, or near, cortical actin patches, which have been proposed to constitute possible sites of osmosensing[317,376], suggest that Cmk2 might play a role in the early steps of HOG signalling pathway or, alternatively, in the reassembly of a polarized actin cytoskeleton.

The ability to alter their localization in response to external stimuli is a common feature of CaMKII kinases[142,313]. This stimuli-induced targeting of Cmk2 to cortical patches may have several purposes. It may increase the kinase specificity of Cmk2 towards specific substrates and/or the sensitivity to second messengers or activators *e.g.*, Ca^{2+} and CaM. In this regard, the repositioning of Cmk2 in polarized cortical patches *de facto* approximates the kinase to the sites where CaM accumulates within the cell[377,378].

4.7 Possible functions of Kns1 and Cmk2 in yeast: Outlook and future perspectives

Comprehensive literature curation of genetic and physical interaction data for Kns1 and Cmk2 together with biochemical and phenotypic data obtained herein suggest the

potential involvement of both proteins in a pathway linked to the Slt2 pathway. Large-scale yeast two-hybrid interaction studies have reported the interaction of Kns1 with stress-inducible dual-specificity MAP kinase phosphatase Sdp1, which negatively regulates the Slt2 MAP-kinase[83]. Slt2 is a component of the cell-wall integrity (CWI) pathway that has been reported to induce a specific transcriptional response upon alkaline stress[171,177] and to be necessary for growth at high pH[171,172]. Importantly, quantitative genetic interaction mapping has revealed an aggravating genetic interaction between the *KNS1* and *SLT2* genes, suggesting that both factors may work in compensatory pathways[331]. It also revealed an alleviating genetic interaction between the *CMK2* and *SLT2* genes, suggesting that their gene products may operate in a common linear pathway[331]. A genetic interaction between *KNS1* and *CMK2* similar to that observed here was not reported, possibly because that genetic analysis was carried out under standard growth conditions *i.e.*, under unstressed conditions where Kns1 and Cmk2 may not functionally interact. Importantly, Cmk2 has been proposed as an *in vitro* candidate substrate for the Slt2 kinase[102]. These findings altogether raise the interesting possibility of Kns1 and Slt2 acting in parallel pathways, which may conceivably converge on Cmk2, to ultimately govern adaptation to alkaline pH stress (pH 8.0). Hence, I suggest that future studies should be aimed at verifying the interaction between Kns1 and Sdp1 and investigating whether it affects Slt2 activity *in vivo*. Moreover, it should be confirmed whether Slt2 *de facto* specifically phosphorylates *in vitro* Cmk2 and, in that case, whether Kns1 function influences this event. Future plans should further include the creation of a combinatorial collection of mutants to analyse the hierarchies of regulation and the genetic relations between Kns1, Cmk2 and components of alkaline-related stress response pathways (*e.g.* Slt2-mediated and calcineurin pathways).

4.8 Concluding remarks

An increase in the external pH has dramatic effects on the physiology of the yeast cell, disrupting internal pH homeostasis and, in turn, optimal enzyme activity, metabolic fluxes, chemical gradients and nutrient acquisition[160,161]. Ultimately, it leads to viability loss[170]. Hence, a thorough understanding of the players and the mechanisms governing the responses of yeast to high pH is of paramount importance for both fundamental and applied research. For instance, the ability of fungi to thrive at high pH is crucial to fungal pathogenicity in plants, insects and animals[379–381]. Mutations that impair the growth of *Candida albicans* at high pH conditions have been shown to correlate with reduced fungal virulence[380]. External alkalinity is a key signal that triggers

antibiotic biosynthesis in other industrially important fungi species[382,383]. I describe in this study a novel and prominent role of the LAMMER kinase Kns1 and its *in vitro* substrate Cmk2 in the adaptation of yeast to environmental alkalinization. Therefore, the implications of my findings may conceivably deliver in the future practical applications in the development of novel antifungal therapies and antibiotic production.

Unicellular organisms that live freely in nature constantly confront sudden and abrupt fluctuations of ambient pH. In multicellular organisms, single cells face pH pertubations in the extracellular environment under both physiological and pathological conditions. For instance, shifts in extracellular pH can be elicited by neurons during synaptic transmission but also by pathological conditions such as hypoxia/ischemia, epilepsy, hyperammonemic encephalopathies, cerebral tumours and HIV (reviewed in [384–386]). Furthermore, changes in extracellular pH have an important impact on the ability of tumour cells to metastasize[387]. Hence, as external pH is a key environmental signal to which all living cells must develop effective molecular responses, it can therefore be envisioned that similarities may exist between the pathways responsible for the ability to endure pH stress from yeast to man. It is thus of utmost interest to determine in the future the extent to which the role of Kns1 and Cmk2 in the control of high pH tolerance are shared with its counterparts in higher eukaryotes. Given the evolutionary conservation of CaM kinases and LAMMER kinases, I anticipate that the information uncovered in the yeast kinases will be likely relevant to the function of their homologues and may potentially have an impact in medical issues.

5. Bibliography

1. Manning, G., Whyte, D.B., Martinez, R., Hunter, T. & Sudarsanam, S. The Protein Kinase Complement of the Human Genome. *Science* **298**, 1912-1934 (2002).
2. Hunter, T. [1] Protein kinase classification. *Protein Phosphorylation Part A: Protein Kinases: Assays, Purification, Antibodies, Functional Analysis, Cloning, and Expression* **Volume 200**, 3-37 (1991).
3. Johnson, L.N. & Barford, D. The effects of phosphorylation on the structure and function of proteins. *Annu Rev Biophys Biomol Struct* **22**, 199-232 (1993).
4. Johnson, L.N. & Lewis, R.J. Structural basis for control by phosphorylation. *Chem. Rev* **101**, 2209-2242 (2001).
5. Hanks, S.K. & Hunter, T. Protein kinases 6. The eukaryotic protein kinase superfamily: kinase (catalytic) domain structure and classification. *The FASEB Journal* **9**, 576 (1995).
6. Lindberg, R.A., Quinn, A.M. & Hunter, T. Dual-specificity protein kinases: will any hydroxyl do? *Trends Biochem. Sci* **17**, 114-119 (1992).
7. Knighton, D. *et al.* Crystal structure of the catalytic subunit of cyclic adenosine monophosphate-dependent protein kinase. *Science* **253**, 407-414 (1991).
8. Hubbard, S.R., Wei, L., Ellis, L. & Hendrickson, W.A. Crystal structure of the tyrosine kinase domain of the human insulin receptor. *Nature* **372**, 746-754 (1994).
9. Taylor, S.S., Radzio-Andzelm, E. & Hunter, T. How do protein kinases discriminate between serine/threonine and tyrosine? Structural insights from the insulin receptor protein-tyrosine kinase. *FASEB J* **9**, 1255-1266 (1995).
10. Hanks, S.K., Quinn, A.M. & Hunter, T. The protein kinase family: conserved features and deduced phylogeny of the catalytic domains. *Science* **241**, 42-52 (1988).
11. Hanks, S.K. & Quinn, A.M. Protein kinase catalytic domain sequence database: identification of conserved features of primary structure and classification of family members. *Meth. Enzymol* **200**, 38-62 (1991).
12. Singh, J. Comparison of conservation within and between the Ser/Thr and Tyr protein kinase family: proposed model for the catalytic domain of the epidermal growth factor receptor. *Protein Eng.* **7**, 849-858 (1994).
13. Howell, B.W. *et al.* STY, a tyrosine-phosphorylating enzyme with sequence homology to serine/threonine kinases. *Molecular and Cellular Biology* **11**, 568 (1991).
14. Ubersax, J.A. & Ferrell, J.E. Mechanisms of specificity in protein phosphorylation. *Nat. Rev. Mol. Cell Biol* **8**, 530-541 (2007).
15. Chaleff, D.T. & Tatchell, K. Molecular cloning and characterization of the STE7 and STE11 genes of Saccharomyces cerevisiae. *Mol. Cell. Biol* **5**, 1878-1886 (1985).
16. Zheng, C.F. & Guan, K.L. Cloning and characterization of two distinct human extracellular signal-regulated kinase activator kinases, MEK1 and MEK2. *J. Biol. Chem* **268**, 11435-11439 (1993).

17. Avruch, J. MAP kinase pathways: the first twenty years. *Biochim. Biophys. Acta* **1773**, 1150-1160 (2007).
18. Dhanasekaran, N. & Premkumar Reddy, E. Signaling by dual specificity kinases. *Oncogene* **17**, 1447-1455 (1998).
19. Widmann, C., Gibson, S., Jarpe, M.B. & Johnson, G.L. Mitogen-activated protein kinase: conservation of a three-kinase module from yeast to human. *Physiol. Rev* **79**, 143-180 (1999).
20. Garrett, S. & Broach, J. Loss of Ras activity in Saccharomyces cerevisiae is suppressed by disruptions of a new kinase gene, YAKI, whose product may act downstream of the cAMP-dependent protein kinase. *Genes Dev* **3**, 1336-1348 (1989).
21. Garrett, S., Menold, M.M. & Broach, J.R. The Saccharomyces cerevisiae YAK1 gene encodes a protein kinase that is induced by arrest early in the cell cycle. *Mol. Cell. Biol* **11**, 4045-4052 (1991).
22. Kassis, S. *et al.* Saccharomyces cerevisiae Yak1p protein kinase autophosphorylates on tyrosine residues and phosphorylates myelin basic protein on a C-terminal serine residue. *Biochem. J* **348 Pt 2**, 263-272 (2000).
23. Kentrup, H. *et al.* Dyrk, a Dual Specificity Protein Kinase with Unique Structural Features Whose Activity Is Dependent on Tyrosine Residues between Subdomains VII and VIII. *Journal of Biological Chemistry* **271**, 3488 - 3495 (1996).
24. Ben-David, Y., Letwin, K., Tannock, L., Bernstein, A. & Pawson, T. A mammalian protein kinase with potential for serine/threonine and tyrosine phosphorylation is related to cell cycle regulators. *EMBO J* **10**, 317-325 (1991).
25. Hartman, H. & Fedorov, A. The origin of the eukaryotic cell: A genomic investigation. *Proceedings of the National Academy of Sciences of the United States of America* **99**, 1420 -1425 (2002).
26. Padmanabha, R., Gehrung, S. & Snyder, M. The KNS1 gene of Saccharomyces cerevisiae encodes a nonessential protein kinase homologue that is distantly related to members of the CDC28/cdc2 gene family. *Mol. Gen. Genet* **229**, 1-9 (1991).
27. Kim, K.H. *et al.* Negative regulation of filamentous growth and flocculation by Lkh1, a fission yeast LAMMER kinase homolog. *Biochem. Biophys. Res. Commun* **289**, 1237-1242 (2001).
28. Bender, J. & Fink, G.R. AFC1, a LAMMEP. kinase from Arabidopsis thaliana, activates STE12-dependent processes in yeast. *PROCEEDINGS-NATIONAL ACADEMY OF SCIENCES USA* **91**, 12105–12105 (1994).
29. Yun, B., Farkas, R., Lee, K. & Rabinow, L. The Doa locus encodes a member of a new protein kinase family and is essential for eye and embryonic development in Drosophila melanogaster. *Genes & Development* **8**, 1160-1173 (1994).
30. Johnson, K.W. & Smith, K.A. Molecular cloning of a novel human cdc2/CDC28-like protein kinase. *J. Biol. Chem* **266**, 3402-3407 (1991).
31. Hanes, J., von der Kammer, H., Klaudiny, J. & Scheit, K.H. Characterization by cDNA cloning of two new human protein kinases. Evidence by sequence comparison of a new family of mammalian protein kinases. *J. Mol. Biol* **244**, 665-672 (1994).
32. Li, J.L., Targett, G.A. & Baker, D.A. Primary structure and sexual stage-specific expression of a LAMMER protein kinase of Plasmodium falciparum. *Int. J. Parasitol* **31**, 387-392 (2001).

33. Lee, K., Du, C., Horn, M. & Rabinow, L. Activity and autophosphorylation of LAMMER protein kinases. *Journal of Biological Chemistry* **271**, 27299 (1996).
34. Nikolakaki, E. *et al.* Phosphorylation by LAMMER protein kinases: determination of a consensus site, identification of in vitro substrates, and implications for substrate preferences. *Biochemistry* **41**, 2055-2066 (2002).
35. Sessa, G., Raz, V., Savaldi, S. & Fluhr, R. PK12, a plant dual-specificity protein kinase of the LAMMER family, is regulated by the hormone ethylene. *Plant Cell* **8**, 2223-2234 (1996).
36. Duncan, P.I. *et al.* Alternative splicing of STY, a nuclear dual specificity kinase. *Journal of Biological Chemistry* **270**, 21524 (1995).
37. Nayler, O., Stamm, S. & Ullrich, A. Characterization and comparison of four serine- and arginine-rich (SR) protein kinases. *Biochem J* **326**, 693-700 (1997).
38. Nayler, O., Schnorrer, F., Stamm, S. & Ullrich, A. The Cellular Localization of the Murine Serine/Arginine-rich Protein Kinase CLK2 Is Regulated by Serine 141 Autophosphorylation. *Journal of Biological Chemistry* **273**, 34341 -34348 (1998).
39. Prasad, J. & Manley, J.L. Regulation and substrate specificity of the SR protein kinase Clk/Sty. *Mol. Cell. Biol* **23**, 4139-4149 (2003).
40. Menegay, H.J., Myers, M.P., Moeslein, F.M. & Landreth, G.E. Biochemical characterization and localization of the dual specificity kinase CLK1. *Journal of Cell Science* **113**, 3241 (2000).
41. Moeslein, F.M., Myers, M.P. & Landreth, G.E. The CLK family kinases, CLK1 and CLK2, phosphorylate and activate the tyrosine phosphatase, PTP-1B. *Journal of Biological Chemistry* **274**, 26697 (1999).
42. Bullock, A.N. *et al.* Kinase Domain Insertions Define Distinct Roles of CLK Kinases in SR Protein Phosphorylation. *Structure* **17**, 352-362 (2009).
43. De Bondt, H.L. *et al.* Crystal structure of cyclin-dependent kinase 2. *Nature* **363**, 595-602 (1993).
44. Taylor, S.S., Knighton, D.R., Zheng, J., Ten Eyck, L.F. & Sowadski, J.M. Structural framework for the protein kinase family. *Annu. Rev. Cell Biol* **8**, 429-462 (1992).
45. Savaldi-Goldstein, S., Sessa, G. & Fluhr, R. The ethylene-inducible PK12 kinase mediates the phosphorylation of SR splicing factors. *The Plant Journal* **21**, 91-96 (2000).
46. Savaldi-Goldstein, S., Aviv, D., Davydov, O. & Fluhr, R. Alternative splicing modulation by a LAMMER kinase impinges on developmental and transcriptome expression. *Plant Cell* **15**, 926-938 (2003).
47. Kang, W.-H., Park, Y.-H. & Park, H.-M. The LAMMER Kinase Homolog, Lkh1, Regulates Tup Transcriptional Repressors through Phosphorylation in Schizosaccharomyces pombe. *J Biol Chem* **285**, 13797-13806 (2010).
48. Colwill, K. *et al.* The Clk/Sty protein kinase phosphorylates SR splicing factors and regulates their intranuclear distribution. *The EMBO Journal* **15**, 265 (1996).
49. Du, C., McGuffin, M.E., Dauwalder, B., Rabinow, L. & Mattox, W. Protein phosphorylation plays an essential role in the regulation of alternative splicing and sex determination in Drosophila. *Mol. Cell* **2**, 741-750 (1998).
50. Kang, W.-H., Park, Y.-D., Hwang, J.-S. & Park, H.-M. RNA-binding protein Csx1 is phosphorylated by LAMMER kinase, Lkh1, in response to oxidative stress in Schizosaccharomyces pombe. *FEBS Lett* **581**, 3473-3478

(2007).
51. Duncan, P.I., Stojdl, D.F., Marius, R.M., Scheit, K.H. & Bell, J.C. The Clk2 and Clk3 dual-specificity protein kinases regulate the intranuclear distribution of SR proteins and influence pre-mRNA splicing. *Exp. Cell Res* **241**, 300-308 (1998).
52. Prasad, J., Colwill, K., Pawson, T. & Manley, J.L. The protein kinase Clk/Sty directly modulates SR protein activity: both hyper- and hypophosphorylation inhibit splicing. *Mol. Cell. Biol* **19**, 6991-7000 (1999).
53. Misteli, T. *et al.* Serine phosphorylation of SR proteins is required for their recruitment to sites of transcription in vivo. *J. Cell Biol* **143**, 297-307 (1998).
54. Xiao, S.H. & Manley, J.L. Phosphorylation of the ASF/SF2 RS domain affects both protein-protein and protein-RNA interactions and is necessary for splicing. *Genes & Development* **11**, 334-344 (1997).
55. Faustino, N.A. & Cooper, T.A. Pre-mRNA splicing and human disease. *Genes Dev* **17**, 419-437 (2003).
56. Venables, J.P. Aberrant and alternative splicing in cancer. *Cancer Res* **64**, 7647-7654 (2004).
57. Tazi, J., Bakkour, N. & Stamm, S. Alternative splicing and disease. *Biochim. Biophys. Acta* **1792**, 14-26 (2009).
58. Muraki, M. *et al.* Manipulation of alternative splicing by a newly developed inhibitor of Clks. *J. Biol. Chem* **279**, 24246-24254 (2004).
59. Park, Y.-D. *et al.* LAMMER kinase homolog, Lkh1, is involved in oxidative-stress response of fission yeast. *Biochem. Biophys. Res. Commun* **311**, 1078-1083 (2003).
60. Rodríguez-Gabriel, M.A. *et al.* RNA-binding protein Csx1 mediates global control of gene expression in response to oxidative stress. *EMBO J* **22**, 6256-6266 (2003).
61. Nakagawa, C.W., Yamada, K. & Mutoh, N. Role of Atfl and Papl in the Induction of the Catalase Gene of Fission Yeast Schizosaccharomyces pombe. *J Biochem* **127**, 233-238 (2000).
62. James, B.P., Staatz, W.D., Wilkinson, S.T., Meuillet, E. & Powis, G. Superoxide dismutase is regulated by LAMMER kinase in Drosophila and human cells. *Free Radical Biology and Medicine* **46**, 821-827 (2009).
63. Myers, M.P., Murphy, M.B. & Landreth, G. The dual-specificity CLK kinase induces neuronal differentiation of PC12 cells. *Mol. Cell. Biol.* **14**, 6954-6961 (1994).
64. Roberts, R.L. & Fink, G.R. Elements of a single MAP kinase cascade in Saccharomyces cerevisiae mediate two developmental programs in the same cell type: mating and invasive growth. *Genes Dev* **8**, 2974-2985 (1994).
65. Ecker The ethylene signal transduction pathway in plants. *Science* **268**, 667-675 (1995).
66. Rodgers, J.T., Haas, W., Gygi, S.P. & Puigserver, P. Cdc2-like kinase 2 is an insulin-regulated suppressor of hepatic gluconeogenesis. *Cell Metab* **11**, 23-34 (2010).
67. Fagerström-Billai, F., Durand-Dubief, M., Ekwall, K. & Wright, A.P.H. Individual subunits of the Ssn6-Tup11/12 corepressor are selectively required for repression of different target genes. *Mol. Cell. Biol* **27**, 1069-1082 (2007).
68. Fan, Y. *et al.* Drosophila translational elongation factor-1gamma is modified in response to DOA kinase activity and is essential for cellular viability. *Genetics* **184**, 141-154 (2010).

69. Rabinow, L., Chiang, S.L. & Birchler, J.A. Mutations at the Darkener of apricot Locus Modulate Transcript Levels of copia and copia-Induced Mutations in Drosophila melanogaster. *Genetics* **134**, 1175-1185 (1993).
70. Bettencourt-Dias, M. *et al.* Genome-wide survey of protein kinases required for cell cycle progression. *Nature* **432**, 980-987 (2004).
71. Björklund, M. *et al.* Identification of pathways regulating cell size and cell-cycle progression by RNAi. *Nature* **439**, 1009-1013 (2006).
72. Gorski, S.M. *et al.* A SAGE approach to discovery of genes involved in autophagic cell death. *Curr. Biol* **13**, 358-363 (2003).
73. Lee, C.-Y. *et al.* Genome-Wide Analyses of Steroid- and Radiation-Triggered Programmed Cell Death in Drosophila. *Current Biology* **13**, 350-357 (2003).
74. Tang, Z. *et al.* The kic1 kinase of schizosaccharomyces pombe is a CLK/STY orthologue that regulates cell-cell separation. *Exp. Cell Res* **283**, 101-115 (2003).
75. Menegay, H., Moeslein, F. & Landreth, G. The dual specificity protein kinase CLK3 is abundantly expressed in mature mouse spermatozoa. *Exp. Cell Res* **253**, 463-473 (1999).
76. Yun, B., Lee, K., Farka, R., Hitte, C. & Rabinow, L. The LAMMER protein kinase encoded by the Doa locus of Drosophila is required in both somatic and germline cells and is expressed as both nuclear and cytoplasmic isoforms throughout development. *Genetics* **156**, 749 (2000).
77. Kumar, A. Subcellular localization of the yeast proteome. *Genes & Development* **16**, 707-719 (2002).
78. Huh, W.-K. *et al.* Global analysis of protein localization in budding yeast. *Nature* **425**, 686-691 (2003).
79. Krogan, N.J. *et al.* Global landscape of protein complexes in the yeast Saccharomyces cerevisiae. *Nature* **440**, 637-643 (2006).
80. Ho, Y. *et al.* Systematic identification of protein complexes in Saccharomyces cerevisiae by mass spectrometry. *Nature* **415**, 180-183 (2002).
81. Yu, H. *et al.* High-Quality Binary Protein Interaction Map of the Yeast Interactome Network. *Science* **322**, 104-110 (2008).
82. Wong, J. *et al.* A protein interaction map of the mitotic spindle. *Molecular Biology of the Cell* **18**, 3800 (2007).
83. Uetz, P. *et al.* A comprehensive analysis of protein-protein interactions in Saccharomyces cerevisiae. *Nature* **403**, 623-627 (2000).
84. Chiolo, I. *et al.* Srs2 and Sgs1 DNA helicases associate with Mre11 in different subcomplexes following checkpoint activation and CDK1-mediated Srs2 phosphorylation. *Mol. Cell. Biol* **25**, 5738-5751 (2005).
85. Keren, H., Lev-Maor, G. & Ast, G. Alternative splicing and evolution: diversification, exon definition and function. *Nat Rev Genet* **11**, 345-355 (2010).
86. Bourgeois, C.F., Lejeune, F. & Stévenin, J. Broad specificity of SR (serine/arginine) proteins in the regulation of alternative splicing of pre-messenger RNA. *Prog. Nucleic Acid Res. Mol. Biol* **78**, 37-88 (2004).
87. Hertel, K.J. & Graveley, B.R. RS domains contact the pre-mRNA throughout spliceosome assembly. *Trends Biochem. Sci* **30**, 115-118 (2005).
88. Zahler, A.M., Lane, W.S., Stolk, J.A. & Roth, M.B. SR proteins: a conserved family of pre-mRNA splicing factors. *Genes Dev* **6**, 837-847 (1992).
89. Lutzelberger, M., Gross, T. & Kaufer, N.F. Srp2, an SR protein family member of fission yeast: in vivo characterization of its modular domains. *Nucl.*

Acids Res. **27**, 2618-2626 (1999).
90. Birney, E., Kumar, S. & Krainer, A.R. Analysis of the RNA-recognition motif and RS and RGG domains: conservation in metazoan pre-mRNA splicing factors. *Nucleic Acids Res* **21**, 5803-5816 (1993).
91. Kadowaki, T. *et al.* Isolation and characterization of Saccharomyces cerevisiae mRNA transport-defective (mtr) mutants. *J. Cell Biol* **126**, 649-659 (1994).
92. Lee, M.S., Henry, M. & Silver, P.A. A protein that shuttles between the nucleus and the cytoplasm is an important mediator of RNA export. *Genes & Development* **10**, 1233-1246 (1996).
93. Windgassen, M. & Krebber, H. Identification of Gbp2 as a novel poly(A)+ RNA-binding protein involved in the cytoplasmic delivery of messenger RNAs in yeast. *EMBO Rep.* **4**, 278-283 (2003).
94. Häcker, S. & Krebber, H. Differential export requirements for shuttling serine/arginine-type mRNA-binding proteins. *J. Biol. Chem.* **279**, 5049-5052 (2004).
95. Kress, T.L., Krogan, N.J. & Guthrie, C. A single SR-like protein, Npl3, promotes pre-mRNA splicing in budding yeast. *Mol Cell* **32**, 727-734 (2008).
96. Gu, Z. *et al.* Role of duplicate genes in genetic robustness against null mutations. *Nature* **421**, 63-66 (2003).
97. Deutscher, D., Meilijson, I., Kupiec, M. & Ruppin, E. Multiple knockout analysis of genetic robustness in the yeast metabolic network. *Nat. Genet* **38**, 993-998 (2006).
98. Papp, B., Pál, C. & Hurst, L.D. Metabolic network analysis of the causes and evolution of enzyme dispensability in yeast. *Nature* **429**, 661-664 (2004).
99. Lockshon, D., Surface, L.E., Kerr, E.O., Kaeberlein, M. & Kennedy, B.K. The sensitivity of yeast mutants to oleic acid implicates the peroxisome and other processes in membrane function. *Genetics* **175**, 77-91 (2007).
100. Petschnigg, J. *et al.* Good Fat, Essential Cellular Requirements for Triacylglycerol Synthesis to Maintain Membrane Homeostasis in Yeast. *Journal of Biological Chemistry* **284**, 30981 -30993 (2009).
101. Rosenberger, S., Connerth, M., Zellnig, G. & Daum, G. Phosphatidylethanolamine synthesized by three different pathways is supplied to peroxisomes of the yeast Saccharomyces cerevisiae. *Biochim. Biophys. Acta* **1791**, 379-387 (2009).
102. Ptacek, J. *et al.* Global analysis of protein phosphorylation in yeast. *Nature* **438**, 679-684 (2005).
103. Simon, J.A. & Bedalov, A. Yeast as a model system for anticancer drug discovery. *Nat. Rev. Cancer* **4**, 481-492 (2004).
104. Menacho-Márquez, M. & Murguía, J.R. Yeast on drugs: Saccharomyces cerevisiae as a tool for anticancer drug research. *Clin Transl Oncol* **9**, 221-228 (2007).
105. Boone, C., Bussey, H. & Andrews, B.J. Exploring genetic interactions and networks with yeast. *Nat Rev Genet* **8**, 437-449 (2007).
106. Castrillo, J.I. & Oliver, S.G. Yeast as a touchstone in post-genomic research: strategies for integrative analysis in functional genomics. *J. Biochem. Mol. Biol* **37**, 93-106 (2004).
107. Muchowski, P.J. & Galarza, V.E.S. Drug targets for the treatment of neurodegenerative disorders. (2009).en http://www.freepatentsonline.com/7504227.html

108. Hellauer, K., Lesage, G., Sdicu, A.M. & Turcotte, B. Large-scale analysis of genes that alter sensitivity to the anticancer drug tirapazamine in Saccharomyces cerevisiae. *Molecular pharmacology* **68**, 1365 (2005).
109. Maier, L.S. Role of CaMKII for signaling and regulation in the heart. *Front. Biosci* **14**, 486-496 (2009).
110. Fährmann, M. & Kaufhold, M.-A. Functional partitioning of epithelial protein kinase CaMKII in signal transduction. *Biochim. Biophys. Acta* **1763**, 101-109 (2006).
111. McGargill, M.A., Sharp, L.L., Bui, J.D., Hedrick, S.M. & Calbo, S. Active Ca2+/calmodulin-dependent protein kinase II gamma B impairs positive selection of T cells by modulating TCR signaling. *J. Immunol* **175**, 656-664 (2005).
112. Wayman, G.A., Lee, Y.-S., Tokumitsu, H., Silva, A. & Soderling, T.R. Calmodulin-Kinases: Modulators of Neuronal Development and Plasticity. *Neuron* **59**, 914-931 (2008).
113. Schulman, H. & Greengard, P. Ca2+-dependent protein phosphorylation system in membranes from various tissues, and its activation by «calcium-dependent regulator». *Proc. Natl. Acad. Sci. U.S.A* **75**, 5432-5436 (1978).
114. Erondu, N.E. & Kennedy, M.B. Regional distribution of type II Ca2+/calmodulin-dependent protein kinase in rat brain. *J. Neurosci* **5**, 3270-3277 (1985).
115. Lisman, J., Schulman, H., Cline, H. & others The molecular basis of CaMKII function in synaptic and behavioural memory. *Nature Reviews Neuroscience* **3**, 175–190 (2002).
116. Braun, A.P. & Schulman, H. The multifunctional calcium/calmodulin-dependent protein kinase: from form to function. *Annual review of physiology* **57**, 417–445 (1995).
117. Hudmon, A. & Schulman, H. Structure-function of the multifunctional Ca2+/calmodulin-dependent protein kinase II. *Biochem J* **364**, 593–611 (2002).
118. Hoelz, A., Nairn, A.C. & Kuriyan, J. Crystal Structure of a Tetradecameric Assembly of the Association Domain of Ca2+/Calmodulin-Dependent Kinase II. *Molecular Cell* **11**, 1241-1251 (2003).
119. Morris, E.P. & Török, K. Oligomeric structure of alpha-calmodulin-dependent protein kinase II. *J. Mol. Biol* **308**, 1-8 (2001).
120. Hanson, P.I., Meyer, T., Stryer, L. & Schulman, H. Dual role of calmodulin in autophosphorylation of multifunctional cam kinase may underlie decoding of calcium signals. *Neuron* **12**, 943-956 (1994).
121. De Koninck, P. Sensitivity of CaM Kinase II to the Frequency of Ca2+ Oscillations. *Science* **279**, 227-230 (1998).
122. Tobimatsu, T. & Fujisawa, H. Tissue-specific expression of four types of rat calmodulin-dependent protein kinase II mRNAs. *Journal of Biological Chemistry* **264**, 17907-17912 (1989).
123. Hudmon, A. & Schulman, H. Neuronal CA2+/calmodulin-dependent protein kinase II: the role of structure and autoregulation in cellular function. *Annu. Rev. Biochem* **71**, 473-510 (2002).
124. Brocke, L., Srinivasan, M. & Schulman, H. Developmental and regional expression of multifunctional Ca2+/calmodulin-dependent protein kinase isoforms in rat brain. *J. Neurosci* **15**, 6797-6808 (1995).
125. Srinivasan, M., Edman, C. & Schulman, H. Alternative splicing introduces a nuclear localization signal that targets multifunctional CaM kinase to the

nucleus. *J. Cell Biol.* **126**, 839-852 (1994).
126. Fink, C.C. *et al.* Selective regulation of neurite extension and synapse formation by the beta but not the alpha isoform of CaMKII. *Neuron* **39**, 283–297 (2003).
127. Griffith, L.C. Regulation of calcium/calmodulin-dependent protein kinase II activation by intramolecular and intermolecular interactions. *Journal of Neuroscience* **24**, 8394 (2004).
128. Schulman, H. Activity-dependent regulation of calcium/calmodulin-dependent protein kinase II localization. *Journal of Neuroscience* **24**, 8399 (2004).
129. Smith, M.K., Colbran, R.J., Brickey, D.A. & Soderling, T.R. Functional determinants in the autoinhibitory domain of calcium/calmodulin-dependent protein kinase II. Role of His282 and multiple basic residues. *Journal of Biological Chemistry* **267**, 1761-1768 (1992).
130. Mukherji, S., Brickey, D.A. & Soderling, T.R. Mutational analysis of secondary structure in the autoinhibitory and autophosphorylation domains of calmodulin kinase II. *Journal of Biological Chemistry* **269**, 20733 (1994).
131. Yang, E. & Schulman, H. Structural examination of autoregulation of multifunctional calcium/calmodulin-dependent protein kinase II. *Journal of Biological Chemistry* **274**, 26199 (1999).
132. Colbran, R.J., Fong, Y.L., Schworer, C.M. & Soderling, T.R. Regulatory interactions of the calmodulin-binding, inhibitory, and autophosphorylation domains of Ca2+/calmodulin-dependent protein kinase II. *Journal of Biological Chemistry* **263**, 18145-18151 (1988).
133. Rich, R.C. & Schulman, H. Substrate-directed Function of Calmodulin in Autophosphorylation of Ca2+/Calmodulin-dependent Protein Kinase II. *Journal of Biological Chemistry* **273**, 28424-28429 (1998).
134. Couchonnal, L.F. & Anderson, M.E. The Role of Calmodulin Kinase II in Myocardial Physiology and Disease. *Physiology* **23**, 151-159 (2008).
135. Colbran, R.J., Smith, M.K., Schworer, C.M., Fong, Y.L. & Soderling, T.R. Regulatory domain of calcium/calmodulin-dependent protein kinase II. Mechanism of inhibition and regulation by phosphorylation. *J. Biol. Chem* **264**, 4800-4804 (1989).
136. Lou, L.L., Lloyd, S.J. & Schulman, H. Activation of the multifunctional Ca2+/calmodulin-dependent protein kinase by autophosphorylation: ATP modulates production of an autonomous enzyme. *Proceedings of the National Academy of Sciences of the United States of America* **83**, 9497-9501 (1986).
137. Meyer, T., Hanson, P.I., Stryer, L. & Schulman, H. Calmodulin trapping by calcium-calmodulin-dependent protein kinase. *Science* **256**, 1199-1202 (1992).
138. Singla, S.I., Hudmon, A., Goldberg, J.M., Smith, J.L. & Schulman, H. Molecular characterization of calmodulin trapping by calcium/calmodulin-dependent protein kinase II. *J. Biol. Chem* **276**, 29353-29360 (2001).
139. Meador, W.E., Means, A.R. & Quiocho, F.A. Modulation of calmodulin plasticity in molecular recognition on the basis of x-ray structures. *Science* **262**, 1718-1721 (1993).
140. Hanson, P.I. & Schulman, H. Inhibitory autophosphorylation of multifunctional Ca2+/calmodulin-dependent protein kinase analyzed by site-directed mutagenesis. *Journal of Biological Chemistry* **267**, 17216-17224 (1992).

141. Erickson, J.R. *et al.* A Dynamic Pathway for Calcium-Independent Activation of CaMKII by Methionine Oxidation. *Cell* **133**, 462-474 (2008).
142. Colbran, R.J. Targeting of calcium/calmodulin-dependent protein kinase II. *Biochemical Journal* **378**, 1 (2004).
143. Bayer, K.U., Harbers, K. & Schulman, H. alphaKAP is an anchoring protein for a novel CaM kinase II isoform in skeletal muscle. *The EMBO Journal* **17**, 5598 (1998).
144. Ohya, Y., Kawasaki, H., Suzuki, K., Londesborough, J. & Anraku, Y. Two yeast genes encoding calmodulin-dependent protein kinases. Isolation, sequencing and bacterial expressions of CMK1 and CMK2. *J. Biol. Chem* **266**, 12784-12794 (1991).
145. Pausch, M.H., Kaim, D., Kunisawa, R., Admon, A. & Thorner, J. Multiple Ca2+/calmodulin-dependent protein kinase genes in a unicellular eukaryote. *The EMBO Journal* **10**, 1511 (1991).
146. Rhoads, A.R. & Friedberg, F. Sequence motifs for calmodulin recognition. *FASEB J* **11**, 331-340 (1997).
147. Miyakawa, T., Oka, Y., Tsuchiya, E. & Fukui, S. Saccharomyces cerevisiae protein kinase dependent on Ca2+ and calmodulin. *Journal of bacteriology* **171**, 1417 (1989).
148. White, R.R., Kwon, Y.-G., Taing, M., Lawrence, D.S. & Edelman, A.M. Definition of Optimal Substrate Recognition Motifs of Ca2+-Calmodulin-dependent Protein Kinases IV and II Reveals Shared and Distinctive Features. *Journal of Biological Chemistry* **273**, 3166-3172 (1998).
149. Gaertner, T.R. *et al.* Comparative analyses of the three-dimensional structures and enzymatic properties of alpha, beta, gamma and delta isoforms of Ca2+-calmodulin-dependent protein kinase II. *J. Biol. Chem* **279**, 12484-12494 (2004).
150. Morris, E.P. & Török, K. Oligomeric structure of alpha-calmodulin-dependent protein kinase II. *J. Mol. Biol* **308**, 1-8 (2001).
151. Londesborough, J. & Nuutinen, M. Ca2+/calmodulin-dependent protein kinase in Saccharomyces cerevisiae. *FEBS Lett* **219**, 249-253 (1987).
152. Dudgeon, D.D., Zhang, N., Ositelu, O.O., Kim, H. & Cunningham, K.W. Nonapoptotic Death of Saccharomyces cerevisiae Cells That Is Stimulated by Hsp90 and Inhibited by Calcineurin and Cmk2 in Response to Endoplasmic Reticulum Stresses. *Eukaryotic Cell* **7**, 2037-2051 (2008).
153. Cyert, M.S. Calcineurin signaling in Saccharomyces cerevisiae: how yeast go crazy in response to stress. *Biochemical and Biophysical Research Communications* **311**, 1143–1150 (2003).
154. Bonilla, M., Nastase, K.K. & Cunningham, K.W. Essential role of calcineurin in response to endoplasmic reticulum stress. *EMBO J* **21**, 2343-2353 (2002).
155. Moser, M.J., Geiser, J.R. & Davis, T.N. Ca2+-calmodulin promotes survival of pheromone-induced growth arrest by activation of calcineurin and Ca2+-calmodulin-dependent protein kinase. *Molecular and Cellular Biology* **16**, 4824 (1996).
156. Dohlman, H.G. & Slessareva, J.E. Pheromone signaling pathways in yeast. *Sci. STKE* **2006**, cm6 (2006).
157. Withee, J.L., Mulholland, J., Jeng, R. & Cyert, M.S. An essential role of the yeast pheromone-induced Ca2+ signal is to activate calcineurin. *Mol. Biol. Cell* **8**, 263-277 (1997).

158. Yoshimoto, H. Genome-wide Analysis of Gene Expression Regulated by the Calcineurin/Crz1p Signaling Pathway in Saccharomyces cerevisiae. *Journal of Biological Chemistry* **277**, 31079-31088 (2002).
159. Casey, J.R., Grinstein, S. & Orlowski, J. Sensors and regulators of intracellular pH. *Nat. Rev. Mol. Cell Biol* **11**, 50-61 (2010).
160. Orij, R., Brul, S. & Smits, G.J. Intracellular pH is a tightly controlled signal in yeast. *Biochim Biophys Acta* (2011).doi:10.1016/j.bbagen.2011.03.011
161. van der Rest, M. *et al.* The plasma membrane of Saccharomyces cerevisiae: structure, function, and biogenesis. *Microbiol. Rev.* **59**, 304-322 (1995).
162. Ferreira, T., Mason, A.B. & Slayman, C.W. The Yeast Pma1 Proton Pump: a Model for Understanding the Biogenesis of Plasma Membrane Proteins. *J. Biol. Chem.* **276**, 29613-29616 (2001).
163. Nass, R., Cunningham, K.W. & Rao, R. Intracellular sequestration of sodium by a novel Na+/H+ exchanger in yeast is enhanced by mutations in the plasma membrane H+-ATPase. Insights into mechanisms of sodium tolerance. *J. Biol. Chem* **272**, 26145-26152 (1997).
164. McCusker, J.H., Perlin, D.S. & Haber, J.E. Pleiotropic plasma membrane ATPase mutations of Saccharomyces cerevisiae. *Mol. Cell. Biol.* **7**, 4082-4088 (1987).
165. Martínez-Muñoz, G.A. & Kane, P. Vacuolar and Plasma Membrane Proton Pumps Collaborate to Achieve Cytosolic pH Homeostasis in Yeast. *Journal of Biological Chemistry* **283**, 20309 -20319 (2008).
166. Brett, C.L., Tukaye, D.N., Mukherjee, S. & Rao, R. The Yeast Endosomal Na+(K+)/H+ Exchanger Nhx1 Regulates Cellular pH to Control Vesicle Trafficking. *Mol. Biol. Cell* **16**, 1396-1405 (2005).
167. Yenush, L., Mulet, J.M., Arino, J. & Serrano, R. The Ppz protein phosphatases are key regulators of K+ and pH homeostasis: implications for salt tolerance, cell wall integrity and cell cycle progression. *EMBO J* **21**, 920-929 (2002).
168. de la Peña, P., Barros, F., Gascón, S., Ramos, S. & Lazo, P.S. The electrochemical proton gradient of Saccharomyces. The role of potassium. *Eur. J. Biochem.* **123**, 447-453 (1982).
169. Valli, M. *et al.* Intracellular pH Distribution in Saccharomyces cerevisiae Cell Populations, Analyzed by Flow Cytometry. *Appl. Environ. Microbiol.* **71**, 1515-1521 (2005).
170. Orij, R., Postmus, J., Ter Beek, A., Brul, S. & Smits, G.J. In vivo measurement of cytosolic and mitochondrial pH using a pH-sensitive GFP derivative in Saccharomyces cerevisiae reveals a relation between intracellular pH and growth. *Microbiology* **155**, 268 -278 (2009).
171. Giaever, G. *et al.* Functional profiling of the Saccharomyces cerevisiae genome. *Nature* **418**, 387-391 (2002).
172. Serrano, R., Bernal, D., Simon, E. & Arino, J. Copper and iron are the limiting factors for growth of the yeast Saccharomyces cerevisiae in an alkaline environment. *Journal of Biological Chemistry* **279**, 19698 (2004).
173. Causton, H.C. *et al.* Remodeling of Yeast Genome Expression in Response to Environmental Changes. *Mol. Biol. Cell* **12**, 323-337 (2001).
174. Viladevall, L. *et al.* Characterization of the calcium-mediated response to alkaline stress in Saccharomyces cerevisiae. *Journal of Biological Chemistry* M403606200v1 (2004).

175. Lamb, T.M., Xu, W., Diamond, A. & Mitchell, A.P. Alkaline Response Genes of Saccharomyces cerevisiaeand Their Relationship to the RIM101 Pathway. *Journal of Biological Chemistry* **276**, 1850 -1856 (2001).
176. Serrano, R., Ruiz, A., Bernal, D., Chambers, J.R. & Ariño, J. The transcriptional response to alkaline pH in Saccharomyces cerevisiae: evidence for calcium-mediated signalling. *Mol. Microbiol* **46**, 1319-1333 (2002).
177. Serrano, R., Martin, H., Casamayor, A. & Arino, J. Signaling Alkaline pH Stress in the Yeast Saccharomyces cerevisiae through the Wsc1 Cell Surface Sensor and the Slt2 MAPK Pathway. *Journal of Biological Chemistry* **281**, 39785-39795 (2006).
178. Hong, S.-P. & Carlson, M. Regulation of Snf1 Protein Kinase in Response to Environmental Stress. *Journal of Biological Chemistry* **282**, 16838 -16845 (2007).
179. Ruiz, A., Serrano, R. & Ariño, J. Direct Regulation of Genes Involved in Glucose Utilization by the Calcium/Calcineurin Pathway. *Journal of Biological Chemistry* **283**, 13923 -13933 (2008).
180. Serrano, R., Bernal, D., Simón, E. & Ariño, J. Copper and iron are the limiting factors for growth of the yeast Saccharomyces cerevisiae in an alkaline environment. *J. Biol. Chem* **279**, 19698-19704 (2004).
181. Bermingham-McDonogh, O., Gralla, E.B. & Valentine, J.S. The copper, zinc-superoxide dismutase gene of Saccharomyces cerevisiae: cloning, sequencing, and biological activity. *Proc. Natl. Acad. Sci. U.S.A.* **85**, 4789-4793 (1988).
182. Nelson, H. & Nelson, N. Disruption of genes encoding subunits of yeast vacuolar H(+)-ATPase causes conditional lethality. *Proceedings of the National Academy of Sciences of the United States of America* **87**, 3503-3507 (1990).
183. Yamashiro, C.T., Kane, P.M., Wolczyk, D.F., Preston, R.A. & Stevens, T.H. Role of vacuolar acidification in protein sorting and zymogen activation: a genetic analysis of the yeast vacuolar proton-translocating ATPase. *Mol. Cell. Biol* **10**, 3737-3749 (1990).
184. Kane, P.M. The Where, When, and How of Organelle Acidification by the Yeast Vacuolar H+-ATPase. *Microbiol. Mol. Biol. Rev.* **70**, 177-191 (2006).
185. Marshansky, V. & Futai, M. The V-type H+-ATPase in vesicular trafficking: targeting, regulation and function. *Curr. Opin. Cell Biol* **20**, 415-426 (2008).
186. Li, S.C. & Kane, P.M. The yeast lysosome-like vacuole: endpoint and crossroads. *Biochim. Biophys. Acta* **1793**, 650-663 (2009).
187. Pina, F.J. *et al.* Hph1 and Hph2 Are Novel Components of the Sec63/Sec62 Posttranslational Translocation Complex That Aid in Vacuolar Proton ATPase Biogenesis. *Eukaryotic Cell* **10**, 63-71 (2011).
188. Sambade, M., Alba, M., Smardon, A.M., West, R.W. & Kane, P.M. A Genomic Screen for Yeast Vacuolar Membrane ATPase Mutants. *Genetics* **170**, 1539-1551 (2005).
189. Ariño, J. Integrative Responses to High pH Stress in S. cerevisiae. *OMICS* (2010).doi:10.1089/omi.2010.0044
190. Ruiz, A. & Arino, J. Function and Regulation of the Saccharomyces cerevisiae ENA Sodium ATPase System. *Eukaryotic Cell* **6**, 2175-2183 (2007).
191. Lamb, T.M. & Mitchell, A.P. The Transcription Factor Rim101p Governs Ion Tolerance and Cell Differentiation by Direct Repression of the Regulatory Genes NRG1 and SMP1 in Saccharomyces cerevisiae. *Mol. Cell. Biol.* **23**, 677-

686 (2003).
192. Stevens, T.H. & Forgac, M. Structure, function and regulation of the vacuolar (H+)-ATPase. *Annu. Rev. Cell Dev. Biol* **13**, 779-808 (1997).
193. Levin, D.E. Cell wall integrity signaling in Saccharomyces cerevisiae. *Microbiol. Mol. Biol. Rev* **69**, 262-291 (2005).
194. GARCIA-SACRISTAN, A., FERNANDEZ-NESTOSA, M.J., HERNANDEZ, P., SCHVARTZMAN, J.B. & KRIMER, D.B. Protein kinase clk/STY is differentially regulated during erythroleukemia cell differentiation: a bias toward the skipped splice variant characterizes postcommitment stages. *Cell Res* **15**, 495-503 (2005).
195. Glatz, D.C. *et al.* The alternative splicing of tau exon 10 and its regulatory proteins CLK2 and TRA2-BETA1 changes in sporadic Alzheimer's disease. *J. Neurochem* **96**, 635-644 (2006).
196. Nothwang, H.G. *et al.* Functional hemizygosity of PAFAH1B3 due to a PAFAH1B3-CLK2 fusion gene in a female with mental retardation, ataxia and atrophy of the brain. *Hum. Mol. Genet* **10**, 797-806 (2001).
197. Brachmann, C.B. *et al.* Designer deletion strains derived from Saccharomyces cerevisiae S288C: a useful set of strains and plasmids for PCR-mediated gene disruption and other applications. *Yeast* **14**, 115-132 (1998).
198. Finley, D., Ozkaynak, E. & Varshavsky, A. The yeast polyubiquitin gene is essential for resistance to high temperatures, starvation, and other stresses. *Cell* **48**, 1035-1046 (1987).
199. Boon, K.-L. *et al.* prp8 mutations that cause human retinitis pigmentosa lead to a U5 snRNP maturation defect in yeast. *Nat. Struct. Mol. Biol* **14**, 1077-1083 (2007).
200. James, P., Halladay, J. & Craig, E.A. Genomic libraries and a host strain designed for highly efficient two-hybrid selection in yeast. *Genetics* **144**, 1425-1436 (1996).
201. Scheich, C., Kümmel, D., Soumailakakis, D., Heinemann, U. & Büssow, K. Vectors for co-expression of an unrestricted number of proteins. *Nucleic Acids Research* **35**, e43 (2007).
202. Janke, C. *et al.* A versatile toolbox for PCR-based tagging of yeast genes: new fluorescent proteins, more markers and promoter substitution cassettes. *Yeast* **21**, 947-962 (2004).
203. Odorizzi, G., Babst, M. & Emr, S.D. Fab1p PtdIns(3)P 5-kinase function essential for protein sorting in the multivesicular body. *Cell* **95**, 847-858 (1998).
204. Gheysen, D. & Fiers, W. Expression and excretion of human fibroblast beta 1 interferon in monkey cells after transfection with a recombinant SV40 plasmid vector. *J. Mol. Appl. Genet.* **1**, 385-394 (1982).
205. Sikorski, R.S. & Hieter, P. A System of Shuttle Vectors and Yeast Host Strains Designed for Efficient Manipulation of DNA in Saccharomyces cerevisiae. *Genetics* **122**, 19-27 (1989).
206. Sambrook, J. & Russell, D.W. *Molecular cloning: a laboratory manual*. (CSHL Press: 2001).
207. Guthrie, C. & Fink, G.R. *Guide to Yeast Genetics and Molecular and Cell Biology*. (Gulf Professional Publishing: 2004).
208. Treco, D.A. & Winston, F. Growth and Manipulation of Yeast. doi:10.1002/0471142727.mb1302s19
209. Gietz, D., Jean, A.S., Woods, R.A. & Schiestl, R.H. Improved method for

high efficiency transformation of intact yeast cells. *Nucleic Acids Research* **20**, 1425 (1992).
210. Winzeler, E.A. *et al.* Functional characterization of the S. cerevisiae genome by gene deletion and parallel analysis. *Science* **285**, 901-906 (1999).
211. Wach, A., Brachat, A., Pöhlmann, R. & Philippsen, P. New heterologous modules for classical or PCR-based gene disruptions in Saccharomyces cerevisiae. *Yeast* **10**, 1793-1808 (1994).
212. Sherman, F. Getting started with yeast. *Meth. Enzymol* **350**, 3-41 (2002).
213. Fields, S. & Song, O.-kyu A novel genetic system to detect protein-protein interactions. *Nature* **340**, 245-246 (1989).
214. Wilkinson, C.R.M. *et al.* Ubiquitin-like protein Hub1 is required for pre-mRNA splicing and localization of an essential splicing factor in fission yeast. *Curr. Biol* **14**, 2283-2288 (2004).
215. Hoffman, C.S. & Winston, F. A ten-minute DNA preparation from yeast efficiently releases autonomous plasmids for transformation of Escherichia coli. *Gene* **57**, 267-272 (1987).
216. Collart, M.A. & Oliviero, S. Preparation of Yeast RNA. doi:10.1002/0471142727.mb1312s23
217. Hartley, J.L., Temple, G.F. & Brasch, M.A. DNA cloning using in vitro site-specific recombination. *Genome Res* **10**, 1788-1795 (2000).
218. Walhout, A.J. *et al.* GATEWAY recombinational cloning: application to the cloning of large numbers of open reading frames or ORFeomes. *Meth. Enzymol* **328**, 575-592 (2000).
219. Landy, A. Dynamic, structural, and regulatory aspects of lambda site-specific recombination. *Annu. Rev. Biochem* **58**, 913-949 (1989).
220. Ma, H., Kunes, S., Schatz, P.J. & Botstein, D. Plasmid construction by homologous recombination in yeast. *Gene* **58**, 201-216 (1987).
221. Hudson, J.R. *et al.* The complete set of predicted genes from Saccharomyces cerevisiae in a readily usable form. *Genome Res* **7**, 1169-1173 (1997).
222. Yoshimoto, H. *et al.* Genome-wide Analysis of Gene Expression Regulated by the Calcineurin/Crz1p Signaling Pathway in Saccharomyces cerevisiae. *Journal of Biological Chemistry* **277**, 31079 -31088 (2002).
223. Bradford, M.M. A rapid and sensitive method for the quantitation of microgram quantities of protein utilizing the principle of protein-dye binding. *Analytical Biochemistry* **72**, 248-254 (1976).
224. Sedmak, J.J. & Grossberg, S.E. A rapid, sensitive, and versatile assay for protein using Coomassie brilliant blue G250. *Analytical Biochemistry* **79**, 544-552 (1977).
225. Laemmli, U.K. Cleavage of structural proteins during the assembly of the head of bacteriophage T4. *Nature* **227**, 680-685 (1970).
226. R. Gallagher, S. Overview of Electrophoresis. *Current Protocols Essential Laboratory Techniques* (2008).en <http://www.currentprotocols.com/protocol/et0701>
227. Burnette, W.N. «Western blotting»: electrophoretic transfer of proteins from sodium dodecyl sulfate--polyacrylamide gels to unmodified nitrocellulose and radiographic detection with antibody and radioiodinated protein A. *Anal. Biochem* **112**, 195-203 (1981).
228. Shevchenko, A., Tomas, H., Havlis, J., Olsen, J.V. & Mann, M. In-gel digestion for mass spectrometric characterization of proteins and proteomes.

Nat Protoc **1**, 2856-2860 (2006).
229. Weisman, L.S., Bacallao, R. & Wickner, W. Multiple methods of visualizing the yeast vacuole permit evaluation of its morphology and inheritance during the cell cycle. *J. Cell Biol* **105**, 1539-1547 (1987).
230. Hasek, J. Yeast Fluorescence Microscopy. *Yeast Protocols* **313**, 085-096 (2005).
231. Rodgers, J.T., Haas, W., Gygi, S.P. & Puigserver, P. Cdc2-like Kinase 2 Is an Insulin-Regulated Suppressor of Hepatic Gluconeogenesis. *Cell Metabolism* **11**, 23-34 (2010).
232. Hampsey, M. A review of phenotypes in Saccharomyces cerevisiae. *Yeast* **13**, 1099-1133 (1997).
233. Hillenmeyer, M.E. *et al.* The Chemical Genomic Portrait of Yeast: Uncovering a Phenotype for All Genes. *Science* **320**, 362-365 (2008).
234. Butt, T.R. *et al.* Copper metallothionein of yeast, structure of the gene, and regulation of expression. *Proceedings of the National Academy of Sciences of the United States of America* **81**, 3332-3336 (1984).
235. Shepard, P.J. & Hertel, K.J. The SR protein family. *Genome Biol* **10**, 242-242 (2009).
236. González, C.I., Bhattacharya, A., Wang, W. & Peltz, S.W. Nonsense-mediated mRNA decay in Saccharomyces cerevisiae. *Gene* **274**, 15-25 (2001).
237. Maquat, L.E. Nonsense-mediated mRNA decay: splicing, translation and mRNP dynamics. *Nat. Rev. Mol. Cell Biol* **5**, 89-99 (2004).
238. Egecioglu, D.E. & Chanfreau, G. Proofreading and spellchecking: A two-tier strategy for pre-mRNA splicing quality control. *RNA* **17**, 383 -389 (2011).
239. Supeková, L., Supek, F. & Nelson, N. The Saccharomyces cerevisiae VMA10 is an intron-containing gene encoding a novel 13-kDa subunit of vacuolar H(+)-ATPase. *J. Biol. Chem* **270**, 13726-13732 (1995).
240. Chen, E.J., Frand, A.R., Chitouras, E. & Kaiser, C.A. A Link between Secretion and Pre-mRNA Processing Defects in Saccharomyces cerevisiae and the Identification of a Novel Splicing Gene, RSE1. *Mol Cell Biol* **18**, 7139-7146 (1998).
241. Clark, T.A., Sugnet, C.W. & Ares, M. Genomewide Analysis of mRNA Processing in Yeast Using Splicing-Specific Microarrays. *Science* **296**, 907-910 (2002).
242. Vijayraghavan, U., Company, M. & Abelson, J. Isolation and characterization of pre-mRNA splicing mutants of Saccharomyces cerevisiae. *Genes Dev* **3**, 1206-1216 (1989).
243. Maddock, J.R., Roy, J. & Woolford, J.L. Six Novel Genes Necessary for Pre-mRNA Splicing in Saccharomyces Cerevisiae. *Nucleic Acids Research* **24**, 1037 -1044 (1996).
244. Burckin, T. *et al.* Exploring functional relationships between components of the gene expression machinery. *Nat. Struct. Mol. Biol* **12**, 175-182 (2005).
245. Balzer, R.J. & Henry, M.F. Snu56p is required for Mer1p-activated meiotic splicing. *Mol. Cell. Biol* **28**, 2497-2508 (2008).
246. Jackson, S.P., Lossky, M. & Beggs, J.D. Cloning of the RNA8 gene of Saccharomyces cerevisiae, detection of the RNA8 protein, and demonstration that it is essential for nuclear pre-mRNA splicing. *Mol. Cell. Biol* **8**, 1067-1075 (1988).
247. Ho, M.N., Hill, K.J., Lindorfer, M.A. & Stevens, T.H. Isolation of vacuolar membrane H(+)-ATPase-deficient yeast mutants; the VMA5 and VMA4 genes

are essential for assembly and activity of the vacuolar H(+)-ATPase. *Journal of Biological Chemistry* **268**, 221 -227 (1993).
248. Hirata, R. *et al.* Molecular structure of a gene, VMA1, encoding the catalytic subunit of H(+)-translocating adenosine triphosphatase from vacuolar membranes of Saccharomyces cerevisiae. *J. Biol. Chem* **265**, 6726-6733 (1990).
249. Roberts, C.J., Raymond, C.K., Yamashiro, C.T. & Stevens, T.H. Methods for studying the yeast vacuole. *Meth. Enzymol* **194**, 644-661 (1991).
250. Yamashiro, C.T., Kane, P.M., Wolczyk, D.F., Preston, R.A. & Stevens, T.H. Role of vacuolar acidification in protein sorting and zymogen activation: a genetic analysis of the yeast vacuolar proton-translocating ATPase. *Mol. Cell. Biol.* **10**, 3737-3749 (1990).
251. Klionsky, D.J., Nelson, H. & Nelson, N. Compartment acidification is required for efficient sorting of proteins to the vacuole in Saccharomyces cerevisiae. *J. Biol. Chem* **267**, 3416-3422 (1992).
252. Morano, K.A. & Klionsky, D.J. Differential effects of compartment deacidification on the targeting of membrane and soluble proteins to the vacuole in yeast. *J. Cell. Sci* **107 (Pt 10)**, 2813-2824 (1994).
253. Plant, P.J., Manolson, M.F., Grinstein, S. & Demaurex, N. Alternative mechanisms of vacuolar acidification in H(+)-ATPase-deficient yeast. *J. Biol. Chem* **274**, 37270-37279 (1999).
254. Bowers, K. & Stevens, T.H. Protein transport from the late Golgi to the vacuole in the yeast Saccharomyces cerevisiae. *Biochim. Biophys. Acta* **1744**, 438-454 (2005).
255. Spormann, D.O., Heim, J. & Wolf, D.H. Biogenesis of the yeast vacuole (lysosome). The precursor forms of the soluble hydrolase carboxypeptidase yscS are associated with the vacuolar membrane. *J. Biol. Chem* **267**, 8021-8029 (1992).
256. Katzmann, D.J., Babst, M. & Emr, S.D. Ubiquitin-dependent sorting into the multivesicular body pathway requires the function of a conserved endosomal protein sorting complex, ESCRT-I. *Cell* **106**, 145-155 (2001).
257. Rubenstein, E.M. & Schmidt, M.C. Mechanisms regulating the protein kinases of Saccharomyces cerevisiae. *Eukaryotic Cell* **6**, 571-583 (2007).
258. Huse, M. & Kuriyan, J. The Conformational Plasticity of Protein Kinases. *Cell* **109**, 275-282 (2002).
259. Zhu, H. *et al.* Analysis of yeast protein kinases using protein chips. *nature genetics* **26**, 283–290 (2000).
260. Chalmers, J.J. *et al.* Effects of temperature on Escherichia coli overproducing beta-lactamase or human epidermal growth factor. *Appl. Environ. Microbiol.* **56**, 104-111 (1990).
261. Schein, C.H. Production of Soluble Recombinant Proteins in Bacteria. *Nat Biotech* **7**, 1141-1149 (1989).
262. Vera, A., González-Montalbán, N., Arís, A. & Villaverde, A. The conformational quality of insoluble recombinant proteins is enhanced at low growth temperatures. *Biotechnol. Bioeng* **96**, 1101-1106 (2007).
263. Palmer, I. & Wingfield, P.T. Preparation and extraction of insoluble (inclusion-body) proteins from Escherichia coli. *Curr Protoc Protein Sci* **Chapter 6**, Unit 6.3 (2004).
264. Hutter, M.C. & Helms, V. Influence of key residues on the reaction mechanism of the cAMP-dependent protein kinase. *Protein Sci* **8**, 2728-2733

(1999).
265. Johnson, L.N., Noble, M.E. & Owen, D.J. Active and inactive protein kinases: structural basis for regulation. *Cell* **85**, 149-158 (1996).
266. Cheng, Y., Zhang, Y. & McCammon, J.A. How does the cAMP-dependent protein kinase catalyze the phosphorylation reaction: an ab initio QM/MM study. *J. Am. Chem. Soc* **127**, 1553-1562 (2005).
267. Díaz, N. & Field, M.J. Insights into the phosphoryl-transfer mechanism of cAMP-dependent protein kinase from quantum chemical calculations and molecular dynamics simulations. *J. Am. Chem. Soc* **126**, 529-542 (2004).
268. Valiev, M., Kawai, R., Adams, J.A. & Weare, J.H. The Role of the Putative Catalytic Base in the Phosphoryl Transfer Reaction in a Protein Kinase: First-Principles Calculations. *Journal of the American Chemical Society* **125**, 9926-9927 (2003).
269. Coker, K.J., Staros, J.V. & Guyer, C.A. A kinase-negative epidermal growth factor receptor that retains the capacity to stimulate DNA synthesis. *Proc. Natl. Acad. Sci. U.S.A* **91**, 6967-6971 (1994).
270. Gibbs, C.S. & Zoller, M.J. Rational scanning mutagenesis of a protein kinase identifies functional regions involved in catalysis and substrate interactions. *J. Biol. Chem* **266**, 8923-8931 (1991).
271. Vitari, A.C. *et al.* WNK1, the kinase mutated in an inherited high-blood-pressure syndrome, is a novel PKB (protein kinase B)/Akt substrate. *Biochem. J* **378**, 257-268 (2004).
272. Schneider, T.D. & Stephens, R.M. Sequence logos: a new way to display consensus sequences. *Nucleic Acids Res* **18**, 6097-6100 (1990).
273. Mok, J. *et al.* Deciphering protein kinase specificity through large-scale analysis of yeast phosphorylation site motifs. *Sci Signal* **3**, ra12 (2010).
274. Shannon, P. *et al.* Cytoscape: A Software Environment for Integrated Models of Biomolecular Interaction Networks. *Genome Res* **13**, 2498-2504 (2003).
275. Heath, V.L., Shaw, S.L., Roy, S. & Cyert, M.S. Hph1p and Hph2p, Novel Components of Calcineurin-Mediated Stress Responses in Saccharomyces cerevisiae. *Eukaryotic Cell* **3**, 695-704 (2004).
276. Estojak, J., Brent, R. & Golemis, E.A. Correlation of two-hybrid affinity data with in vitro measurements. *Mol. Cell. Biol* **15**, 5820-5829 (1995).
277. McAlister-Henn, L., Gibson, N. & Panisko, E. Applications of the yeast two-hybrid system. *Methods* **19**, 330-337 (1999).
278. Avery, L. & Wasserman, S. Ordering gene function: the interpretation of epistasis in regulatory hierarchies. *Trends in Genetics* **8**, 312-316 (1992).
279. Hartman, J.L., Garvik, B. & Hartwell, L. Principles for the Buffering of Genetic Variation. *Science* **291**, 1001-1004 (2001).
280. Segrè, D., Deluna, A., Church, G.M. & Kishony, R. Modular epistasis in yeast metabolism. *Nat. Genet* **37**, 77-83 (2005).
281. Drees, B. *et al.* Derivation of genetic interaction networks from quantitative phenotype data. *Genome Biology* **6**, R38 (2005).
282. Costanzo, M. *et al.* The genetic landscape of a cell. *Science* **327**, 425-431 (2010).
283. Tong, A.H.Y. *et al.* Global mapping of the yeast genetic interaction network. *Science* **303**, 808-813 (2004).
284. St Onge, R.P. *et al.* Systematic pathway analysis using high-resolution fitness profiling of combinatorial gene deletions. *Nat. Genet* **39**, 199-206 (2007).

285. Schuldiner, M. *et al.* Exploration of the function and organization of the yeast early secretory pathway through an epistatic miniarray profile. *Cell* **123**, 507-519 (2005).
286. Elena, S.F. & Lenski, R.E. Test of synergistic interactions among deleterious mutations in bacteria. *Nature* **390**, 395-398 (1997).
287. Phillips, P.C. The language of gene interaction. *Genetics* **149**, 1167-1171 (1998).
288. Mani, R., St.Onge, R.P., Hartman, J.L., Giaever, G. & Roth, F.P. Defining genetic interaction. *Proceedings of the National Academy of Sciences* **105**, 3461 -3466 (2008).
289. Phillips, P.C. Epistasis--the essential role of gene interactions in the structure and evolution of genetic systems. *Nat. Rev. Genet.* **9**, 855-867 (2008).
290. Järvinen, A.P., Hiissa, J., Elo, L.L. & Aittokallio, T. Predicting Quantitative Genetic Interactions by Means of Sequential Matrix Approximation. *PLoS ONE* **3**, e3284 (2008).
291. Onge, R.P.S. *et al.* Systematic pathway analysis using high-resolution fitness profiling of combinatorial gene deletions. *Nat Genet* **39**, 199-206 (2007).
292. Collins, S.R. *et al.* Functional dissection of protein complexes involved in yeast chromosome biology using a genetic interaction map. *Nature* **446**, 806-810 (2007).
293. Sopko, R. & Andrews, B.J. Linking the kinome and phosphorylome--a comprehensive review of approaches to find kinase targets. *Mol Biosyst* **4**, 920-933 (2008).
294. Sopko, R. *et al.* Mapping pathways and phenotypes by systematic gene overexpression. *Mol. Cell* **21**, 319-330 (2006).
295. Albuquerque, C.P. *et al.* A multidimensional chromatography technology for in-depth phosphoproteome analysis. *Mol. Cell Proteomics* **7**, 1389-1396 (2008).
296. Li, X. *et al.* Large-scale phosphorylation analysis of alpha-factor-arrested Saccharomyces cerevisiae. *J. Proteome Res* **6**, 1190-1197 (2007).
297. Smolka, M.B., Albuquerque, C.P., Chen, S.-hong & Zhou, H. Proteome-wide identification of in vivo targets of DNA damage checkpoint kinases. *Proc. Natl. Acad. Sci. U.S.A* **104**, 10364-10369 (2007).
298. Breitkreutz, A. *et al.* A global protein kinase and phosphatase interaction network in yeast. *Science* **328**, 1043-1046 (2010).
299. Ballif, B.A., Carey, G.R., Sunyaev, S.R. & Gygi, S.P. Large-scale identification and evolution indexing of tyrosine phosphorylation sites from murine brain. *J. Proteome Res* **7**, 311-318 (2008).
300. Oppermann, F.S. *et al.* Large-scale proteomics analysis of the human kinome. *Mol. Cell Proteomics* **8**, 1751-1764 (2009).
301. Trinidad, J.C., Thalhammer, A., Specht, C.G., Schoepfer, R. & Burlingame, A.L. Phosphorylation state of postsynaptic density proteins. *J. Neurochem* **92**, 1306-1316 (2005).
302. Trinidad, J.C. *et al.* Quantitative analysis of synaptic phosphorylation and protein expression. *Mol. Cell Proteomics* **7**, 684-696 (2008).
303. Tweedie-Cullen, R.Y., Reck, J.M. & Mansuy, I.M. Comprehensive mapping of post-translational modifications on synaptic, nuclear, and histone proteins in the adult mouse brain. *J. Proteome Res* **8**, 4966-4982 (2009).
304. Hunter, T. & Plowman, G.D. The protein kinases of budding yeast: six score and more. *Trends Biochem. Sci* **22**, 18-22 (1997).

305. Brocke, L., Chiang, L.W., Wagner, P.D. & Schulman, H. Functional Implications of the Subunit Composition of Neuronal CaM Kinase II. *Journal of Biological Chemistry* **274**, 22713-22722 (1999).
306. Takeuchi, Y., Yamamoto, H., Fukunaga, K., Miyakawa, T. & Miyamoto, E. Identification of the isoforms of Ca(2+)/Calmodulin-dependent protein kinase II in rat astrocytes and their subcellular localization. *J. Neurochem* **74**, 2557-2567 (2000).
307. Urquidi, V. & Ashcroft, S.J. A novel pancreatic beta-cell isoform of calcium/calmodulin-dependent protein kinase II (beta 3 isoform) contains a proline-rich tandem repeat in the association domain. *FEBS Lett* **358**, 23-26 (1995).
308. Tombes, R.M., Faison, M.O. & Turbeville, J.M. Organization and evolution of multifunctional Ca(2+)/CaM-dependent protein kinase genes. *Gene* **322**, 17-31 (2003).
309. Aimes, R.T., Hemmer, W. & Taylor, S.S. Serine-53 at the tip of the glycine-rich loop of cAMP-dependent protein kinase: role in catalysis, P-site specificity, and interaction with inhibitors. *Biochemistry* **39**, 8325-8332 (2000).
310. Mann, M. *et al.* Analysis of protein phosphorylation using mass spectrometry: deciphering the phosphoproteome. *Trends Biotechnol* **20**, 261-268 (2002).
311. Tsui, J., Inagaki, M. & Schulman, H. Calcium/calmodulin-dependent protein kinase II (CaMKII) localization acts in concert with substrate targeting to create spatial restriction for phosphorylation. *J. Biol. Chem* **280**, 9210-9216 (2005).
312. Schulman, H. Activity-Dependent Regulation of Calcium/Calmodulin-Dependent Protein Kinase II Localization. *J. Neurosci.* **24**, 8399-8403 (2004).
313. Bayer, K.U. & Schulman, H. Regulation of signal transduction by protein targeting: the case for CaMKII. *Biochem. Biophys. Res. Commun* **289**, 917-923 (2001).
314. Scott, J.D. & Pawson, T. Cell Signaling in Space and Time: Where Proteins Come Together and When They're Apart. *Science* **326**, 1220-1224 (2009).
315. Gasch, A.P. *et al.* Genomic expression programs in the response of yeast cells to environmental changes. *Molecular biology of the cell* **11**, 4241 (2000).
316. Ayscough, K.R. Coupling actin dynamics to the endocytic process in Saccharomyces cerevisiae. *Protoplasma* **226**, 81-88 (2005).
317. Gustin, M.C., Albertyn, J., Alexander, M. & Davenport, K. MAP Kinase Pathways in the Yeast Saccharomyces cerevisiae. *Microbiol Mol Biol Rev* **62**, 1264-1300 (1998).
318. Mulholland, J. *et al.* Ultrastructure of the yeast actin cytoskeleton and its association with the plasma membrane. *J. Cell Biol* **125**, 381-391 (1994).
319. Chowdhury, S., Smith, K.W. & Gustin, M.C. Osmotic stress and the yeast cytoskeleton: phenotype-specific suppression of an actin mutation. *The Journal of Cell Biology* **118**, 561 -571 (1992).
320. Romano, G.H. *et al.* Different sets of QTLs influence fitness variation in yeast. *Mol. Syst. Biol* **6**, 346 (2010).
321. Grummt, I. Regulation of mammalian ribosomal gene transcription by RNA polymerase I. *Prog. Nucleic Acid Res. Mol. Biol* **62**, 109-154 (1999).
322. Gilbert, W., Siebel, C.W. & Guthrie, C. Phosphorylation by Sky1p

promotes Npl3p shuttling and mRNA dissociation. *RNA* **7**, 302-313 (2001).
323. Ross-Macdonald, P. *et al.* Large-scale analysis of the yeast genome by transposon tagging and gene disruption. *Nature* **402**, 413-418 (1999).
324. Wa, C., Cerny, R. & Hage, D.S. Obtaining high sequence coverage in matrix-assisted laser desorption time-of-flight mass spectrometry for studies of protein modification: analysis of human serum albumin as a model. *Anal. Biochem* **349**, 229-241 (2006).
325. Krause, E., Wenschuh, H. & Jungblut, P.R. The dominance of arginine-containing peptides in MALDI-derived tryptic mass fingerprints of proteins. *Anal. Chem* **71**, 4160-4165 (1999).
326. Dreisewerd, K., Berkenkamp, S., Leisner, A., Rohlfing, A. & Menzel, C. Fundamentals of matrix-assisted laser desorption/ionization mass spectrometry with pulsed infrared lasers. *International Journal of Mass Spectrometry* **226**, 189-209 (2003).
327. Kpebe, A. & Rabinow, L. Dissection of Darkener of Apricot Kinase Isoform Functions in Drosophila. *Genetics* **179**, 1973-1987 (2008).
328. Collins, S.R. *et al.* Functional dissection of protein complexes involved in yeast chromosome biology using a genetic interaction map. *Nature* **446**, 806-810 (2007).
329. Roguev, A. *et al.* Conservation and Rewiring of Functional Modules Revealed by an Epistasis Map in Fission Yeast. *Science* **322**, 405-410 (2008).
330. Kelley, R. & Ideker, T. Systematic interpretation of genetic interactions using protein networks. *Nat Biotech* **23**, 561-566 (2005).
331. Fiedler, D. *et al.* Functional Organization of the S. cerevisiae Phosphorylation Network. *Cell* **136**, 952-963 (2009).
332. Segre, D., DeLuna, A., Church, G.M. & Kishony, R. Modular epistasis in yeast metabolism. *Nat Genet* **37**, 77-83 (2005).
333. Carter, G.W., Galas, D.J. & Galitski, T. Maximal Extraction of Biological Information from Genetic Interaction Data. *PLoS Comput Biol* **5**, e1000347 (2009).
334. Connerth, M. *et al.* Oleate Inhibits Steryl Ester Synthesis and Causes Liposensitivity in Yeast. *Journal of Biological Chemistry* **285**, 26832 -26841 (2010).
335. Castrejon, F., Gomez, A., Sanz, M., Duran, A. & Roncero, C. The RIM101 Pathway Contributes to Yeast Cell Wall Assembly and Its Function Becomes Essential in the Absence of Mitogen-Activated Protein Kinase Slt2p. *Eukaryotic Cell* **5**, 507-517 (2006).
336. Steen, H., Jebanathirajah, J.A., Rush, J., Morrice, N. & Kirschner, M.W. Phosphorylation Analysis by Mass Spectrometry. *Molecular & Cellular Proteomics* **5**, 172 -181 (2006).
337. Dutil, E.M., Toker, A. & Newton, A.C. Regulation of conventional protein kinase C isozymes by phosphoinositide-dependent kinase 1 (PDK-1). *Curr. Biol* **8**, 1366-1375 (1998).
338. Sweeney, F.D. *et al.* Saccharomyces cerevisiae Rad9 acts as a Mec1 adaptor to allow Rad53 activation. *Curr. Biol* **15**, 1364-1375 (2005).
339. Toker, A. & Newton, A.C. Akt/Protein Kinase B Is Regulated by Autophosphorylation at the Hypothetical PDK-2 Site. *Journal of Biological Chemistry* **275**, 8271 -8274 (2000).
340. Li, X. *et al.* Large-scale phosphorylation analysis of alpha-factor-arrested Saccharomyces cerevisiae. *J. Proteome Res* **6**, 1190-1197 (2007).

341. Bayer, K.U., Koninck, P.D. & Schulman, H. Alternative splicing modulates the frequency-dependent response of CaMKII to Ca2+ oscillations. *EMBO J* **21**, 3590-3597 (2002).
342. Caran, N. Cytosolic Targeting Domains of gamma and delta Calmodulin-dependent Protein Kinase II. *Journal of Biological Chemistry* **276**, 42514-42519 (2001).
343. GuptaRoy, B. *et al.* Alternative splicing of Drosophila calcium/calmodulin-dependent protein kinase II regulates substrate specificity and activation. *Brain Res. Mol. Brain Res* **80**, 26-34 (2000).
344. Heist, E.K., Srinivasan, M. & Schulman, H. Phosphorylation at the nuclear localization signal of Ca2+/calmodulin-dependent protein kinase II blocks its nuclear targeting. *Journal of Biological Chemistry* **273**, 19763 (1998).
345. Shen, K., Teruel, M.N., Subramanian, K. & Meyer, T. CaMKIIbeta functions as an F-actin targeting module that localizes CaMKIIalpha/beta heterooligomers to dendritic spines. *Neuron* **21**, 593-606 (1998).
346. Rosenberg, O. Structure of the Autoinhibited Kinase Domain of CaMKII and SAXS Analysis of the Holoenzyme. *Cell* **123**, 849-860 (2005).
347. Brickey, D.A. *et al.* Mutational analysis of the autoinhibitory domain of calmodulin kinase II. *J. Biol. Chem* **269**, 29047-29054 (1994).
348. Fong, Y.L., Taylor, W.L., Means, A.R. & Soderling, T.R. Studies of the regulatory mechanism of Ca2+/calmodulin-dependent protein kinase II. Mutation of threonine 286 to alanine and aspartate. *Journal of Biological Chemistry* **264**, 16759 -16763 (1989).
349. Waldmann, R., Hanson, P.I. & Schulman, H. Multifunctional Ca2+/calmodulin-dependent protein kinase made Ca2+ independent for functional studies. *Biochemistry* **29**, 1679-1684 (1990).
350. Hoekstra, M.F. *et al.* Budding and fission yeast casein kinase I isoforms have dual-specificity protein kinase activity. *Mol. Biol. Cell* **5**, 877-886 (1994).
351. Lim, M.Y., Dailey, D., Martin, G.S. & Thorner, J. Yeast MCK1 protein kinase autophosphorylates at tyrosine and serine but phosphorylates exogenous substrates at serine and threonine. *J. Biol. Chem* **268**, 21155-21164 (1993).
352. Malathi, K., Xiao, Y. & Mitchell, A.P. Catalytic roles of yeast GSK3beta/shaggy homolog Rim11p in meiotic activation. *Genetics* **153**, 1145-1152 (1999).
353. Stern, D.F., Zheng, P., Beidler, D.R. & Zerillo, C. Spk1, a new kinase from Saccharomyces cerevisiae, phosphorylates proteins on serine, threonine, and tyrosine. *Mol. Cell. Biol* **11**, 987-1001 (1991).
354. Wang, Q.M., Fiol, C.J., DePaoli-Roach, A.A. & Roach, P.J. Glycogen synthase kinase-3 beta is a dual specificity kinase differentially regulated by tyrosine and serine/threonine phosphorylation. *Journal of Biological Chemistry* **269**, 14566 -14574 (1994).
355. Wilson, L.K., Dhillon, N., Thorner, J. & Martin, G.S. Casein kinase II catalyzes tyrosine phosphorylation of the yeast nucleolar immunophilin Fpr3. *J. Biol. Chem* **272**, 12961-12967 (1997).
356. Sugiyama, Y., Ishida, A., Sueyoshi, N. & Kameshita, I. Tyrosine kinase activity of a Ca2+/calmodulin-dependent protein kinase II catalytic fragment. *Biochemical and Biophysical Research Communications* **377**, 648-652 (2008).
357. Lundgren, K. *et al.* mik1 and wee1 cooperate in the inhibitory tyrosine phosphorylation of cdc2. *Cell* **64**, 1111-1122 (1991).

358. Atherton-Fessler, S., Parker, L.L., Geahlen, R.L. & Piwnica-Worms, H. Mechanisms of p34cdc2 regulation. *Mol. Cell. Biol.* **13**, 1675-1685 (1993).
359. Gould, K.L. & Nurse, P. Tyrosine phosphorylation of the fission yeast cdc2+ protein kinase regulates entry into mitosis. *Nature* **342**, 39-45 (1989).
360. Welburn, J.P.I. *et al.* How Tyrosine 15 Phosphorylation Inhibits the Activity of Cyclin-dependent Kinase 2-Cyclin A. *Journal of Biological Chemistry* **282**, 3173 -3181 (2007).
361. Döppler, H. & Storz, P. A Novel Tyrosine Phosphorylation Site in Protein Kinase D Contributes to Oxidative Stress-mediated Activation. *Journal of Biological Chemistry* **282**, 31873-31881 (2007).
362. Storz, P., Döppler, H., Johannes, F.-J. & Toker, A. Tyrosine Phosphorylation of Protein Kinase D in the Pleckstrin Homology Domain Leads to Activation. *Journal of Biological Chemistry* **278**, 17969-17976 (2003).
363. Wu, Y., Spencer, S.D. & Lasky, L.A. Tyrosine Phosphorylation Regulates the SH3-mediated Binding of the Wiskott-Aldrich Syndrome Protein to PSTPIP, a Cytoskeletal-associated Protein. *Journal of Biological Chemistry* **273**, 5765-5770 (1998).
364. Xie, J., Supekova, L. & Schultz, P.G. A genetically encoded metabolically stable analogue of phosphotyrosine in Escherichia coli. *ACS Chem. Biol* **2**, 474-478 (2007).
365. Pruyne, D. & Bretscher, A. Polarization of cell growth in yeast. *Journal of Cell Science* **113**, 571 -585 (2000).
366. Munn, A.L. Molecular requirements for the internalisation step of endocytosis: insights from yeast. *Biochimica et Biophysica Acta (BBA) - Molecular Basis of Disease* **1535**, 236-257 (2001).
367. Waddle, J.A., Karpova, T.S., Waterston, R.H. & Cooper, J.A. Movement of cortical actin patches in yeast. *J. Cell Biol* **132**, 861-870 (1996).
368. Robertson, A.S., Smythe, E. & Ayscough, K.R. Functions of actin in endocytosis. *Cell. Mol. Life Sci* **66**, 2049-2065 (2009).
369. Michelot, A. *et al.* Reconstitution and protein composition analysis of endocytic actin patches. *Curr. Biol* **20**, 1890-1899 (2010).
370. Lew, D.J. & Reed, S.I. Cell cycle control of morphogenesis in budding yeast. *Curr. Opin. Genet. Dev* **5**, 17-23 (1995).
371. Madden, K. & Snyder, M. Cell polarity and morphogenesis in budding yeast. *Annu. Rev. Microbiol* **52**, 687-744 (1998).
372. Cid, V.J. *et al.* Orchestrating the cell cycle in yeast: sequential localization of key mitotic regulators at the spindle pole and the bud neck. *Microbiology (Reading, Engl.)* **148**, 2647-2659 (2002).
373. Gagny, B. *et al.* A novel EH domain protein of Saccharomyces cerevisiae, Ede1p, involved in endocytosis. *J. Cell. Sci* **113 (Pt 18)**, 3309-3319 (2000).
374. Stimpson, H.E.M., Toret, C.P., Cheng, A.T., Pauly, B.S. & Drubin, D.G. Early-arriving Syp1p and Ede1p function in endocytic site placement and formation in budding yeast. *Mol. Biol. Cell* **20**, 4640-4651 (2009).
375. Brewster, J.L. & Gustin, M.C. Positioning of cell growth and division after osmotic stress requires a map kinase pathway. *Yeast* **10**, 425-439 (1994).
376. Hohmann, S. Osmotic stress signaling and osmoadaptation in yeasts. *Microbiol. Mol. Biol. Rev* **66**, 300-372 (2002).
377. Brockerhoff, S.E. & Davis, T.N. Calmodulin concentrates at regions of cell growth in Saccharomyces cerevisiae. *The Journal of Cell Biology* **118**, 619 -

629 (1992).
378. Sun, G.-H., Ohya, Y. & Anraku, Y. Yeast calmodulin localizes to sites of cell growth. *Protoplasma* **166**, 110-113 (1992).
379. Davis, D.A. How human pathogenic fungi sense and adapt to pH: the link to virulence. *Curr. Opin. Microbiol* **12**, 365-370 (2009).
380. Davis, D. Adaptation to environmental pH in Candida albicans and its relation to pathogenesis. *Curr. Genet* **44**, 1-7 (2003).
381. Peñalva, M.A. & Arst, H.N. Regulation of gene expression by ambient pH in filamentous fungi and yeasts. *Microbiol. Mol. Biol. Rev* **66**, 426-446, table of contents (2002).
382. Shah, A.J., Tilburn, J., Adlard, M.W. & Arst Jr., H.N. pH regulation of penicillin production in Aspergillus nidulans. *FEMS Microbiology Letters* **77**, 209-212 (1991).
383. Espeso, E.A., Tilburn, J., Arst, H.N. & Peñalva, M.A. pH regulation is a major determinant in expression of a fungal penicillin biosynthetic gene. *EMBO J* **12**, 3947-3956 (1993).
384. Obara, M., Szeliga, M. & Albrecht, J. Regulation of pH in the mammalian central nervous system under normal and pathological conditions: facts and hypotheses. *Neurochem. Int* **52**, 905-919 (2008).
385. Chesler, M. Regulation and modulation of pH in the brain. *Physiol. Rev* **83**, 1183-1221 (2003).
386. Chesler, M. & Kaila, K. Modulation of pH by neuronal activity. *Trends Neurosci* **15**, 396-402 (1992).
387. Stock, C. & Schwab, A. Protons make tumor cells move like clockwork. *Pflugers Arch - Eur J Physiol* **458**, 981-992 (2009).

6. Appendix

6.1 Additional info

Table 6.1. Summary of Kns1 interactors identified in other studies.

ORF Name	St. Name	Description	Exp.	Reference
YIL113W	SDP1	Stress-inducible dual-specificity MAP kinase phosphatase, negatively regulates Slt2p MAP kinase by direct dephosphorylation, diffuse localization under normal conditions shifts to punctate localization after heat shock	TH	Uetz P (2000)
YOL054W	PSH1	Nuclear protein, putative RNA polymerase II elongation factor; isolated as Pob3p/Spt16p-binding protein	AC	Ho Y (2002)
YDL185W	TFP1	Subunit A of the eight-subunit V1 peripheral membrane domain of the vacuolar H+-ATPase; protein precursor undergoes self-catalyzed splicing to yield the extein Tfp1p and the intein Vde (PI-SceI), which is a site-specific endonuclease	AC	Ho Y (2002)
YBR126C	TPS1	Synthase subunit of trehalose-6-phosphate synthase/phosphatase complex, which synthesizes the storage carbohydrate trehalose; also found in a monomeric form; expression is induced by the stress response and repressed by the Ras-cAMP pathway	AC	Ho Y (2002)
YLR438W	CAR2	L-ornithine transaminase (OTAse), catalyzes the second step of arginine degradation, expression is dually-regulated by allophanate induction and a specific arginine induction process; not nitrogen catabolite repression sensitive	AC	Ho Y (2002)
YDR510W	SMT3	Ubiquitin-like protein of the SUMO family, conjugated to lysine residues of target proteins; regulates chromatid cohesion, chromosome segregation, APC-mediated proteolysis, DNA replication and septin ring dynamics; phosphorylated at Ser2	TH	Hannich JT (2005)
YJL092W	SRS2	DNA helicase and DNA-dependent ATPase involved in DNA repair, needed for proper timing of commitment to meiotic recombination and transition from Meiosis I to II; blocks trinucleotide repeat expansion; affects genome stability	TH	Chiolo I (2005)
YGR037C	ACB1	Acyl-CoA-binding protein, transports newly synthesized acyl-CoA esters from fatty acid synthetase (Fas1p-Fas2p) to acyl-CoA-consuming processes; subject to starvation-induced, Grh1p-mediated unconventional secretion	AC	Krogan NJ (2006)

YPL209C	IPL1	Aurora kinase subunit of the conserved chromosomal passenger complex (CPC; Ipl1p-Sli15p-Bir1p-Nbl1p), involved in regulating kinetochore-microtubule attachments; helps maintain condensed chromosomes during anaphase and early telophase	TH	Wong J (2007)
YIL144W	TID3	Component of the evolutionarily conserved kinetochore-associated Ndc80 complex (Ndc80p-Nuf2p-Spc24p-Spc25p); conserved coiled-coil protein involved in chromosome segregation, spindle checkpoint activity, kinetochore assembly and clustering	TH	Wong J (2007)
YJR076C	CDC11	Component of the septin ring of the mother-bud neck that is required for cytokinesis; septins recruit proteins to the neck and can act as a barrier to diffusion at the membrane, and they comprise the 10nm filaments seen with EM	TH	Yu H (2008)
YGL173C	KEM1	Evolutionarily-conserved 5'-3' exonuclease component of cytoplasmic processing (P) bodies involved in mRNA decay; plays a role in microtubule-mediated processes, filamentous growth, ribosomal RNA maturation, and telomere maintenance	AC	Breitkreutz A (2010)
YOR201C	MRM1	Ribose methyltransferase that modifies a functionally critical, conserved nucleotide in mitochondrial 21S rRNA	AC	Breitkreutz A (2010)
YOL041C	NOP12	Nucleolar protein involved in pre-25S rRNA processing and biogenesis of large 60S ribosomal subunit; contains an RNA recognition motif (RRM); binds to Ebp2; similar to Nop13p and Nsr1p	AC	Breitkreutz A (2010)
YPL043W	NOP4	Nucleolar protein, essential for processing and maturation of 27S pre-rRNA and large ribosomal subunit biogenesis; constituent of 66S pre-ribosomal particles; contains four RNA recognition motifs (RRMs)	AC	Breitkreutz A (2010)
YOR017W	PET127	Protein with a role in 5'-end processing of mitochondrial RNAs, located in the mitochondrial membrane	AC	Breitkreutz A (2010)
YEL055C	POL5	DNA Polymerase phi; has sequence similarity to the human MybBP1A and weak sequence similarity to B-type DNA polymerases, not required for chromosomal DNA replication; required for the synthesis of rRNA	AC	Breitkreutz A (2010)
YLR196W	PWP1	Protein with WD-40 repeats involved in rRNA processing; associates with trans-acting ribosome biogenesis factors; similar to beta-transducin superfamily	AC	Breitkreutz A (2010)
YPL012W	RRP12	Protein required for export of the ribosomal subunits; associates with the RNA components of the pre-ribosomes; contains HEAT-repeats	AC	Breitkreutz A (2010)
YMR229C	RRP5	RNA binding protein with preference for single stranded tracts of U's involved in synthesis of both 18S and 5.8S rRNAs; component of both the ribosomal small subunit (SSU) processosome and the 90S preribosome	AC	Breitkreutz A (2010)

YNL189W	SRP1	Karyopherin alpha homolog, forms a dimer with karyopherin beta Kap95p to mediate import of nuclear proteins, binds the nuclear localization signal of the substrate during import; may also play a role in regulation of protein degradation	AC	Breitkreutz A (2010)
YDR212W	TCP1	Alpha subunit of chaperonin-containing T-complex, which mediates protein folding in the cytosol; involved in actin cytoskeleton maintenance; overexpression in neurons suppresses formation of pathogenic conformations of huntingtin protein	AC	Breitkreutz A (2010)
YPL093W	NOG1	Putative GTPase that associates with free 60S ribosomal subunits in the nucleolus and is required for 60S ribosomal subunit biogenesis; constituent of 66S pre-ribosomal particles; member of the ODN family of nucleolar G-proteins	AC	Breitkreutz A (2010)
YJL010C	NOP9	Essential subunit of U3-containing 90S preribosome involved in production of 18S rRNA and assembly of small ribosomal subunit; also part of pre-40S ribosome and required for its export into cytoplasm; binds RNA and contains pumilio domain	AC	Breitkreutz A (2010)
YCL011C	GBP2	Poly(A+) RNA-binding protein, involved in the export of mRNAs from the nucleus to the cytoplasm; similar to Hrb1p and Npl3p; also binds single-stranded telomeric repeat sequence in vitro	AC	Breitkreutz A (2010)
YBR142W	MAK5	Essential nucleolar protein, putative DEAD-box RNA helicase required for maintenance of M1 dsRNA virus; involved in biogenesis of large (60S) ribosomal subunits	AC	Breitkreutz A (2010)
YGR090W	UTP22	Possible U3 snoRNP protein involved in maturation of pre-18S rRNA	AC	Breitkreutz A (2010)
YNL004W	HRB1	Poly(A+) RNA-binding protein, involved in the export of mRNAs from the nucleus to the cytoplasm; similar to Gbp2p and Npl3p	AC	Breitkreutz A (2010)
YGL120C	PRP43	RNA helicase in the DEAH-box family, functions in both RNA polymerase I and polymerase II transcript metabolism, involved in release of the lariat-intron from the spliceosome	AC	Breitkreutz A (2010)

[1]ORF names, standard names and descriptions according to Biogrid/Saccharomyces Genome Database (http://www.yeastgenome.org/). AC: affinity copurification. TH: yeast Two-hybrid

6.2 Abbreviations

% v/v	percent per volume
% w/v	percent per weight
2-ME	2-β-mercaptoethanol
aa	amino acid
APS	ammoniumpersulfate
ATP	adenosintriphosphate

bp	base pair(s)
BSA	bovine serum albumin
C-	carboxy-
ddH2O	double deionized H2O
DNA	2'-desoxyribonucleic acid
DTT	dithiothreitol
e.g.	*exempli gratia* (for example)
ECL	enhanced chemiluminescence
EDTA	ethylenediaminetetraacetic acid
ER	endoplasmic reticulum
et al.	et alii (and others)
g	gram
g	gravity
h	hour(s)
HEPES	4-(2-hydroxyethyl)-1-piperazineethanesulfonic acid
i.e.	id est (that is)
Ig	immunoglobulin
IP	immunoprecipitation
IPTG	isopropylthio-ß-D-galactoside
kb	kilo base pair(s)
kDa	kilo Dalton
KOAc	potassium acetate
l	litre
LiOAc	lithium acetate
m	meter
M	molar (mol x l^{-1})
mA	milli Amper
mg	milligram (10^{-3} g)
min	minute(s)
ml	millilitre (10^{-3} l)
mM	millimolar (10^{-3} M)
mRNA	messenger RNA
MYC	c-myc epitope
N-	amino-
NaOAc	sodium acetate
nm	nanometer (10^{-9} m)
OD	optical density

ORF	open reading frame
PAGE	polyacrylamide gel electrophoresis
PCR	polymerase chain reaction
PMSF	phenyl methyl sulfonyl fluoride
r.m.p.	rotation per minute
RNA	ribonucleic acid
RNase	ribonuclease
RT	room temperature
s	second(s)
SDS	sodium dodecyl sulfate
TBS	tris buffered saline
TCA	thrichloroacetic acid
TEMED	1,2-bis-(dimethylamino)-ethane
Tris	tris(hydroxymethyl)aminomethane
U	units
v/v	volume/volume
w/o	without
w/v	weight/volume
wt	wild-type
YPD	yeast extract, peptone, dextrose
µg	microgram (10^{-6} g)
µl	microlitre (10^{-6} l)
µm	micrometer (10^{-6} m)
µM	micromolar (10^{-6} M)

7. Acknowledgments

The experimental work of this Ph.D. thesis was carried out at the Max-Delbrück-Center for Molecular Medicine, Berlin (Germany).

First, I would like to express my sincere gratitude to Dr. Gunnar Dittmar who gave me the opportunity to start my PhD project and develop as a scientist in his laboratory. I appreciate his support, his mentoring and scientific discussions. Furthermore, I would like to thank him for the mass spectrometric analysis and for critical revision of the manuscript.

I am indebted to Prof. Dr. Thomas Sommer for lending me his help when I most needed it, for his encouragement, for his advice and for providing financial support and resources throughout this work.

I wish to express my gratitude to Prof. Dr. Saumweber for being my supervisor at the Humboldt University and for his critical revision of this manuscript.

I am grateful to Dr. Mathias Dahlmann for his help in countless occasions. I also would like to thank all members of the Prof. Thomas Sommer lab for providing technical advice and fruitful scientific discussions.

8. Selbstständigkeitserklärung

Hiermit erkläre ich eidesstattlich, dass die von mir vorgelegte Dissertation selbständig angefertigt wurde und ich die Stellen der Arbeit, die anderen Werken in Wortlaut oder Sinn nach entnommen sind, in jedem Einzelfall als Entlehnung kenntlich gemacht habe. Ich versichere, dass ich mich nicht anderwärtig um einen Doktorgrad beworben habe oder einen entsprechenden Doktorgrad besitze. Diese Dissertation habe ich bei keinem anderen Fachbereich oder keiner anderen Universität vorgelegt. Die Promotionsordnung der Mathematisch-Naturwissensachftlichen Fakultät I der Humboldt-Universität zu Berlin habe ich gelesen und akzeptiert.

M. Nieves Martínez Marshall

Berlin, 27. Oktober 2011